The Effect of Mechanical Stimulation on Osteogenesis of Cell Seeded Collagen Microspheres

Maryam Shariatzadeh

Supervisors: Prof Damien Lacroix
Dr Cecile M Perrault

Submitted in accordance with the requirements for the degree of Doctor of Philosophy.

The University of Sheffield,
Department of Mechanical Engineering

The candidate confirms that the work submitted is her own and that appropriate credit has been given where reference has been made to the work of others.
This copy has been supplied on the understanding that it is copyright material and that no quotation from the thesis may be published without proper acknowledgement.
The right of Maryam Shariatzadeh to be identified as Author of this work has been asserted by her in accordance with the Copyright, Designs and Patents Act 1988.

Acknowledgements

I would like to thank both my supervisors, Prof Damien Lacroix and Dr Cecile Perrault for giving me the opportunity to undertake this PhD project and for all their continued support, guidance, patience and encouragement.

I would like to thank Dr Nicola Green for her technical assistance regarding confocal and SHG microscopes. I also would like to thank Ms Orla Gallagher and Mr Mark Kinch for their valued work regarding histology samples. I would specially like to thank Mr Neil Bramall for his technical assistance regarding ICP-ES machine. I would also like to thank Mr Chris Hill for his technical support, training and work with SEM samples. I would like to thank Tom Paterson for his valued work regarding laser 3D print.

I would like to thank my main PhD financial sponsor, European Research Council (ERC). Without which I would not have been able to carry out this research.

I would like to show my appreciation towards everyone in INSIGNEO Institute for in silico Medicine lab who has either given me training or advice and helped me to carried out my work. My special thank to Mrs Julie Marshall our lab manager for her support and understanding.

I would like to say big thank you to Dr Detlev Conrad Mielczarek for his patience and providing huge support regarding Latex. I would like to thank Dr Adrien Adrien Baldit for his valued work regarding computational modelling part of my project.

I would like to thank my husband Dr Ehsan Alborzi for his huge understanding and endless support and also putting up with me over the course of these three years. I have worked many late nights and weekends and without his understanding and patience I would not have been able to finish my project. I truly appropriate both

his and my son Ayeen supports and thank them again that I have been able to reach where I am today.

I would like to thank my very first teachers, my parents, for their support and encouragement and appreciate everything they ever done for me since I started school and University many years ago.

My final huge thank you goes out once more to Damien, you have been so understanding and supportive from the start I am truly grateful to you for giving me this opportunity and treasure everything you have taught me.

Abstract

Mesenchymal stem cells (MSCs) are widely implicated as a cell source for tissue engineering of skeletal tissue in cell based therapy. Mechanical forces can stimulate the differentiation of MSCs in micro environment and the resulting mechanotransduction would provide crucial adjuncts to customary biochemical signalling pathways. This study indicated that collagen concentration, hence cells micro environment mechanical properties are important in cell proliferation and differentiation process. The experimental results showed that collagen concentration of 2 mg/mL supports proliferation of MSCs while, higher concentrations promote the viability of more differentiated cell lines human osteosarcoma (MG-63s).

Encapsulated human embryonic stem cell-derived mesenchymal progenitor (hES-MPs) contraction is vital in cell adaptation and remodeling of their new environment. hES-MPs seeded collagen microspheres were subjected to two cyclic compression regimes and cell viability, alkaline phosphatase (ALP) activity and mineralisation of differentiated cells were assessed over 28 days experiment. It has been shown that cyclic compression of very low cell number seeded on soft natural scaffold can encourage osteogenesis of undifferentiated cells.

Applying mechanical stimulation can affect cell commitment but at the same time it shows that mechanical loading and in particular fluid-induced shear stress (FSSs) on their own fail to provide all the necessary signals in osteogenic differentiation of hES-MPs.
Combining microfluidic systems with mechanical stimulation for osteogenesis represents a scientific and technological innovation. This study demonstrated a microfluidic chamber design for mechanical stimulation of flexible cellular microspheres and a possible high-throughput microfluidic system for parallel processing of stem cell aggregation. Microfluidic system can increase the ALP activity of cells while maintaining cell viability and proliferation. Self-assembled hES-MPs

collagen microspheres present exceptional cell delivery model in bone healing and repair process and in addressing many inadequacies of the existing cell delivery approaches. Cell seeded collagen microspheres offer great possibilities in facilitating the clinical application of cell-based therapy in local bone remodelling and regenerative medicine.

Contents

Abstract **vi**

Table of Contents **xii**

List of Figures **xxvi**

List of Tables **xxvii**

Nomenclature **xxxiii**

1 Literature review **5**

1.1 Recent advances and challenges in bone tissue engineering 5

1.2 Fundamental of bone and developmental biology 6

1.3 Main clinical bone disease and disorders 8

1.4 Application of biomaterials in tissue engineering 9

1.4.1 Biocompatibility 10

1.4.2 Biodegradability 11

1.4.3 Mechanical properties 11

1.4.4 Scaffold architecture 11

1.5 Type of biomaterials 12

1.5.1 Osteoinductive materials 12

1.5.2 Hybrid materials 13

1.5.3 Advanced hydrogels 14

1.5.4 Immuno modulatory biomaterials 15

1.6 Cellular approaches 16

1.7 Mechanotransduction 18

1.8 Mechanical stimulations 20

1.8.1 Overview 20

1.8.2 Molecules and genetic pathways involved in MSCs response to mechanical loading 21

1.8.2.1 Wnt signalling and MSC differentiation 21
1.8.2.2 The TGF-β superfamily 23
1.8.3 Compression 25
1.8.4 Tension 28
1.8.5 Fluid flow-induced shear stress 31
1.9 Cells ability in sensing their local environment 34
1.10 Collagen micro encapsulation 36
1.10.1 Advantages of collagen micro encapsulation application . . 36
1.10.2 Advantages of collagen application in drug delivery system 38
1.10.3 Collagen nanoparticles and microspheres 38
1.11 Microfluidic system 40
1.12 Potential clinical applications in regenerative medicine and tissue engineering 44
1.13 Aim and objectives 45

2 Materials and Methods **47**
2.1 Materials 47
2.2 Methods 51
2.2.1 Cell preparation 51
2.2.1.1 General cell culture conditions 51
2.2.1.2 MG-63 cell line 51
2.2.1.3 Human embryonic stem cell derived mesenchymal progenitors (hES-MPs) 51
2.2.2 Cell culture in 2D 52
2.2.3 Cell culture in 3D 52
2.2.3.1 Collagen microsphere formation 52
2.2.3.2 Cell seeding 52
2.2.4 Fluorescent staining of live and dead cells 53
2.2.5 Evaluation of cell viability and cell number 53
2.2.5.1 PrestoBlue assay 53
2.2.5.2 Total DNA count 54
2.2.6 Analysis of collagen fibres organisation and remodeling . . 55
2.2.6.1 Fluorescent staining of collagen fibres 55
2.2.6.2 Second harmonic generation microscopic imaging 56
2.2.7 Assessment of osteogenesis 57
2.2.7.1 BCIP/NBT Liquid Substrate System for extracellular ALP staining 57
2.2.7.2 Quantification of total ALP activity of cells . . . 57

2.2.7.3 Alizarin red S staining . . . 58
2.2.7.4 Alcian blue staining . . . 60
2.2.8 Scanning electron microscopy . . . 60
2.2.9 Histological staining of samples . . . 61
2.2.10 Statistical analysis . . . 61

3 Cell Seeded Collagen Microspheres 63
3.1 Introduction . . . 63
3.2 Methods . . . 65
3.2.1 Collagen gelation procedure . . . 65
3.2.2 Assessment of collagen mechanical properties . . . 67
3.2.3 Evaluation of collagen fibres density and microstructure . . . 67
3.2.4 Measurement of collagen microsphere contraction . . . 68
3.2.5 Examining short and long cell viability of cell seeded collagen microspheres . . . 68
3.2.6 Assessment of collagen fibres micro structure in hES-MPs seeded bovine and rat tail collagen I microspheres . . . 69
3.2.7 Effect of different hES-MPs passages on level of ALP activity and calcium deposition . . . 69
3.2.8 2D versus 3D hES-MP cell culture . . . 69
3.2.9 Cell culture . . . 70
3.2.10 Cellular assay . . . 70
3.2.11 Statistics . . . 71
3.3 Results . . . 72
3.3.1 Collagen gel mechanical properties . . . 72
3.3.2 Identification of collagen fibre micro structure . . . 72
3.3.3 Assessment of short and long term cell viability of seeded hES-MPs/collagen microspheres . . . 78
3.3.4 Determination of seeded MG-63s collagen I microspheres viability . . . 81
3.3.5 Collagen gel contraction . . . 83
3.3.6 Effect of different hES-MPs passages on level of ALP activity and calcium deposition . . . 85
3.3.7 2D versus 3D hES-MP cell culture . . . 90
3.4 Discussion . . . 93
3.5 Conclusions and future work . . . 96

4 Design of a microfluidic chamber for cell compression 99
4.1 Introduction . . . 99
4.2 Methods . . . 101
4.2.1 Fabrication of microfluidic chamber by glass capillary template . . . 102
4.2.2 Fabrication of a microfluidic chamber using shrinking tube 102
4.2.3 Fabrication of microfluidic chamber using play dough . . . 102
4.2.4 Fabrication of microfluidic system by vinyl paper template 103
4.2.5 Fabrication of rapid prototyping and photo mask of vinyl paper template . . . 103
4.2.6 Fabrication of microfluidic chamber via laser 3D printing . 104
4.2.6.1 Photo-curable monomer preparation . . . 105
4.2.6.2 UV laser set up . . . 105
4.2.6.3 PDMS molding of microfluidic chamber . . . 106
4.2.6.4 Flow regime and calculation of shear stress . . . 106
4.2.7 Fabrication of injected PEG as a template for microfluidic chamber . . . 106
4.2.8 Fabrication of a microfluidic chamber by using brass rod replica . . . 107
4.2.9 Cell culture . . . 107
4.2.10 Cellular assay . . . 107
4.2.11 Statistics . . . 109
4.3 Results . . . 109
4.3.1 Fabrication of microfluidic chamber using glass capillary, shrinking tubes or dough as a template . . . 109
4.3.2 Fabrication of microfluidic chamber via laser 3D printing . 111
4.3.2.1 Compression of cell seeded collagen microspheres using microfluidic chamber . . . 111
4.3.2.2 Effect of optimisation of fluid flow rate on cell proliferation . . . 113
4.3.3 Optimisation of chamber design . . . 118
4.3.3.1 Enhancing the geometry via laser 3D print . . . 118
4.3.3.2 Rapid prototyping and photo mask of vinyl paper template . . . 120
4.3.3.3 Optimisation of chamber design via injected PEG method . . . 122

4.3.3.4 Application of metal rod template in optimisation of chamber design . . . 122
4.3.4 Assessment of hES-MPs viability in microfluidic experiment 123
4.3.4.1 Microfluidic system can induce osteogenesis of hES-MPs by increasing early stage bone marker . . . 125
4.4 Discussion . . . 127
4.5 Conclusions and future work . . . 129

5 Mechanical conditioning of hES-MPs/collagen microspheres 131
5.1 Introduction . . . 131
5.2 Methods . . . 133
5.2.1 Design of a PDMS made loading chamber . . . 133
5.2.2 Characterisation of PDMS mechanical properties . . . 133
5.2.3 Cyclic compression protocol . . . 134
5.2.4 Assessment of collagen fibre alignment . . . 135
5.2.5 Evaluation of collagen microsphere surface micro structure 136
5.2.6 Cell culture . . . 136
5.2.7 Cellular assay . . . 136
5.2.8 Statistics . . . 138
5.3 Results . . . 138
5.3.1 Design of a PDMS made compression chamber . . . 138
5.3.2 Characterisation of PDMS mechanical properties . . . 141
5.3.3 Application of cyclic mechanical conditioning . . . 142
5.3.4 Comparison of cell proliferation, ALP activity and mineralisation between adjusted and constant loading protocols . . 142
5.3.5 Assessment of collagen fibre alignment . . . 156
5.3.6 Evaluation of collagen fibre organisation using SEM microscopy . . . 158
5.4 Discussion . . . 160
5.5 Conclusions and future work . . . 164

6 Effect of fluid flow on osteogenesis of hES-MPs/collagen microspheres 167
6.1 Introduction . . . 167
6.2 Methods . . . 168
6.2.1 Application of fluid flow-induced shear stress on microspheres by orbital shaker . . . 168

6.2.2 Application of fluid flow-induced shear stress on microspheres by platform rocker . . . 169
6.2.3 Cell culture . . . 170
6.2.4 Cellular assay . . . 170
6.2.5 Statistics . . . 171
6.3 Results . . . 171
6.3.1 Effect of FSS on total DNA and proliferation of hES-MPs 171
6.3.2 Evaluation of shear stress induced ALP activity level . . . 173
6.3.3 Assessment of mineralisation . . . 175
6.4 Discussion . . . 180
6.5 Conclusions and future work . . . 184

7 Discussion and Conclusions 187
7.1 Collagen I microspheres . . . 187
7.2 Mechanical conditioning of cells . . . 189
7.2.1 Microfluidics . . . 189
7.2.2 Mechanical stimulation . . . 190
7.2.3 Fluid flow induced shear stress . . . 193
7.3 Conclusions . . . 195

Bibliography 221

List of Figures

1.1 Schematic of different types of organ transplantation and comparison between autograft, allograft and xenograft[1]. 6

1.2 Schematic of the effect of mechanical stimulation on the bone through structural adaptation and the maintenance of physiological homeostasis. Load is transferred to the skeleton through direct activation of the bone mechanosensor and by indirect stimulation through dynamic muscle activity[2]. 7

1.3 Scaffold properties should be considered in designing an optimum construct for tissue engineering applications including geometry, biocompatibility of material, porosity, degradation rate, mechanical strength and incorporation of signalling molecules. Optimising these factors is essential in addressing various physiological specifications of an engineered tissue.[3]. 10

1.4 Osteoinductive CaP based biomaterials in the form of sintered ceramics, cements coatings, coral-derived ceramics, alumina ceramic and porous bioglass and their various applications in tissue engineering and animal models. 13

1.5 Schematic of Mesenchymal stem cells capability to differentiate into other cell linages[4]. 17

1.6 Cell response to mechanical stimuli initiates by triggering multiple intracellular signalling pathways that regulate cellular functions including maintenance, proliferation and differentiation[5]. 19

1.7 Role of Wnt signalling pathway in osteogenesis. Taken from http://www.nature.com/bonekey 22

1.8 Schematic Illustration: TGF-β signalling pathway. TGF-β ligand binds to TGF-βRII that activates TGF-βRI and induces the downstream SMAD mediated signal transduction. Taken from hindawi.com 24

1.9 Transduction of external mechanical stimulation into the biochemical signals: When a mechanical signal (i.e. mechanical stress or compression) is applied onto the cell surface, it activates various biological molecules and signalling pathways. The resulting cellular responses will be cell proliferation, differentiation or apoptosis depending on the cell's requirements that determines the cell's fate[6]. 26

1.10 Anatomical locations of and mechanical strain experienced by bone cells. Osteocytes are embedded in osteons and organised parallel to the Haversian canal. An osteocyte located in a lacuna and connects to other osteocytes through the cannaliculi. Mechanical stimulations induce fluid flow in the canalicular space[7]. 31

1.11 Mesenchymal stem cells and many other cells have the capacity to response to fluid shear stress, pressure, electric fields and tissue strain[2]. 32

1.12 Schematic of ECM-integrin-cytoskeleton formation in the focal adhesion site by applying an external tensile load[8]. 34

1.13 Schematic Illustration of cell encapsulation technology. The semi permeable membrane enables nutrients, oxygen, therapeutic molecules and waste to bidirectionally diffuse through. Also membrane prevents the entrance of immune cells and antibodies[9]. 36

1.14 PDMS made microfluidic chip: (a) individual channel acting as a diffusion barrier; (b) reaction chamber;(c) network of channels; (d) assembly of the independent channels; (e) integrating the channels into an outlet channel that can be connected to the withdrawal mode of a syringe pump[9]. 42

2.1 A schematic representation showing reduction of resazurin to resorofin. This reduction takes place in only viable cells. The resazurin is reduced by cells into a fluorescent red colour compound and the conversion is often used as an indicator of living cells. Adapted from www.promega.com/resources/protocols/technical-bulletins/101/celltiter-blue-cell-viability-assay-protocol. 54

2.2 Molecular structure of Oregon Green 488 Carboxylic Acid, Succinimidyl Ester, 5-isomer fluorescent dye that used to stain collagen fibres of bovine and rat tail microspheres. Image was taken from www.thermofisher.com. 56

2.3 Molecular structure of Alizarin red dye in staining the deposited calcium in extracellular matrix of mineralised cells. Each calcium ion chelates with two molecules of Alizarin red[10]. 59

3.1 Undertaken experiments and conditions that applied on cell seeded collagen microspheres during 28 days pc. 68

3.2 Standard curve of DNA pico green assay used to evaluate hES-MP cell viability within 28 days of post en-capsulation. 70

3.3 SEM images of bovine collagen I microspheres, micro structure and mesh work of collagen fibres after gelation, a-f; different cross section area and magnification of collagen gel. Scale bar for (a)-(b) 2 µm, (c) 1 µm, (d) 5 µm, (e)-(f) 20 µm. 73

3.4 Microstructure and fibre density of three bovine and rat tail collagen I microspheres were compared using SHG confocal microscope at 24 h post gelation. Bovine collagen fibre presented higher intensity of signals suggesting the presence of more collagen fibres in the samples. Microscopic images were taken by Dr Green at Kroto Research Institute, Department of Material Sciences, University of Sheffield. Scale bar for (a)-(h) 20 µm. 74

3.5 Microstructure and density of bovine and rat tail collagen I fibres were compared using Oregon Green® 488 carboxylic acid, succinimidyl ester, 5-isomer collagen tracker at 24 h post gelation. No considerable differences was recorded between microstructure of collagen fibres from bovine and rat tail origins. Scale bar for (a)-(d) 200 µm, (e)-(h) 50 µm. 75

3.6 SEM images of hES-MPs seeded bovine collagen I microspheres. Cells attached to the hydrogel surface and presented more elongated morphology on day 16 pc. Scale bars for (a) and (c) 20 µm and (b) 10 µm. 76

3.7 Microstructure and fibres density of hES-MPs seeded bovine and rat tail collagen I microspheres were compared using SHG confocal microscope. Rat tail collagen fibre presented slightly higher intensity of signals suggesting the presence of more collagen fibres in the samples on day 7 pc. Microscopic images were taken by Dr Green at Kroto Research Institute, Department of Material Sciences, University of Sheffield. Scale bars for (a)-(i) are 20 µm. . 77

3.7 Effect of collagen concentration and cell seeding density on viability of hES-MPs 24 h after encapsulation in bovine collagen I using fluorescence live and dead assay. c: collagen concentration. Scale bars for (a)-(f) are 200 µm. 79

3.7 Short term cell viability of seeded hES-MPs collagen I microsphere was checked by bright field and fluorescent imaging of live/dead cells over 7 days pc. Live cells were shown by green colour while, dead cells were stained red. Scale bars for (a)-(k) are 200 µm. . . . 80

3.7 Long term cell viability of seeded hES-MPs collagen I microsphere on day 35 pc was evaluated by fluorescent imaging of live/dead cells and presented by different magnification. Live cells were shown by green stain while, dead cells were stained red. Scale bars for (a)-(e) are 200 µm. 81

3.8 hES-MPs cell viability was evaluated over 28 days pc by using DNA pico green assay at different time points. 81

3.9 Long term cell viability of seeded MG-63s collagen I microsphere was checked by fluorescent imaging of live/dead cells over 21 days pc. Scale bars for (a)-(i) are 200 µm and (j) 50 µm. 82

3.10 Microscopic images of cell seeded collagen I contraction over 7 days pc, from top left to bottom right, embedded hES-MPs ability to contract the collagen gel at 24 h, 72 h, 120 h and 168 h pc. Seeded hES-MPs contracted collagen gel to nearly half its diameter within first 7 days pc. Scale bars are 200 µm. 83

3.11 Microscopic images of cell seeded collagen I contraction over 7 days pc, from top left to bottom right, embedded MG-63s ability to contract the collagen gel at 24 h, 72 h, 120 h and 168 h pc. Seeded MG-63s contracted collagen gel far less that hES-MPs within first 7 days of en-capsulation. Scale bars are 200 µm. 84

3.12 Effect of two cell lines and collagen I sources on the contraction of collagen I gel with concentration of 2 mg/mL were investigated, a: collagen contractibility of hES-MPs/bovine collagen I was compared with rat tail collagen I by measuring the diameter of 12 samples at each time point, b: ability of hES-MPs versus MG-63 cell line in contracting collagen gel was assessed,* indicates statistical significance, (** $p < 0.01$, *** $p < 0.001$, **** $p < 0.0001$). Data is mean ± SD n=9. 85

3.12 Microscopic images of hES-MPs live and dead assay and comparison of collagen gel contraction in different passages of hES-MP seeded hES-MPs collagen microsphere over 7 days pc. Ps5 hES-MPs showed slightly stronger fluorescent signals compared to Ps 12. Scale bars for (a)-(h) are 200 µm. 86

3.13 Alkaline phosphatase staining of different passages of hES-MPs seeded collagen microsphere over 14 days pc. OS media; osteogenic media, nFGF; control media with no treatment. ALP activity of both passages were similar during 14 day experiment with osteogenic media treated samples in both passages showed higher intensity of ALP stain from day 5 pc. Stain intensity in osteogenic media treated samples was reported as minimal on day 14 pc. All images taken by light microscope, 1.5x. 87

3.14 Alizarin red staining of different passages of hES-MPs seeded collagen microsphere over 14 days pc. OS media; osteogenic media, nFGF; control media with no treatment. Deposited stain accumulated much more in osteogenic media treated samples in both passages from day 5 pc. Stain intensity in osteogenic media treated samples was reported highest on day 14 pc in both passages but ps 12 showed slightly higher deposition of stain compared with ps 5. All images taken by light microscope, 1.5x. 88

3.15 Characterisation of hES-MPs/collagen microspheres behaviour in ps 5 and 12, a: cell proliferation of hES-MPs was assessed over 28 days pc using DNA pico green, b: total Alkaline phosphatase activity level was investigated by ALP fluorescent kit over 21 days pc, * indicates statistical significance, (*** p <0.0001). Data is mean ± SD n=9. 90

3.16 Alkaline phosphatase staining of 2D culture of ps 5 hES-MPs was assessed in three conditions of added FGF-β, nFGF-β (control media with no treatment) and cultured in osteogenic media (OS media) over 28 days. Ostegenic media treated samples showed higher deposition of ALP stain from day 8 pc onward. All images taken by light microscope, 10x. 91

3.17 Alizarin red staining of 2D culture of ps 5 hES-MPs was examined in three conditions of added FGF-β, nFGF-β (control media with no treatment) and cultured in osteogenic media (OS media) over 28 days. Ostegenic media treated samples showed higher deposition of ALP stain from day 6 pc onward. All images taken by light microscope, 10x. 92

3.18 Total alkaline phosphatase activity of hES-MPs 2D culture was compared with seeded hES-MPs collagen microspheres over 28 days pc using ALP fluorescent kit,* indicates statistical significance, (* p <0.05). Data is mean ± SD n=9. 93

4.1 Schematic of various undertaken approaches in designing a PDMS made microfluidic chamber, loading/flow rate protocol and duration of experiment. 101

4.2 Vertical pipette puller, Narishige PP830 102

4.3 Geometry design of microfluidic chamber using inkscape software which contains 14 repeats of 1 mm diameter main channels with the length of 2.5 mm and 14 repeats of narrow channels (D=0.5 mm, L=2.5 mm). 103

4.4 Geometry design of microfluidic chamber that contained a main channel (I.D=1 mm) and a narrow channel (I.D=0.5 mm). 104

4.5 Geometry design of microfluidic chamber by solid work software that contained 10 repeats of 7.83 mm long main channels (I.D=1 mm) and 10 repeats of 7.68 mm long narrow channels (O.D=0.75 mm, I.D=0.5 mm). 105

4.6 Standard curve of a; DNA pico green and b; ALP 4-MU that was employed to analyse hES-MPs viability and early stage mineralisation marker. 108

4.7 Standard curve of presto blue assay used to evaluate MG-63 cell viability at different time points. 108

4.8 A; Capillary glass molded in PDMS, B; microscopic image of chamber micro structure bright filed filter 4x. 110

4.9 A; shrinking tubes molded in PDMS, B; microscopic image of chamber micro structure bright filed filter 4x. 110

4.10 A; PDMS made chamber using play dough as a template, B; Microscopic image of chamber micro structure bright filed filter 4x. . 111

4.11 a; microscopic images of PDMS chamber made by laser 3D printing, b; compression of collagen beads by being passed through microfluidic chamber 112

4.12 Microscopic images of viable MG-63s on day 3 pc before and 24 h after being subjected to flow rate of 0.4 ml/min using fluorescent live and dead stain and phase contrast microscopy. (g)-(i) shows collagen microspheres damage after being subjected to flow rate compared with free floating control (f). Scale bars for (a)-(i) are 200 µm. 113

4.13 Microscopic images of viable MG-63s on day 5 pc before and 24 h after being subjected to flow rate of 0.32 ml/min. (a)-(f); phase contrast microscopy, scale bars are 200 µm, (g)-(i); live and dead fluorescent images of cell seeded microspheres, scale bars are 50 µm. 115

4.14 Microscopic images of viable MG-63s on day 7 pc that were subjected to fluid flow compared with free floating controls. (a)-(e); phase contrast microscopy, scale bars are 200 µm, (f)-(i); live and dead fluorescent images of cells, scale bare for (f) and (g) are 50 µm and for (h) and (i) are 100-200 µm. 116

4.15 Cell viability of MG-63s seeded collagen microspheres. Comparison of compressed samples vs free floating controls using presto blue assay from 24 h to day 7 pc, * indicates statistical significance, (* $p < 0.01$, **** $p < 0.0001$). Data is mean ± SD for 9 samples. . . 117

4.16 Collagen microspheres trapped in the constricted channel of microfluidic chamber objective 4x. 118

4.17 PDMS microfluidic chamber was made by laser 3D printing and its microstructure, a; PDMS chamber consisted of 14 repeats of main and restricted channels, images b-f show appearance of micro grooves, uneven inner surface on the channels and partially to fully blockage of narrow channels caused by uncured PDMS. Scale bars for (b) and (c) are 1000 µm and for (d)-(f) are 500 µm. 119

4.18 Broken and missing parts in PDMS chamber caused by application of UV photo mask technique and vinyl paper template. 120

4.19 Vinyl paper used as a template to create microfluidic chamber. Images b-g show micro patterns and groove on the inner surface of template. Scale bars for (b), (d)-(f) are 1000 µm and for (c) and (g) are 500 µm. 121

4.20 Vinyl paper template and UV photo mask were used to create microfluidic chamber. Scale bars for (b)-(e) are 500 µm. 122
4.21 Metal rod was used as a template to fabricate PDMS microfliudic chamber. 123
4.22 Microscopic images of hES-MPs viability and collagen bead's geometry of free floating control on 24 h, days 2, 3, 4 and 5 pc. ff; free floating control. Samples were passed through the compression chamber on day 3 pc and fluorescent images of collagen microspheres were recorded 24 h after applying the first and the second compression cycles. Scale bars for images (a)-(i) are 200 µm. . . . 124
4.23 Microscopic images of viable hES-MPs and collagen microspheres geometry of fluorescently stained free floating controls and compressed samples 24 h after applying 3rd compression cycle at day 6 and day 7 pc. ff; free floating control. Scale bars for (a)-(i) are 200 µm. 125
4.24 a; Cell proliferation comparison between free floating controls and microfluidic samples, b; alkaline phosphatase activity of free floating controls and compressed sample was assessed by fluorometric assay. * indicates statistical significance (* $p < 0.01$, ** $p < 0.001$). Data is mean ± SD for 9 samples. 126
4.25 Evaluation of deposited extracellular matrix phosphorous level between microfluidic compressed samples and free floating controls over 28 days pc. * indicates statistical significance (*** $p < 0.0001$). Data is mean ± SD for 9 samples. 127

5.1 Schematic of the loading protocols, durations and mechanical conditioning of hES-MPs seeded collagen microspheres within 28 days post en-capsulation. Samples were subjected to either 15-40 mind, 10% strain, 1 Hz for 5 and 10 days. The DNA content, ALP activity level and mineralisation of 12 samples were analysed for each time points. 134
5.2 Schematic of the applied constant strain on PDMS made loading chamber which resulted in inconsistent load transfer to the microspheres. 135
5.3 Schematic of the applied adjusted strain which shows subtracting the calculated PDMS plastic elongation from global strain may result in more consistent and uniform load transfer to the microspheres. 135

5.4 Standard curve of a; DNA pico green and b; ALP 4-MU that was employed to analyse hES-MPs viability and early stage mineralisation marker. 137

5.5 PDMS strain field corresponding to 10% of strain applied macroscopically (Abaqus). Strong stress appears close the sample ends but locally in the centre and along half sample height the strain is quite constant and close to 10% equivalent to the macroscopic load. 139

5.6 Beads strain field corresponding to 10% of strain applied macroscopically on the PDMS sample (Abaqus). Microspheres inside the loading chamber would sense the maximal strain of around 5% by applying 5% tensile strain to the loading chamber to reach the contact with beads. Contact sensitivity is related the to the geometry of PDMS sample as with the rectangular cross section, it appears that the contact is first reached in the direction corresponding to the shortest geometry length compared with the square sample. . 140

5.7 PDMS made compression chamber, ID: 0.9 mm, a and viscoelastic behaviour of PDMS under 10% strain was shown by stress/strain curve along a cyclic loading, b. 141

5.8 Measurement of transversal and longitudinal strains on the PDMS surface when subjected to 10% global strain using Kelkins software. 141

5.9 Characterisation of PDMS Young's modulus and plastic elongation using Bose biodynamic system. 142

5.10 Evaluation of cell viability in loaded samples of constant protocol versus control over 28 day pc. Total DNA content of loaded samples 15 min/day and 40 min/day for 5 and 10 days, compared with controls in the constant protocol and DNA level shows steady viability of cells in all conditions. Free floating controls showed significant higher DNA concentration compared with other experimental samples. * indicates statistical significance, (**** p <0.0001, *** p <0.001). Data is mean ± SD n=9. 143

5.11 Evaluation of ALP activity in loaded samples of constant protocol versus control over 28 day pc. Enzyme level did not show any significant increase in different time points and apart from free floating controls, ALP activity remained unchanged during 28 day pc. * indicates statistical significance, (**** p <0.0001, *** p <0.001, * p <0.1). Data is mean ± SD n=9. 144

5.12 Evaluation of cell viability in loaded samples of adjusted protocol versus control over 28 day pc, a; total DNA content of loaded samples 15 min/day and 40 min/day for 5 and 10 days, compared with controls in the constant protocol. Total DNA concentration presented steady cell viability in all conditions during 28 day experiment with no significant changes between different time points. * indicates statistical significance, (*** p <0.001). Data is mean ± SD n=9. 144

5.13 Evaluation of ALP activity in loaded samples of adjusted protocol versus control over 28 day pc. ALP activity reported significantly higher in loaded samples of 40 min in both 5 and 10 days loading regimes on day 14 pc in comparison with other conditions. Enzyme activity of all experimental conditions dropped to the lower level from day 21 pc onwards. * indicates statistical significance, (**** p <0.0001, ** p <0.01). Data is mean ± SD n=9. 145

5.14 Alizarin red staining of hES-MPs seeded collagen microspheres loaded under constant loading protocol versus controls over 28 days pc. Both 15-40 min/day loaded samples of 5 and 10 days experiment presented higher accumulation of deposited Alizarin red stain compared to unloaded controls from day 21 pc onward. All images taken by light microscope, 20x. 146

5.15 H&E staining of 10 µm thick seeded hES-MPs collagen microspheres cross sections over 28 days pc in 10 days cyclic loading regime. ffc; free floating control. cls; constant loading sample. uc; unloaded control. als; adjusted loading sample. All images taken by light microscope, 20x. 148

5.16 Alkaline phosphatase staining of 10 µm thick seeded hES-MPs collagen microspheres over 21 days pc in 10 days cyclic loading regime. ffc; free floating control. cls; constant loading sample. uc; unloaded control. als; adjusted loading sample. All images taken by light microscope, 20x. 149

5.17 Alkaline phosphatase staining of 10 µm thick seeded hES-MPs collagen microspheres on day 28 pc in 10 days cyclic loading regime. ffc; free floating control. cls; constant loading sample. uc; unloaded control. als; adjusted loading sample. All images taken by light microscope, 20x. 150

5.18 Alizarin red staining of 10 µm thick seeded hES-MPs collagen microspheres over 21 days pc in 10 days cyclic loading regime. ffc; free floating control. cls; constant loading sample. uc; unloaded control. als; adjusted loading sample. All images taken by light microscope, 20x. 151

5.19 Alizarin red staining of 10 µm thick seeded hES-MPs collagen microspheres on day 28 pc in 10 days cyclic loading regime. ffc; free floating control. cls; constant loading sample. uc; unloaded control. als; adjusted loading sample. All images taken by light microscope, 20x. 152

5.20 Evaluation of deposited extracellular matrix calcium and phosphorous in loaded samples of 40 min/day in 10 days loading regime of constant and adjusted protocols versus controls over 28 days pc, a; measurement of deposited calcium in the loaded samples compared with controls, b; comparison of phosphorous level in the loaded samples versus controls, * indicates statistical significance, (**** p <0.0001, *** p <0.001, ** p <0.01). Data is mean ± SD n=9. . . 154

5.21 Measurement extracellular zinc level in the loaded samples of 40 min/day in 10 days loading regime of constant and adjusted protocols versus controls over 28 days pc, * indicates statistical significance, (**** p <0.0001). Data is mean ± SD n=9. 155

5.22 Alcian blue staining of 10 µm thick seeded hES-MPs collagen microspheres over 14 days pc in 10 days cyclic loading regime, ffc; free floating control. cls; constant loading sample. uc; unloaded control. als; adjusted loading sample. All images taken under light microscope, 20x. 155

5.23 Alcian blue staining of 10 µm thick seeded hES-MPs collagen microspheres on days 21 and 28 pc in 10 days cyclic loading regime, ffc; free floating control. cls; constant loading sample. uc; unloaded control. als; adjusted loading sample. All images taken by light microscope, 20x. 156

5.24 SHG microscopic images of reorientation and alignment of collagen fibres on day 21 pc in 10 days cyclic loading experiment. SHG signal intensity was higher in loaded samples compared to the controls. Ffc; free floating control. Cls; constant loading sample. Uc; unloaded control. Als; adjusted loading sample. Collagen fibres of loaded sample in adjusted protocol visibly reorganised and aligned in comparison with more random organisation of collagen fibre in other conditions. Settings for images taken at 50-75 µm on all samples were optimised to visualise collagen SHG. All images taken by confocal microscope, EC 40x/1.3 plan-Neofluar oil DIC. 157

5.25 SEM microscopy of hES-MPs seeded collagen microspheres surface on day 28 pc. ffc; free floating control. cls; constant loading sample. uc; unloaded control. als; adjusted loading sample. Accumulation of mineral deposits is more evident in both loaded samples and free floating controls compared to free floating controls on day 6 pc. . 159

6.1 Cell seeding and experimental time line of orbital shaker experiment. (1000-2000) hES-MPs were seeded in collagen microspheres that were fixed at the centre of each well. DNA assay, ALP activity level and quantification of mineralisation were performed on samples at 24 h, day 6, 14, 21 and 28 pc. 169

6.2 Cell seeding and experimental time line of platform rocker. (1000-2000) hES-MPs were seeded in collagen microspheres that were fixed at the centre of each well. DNA assay, ALP activity level and quantification of mineralisation were performed on samples at 24 h, day 6, 14, 21 and 28 pc. 170

6.3 Cell viability of shear stress induced samples were assessed against static free floating controls over 28 days pc, total DNA measurement was performed for cell proliferation, * indicates statistical significance (*** $p < 0.001$, ** $p < 0.01$ and * $p < 0.1$). Data is mean ± SD for n=9 samples. 172

6.4 ALP activity level of shear stress induced samples were assessed against static free floating controls over 28 days pc, ALP activity was evaluated to study the osteogenic effect of fluid flow-induced shear stress on cells, * indicates statistical significance (**** $p < 0.0001$ and * $p < 0.1$). Data is mean ± SD for n=9 samples. . . 173

6.5 Measurement of alkaline phosphatase activity and deposited calcium in shaker experiment compared with static controls over 28 days pc, a; samples that were treated with osteogenic media (OS) presented significantly higher ALP level from day 14 pc onward, b; deposited calcium up regulated considerably from day 21 pc onward in static controls compared with the shaker samples, * indicates statistical significance (**** p <0.0001 and *** p <0.001). Data is mean ± SD for n=9 samples. 174

6.6 Comparison of ARS red S staining intensity between shaker samples and static free floating controls that were treated with osteogenic, basal media with added FGF-β and basal media. Deposited ARS stain was considerably higher in shaker samples that were treated with osteogenic media compared with other experimental conditions from day 14 pc onward. 175

6.7 Deposited zinc and phosphorous level of shear stress induced samples were assessed against static free floating controls over 28 days pc, a; quantitative measurement of deposited zinc showed significantly higher concentration of minerals in static controls that fluid flow induced samples was performed for cell proliferation, b; phosphorous level was up regulated significantly in static controls than shaker samples, * indicates statistical significance (*** p <0.001). Data is mean ± SD for n=9 samples. 176

6.8 Comparison of ALP activity level between shaker, platform rocker samples and free floating controls over 28 day pc. Alkaline phosphatase level was reported significantly higher free floating controls compared to fluid flow-induced samples of rocker and orbital shaker conditions. * indicates statistical significance (*** p <0.001 and **** p <0.0001). Data is mean ± SD for n=9 samples. 177

6.9 ALP staining of 10 µm thick cross sections of of shear stress induced samples were performed against static free floating controls over 28 days pc. ff; free floating control, sc; static control, ss; shaker sample. Static free floating controls presented higher ALP stain intensity on both days 21 and 28 pc compared to shaker experiment samples. 178

6.10 Alizarin red S staining of 10 µm thick cross section of shear stress induced samples were assessed against static free floating controls over 28 days pc. ff; free floating control, sc; static control, ss; shaker sample . Static controls presented more accumulation of deposited ARS stain on both days 21 and 28 pc compared to shaker experiment samples. 178
6.11 Histological staining of 10 µm thick cross section of shear stress induced samples against static free floating controls over 28 days pc. ff; free floating control, sc; static control, ss; shaker sample. Static controls presented darker stain colour that suggested more mineralised cells on both days 21 and 28 pc compared to shaker experiment samples. 179
6.12 Alcian blue staining of 10 µm thick cross section of shear stress induced samples against static free floating controls over 28 days pc. ff; free floating control, sc; static control, ss; shaker sample. Shaker sample presented higher accumulation of deposited stain on day 14 pc that suggested initiation of chondrogenic differentiation compared to static controls. 180

List of Tables

3.1 Number of cells/droplet with different initial cell density, collagen concentration and droplet volume used in hES-MPs and MG-63s encapsulation. 66

5.1 Mechanical properties of PDMS polymer were characterised using 10 step blocks of sinusoidal waves and ramps. Sine wave; sinusoidal wave of displacement to load. Dwell; sample was hold at a displacement level for a specific time. Ramp; sample was moved from displacement level 1 to displacement level 2 with specific rate. PDMS sample was subjected to relative tensile loading of 2.35 mm that applied from 0 mm to 2.35 mm, the sample was then hold at 2.35 mm for 400 s. PDMS sample then was pulled from relative 0 mm to 2.4 mm with rate of 0.01 mm/s, was hold for 400 s and moved back to relative 0 mm with the same rate. The experiment was repeated one more time with a different rate. 133

Nomenclature

Abbreviations

2D	two dimensional
3D	three dimensional
AA	amino acid
ADMSC	adipose-derived mesenchymal stem cell
AFFD	axisymmetric flow focusing device
ALP	alkaline phospahtase
AMH	anti mullerian hormone
ANOVA	analysis of variance
ARS	Alizarin red S
ASC	adult stem cell
BMP	Bone morphogenetic protein
BMSC	bone marrow stem/stormal cell
BSA	bovine serum albumin
BSP	bone sialoprotein
BTE	bone tissue engineering
Ca^{2+}	calcium
cAMP	Cyclic adenosine monophosphate
CaP	calcium phosphate

CDMP1	cartilage-derived morphogenetic protein1
COLI	collagen type I
COLIII	collagen type III
COLIV	collgen type 4
DAPI	4',6-diamidino-2-phenylindole
Dex	dexamethasone
DMEM	Dulbecco's Modifield Eagle's Medium
DMSO	dimethyl sulphoxide
DNA	deoxyribonucleic acid
ECM	extra cellular matrix
EDTA	ethylenediaminetetraacetic acid
ERK1/2	extra cellular signal-regulated kinase
ESC	embryonic stem cell
FBS	fetal bovine serum
FGF-β	fibroblast growth factor beta
FSS	fluid shear stress
GDF	growth and differentiation factor
GPC	gas phase chromatography
HA	hyaluronic acid
HCL	hydrochloric acid
hES-MP	human embryonic stem cell-derived mesenchymal progenitor
HPLC	high pressure liquid chromatography
HSP	heat-shock protein
ICP-ES	inductively coupled emission spectrometry

ILs	interleukins
JNK	C-jun N-terminal kinase
MAPK	mitogen-activated protein kinase
MG-63	human osteosarcoma cell
MLO-A5	murine long bone osteocyte A5
mRNA	messenger ribonucleic acid
NaOH	sodium hyroxide
nFGF-β	non-treated with fibroblast growth factor beta
OCN	osteocalcin
OPN	osteopontin
P/S	penicillin/steptomycin
PBS	Phosphate-buffered saline
pc	time post encapsulation
PCL	Polycaprolactone
PDGF	platelet-derived growth factor
PDMS	polydimethylsiloxane
PETG	ploye thylene terephthalate glycol
PLGA	ploy (lactic-coglycolic acid)
PLLA	ploy (L-lactic acid)
PLLA/HA	ploy (L-lactic acid/hyaluronic acid)
PMMA	ploymethyl methacrylate
Ps	passage number
qPCR	quantitative polymerase chain reaction
RGD	tripeptide composed of L-arginine, glycine, and L-aspartic acid

RT	room temperature
RT-PCR	reverse transcription polymerase chain reaction
RUNX2	runt-related transcription factor 2
SD	standard deviation
SEM	scanning electron microscopy
SHG	second harmonic generation
SMAD	intracellular protein that transduce extracellular signals from FGβ ligands
SOX	transcription factor SOX
TE	tissue engineering
TNFα	tumor necrosis factor alpha
TNFβ	tumor necrosis factor beta
TP508	thrombin peptide508
VEGF	vascular endothelial growth factor

Non-Standard Units

Hz	hertz
µg	microgram
µL	microlitre
µM	micromolar
ng	nanogram
nM	nanomolar
nm	nanometre
g	gram
kPa	kilopascal
kDa	kilodalton

MPa	megapascal
M	molar
nmol	nanomole

Introduction

Cell therapies serve as the most challenging yet, potentially the most successful application of stem cells. Mesenchymal stem cells (MSCs) are defined as multipotent progenitor cells with capability of self-renewal and differentiation into specialized lineage, in response to appropriate signals[11,12]. Using cells seeded in suitable biomaterials to mimic the in-vivo condition and provide necessary biochemical and biophysical micro environment is a one of the tissue engineering strategy which that has shown promising results in the field of regenerative medicine[13]. Nevertheless, before stem cell-based therapies are applied in clinics, a fundamental issue needs to be elucidated to gain a precise control over cell self-renewal and differentiation and a better understanding of the interplay between MSCs and their surrounding micro environment components including: growth factors, cell-cell network, and cell-extracellular matrix interactions[14]. Recent studies have shown the importance of mechanical cues, including the stiffness of the substrate, the nano topography of surface, and extracellular forces, in directing stem cell fate in vitro, even in the absence of biochemical factors[15].

Cells sense and respond to the mechanical properties of their extracellular matrix. Applied external forces, such as compressive, tensile, and fluid-induced shear forces can affect the mechanical properties of extracellular matrix through changes in cell function and most importantly differentiation of MSCs into distinct cell lines[16].

Mechanical stimulation can regulate most of our body cells and tissues and among them; bone function. This role in supporting our body weight appears to be particularly controlled by mechanical forces[17]. From a physiological point of view, healthy bone function is essential in body movement, organ protection and, mineral and marrow storage. The results of numerous studies indicate that bone cells too can regulate the magnitude of strain through functional adaptation[18]. Bone that are not subjected to proper external mechanical loading demonstrate bone loss through lower bone formation and/or increase in the rate of bone resorption. For instance, astronauts' bones who experience no mechanical load due to lack of

gravity and in long term immobilisation, the number of bone-forming osteoblasts decreases to keep the bone site specific strain at more or less the same level. Mechanical forces are thus recognized as a key player in maintaining the healthy bone[19].

The micro encapsulation technique is a novel approach in fabricating self-assembled collagen/human embryonic stem cell-derived mesenchymal progenitors (hES-MPs) microspheres that can be used as delivery devices for MSCs[20]. Collagen microspheres are comprised of fibrous networks of collagen that provide a protective matrix for MSCs viability. These collagen based carriers support growth and migration and may overcome many inadequacies of the existing cell delivery approaches by facilitating the application of MSC-based therapy in tissue engineering and regenerative medicine. In addition, cell/collagen microspheres can be used to monitor the response of the embedded cells to the applied external mechanical forces in soft materials and investigate how cells react to the changes in rigidity of their micro environment in combination with mechanical stimulation. Studying the effect of applied external forces in inducing MSCs differentiation into specific cell line may thus provide key adjuncts to prevalent biochemical signalling pathways in tissue engineering.

Mechanical forces play a key role in MSCs adhesion, proliferation, and differentiation[21]. External forces are able to manipulate the intracellular cytoskeletal arrangement and are competent in regulating nuclear shape and cell activities. As it is difficult to precisely evaluate the mechanisms of cytoskeletal conformational changes in vivo, biomimetic mechanical stimulation such as compression, stretching, and fluid-induced shear stress, have been employed to study these mechanisms in vitro[22]. Indeed mechanical stimulations have been reported to control developmental processes as diverse as gastrulation in Drosophili[23], cardiogenesis[24], and skeletogenesis[15].

Bioreactors are the vessels which accommodate controlled environment for efficient cell growth, cell conditioning and formation of specific product. Microfluidic chambers are an alternative approach to bioreactors, in applying mechanical loading to the cell-seeded biomaterial constructs. These systems can provide chemical and mechanical stimulations essential for cell differentiation in a controlled environment. Compared to current bulky bioreactor designs that require large amount

of reagents and lack high-throughput capabilities, microfluidic systems can offer a reduction in the overall volume of the systems and cost while providing the possibility of high-throughput testing. Mechanostimulation applied by microfluidic designs hence facilitates the confirmation of osteogenesis in cellular microsphere while allowing the optimization of mechanical stimulation and culture conditions for enhanced osteogenesis. Self-assembled hES-MPs seeded collagen microspheres present exceptional cell delivery devices in bone healing and repair process that have addressed many inadequacies of the existing cell delivery approaches and would facilitate the clinical application of cell based therapy in local bone remodelling, repair and, regenerative medicine.

This work is presented in seven chapters with the first chapter containing an abstract, introduction and literature review. Chapter 2 mainly focuses on general material and methods that were employed in this research. Chapter 3 contains experimental methods providing more in depth description of cell/collagen micro encapsulation design, cell viability and proliferation, characterisation of hES-MPs and assessing the effect of chemical stimulation on cell differentiation. Chapter 4 main focus is on experimental design and fabrication of microfluidic device to mechanically manipulate progenitor cells and to encourage osteogenesis. The effect of cyclic compression conditioning of osteogenesis hES-MPs/collagen microspheres was assessed in Chapter 5. The effect of fluid flow-induced shear stress on osteogenesis of hES-MPs/collagen microspheres was investigated in Chapter 6. Discussion and conclusions are presented in Chapter 7.

1

Literature review

1.1 Recent advances and challenges in bone tissue engineering

Bone grafts are used in a wide range of clinical settings to enhance application of bone repair and regeneration. Employing the tissue engineering approach for bone defect repair increasingly became more recognised as a better approach because the repair and healing begin with the patient's own tissue[25,26].

To date, autografts are commonly used as the gold standard for bone grafts because they are histo-compatible, non-immunogenic and also offer all of the essential required properties of a bone graft material (Figure 1.1). Additionally, autografts can stimulate and enhance osteoinduction, osteogenesis and osteoconduction. However, autografts have considerable disadvantages that involve harvesting bone from the patients, costly procedures and donor site injury and morbidity[26,27]. Allografts represent the second most common bone-grafting technique that involves transplanting donor bone tissue and depending on the host-site requirements is available in various forms from demineralized bone matrix and cancellous chips to osteochondral and whole-bone segments. Allografts are devitalized via irradiation or freeze-drying processing therefore are associated with risks of immuno reactions, reduced osteoinductive properties compared to autografts[28,29]. Although the clinical interventions improved the process of bone repair and regeneration, they do not possess all required characteristics of a transplant such as angiogenic potentials, biological safety, no size restrictions, ready access to surgeons, low patient morbidity, long shelf life and lower cost.

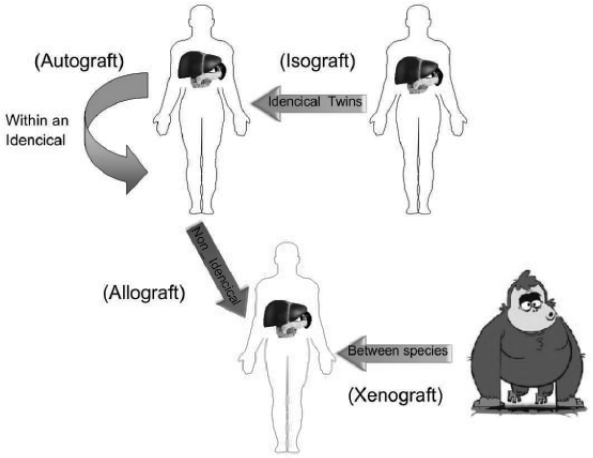


Figure 1.1: Schematic of different types of organ transplantation and comparison between autograft, allograft and xenograft[1].

Since thirty years ago that bone tissue engineering (BTE) was first initiated, both interest and progress in the field have increased tremendously. These advances involve design of biocompatible scaffolds that closely mimic the natural bone extracellular matrix niche, embedding of osteogenic cells to lay down the bone tissue matrix and employing the biochemical signals that help to direct the cells to the phenotypically desirable type. Yet, many crucial complications remain to be cleared on the way to BTE becoming a true clinical reality. Tissue engineers are attempting to tackle both enhanced vascularization and inhibition of fibrous tissue formation by integrating growth factors to the scaffold or use of genetically modified cells that release higher levels of angiogenic VEGF and coating the scaffold with anti-inflammatory drugs such as Dexamethasone[30,31]. In addition to bioreactors that can incorporate scaffolds, cells and growth factors have been proposed to drive safer and more effective bone tissue engineering application. Nevertheless, the ultimate bioreactor for BTE scaffolds is bone itself therefore, further efforts must be made to establish efficient intraoperative cell seeding approaches to minimize in vitro culture of the tissue engineered constructs and to maximize bone tissue regeneration in vivo[26].

1.2 Fundamental of bone and developmental biology

The understanding of bone structure, bone mechanics and tissue formation is crucial in inducing new functional bone tissues in application of bone repair and regeneration. Bone responds to a variety of external and internal stimuli including:

metabolic, physical and endocrine and provides load-bearing capacity to our skeleton and protection to our internal organs[32]. In addition, bone serves as a home of the biological elements required for hematopoiesis while, maintaining the homeostasis of key electrolytes by storage of calcium and phosphate ions[33]. Bone is constantly engaged in resorption and renewal cycles and undergoes perpetual biochemical exchange and remodelling to adapt to both internal mediators and external mechanical stimulations.

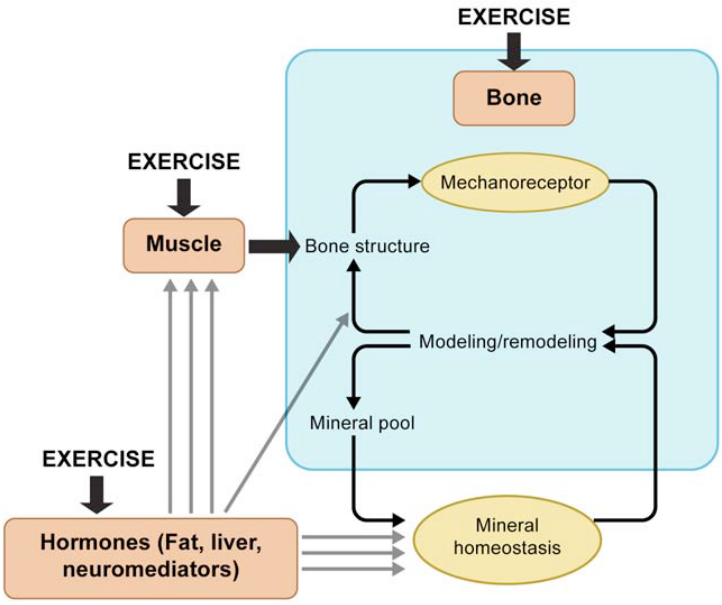


Figure 1.2: Schematic of the effect of mechanical stimulation on the bone through structural adaptation and the maintenance of physiological homeostasis. Load is transferred to the skeleton through direct activation of the bone mechanosensor and by indirect stimulation through dynamic muscle activity[2].

Bone is a highly dynamic, structural and functional tissue and its macroscopic structure and mechanical properties are extensively influenced by loading conditions. Skeletal structures categorise into long bones (tibia, ulnar, etc.), short bones (phalanges, etc.), flat bones (skull, sternum, etc.), and irregular bones (pelvic, vertebrae, etc.) while, bone tissue consists of compact (cortical bone) or trabecular (cancellous bone) pattern arrangement which vary in mechanical strength and stiffness. Despite these complex features and forms, bone possess relatively simple microscopic and hierarchical organisation in its structure[26].

Bone formation happens via distinct pathways of intramembraneous and endochondral ossification. Intra membraneous bone formation occurs when mesenchymal

progenitor cells differentiate directly into osteoblasts which later initiates the development of clavicle and many cranial bones. However, most bones in the body including all long bones and vertebrae are initiated through endochondral bone formation via differentiation of mesenchymal progenitor cells into chondrocytes and formation of a cartilaginous template that is subsequently mineralized and replaced by bone. Furthermore, bone remodeling and balance between osteoclastic bone resorption and osteoblastic bone formation are necessary in both processes for the maintenance of healthy bone[34].

Upon a fracture, bone is repaired and healed through a process that summarises many intra membraneous and endochondral bone formation events and without the formation of scar tissue[35]. Following an immune response and formation of hematoma, many of the signalling molecules involved in the regulation of new bone formation (ILs, TNFα, FGFs, BMPs, PDGF, VEGF, etc.) pervade the site of injury. The external soft tissues then stabilize the fracture by producing a callus which undergoes chondrogenesis and matrix ossification. In-growing blood vessels transport chondroclasts to resorb the calcified cartilage and also osteoblastic progenitors to initiate the process of new bone formation.

1.3 Main clinical bone disease and disorders

Bone disorders and diseases can be classified as following:

1) Osteoporosis
Osteoporosis is a progressive yet silent bone disease that cause weakening of porous bones and bones incapability in maintaining normal bone functions. Continuous weakening of bones will result in fracture with huge pain and discomfort, increase in risk of pathological fractures, poor healing and further dislocation of fractured bone. The most common site of fractures are in forearm, hip and vertebrate. Treatment of osteoporosis involve bisphosphonates, calcium and vitamin D supplements in addition to healthy and balanced diet and life style as well as regular physical activity[31].

2) Osteogenesis Imperfecta
Osteogenesis imperfecta is a genetic disorder of bones which consists of pathological bone fractures in the absence of external force or injury. Treatment of this bone disorder is a multi-dimensional and complex process that contains

bone strengthening exercise, medication (bisphosphonate), gene therapy, physical therapy and surgical treatment for more extreme cases[26].

3) Paget Disease
Paget disease is a musculoskeletal issue that can affect other systems like hearing and is characterized by high growth potential, weakening, high risks of fracture and dislocation of long bones. Excessive bone resorption with abnormal bone formation eventually replaces the marrow with fibrous and vascular tissue and results in bone vulnerability to injuries. treatment is mainly pharmacological to stop the formation of abnormal bone and dissolution (risedronate) combined with exercise and healthy diet[26].

4) Osteomalacia
Osteomalacia is caused by vitamin D deficiency in adults that affects bone remodeling process and leads to building of soft and weak bones, bone pain and muscle weakness. Treatment is mainly to increase calcium and vitamin D level by oral or intra-muscular supplementation[30,31].

Pharmacological agents including; inhibitors of bone resorption, anti-inflammatory drugs, growth factors as well as hormone therapy (estrogen and selective estrogen receptor modulators, parathyroid hormone and calcitonin) are major therapies in treatment of bone diseases but their severe side effect, patient body resistance and carcinogenicity limited their application bone therapy.
Bone grafts provide safer approaches in bone repair and regeneration compared to conventional methods and combing these approaches with micro en-capsulation offers greater protection of pharmacological agents/cells from host immune system. This approach therefore, grantees the therapeutic concentration of specific agents in the targeted areas which leads to more effective treatment of bone diseases[26].

1.4 Application of biomaterials in tissue engineering

Several scaffolds were produced from a variety of biomaterials and manufactured through ranges of fabrication techniques in attempts to regenerate different tissues and organs in vitro and in vivo[36]. Regardless of the tissue type, there are several key considerations in designing and assessing scaffold suitability for use in tissue engineering as shown in Figure 1.3.

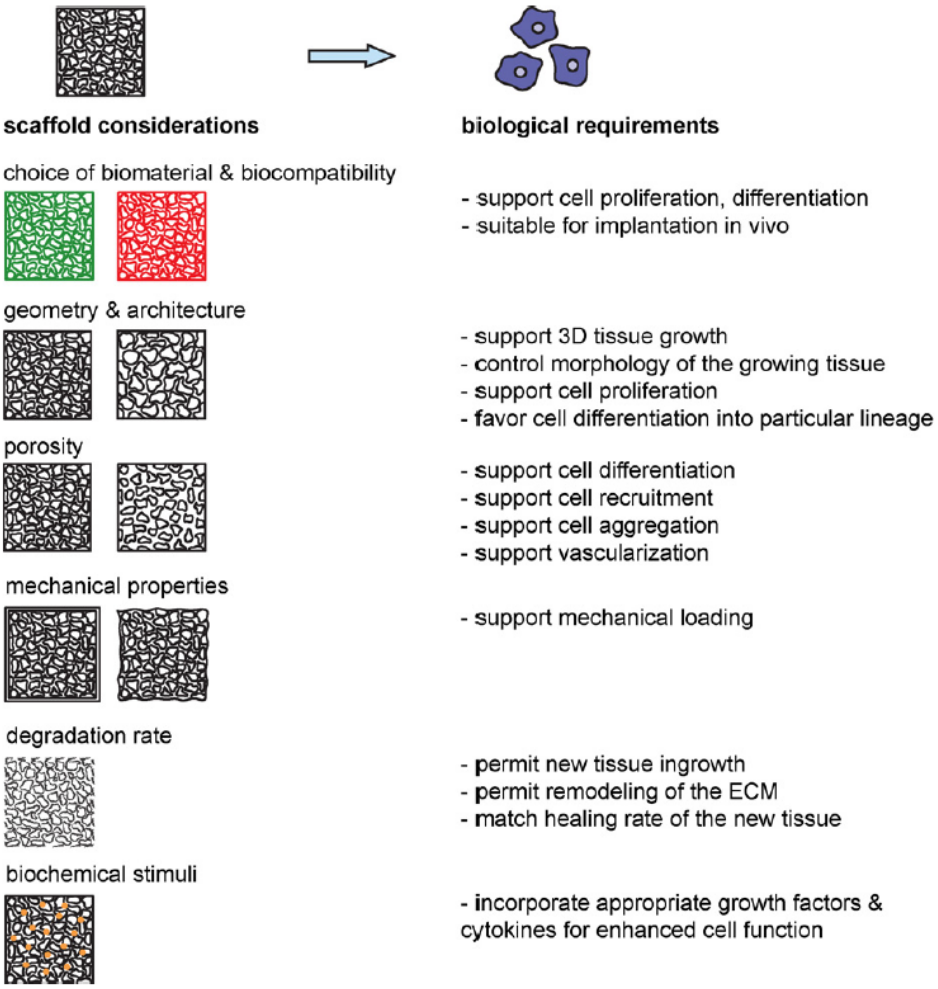


Figure 1.3: Scaffold properties should be considered in designing an optimum construct for tissue engineering applications including geometry, biocompatibility of material, porosity, degradation rate, mechanical strength and incorporation of signalling molecules. Optimising these factors is essential in addressing various physiological specifications of an engineered tissue.[3].

1.4.1 Biocompatibility

Biocompatibility is the very first criterion of any scaffold for tissue engineering; a biocompatible scaffold helps cells to adhere, migrate onto the surface, proliferate and lay down new extracellular matrix. Additionally, the implanted scaffold or tissue engineered construct must trigger minimum immune reaction and inflammatory response that can prolong the healing process or cause implant rejection by the body.

1.4.2 Biodegradability

Scaffolds and constructs are not permanent implants therefore, ideally they should be biodegradable to allow cells to produce their own extracellular matrix. Also the by-products of this degradation should be non-toxic and have negligible interference with other organs when exit the body. An inflammatory response is required to initiate the controlled infusion of cells such as macrophages and to allow the cycle of degradation and new bone formation to occur[37].

1.4.3 Mechanical properties

Ideally, the scaffold should possess mechanical properties compatible with the anatomical site which it be implanted into and, it must be mechanically strong enough to endure the surgical handling during implantation. Mechanical properties of tissue engineered constructs can be challenging especially for cardiovascular and orthopedic applications. Designing scaffolds with sufficient mechanical properties is one of the major challenges in the field of tissue engineered bone or cartilage as, the implanted construct must have adequate mechanical strength to operate from the time of implantation to the completion of the remodeling process[38].
Healing rates vary considerably with age as in younger patients the process of fracture healing takes about six weeks to the point of weight-bearing while, complete mechanical integrity returns around approximately one year after fracture. However, the rate of repair slows down substantially in elderly which must be taken into account when designing constructs for orthopaedic applications. Nevertheless, numerous materials have been manufactured with sufficient mechanical properties and less porosity and many materials, which have demonstrated potential in vitro have failed when implanted in vivo because of limited capability for vascularization. Keeping the balance between mechanical properties and porous architecture is key to the success of any scaffold which allows cell infiltration and vascularization[36].

1.4.4 Scaffold architecture

The architecture of scaffolds is critically important in the application of tissue engineering. Scaffolds should have a high interconnected pore structure, porosity and adequate pore size for cellular penetration, diffusion of nutrients to cells and their extra-cellular matrix. In addition, a porous interconnected structure is equally important to ensure diffusion of waste products and scaffold degradation out of the scaffold without interfering with other organs and surrounding tissues. A major concern in the field of tissue engineering is the issue of degradation due to lack of

vascularization and waste removal from the centre of tissue engineered constructs[39].

Another main component is the mean pore size of the engineered construct as cells predominately interact with chemical groups (ligands) on the surface of scaffold. Scaffolds synthesized from natural biomaterials such as collagen have these ligands in the form of Arg-Gly-Asp (RGD) binding sequences while, synthetic scaffolds may require addition of these ligands via protein adsorption. Also, the ligand density is affected by the specific surface area of the pores to which cells can adhere and depends on the mean pore size in the scaffold. Therefore, construct pores are required to be large enough to enable cell migration into the structure, where they eventually bind to the ligands. Yet, the pore size should be small enough to create a sufficiently high specific surface that leads to a minimal ligand density and allow efficient binding of cells to the scaffold[40].

1.5 Type of biomaterials

1.5.1 Osteoinductive materials

Osteoinductive or smart biomaterials have the ability to promote the formation of ectopic bone through directing its surrounding in vivo environment to form bone[41]. While, the biological mechanisms of this phenomenon have not been fully understood, it is well identified that these materials possess great potential for bone tissue regeneration. Two possible mechanisms include the biomaterial surface chemistry structure that absorbs and presents osteoinductive factors to the surrounding cells. Also, the release of calcium and phosphate ions from calcium phosphate based materials that can influence stem cell differentiation into bone cells. A range of biomaterial families have exhibited osteoinductive properties, including hydroxyapatite, several calcium phosphate (CaP) compositions, and their composites such as poly lactic coglycolic acid (PLGA)(Figure 1.4). Many studies have presented osteoinduction in various animal models by CaP based biomaterials specifically, in the form of sintered ceramics, cements coatings and coral-derived ceramics[42–44]. In addition, other ceramics, such as alumina ceramic and porous bioglass, have also recently demonstrated osteoconductive properties[45]. However, other material properties play a critical role in osteoinduction including chemical composition of the biomaterial, construct porosity, nano/micro topography[46].

Product	Type	Form
Collagraft	Bovine collagen, hydoxyapatite, tricalcium phosphate	Granular and strip forms
Pro Osteon	cross coralline hydroxyapatite	Granules,blocks; 200, 500, and R forms
Osteoset	Calcium sulfate	pellets
Allomatrix	Demineralized human bone matrix in an Osteoset medium	
NovaBone	Bioactive glass (SiO2 and minerals)	
Endobon	Hydroxyapatite (bovine)	Cancellous bone blocks
Vitoss	Ultraporous beta-tricalcium phosphate	
SRS	Calcium phosphate (carbonated apatite)	Injectable cement

Figure 1.4: Osteoinductive CaP based biomaterials in the form of sintered ceramics, cements coatings, coral-derived ceramics, alumina ceramic and porous bioglass and their various applications in tissue engineering and animal models.

1.5.2 Hybrid materials

Biomaterials for bone construct applications should exhibit certain physical, chemical, and biological properties. Hybrid biomaterials are made by combination of two or more biomaterials, with enhanced functionalities, in the form of copolymers, polymer polymer blends, or polymer ceramic composites that are considered advanced class of biomaterials for bone scaffolding applications.

A. Copolymers: Copolymers are derived from two or more monomeric species. For example, PLGA copolymer are derived from poly lactide and poly glycolide that allowed for the tuning of glass transition temperature (Tg) and degradation. Other copolymer systems include PLGA-PCL, PLGA copolymerized with PLL, and PLA copolymerized PCL[47].

For example, acidic degradation products of PLAGA could be neutralized by the degradation products of polyphosphazenes but, the mechanical properties of this copolymer would not be in favour of bone tissue engineering applications. In

addition, the presence of bulky aromatic side groups in poly[(50% ethyl alanato) (50% p-phenyl phenoxy) phosphazene cause higher Tg value and more improved mechanical properties therefore, make this copolymera better scaffold material candidate for the application of bone tissue engineering[47].

B. Polymer-polymer blends: Polymer blends consist of a mixture of two polymers with intermolecular or Van der Walls interactions which exhibit enhanced properties for example PLGA blends with polyphosphazenes. PLGA biomaterials produce acidic byproducts upon degradation and long-term tissue exposure to acidic products may lead to tissue necrosis and implant failure. In contrast, polyphosphazenes release neutral or basic products during degradation, therefore, blend of PLGA with polyphosphazenes results in release of near neutral degradation products[48].

C. Polymer ceramic composites: Composite materials are attractive candidates for BTE applications as bone itself is a composite material comprised of inorganic hydroxyapatite crystals and organic collagen fibers[33]. Composites of hydroxyapatite and different polymers such as PLGA, collagen, chitosan, etc have been successfully produced and have presented enhanced bone formation both vitro and in vivo[49,50]. These materials are defined as biomimetic, can promote the formation and deposition of CaP from simulated body fluid which result in stronger and more enhanced bone matrix interface[51]. Additionally, it has been demonstrated that porous poly(L lactic acid) (PLLA)/HA composite scaffolds possess superior osteoconductivity properties and stimulate enhanced osteoblasts proliferation, and expression of bone specific markers such as osteocalcin compared to pure PLLA scaffolds[52]. Addition of HA to natural polymer scaffolds has been reported to improve the bioactivity and mechanical properties of in vivo implanted composite in comparison with polymer control scaffolds[53]. Furthermore, it has been demonstrated that composite PLA/HA construct in a rat femur defect model can increase bone formation compared to pure PLA scaffolds and polymer/HA composites have osteoconductivity properties that is superior to their pure polymer counterparts[54].

1.5.3 Advanced hydrogels

Hydrogels have long been used for tissue engineering application because of their remarkable biocompatibility and physical characteristics. Hydrogels are employed as matrices for tissue engineering and regenerative therapy and can

mimic ECM topography while, delivering required bioactive agents that encourage tissue regeneration[55]. For Example, collagen fibres of ECM serve as a reservoir (making growth factors insoluble, unavailable and none bioactive) and distributors of growth factors following the action of enzymes and induce the remodeling of ECM components in stem cells niche.
Recently, self-assembling peptides have been used as scaffolds because of their complete biological, biocompatibility and biodegradability properties as well as their capability in mimicking the natural extracellular matrix. In addition, these self assembling nano featured biomaterials have been demonstrated non immunogenicity and can safely break down into amino acids and be cleared in vivo. Therefore, advance hydrogels represent a novel class of biomaterials that offers a promising option for tissue engineering applications[56].

1.5.4 Immuno modulatory biomaterials

Tissue engineering aims to fabricate materials that have the ability to modulate or control the immune system for enhanced bone repair and regeneration[57]. Several specific strategies have been used in immuno bioengineering including biomaterial surface modulation through surface treatments and surface topography, and addition of artificial extracellular matrix and bioactive molecules. Whilst, it has been accepted that the implants should be immune inert, it has been shown that designing materials with ability of promoting enhanced cell specific responses results in accelerated wound healing and bone tissue regeneration. Furthermore, the biomaterial surfaces are required to be modified to become more immunocompatible because the biomaterial surface is the most crucial factor for host acute immune response after implantation. This is due to the surface chemistry key role in absorption of the type, intensity, and conformation of serum proteins. The surface should control macrophage adhesion, activation and fusion into foreign body giant cells. For instance, hydrophilic surfaces with low integrin binding sites are associated with decreased dendritic cell maturation and increased macrophage apoptosis[58].

Biomaterial surface topography and micro/nano scale architecture play a critical role in modulating and activating the immune system. Thus, biomaterial surface treatments including coating with microparticle hydrogels and surfactant polymers have been employed to shield the biomaterial from protein absorption or to deliver bioactive molecules such as growth factors and anti inflammatory drugs[59]. Various immuno bioengineering studies have shown the effects of pharmacologic modula-

tion of the inflammatory response on bone regeneration including cytokine specific agents, corticosteroids, prostaglandins and their selective agonists[60]. For instance, a single injection of TP508 (pro inflammatory synthetic thrombin peptide) into a femoral fracture of a rat model, increased vascularization of fracture site and accelerated fracture repair and regeneration[61].

Selective prostaglandin agonists manifest an alternative immuno modulating target for enhanced bone regeneration. Previously, prostaglandins have been avoided as a therapeutic agent for bone repair, because of their side effects including severe systemic inflammation. However, its been shown that prostaglandins induce the bone formation through prostaglandins E2 and E4 receptors[62]. Despite the promising results, further studies are required to identify and assess more immuno modulating targets and also establish strategies to integrate inflammatory modulation into tissue engineering application for enhancement of bone regeneration.

1.6 Cellular approaches

MSCs also called stromal cells are multipotent adult stem cells (ASCs) that are localized within the stroma of the bone marrow and other tissues. HMSCs have been isolated from several tissue types including, adipose tissue[20], umbilical cord blood[63], peripheral blood, as well as amniotic fluid[64]. Mesenchymal stem cells have created a great deal of interest as a potential source for cell based therapeutic strategies. Their rather ease of isolation from embryo/bone marrow or umbilical cord blood, generation of single cell derived colonies as well as their expansion and differentiation ability to a variety of cell types such as osteocyte, adipocytes, myocytes and neurons have already made them a popular choice in treating children with osteogenesis imperfecta, hematopoietic recovery and bone tissue regeneration studies[16].

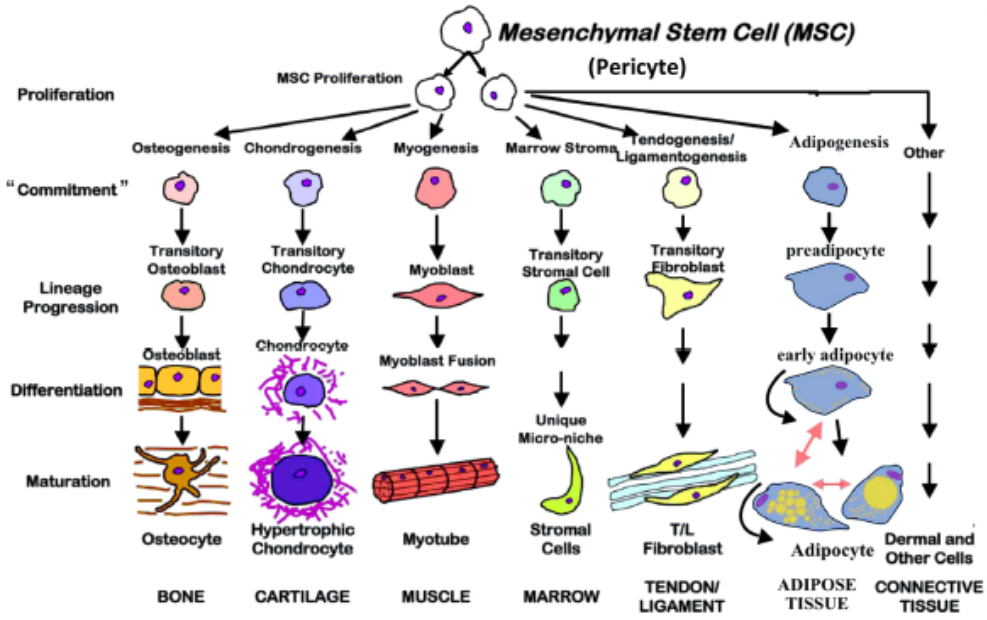


Figure 1.5: Schematic of Mesenchymal stem cells capability to differentiate into other cell linages[4].

Stem cells plasticity differs according to the sources they have been isolated from. Adult stem cells comprise of neural stem cells, skin stem cells, and blood (hematopoietic) stem cells. Hematopoietic stem cells can be isolated from adult bone marrow, blood and umbilical cord blood and are used in standard therapies in making new blood cells. Adult bone marrow stem cells are used in repopulation of the bone marrow and white blood cells (leukocytes) in treatment of cancer such as leukaemia and blood disorders[63]. A particularly promising source of stem cells is collected from umbilical cord blood, as they are less likely to reject from a transplant recipient's body than cells or tissues transplanted from another individual. Additional sources of stem cells include foetal stem cells that are derived from discarded foetal tissue, and human embryonic stem cells (hES cells) that are derived from 5 day-old blastocyst precursors to embryos. A blastocyst is a sphere of cells with an inner cell mass of about 30-34 undifferentiated cells (hES cells) that have the potential to form all the tissues in the human body. The isolation and removal of those hES cells from the blastocyst necessarily makes it unsuitable for transfer into a woman. In other words, the removal of the hES cells from a blastocyst compromises the ability of that blastocyst to ever become an embryo, and hence its potential to develop into a baby were it implanted in a woman and born alive. This primarily destruction of the human blastocyst causes hES research to be controversial.

These cells have been shown to differentiate into skeletal tissues originated from mesoderm, yet may differentiate into ectodermal and endodermal cell types as well (Figure 1.5). MSCs were first isolated from bone marrow by Friedenstein et al. who revealed their osteogenic potential, but cell populations with similar characteristics have been obtained from other tissues since[64]. Although there are some general guidelines for defining MSCs, these cell lines are a heterogeneous population and no unique cell-surface markers for their identification have yet been found[16]. According to guidelines, MSCs should adhere to tissue culture plastic and express the specific surface antigen markers CD73, CD90, and CD105; while being negative for CD11b, CD19 or CD34, CD45, CD79a, and HLA-DR: and they must also have the ability to differentiate into osteoblasts, chondroblasts, and adipocytes in vitro[65].

Cells and tissues in the body are subjected to a wide range of external mechanical forces including compression, tension, torsion, fluid shear stress, and hydrostatic pressure, each of which has an impact in their growth, development, and maintenance[66]. Since almost all cell types that MSCs differentiate into are strongly mechanosensitive, it is not surprising that undifferentiated MSCs are also mechanosensitive. However the mechanism through which cells sense mechanical loading and translate them into biochemical signals (mechanotransduction), is not still well understood[67]. In addition to external mechanical stimuli, there are also intracellular tensile forces at focal adhesions as a result of cells and extracellular matrix (ECM) interactions and recent studies suggest that both intrinsic and extrinsic forces play a key role in MSC differentiation[21].

1.7 Mechanotransduction

The ability of cells to sense and respond to mechanical loading and translate them into biochemical signals is called mechanotransduction as shown in Figure 1.6[67]. Regardless of their cell type all cells can experience this phenomenon that are caused by some collective mechanisms. One theoretical explanation for mechanotransduction is the response that is caused by integrin pulling and results in deformation of cytoskeletal elements[18].

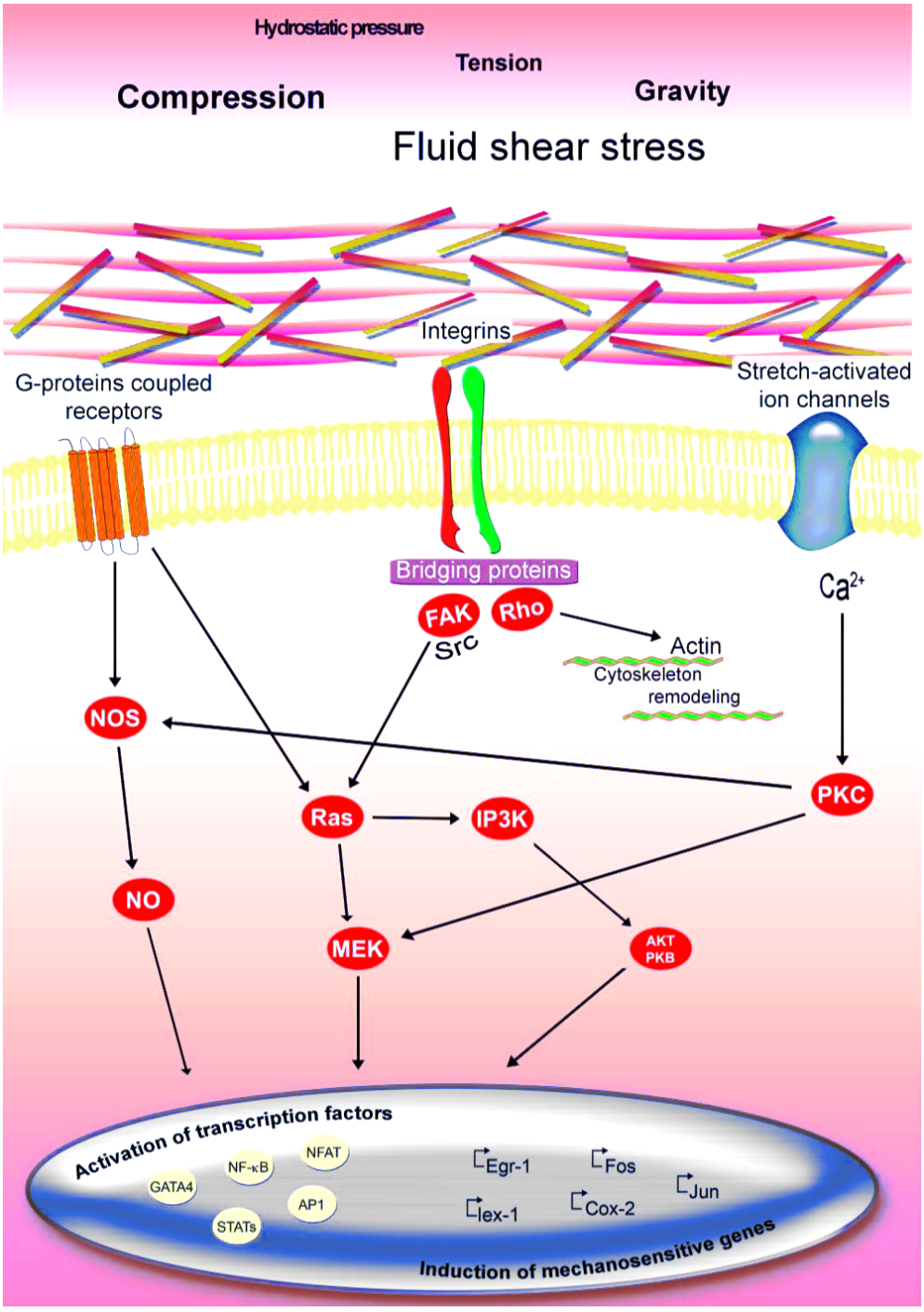


Figure 1.6: Cell response to mechanical stimuli initiates by triggering multiple intracellular signalling pathways that regulate cellular functions including maintenance, proliferation and differentiation[5].

Integrins are transmembrane proteins that connect the intracellular cytoskeleton to the ECM. The integrin-ligand bond, at focal adhesion points of the cell surface, resists external forces, which leads to transferring the force across the plasma mem-

brane and into the cytoplasm and results in deformation of the cytoskeleton. A second theory involves regulation of membrane proteins such as stretch-activated ion channels, or G-protein coupled receptors, where the plasma membrane is deformed by an external force which leads to an influx and /or efflux of ions into or out of the cell[16]. Other sensors of external forces exist such as of the primary cilia and the cell glycocalyx (GAG-proteoglycan layer), which surrounds the cell membrane. When fluid moves past the cell this surrounding layer creates a drag force that results in deformation of the cellular membrane and transferring the external force[68]. Primary cilia are immotile microtubule-based organelles, one per cell, that protrude from the cell surface in most mammalian tissue types[69]. They are occupied with receptors that are involved in numerous signalling events in sensing fluid flow.

In most cells, mechanotransduction is not well understood. It is not yet clear how universal these mechanisms are and only a few studies have investigated mechanotransduction mechanisms in MSCs but research have reported many common mechanisms with mature mesenchymal cells such as the cytoskeletal changes referred to previously[16]. For instance mechanically mediated up regulation of ERK1/2 is common between osteogenic MSCs[70,71] and both precursor[72] and mature bone cells[73]. It has been reported that the primary cilia of hMSCs are essential for the regulation of osteogenic and adipogenic differentiation pathways in static conditions which suggests the participation of these organelles in mediation of mechanically activated differentiation pathways in the cells[16].

1.8 Mechanical stimulations

1.8.1 Overview

Cell response to mechanical stimulation categorises into rapid and late response. Rapid responses occur within few seconds after applying load and have been reported as cellular influxes of calcium activation of transcription factors protein activation and release of nitric oxide[73]. Late responses develop in matter of hours, days or weeks and usually are described by secretion of hormones, modulation of gene expressions, and/or deposition of matrix[74]. Due to the difficulty of undertaking multiple loading regimens within one set of experiments, the optimum conditions for duration, magnitude, and frequencies of mechanical loading for

lineage specific differentiation of MSCs is not yet defined.

MSCs response to loading may be specific to the site of origin, the stage of cell differentiation at the time of loading, as well as the combination of chemical and mechanical stimulation regime. There are different types of mechanical forces that can stimulate cells. For each stimulation mode the stimulus can be applied in either 2D (monolayer) or 3D cell culture to determine the differences between these two systems in terms of cellular morphology, migration strategies, matrix adhesion, gene and protein expression, and responses to fluid flow[75]. Major types of mechanical stimulation will be described here in three parts: compression, tension, and fluid induced shear stress, along with brief examples of studies on stem cells.

1.8.2 Molecules and genetic pathways involved in MSCs response to mechanical loading

Although the precise cellular signalling mechanisms that controls bone synthesis within developing osteoblasts and progenitor cells is not still fully understood, this process most likely includes early electro physiological responses that are mediated by integrins and stretch activated ion channels and results in activation of intracellular signalling pathways. The regulatory effect of these mechanisms on transcription levels of various transcription factors modulates osteoblast phenotype and regulation of the genes that code for bone matrix protein. This report focuses mainly on genes and transcription factors involved in two key regulation pathways: Wnt canonical pathway and the TGF-β superfamily pathway regulating the differentiation of MSCs[76].

1.8.2.1 Wnt signalling and MSC differentiation

Wnt super family genes consist of 19 genes in humans and mice that mainly mediate cell proliferation, differentiation, and apoptosis in both embryonic tissue development and adult tissue regeneration. Studies carried out by Gong and colleagues revealed the significance of Wnt proteins in bone development and homeostasis[77]. Their result indicated that LRP5 mutation or lack of activity could contribute to decreased osteoblast proliferation. Other studies have supported the initial reports, showing that loss of function in LRP5 gene could also have negative impact on bone formation via indirect mechanisms, including Htr1b

(5-hydroxytryptamine) that serves as serotonin receptor1B and cAMP response element-binding protein, and interestingly the gain of function mutation in Lrp5 may not influence bone density[78]. It appears therefore that Lrp5 could affect bone mass in a Wnt-independent way and that Lrp6 could be more relevant when considering Wnt signalling in osteoblasts. Wnt genes and proteins also regulate cartilage differentiation by acting on cartilage-related transcription factors. Day et al. have demonstrated the key role of ectopic canonical Wnt signalling in augmenting ossification and suppression of chondrocyte formation during skeletogenesis[79]. While, Hill et al. indicated canonical Wnt signalling regulating skeletal line age differentiation by inhibiting the trans differentiation of osteoblasts into chondrocytes, and most importantly β-catenin essential role in differentiation of mesenchymal progenitors to osteoblasts in the developing embryo[80].

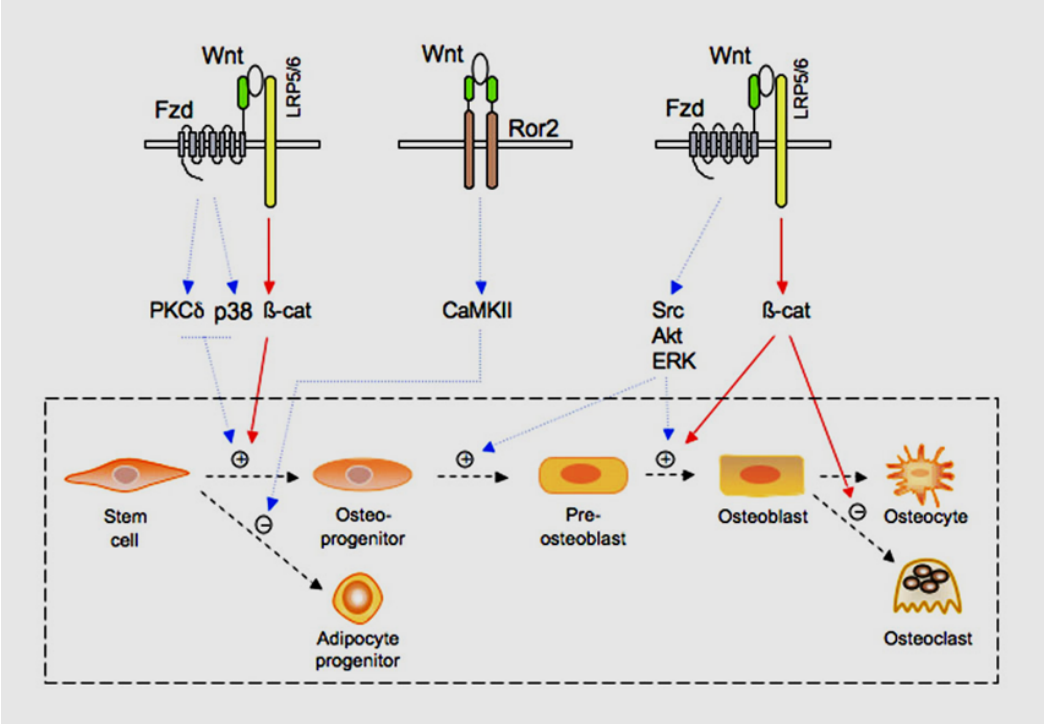


Figure 1.7: Role of Wnt signalling pathway in osteogenesis. Taken from http://www.nature.com/bonekey

It has been suggested that the WNT/β-catenin pathway modulates stem cell renewal, proliferation and its lineage specification by regulation of the FGF and BMP pathways. Etheridge and colleagues have drawn their attention from osteoblast to the cells that originate them and showed that MSCs express several Wnt ligands, including Wnt2, 4, 5a, 11, and 16. In addition, a number of Wnt

receptors and coreceptors, including FZD2, 3, 4, 5, and 6 and several Wnt inhibitors were identified and it was shown that MSCs upregulate a number of Wnt related molecules while down regulating others[81]. Recently, it has been revealed that canonical Wnt signalling stimulates the differentiation of MSCs to osteogenic lineage, while suppressing the terminal differentiation of mature osteoblasts. Im and Quan presented the stimulatory effect of Wnt pathway inhibitors on early chondrogenesis of MSCs, but due to lack of synergistic effect with TGF-β in the longer term culture, their finding did not prove Wnt enhancing role in the cartilage tissue engineering of MSCs[76].

Many studies have focused on microRNA involvement in potentiate and regulation of Wnt signalling. Kapinas et al. report provides vital details on stimulation of miR-29a by canonical Wnt signalling and its role in potentiating Wnt signalling. It has been suggested that miR-27 regulates adipogenesis and myogenesis, while, miR-27 microRNA affects the differentiation of a foetal osteoblasts by enhancing Wnt signalling activity and accumulation of β-catenin[82].

1.8.2.2 The TGF-β superfamily

Transforming growth factor beta (TGF-β) is a protein that regulates proliferation and cellular differentiation in most cells. This cytokine plays a key role in immunity and many disease and disorders such as cancer, bronchial asthma, heart disease, diabetes, Marfan syndrome, Loeys Dietz syndrome, and AIDS. TGF-β is a secreted protein that consists of three isoforms; TGF-β1, TGF-β2 and TGF-β3[82]. Most tissues have high expression of the TGF-β gene in comparison with other anti-inflammatory cytokines such as IL-10, whose expression is minimal and requires triggering by commensal or pathogenic flora. Some cells that secrete TGF-β also have receptors for this protein that is known as autocrine signalling[83].

TGF-β superfamily comprises many growth factors and morphogens that regulate skeletal development and homeostasis. This family of ligands includes bone morphogenetic proteins (BMPs), growth and differentiation factors (GDFs), anti mullerian hormone (AMH), activin, nodal, and TGF-β. Many studies have established the chondro/osteo stimulatory/modulatory effects of the TGF-βs and BMPs in embryonic and adult mesenchymal cells differentiation[83]. TGF-β induce cartilage specific genes expressions via SMAD intracellular signalling, extracellular signal regulated kinase (ERK)-1, the mitogen activated protein (MAP) kinases, p38 and c-Jun N-terminal kinase (JNK). Tuli and colleagues showed that TGF-β1

triggers and maintains chondrogenesis of MSCs by chondro stimulatory activities of ERK-1, as well as JNK and p38 which regulates the expression level of N-cadherin and WNT-7A, along with Wnt mediated signalling via intracellular β-catenin pathway, with the latest modulates the early steps of MSC chondrogenesis[84].

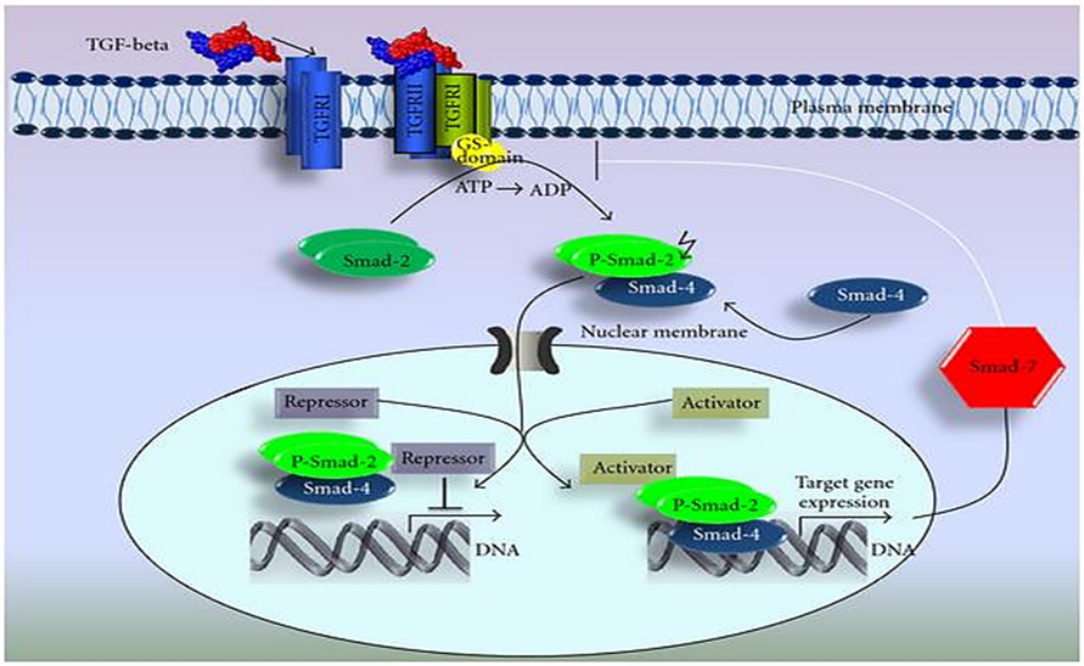


Figure 1.8: Schematic Illustration: TGF-β signalling pathway. TGF-β ligand binds to TGF-βRII that activates TGF-βRI and induces the downstream SMAD mediated signal transduction. Taken from hindawi.com

BMPs are characterized based on their signalling through SMAD proteins 1, 5, 8.Several studies have demonstrated the role of BMPs on differentiation MSCs. Rickard and colleagues showed that BMP2 enhances the expression level of osteogenic markers including ALP and OCN[85]. Sekiya et al. evaluated the chondrogenic effect of BMP2, BMP4, and BMP6 on hBMSCs and highlighted the chondro inductory role of BMP2 by analysing microarray data that confirmed correct pattern and time sequence of chondrogenesis[83]. Nonetheless, the chondrogenic stimulatory effect of TGF-β1 reported much higher in comparison with BMP2, BMP4, BMP7, and GDF5/CDMP1 (cartilage derived morphogenetic protein1)[82].

Wnt pathway can be affected by BMP2 signalling through interaction of β-catenin and N-cadherin. As, Modarresi et al.report pointed to normal levels of N-cadherin expression were crucial for regulatory effect of temporal MAP kinase and BMP2 on chondrogenic genes including type II collagen, aggrecan, and Sox9[86]. BMP and Wnt signalling activity seem to be essential in bone formation as inhibition of endogenous BMP and Wnt signalling by overexpression of their secreted antagonists seeded MSCs on calcium phosphate carriers can prevent induction of osteogenesis[87].

1.8.3 Compression

Compressive strain happens when an object pushes against a sample and causes size reduction in that plane. Hydrostatic pressure and direct contact compression (platen abutment) are two main types of compressive strain. There are no direct contact of the load platform with the cells in hydrostatic pressure and a plate is in direct contact with the cell-seeded scaffold providing the compressive force in direct contact compression. It has been reported that hydrostatic pressure may play a substantial role in the mechanical environment of bone marrow in vivo[88]. Direct contact compression is applied on a cell seeded scaffold which involves a plate in direct contact with the scaffold exerting compressive force. This type of compression is important as it can mimic the compression when bone or cartilage is loaded in vivo[16].

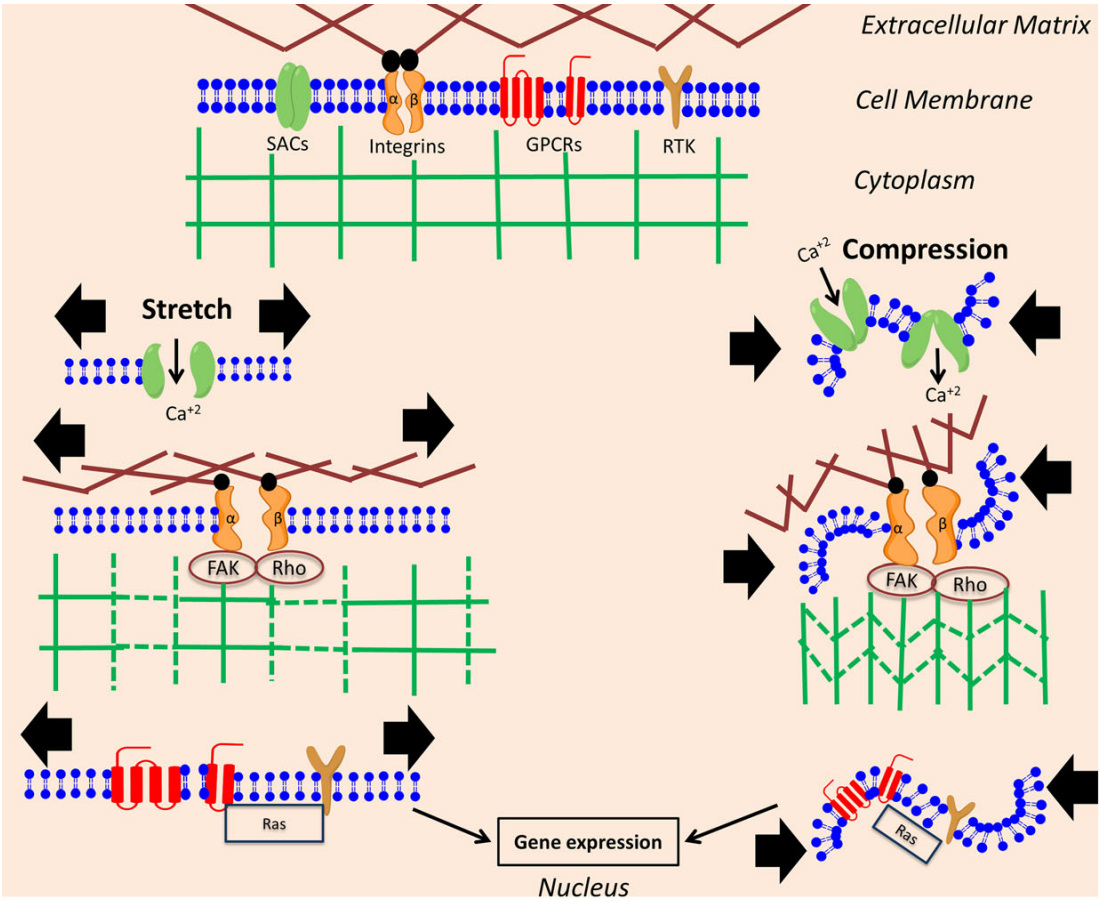


Figure 1.9: Transduction of external mechanical stimulation into the biochemical signals: When a mechanical signal (i.e. mechanical stress or compression) is applied onto the cell surface, it activates various biological molecules and signalling pathways. The resulting cellular responses will be cell proliferation, differentiation or apoptosis depending on the cell's requirements that determines the cell's fate[6].

In both compression and tensile forces; there can be a post response from fluid drawn in and out of the scaffold, which causes fluid-induced shear stresses and nutrient transfer (Figure 1.11). Tanaka et al suggests that fluid-induced shear stress has the dominant role in the compression of a porous scaffold[75]. The compression load generates hydrostatic forces from the pressure of the media pushing down on the cells. The scaffold architecture and microstructure modulate the magnitude of the applied force received by the cells. For example a cell-seeded gel transfers most of the force while sponge-like construct displays a heterogenous distribution of force therefore, individual cells may experience tensile rather than compressive strain or any strain at all.

MSCs subjected to compressive loading have mainly been investigated for the

potential of compression to promote differentiation toward chondrogenesis. Angele et al. showed that applying unconfined cyclic compression on human bone marrow stromal cells (hBMSCs) seeded in 3D hyaluronic gelatin composite and in a chondrogenic media results in higher level of COLII and proteoglycan gene expression on day 21 post loading[89]. Haudenschild et al. also reported increased aggrecan, BMP-6, COLXI mRNA and COLI mRNA level with cyclic compression loading on human BMSCs seeded alginate gel within 25h. Chondrogenetic differentiation of MSCs has been confirmed in both studies[16].

Few studies have investigated the different compressive strain regimes on bovine BMSCs embedded in 3D agarose gels with common global strain of 10% and frequency range between 0.01-3 Hz[90]. These forces were applied on a one off basis or over a short period of 5 days[91], or 3 weeks[92]. In all cases, changing the load frequency and duration did not affect the differentiation, except in Mauck et al. results where they demonstrate highest increase in aggrecan promoter activity when applying 3 Hz for 180 min[91]. However, media conditions and timing of the load are crucial factors as well. Thorpe et al. showed that differentiation stage of cells can be influenced by time of loading and presence of TGF-β[93]. Loading initiated before MSCs have gone through chondrogenic differentiation can inhibit chondrogenesis and without the presence of TGF-β, loading alone has a minimal effect on chondrogenic differentiation.

To summarize, timing of loading, along with media conditions are two crucial parameters that can influence the outcome of MSC's chondrogenic differentiation subjected to compression loading. Most studies showed that compression forces can induce chondrogenic differentiation rather than osteogenesis. In general, TGF-β alone can stimulate chondrogenesis in MSCs but its effect on differentiation in combination with loading is still not very well comprehended. The results of few studies indicate that compressive loading alone can induce chondrogenic differentiation while, others have pointed to the inhibitory effect of TGF-β treatment in combination with compressive loading on the chondrogenesis. Nevertheless, it is now widely agreed that addition of TGF-β seems to be favourable and its exclusion may results in down regulation of key chondrogenic markers. In addition, very limited studies have demonstrated that compressive loading can induce COLI and ALP activity and osteogenesis[16].

1.8.4 Tension

By applying tensile force to an object, its length will increase and the sample gets stretched. Many tissues including bone, tendons and ligaments, skin and vascular tissue experience stretching in vivo. Currently in vitro experiments are mainly based on two primary designs: uniaxial (and multi axial) grip tension and substrate bending. Longitudinal stretch is either static stretch which requires a deformable material that is retained at a specific strain over a period of time, or dynamic stretching where cyclic strain is exerted to a sample. Gripped tensile loading is performed on cell seeded scaffolds with gripping the sample at both ends and the cells seeded in the middle of the sample while, in substrate bending cells seeded on a flexible substrate are placed over a number of pivot points and an external load or displacement is exerted to the ends. In 2D models, compression forces will be applied as a result of substrate deformation which is perpendicular to the applied tension (Poisson effect). In addition, due to cells movement through the media and simulation of flow of fluid over the cells, cyclic tension can subject the cells to fluid shear stresses[94].

In 3D tensile loading, cells are embedded in a gel or porous construct which can similarly stimulate the flow of media/nutrients in and out of the scaffold. In this model, the forces that the cells would experience will depend on the architecture of the construct. For instance, a gel-based scaffold will deform almost uniformly, therefore the forces resulting from the applied strain will be homogeneously exerted on each cell through the scaffold. In comparison, cells seeded in randomly orientated fibrous scaffold or a foam scaffold experience heterogenous forces throughout the scaffold as attached cells to fibers or struts are not in the same plane as the applied strain. In this case the applied tensile strain is referred to as a global strain.

Tensile loading of MSCs has mainly been used to initiate osteogenic or tenogenic differentiation. Large number of studies reported bone marrow as a source for stem cells while few others stimulated adipose tissue for their purpose[95]. In comparison with 3D cultures where grip and pull method was used to stimulate cells, 2D cultures tended to be stimulated by bending flexible substrates. However, both these tensile strains are usually uniaxial and cyclic.

Application of tensile strain to MSCs, regardless of osteogenic media presence reported as an increased expression of early osteogenic makers and matrix secretion.

In the study carried out by Yang and his team on MSCs seeded 2D substrates in a osteogenic media, both RUNX2 and BMP-2 mRNA expression levels showed substantial increase after applying one bout of 2% continuous strain for 6 h, but not when cells were stretched for 17 min daily[95]. Ngiam et al. demonstrated the stimulation by continuous cycling strain on human BMSCs differentiation by loading human BMSCs seeded on PLLA/COLI films or fibres over a period of up to 4 weeks in osteogenic media[96]. After one week of stretching regime, cells seeded on the fibrous scaffold reported to have high ALP activity level and, this level remained unchanged in cells seeded in PLLA/ COLI film. However, continuous loading longer than one week seemed to have no effect on the osteogenic differentiation of cells on either constructs. Their findings confirm that not only prolonged continuous tensile loading may not be fit for osteogenic differentiation purposes but the cellular response is partially modulated by cell/scaffold surface adhesion.

The effect of combining tensile loading with dexamethasone (DEX) (an osteogenesis inducing agent) was presented by Jagodzinski et al. revealed stretching, with and without DEX, upregulates COLI mRNA and ALP activity, but only at the higher strain rate whereas COLIII mRNA expression level showed a surge in the presence of both stretching and DEX[97]. Furthermore, stretching alone seemed to be as effective as DEX treatment alone. Mauney et al. investigated the role of different DEX concentration (0 , 10 , or 100 nM) in loading induced osteogenic initiation[98]. Loading alone upregulates the ALP activity and expression, but it had no effect on expression level of OPN and OCN. Addition of 10 nM DEX caused a synergistic response with enhancing ALP activity and a small, significant increase in OPN gene expression while higher DEX levels 100 nM seemed to suppress the effect of loading.

Other studies have also proved higher level of ALP activity and mineralized matrix deposition after tensile loading and in the absence of osteogenic media. Human BMSCs were seeded on substrates with different ECM surface coatings and continuous short-term stretching was applied at a low frequency of 0.1 Hz. Mechanical loading was shown to up regulate osteogenic markers on all surfaces and fibronectin and lamanin supported the greatest differentiation potential, which indicates that cell, ECM interactions and how cells sense the load may have an influence on the outcome[99].

In contrast to above studies that support the regulatory effect of cyclic ten-

sion on osteogenesis differentiation of MSCs, Byrne et al. revealed that subjecting rat BMSCs seeded in a collagen-GAG scaffold to 3 days of tensile loading could have an inhibitory effect on osteogenesis of the cells in the first week. OPN, OCN, and BSP gene expressions were down regulated, while COLI mRNA expression levels remained unchanged[100].

It has been suggested that using collagen-based or collagen coated scaffold as a substrate for the cyclic loading of MSCs could induce tenogenesis. Chen et al showed that seeded human BMSCs on COLI coated flexible substrates in the presence of basal media subjected to 3% and 10% global strains for 8 or 48 h presented higher level of COLI, COLIII, and tenascin-C mRNA compared to controls with applying 10% strain for 48 h whereas 3% strain seemed to increase ALP mRNA after 8 h and OCN gene expression after 48 h of loading 48 h relaxation period. This finding implies that different levels of strain alone can stimulate the differentiation pathway of MSCs, with lower strains favouring osteogenesis over tenogenesis[16].

While tensile loading appears to be influencing osteogenesis and not chondrogenesis, there are a number of studies that have observed that, in cyclic loading, culture conditions can regulate chondrogenesis. Connelly et al. also proposed that TGF-β could prevent the loading induced chondrogenic differentiation at later time points, as seen from lack of chondrogenic markers[101]. MSCs also have the potential of differentiating into cardiomyocyte-like phenotypes with addition of DEX, insulin, and AA in their cardiomyogenic medium but the proportion of MSCs that have shown a cardiomyocyte phenotype after these different treatments has been low. Therefore, alternative methods such as mechanical loading have been sought to enhance this response. Colazzo et al. seeded human BMSCs and ADMSCs on a collagen coated BioFlex plate and subjected both cell types to continuous stretching at 14% strain for 3 days[102]. Their results showed that production of collagen was increased in both cell types however, only COLIII mRNA expression level seemed to be upregulated in ADMSCs with a higher degree of collagen and elastin crosslink. Although there was no change in the expression level of COLII, COLIV mRNA level showed to be up regulated in both cell types with stretching.

In summary, above findings indicate that, tensile loading can initiate or enhance osteogenesis, tenogenesis, and cardiomyogenesis of MSCs, but tend to inhibit adipogenesis and have no or limited effect on chondrogenesis. The osteogenesis of MSCs seems to be initiated at lower strain magnitudes than that for tenogenesis

while cardiomyogenesis is more likely to occur under larger strains. Upregulation of early ALP activity and late osteogenic markers have been detected in the absence of osteogenic media, and depending on DEX concentration in media it can inhibit differentiation of MSCs. In addition, stretching prevents adipogenesis in the presence of adipogenic media with no increase in GAG secretion[98,101].

1.8.5 Fluid flow-induced shear stress

When a fluid passes over the surface of an object it generates fluid flow-induced shear stress (FSS). This force is believed to be one of the main mechanical stimuli in vivo and for bone in particular, as interstitial fluid movement in the lacunar-canalicular system can create high shear forces on osteocytes and trigger a biochemical response to initiate remodelling[103] (Figure 1.10). In 2D systems, the most common systems shear stress on monolayers of cells include: an oscillating orbital shaker system, the cone and plate system, the parallel plate flow chamber system, the rotating disk or radial flow devices, the rocking see-saw systems[34].

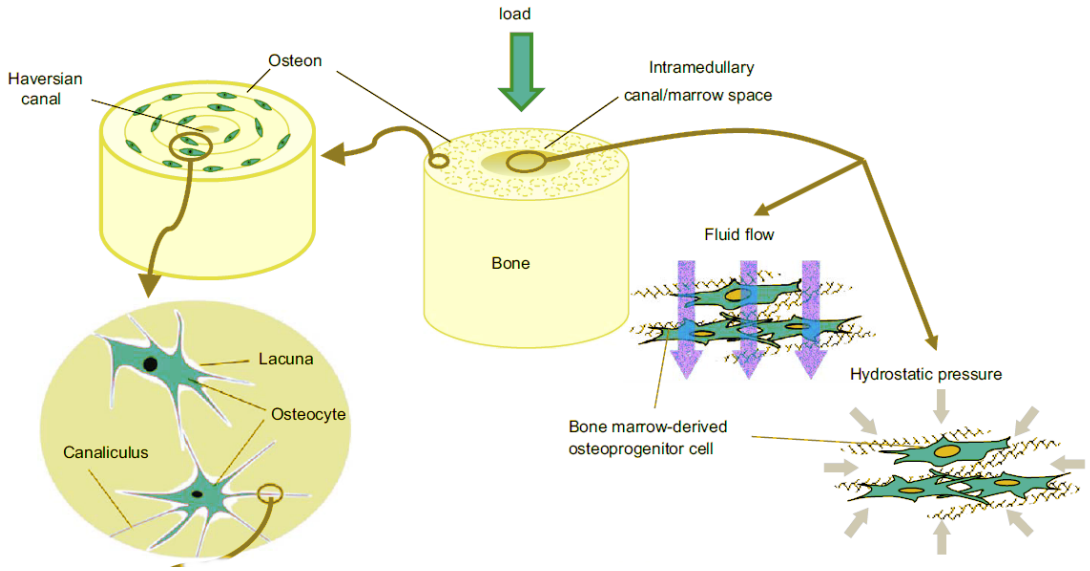


Figure 1.10: Anatomical locations of and mechanical strain experienced by bone cells. Osteocytes are embedded in osteons and organised parallel to the Haversian canal. An osteocyte located in a lacuna and connects to other osteocytes through the cannaliculi. Mechanical stimulations induce fluid flow in the canalicular space[7].

In order to allow seeded cells on scaffold materials to experience the flow-induced shear forces, 3D culture bioreactors including rotating wall vessels, spinner flasks, and perfusion systems have been designed[104]. In bioreactors the transfer of nutrients to cells is improved since the media constantly forced the media through

the scaffold, and cells in the centre will receive a greater supply of nutrients. In perfusion system of both 2D and 3D culture, separating the effects of enhanced nutrient transfer from a direct mechanical effect of shear stress at the cell membrane still remains challenging. Bakker et al. investigated this in 2D bone cells by altering media viscosity so that for a given flow rate the shear stress is changed and showed that cell response mainly depended on shear stress and nutrient transport more than flow rate[105]. Applying similar technique in 3D, calcium phosphate porous scaffolds indicated that mineralized matrix deposition was dependant on both shear stress and flow rate (mass transport) and too high flow rate played an inhibitory role in ECM deposition[105]. For that reason, biochemical/nutrient movement alone cannot explain the effects of flow within perfusion systems on MSCs ECM production.

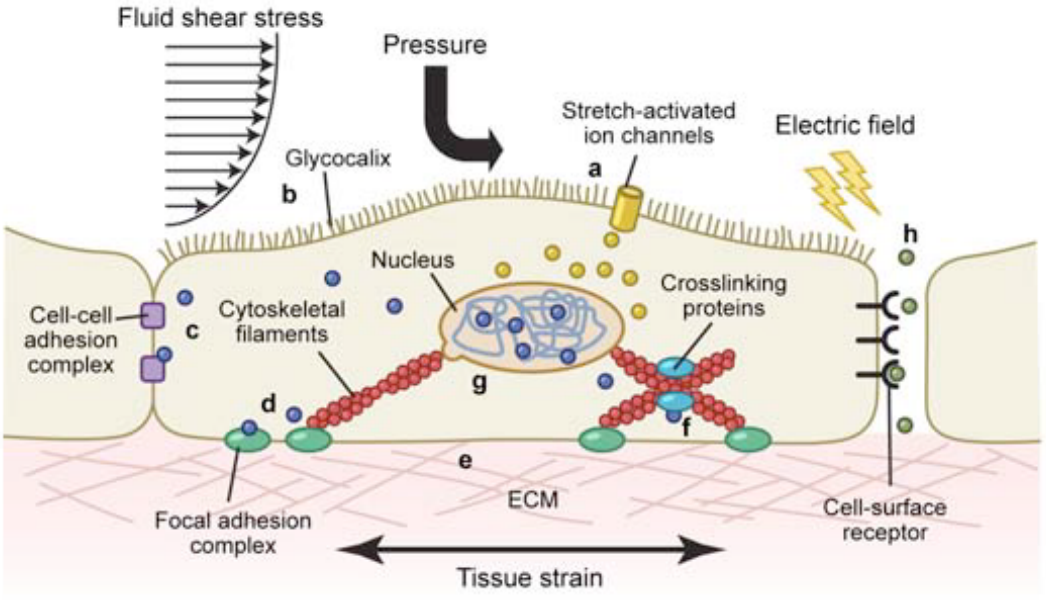


Figure 1.11: Mesenchymal stem cells and many other cells have the capacity to response to fluid shear stress, pressure, electric fields and tissue strain[2].

McCoy and O'Brien findings illustrated that MSCs seeded on 2D substrates are usually subjected to levels of shear stress around 0.1-2 Pa while in 3D constructs these levels are often much lower (0.1 m Pa and 0.03 Pa)[106,107]. 3D perfusion systems apply fluid flow over the seeded constructs for the entire length of the culture period[108], whereas in 2D systems cells are subjected to shear forces more erratically and for relatively shorter amounts of time, for example, from 30 min to 24 h[109]. But recently Jaasma et al. revealed that short bouts of flow applied to 3D

scaffolds induced osteogenic differentiation in both MSCs and osteoblast[110]. This response may also vary with the type of flow, for example, both oscillatory flow and unidirectional steady flow tend to upregulate variety of mechanotransduction pathways in mature bone cells and also were shown to have a similar osteogenic effect on a preosteoblast cell line[111].

Grellier et al. work indicated the dual role of fluid shear forces in induction as well as enhancement of osteogenesis in MSCs[109]. By subjecting 1.2 Pa shear forces to human BMSCs seeded in a parallel plate flow chamber, pre cultured in osteogenic media, for 30 or 90 min, the measured ALP activity level was shown to increase with, 30 min of stimulation showing the highest levels while RUNX2 expression level remaining unchanged and COLI gene expression was reported lower after applying the flow. Some studies, however, have pointed to inhibition of ALP activity by flow. Steady perfusion of 3D cell seeded constructs seems to induce ALP activity, with the highest response occurring at the earlier time points of 4-8 days before levelling off [108,112]. In 3D perfusion systems ALP activity level is not affected by increasing the rate of shear forces; however, higher calcium production emphasized that increasing the fluid shear force rather regulates later stages of differentiation and is essential for ECM formation more than for stimulation of differentiation[77]. Also Augst et al. revealed an increase in COLI and Calcium production in osteogenic differentiation of seeded human BMSCs on 3D silk scaffolds that were subjected to 16 rpm of steady rotation for 6 weeks[78].

Porosity, scaffold architecture and the mechanical properties of the scaffold can influence the forces experienced by seeded cells. Perfusion fluid rate (1 ml/min) applied to rat BMSCs that were seeded on titanium mesh scaffolds with 20 and 40 mm pore sizes revealed the highest levels of calcium produced at day 8 in the 40 mm mesh while, the 20 mm mesh showing the highest levels at day 16. Van Gordonat et al. study also reported similar results with seeded rat BMSCs on PLA foam or fibrous scaffolds that were subjected to daily perfusion flow of 0.5 ml/min[108].

In brief, within a tissue engineered scaffold matrix distribution and/or production arev enhanced when subjected to flow[112]; However, it is still not clear whether fluid flow alone is able to stimulate the necessary mechanical signals for differentiation of MSCs and matrix production or additional strain stimuli are required. Bearing

in mind the significance of rest periods in mechanical loading to induce tissue formation, it can be emphasized that rest periods are vital in obtaining ideal stimulation regimens for MSCs; but the best rest periods to use within any specific MSC-stimulating flow regimen is yet to be identified[113].

1.9 Cells ability in sensing their local environment

The mechanism by which cells sense the rigidity of their substrate and respond by expressing the appropriate adhesions and morphology is not yet fully understood. One theory assumes that cells integrate global cues around their surfaces that contribute in sensing the spatial organization of activated adhesions. This sensing results in ECM active deformation and remodelling by cells and their differentiation into specific lineage[114]. Burdick and colleagues revealed that the encapsulated MSCs in non degradable, alginate hydrogels have used matrix rigidity as a regulator for their differentiation in 3D. While, MSCs fate is mediated independently of matrix rigidity and by degradation-specific traction stresses in degradable hyaluronic hydrogels which showed more rounded morphology and differentiation into adipocytes[115]. Another notion suggests involvement of a molecularly complex substrate in 3D matrix adhesions formation. Cell derived 3D matrices that have been stiffened by crosslinking with glutaraldehyde show no attachment to 3D matrix while forming structures similar to focal adhesion , which indicates the role of mechanical cues to offer a key input to the cells probing their environment[116].

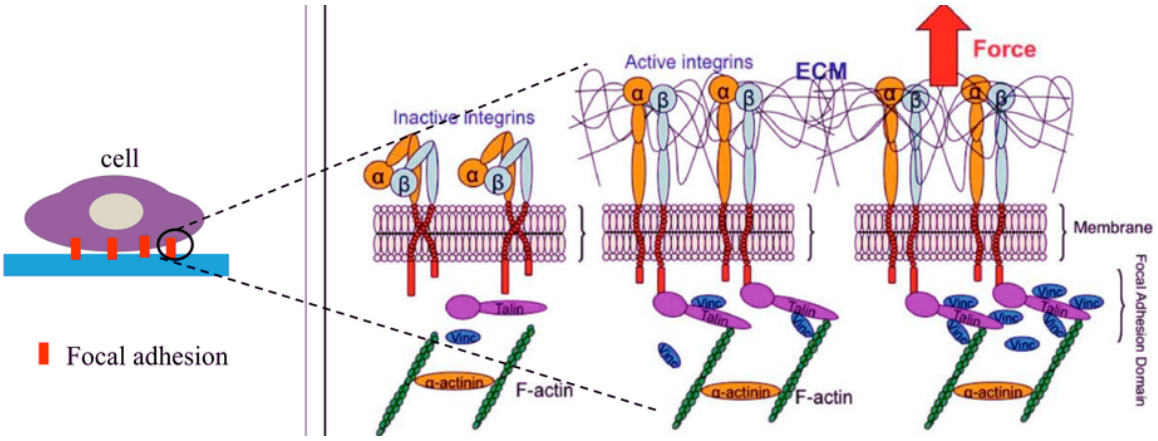


Figure 1.12: Schematic of ECM-integrin-cytoskeleton formation in the focal adhesion site by applying an external tensile load[8].

Burdick and co-authors also showed the need of local degradability to enable the entrapped cells rearranging their cytoskeletal structure and their osteogenic differentiation[115]. It has been reported that compared to 2D, in 3D constructs matrix driven cell tension determines cell fate regardless of cell morphology or spreading area. This notion has been examined by investigating the effect of matrix rigidity on MSCs encapsulated in ionically crosslinked alginate hydrogels, which interestingly suggested that matrix rigidity did directly, regulate cell differentiation. Therefore, it can be concluded that either cells ability to deform rigid substrates could directly affect cell tractions and differentiation or it could have an indirect impact by cells capability to degrade the matrix before contraction[114,116].

In addition, both the likelihood of ligand bonding and the cross linked matrix, regulate the mechanical feedback resulting from en-capsulated cell matrix interactions. A report also by Burdick and colleagues indicated the MSCs suppression of traction forces and adipogenic differentiation caused by delayed restriction of cell mediated degradation. As cell-generated forces are dynamic in time and space, active cytoskeletal rearrangements are vital in inducing osteogenesis as well as maintaining traction stresses over time[8].

Conversely, encapsulated MSCs in rigid ionically crosslinked alginate gels were shown to rearrange their local matrix-bound ligands within a limited distance from the cell suggesting the role of ligands/integrins interactions as active molecular force sensors probing substrate mechanics. Others have highlighted vinculin ability in bearing a mechanical load which involves a regulatory process in stabilizing focal adhesion dynamics caused during adhesion maturation of protein talin and exposure of its hidden binding sites for vinculin [117,118].

In conclusion, the fate of encapsulated stem cells is considered to be closely related to ligand density and its type, stiffness of substrate, and the occurrence of covalent crosslinks that negatively affect cell movement and morphology. It has been emphasized that cells contractibility, as a precise representative of traction force measurement, drives cellular differentiation and requires more in depth investigation on the dynamics of integrin/ECM ligand interaction at individual focal adhesions level.

1.10 Collagen micro encapsulation

1.10.1 Advantages of collagen micro encapsulation application

Micro encapsulation is defined as the process of entrapping cells within a confined semi permeable membrane to generate a microcapsule or within a homologous solid mass to create a microsphere. This technique has been developed for allogenic or xenogenic cell transplantation and cell based biosensors[119]. As well as agarose and polyethylene glycol, sodium alginate has been one of the most commonly used materials in this process, yet limitations of these materials in supporting cell attachment and growth and not being penetrable to the cells has made collagen a strong alternative supplement for enhancement in viability of the encapsulated cells and expanded its use in regenerative medicine and tissue engineering, which involves close host implant interaction at the cellular level and uniform microsphere dimensions and morphology[120,121].

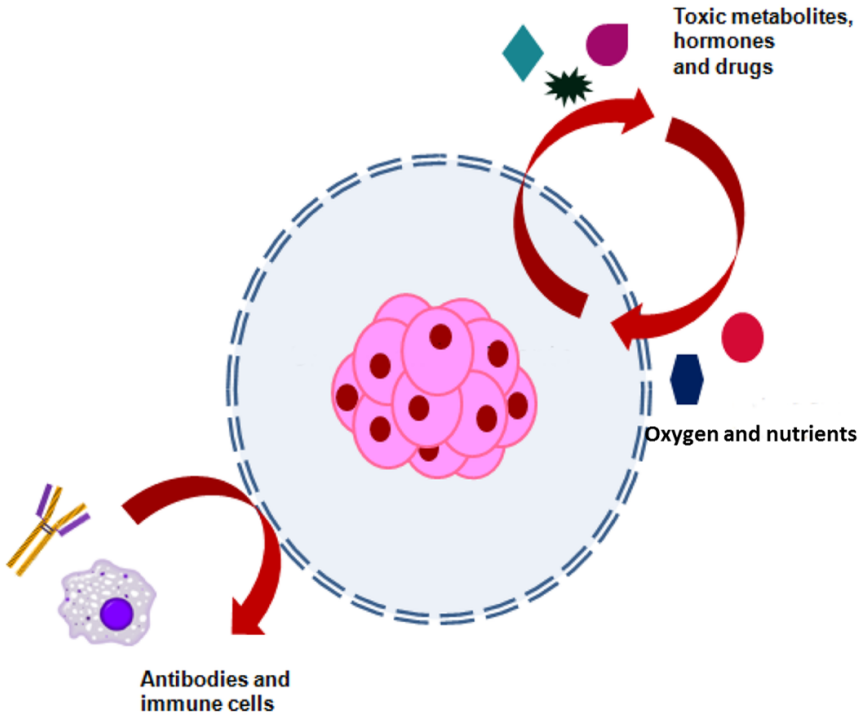


Figure 1.13: Schematic Illustration of cell encapsulation technology. The semi permeable membrane enables nutrients, oxygen, therapeutic molecules and waste to bidirectionally diffuse through. Also membrane prevents the entrance of immune cells and antibodies[9].

Natural extracellular matrices such as collagen are encapsulation materials of

choice due to being the most abundant scaffold protein in tissues, their specific cell binding sites involve in normal cell function together with their excellent biocompatibility and negligible immunogenicity[122]. It has widely been used as carriers of antibiotics genes and proteins, as well as scaffolds[20]. Collagen poor mechanical and shape stability and the fact that no micro encapsulation system has been fully developed before has made them incompatible with current micro encapsulation techniques, which involves vigorous mechanical disturbances including pressurized nozzle, emulsification or stirring during droplet generation[123].

Collagen microspheres generation involves forming micro droplets of cells in collagen via direct aliquoting or via emulsification, and consequently gelation of the collagen which forms microspheres. In emulsification, microdroplets are made by dispersing the aqueous collagen solution within a continuous oil phase solution and separating the microsphere from oil phase by centrifugation. In aliquoting, on the other hand, small volumes (a few microliters) of aqueous collagen solution is dispersed onto a surface. Major drawbacks of these techniques are: the production process is a tedious task and it requires that each step of droplet generation, gelation, and extraction be performed separately. Another downside would be the challenge to maintain uniform microsphere dimensions and shapes at a high production rate. In one approach, collagen microspheres were generated by an axisymmetric flow-focusing device (AFFD) which consisted of the mono-dispersed collagen microdroplets being formed at the orifice of a nozzle, collected in a test tube, then go through gelation process for 45 min at 37 °C. The dimensions and shapes of collagen microspheres were reported as non-uniform as a result of microdroplets coalescence by forces generated during centrifugation which also caused low cell viability[124].

Few studies have used bio-printing platform technique in producing cell encapsulated collagen droplets involved long-term cell viability, multi layered 3D cell laden hydrogel structures and high throughput droplet generation, yet unable to produce spherical collagen droplets due to gravity effect[125,126]. More recently, an integrated high throughput microfluidic platform was designed to generate more uniform collagen microspheres size and shape with high cell viability. Since both the collagen microdroplet generation and the gelation processes occurred on a chip, the time lag between these two steps was adequately short to eliminate microdroplets coalescence; also by employing microfluidic extraction approach cell viability was considerably improved[119].

In 2007 Chen and her group introduced a novel cell micro en-capsulation technique by entrapping hMSCs in a dense meshwork of reconstructed rat tail collagen I fibres that generated self-assembled collagen hMSC microspheres. Their approach illustrated the feasibility of utilising these microspheres for MSC delivery by investigating the microspheres injectability, the cellular growth kinetics and the migration capability in addition to their self renewal capacity and multi-potent differentiating potential[120].

1.10.2 Advantages of collagen application in drug delivery system

Collagen has numerous advantages as a biomaterial and is extensively used as carrier systems for delivery of drug, protein and gene. Collagen possesses remarkable properties which make it a very applicable biomaterial for drug delivery including: its biocompatibility, high absorbability on biological membranes, non antigenicity, low toxicity and synergism with other bioactive compounds (Figure 1.13). Despite many applications of collagen as a drug vehicle, it should be noted the information regarding collagen in literature is much lower as compared to synthetic polymers due to the high cost of pure collagen I, variability in different forms, complexity of handling processes and risk of bovine spongiform encephalopathy (BSE) disease[127].

Collagen can be used as a biomaterial for drug delivery because; it is biodegradable and simply absorbed in the body and its biodegradability can be controlled by degree of cross-linking. Also, collagen is a main component of cellular structure and therefore, it is nonantigenic and nontoxic biopolymer. It shows synergy with other bioactive compounds and is haemostatic in nature and can encourage blood coagulation. In addition, collagen is compatible with synthetic polymers and can be easily modified to produce desired materials[127,128].

1.10.3 Collagen nanoparticles and microspheres

The fabrication of nanospheres is determined by electronic, electrostatic forces and using sodium sulphate as a liquefying reagent to promote greater charge-charge relations between plasmid DNA and collagen[128]. The stability of the produced

collagen nanoparticles is controlled by different factors such as the molecular weight of collagen, temperature and pH which significantly affects the molecular weight profile of the collagen solution. These factors also further regulate the non-covalent interactions responsible for the molecular structure of collagen. The nanoparticles and nanospheres based on biodegradable collagen allow and enhance uptake of exogenous compounds such as anti-HIV in a number of cells including macrophages and they are also thermally stable and sterilized[129]. Some other drugs like steroids[127], cytotoxic drugs such as Campthocin[130] can also be delivered in systemic circulation by use of collagen nanoparticles. Collagen based nanoparticles can be readily used in sustained and delayed release formulation for steroids and antibiotics[131] because of their large surface area and smaller size. In addition, collagen nanoparticles possess great absorptive capability and can be easily diffused in water to form a colloidal solution. One example is dermal delivery of retinol enhanced in collagen nanoparticles that revealed a quicker transportation of incorporated drug through the skin[132].

Microcapsules, characterized by dimensions (hundreds of microns or less), are spherical in shape to enable optimal surface-to-volume ratio for enhanced protein and nutrient diffusion and good cell viability[133]. The microscale size of microcapsules makes them ideal transplant barriers to be used in microvascularized and deep tissue sites. Natural polymers derived from non animal sources or synthetic polymers with no cell binding sites are better materials for use as barriers. Cells are mainly encapsulated within nanoporous biodegradable hydrogels including hyaluronic acid, fibrin, or gelatin, or nondegradable hydrogels like alginate and PEG, which control cross membrane diffusion of nutrients and waste, oxygen, and the products of encapsulated cells such as therapeutic agents[134].

Alginate is the most commonly used polymer matrix in making cell laden microcapsules which showed great success in short or intermediate term cell therapy[135]. Cells are suspended in alginate pre-solution, which is released via a droplet generator into a calcium chloride solution, leading to formation of microcapsules. Alginate's mechanical stability has been improved by using different techniques including: layering poly-L-lysine[133], poly-l-orinthine 9[136], and poly(methylene-co-guanide) on surface of the microcapsules[137], and control homogeneity of its porosity using multilayered poly-electrolytes[138].

Another approach to form micro encapsulation is conformal coating of cells,

where a thin coating covered on embedded cells could minimise molecular diffusion rate between transplants and host therefore, prolong graft to host response[137]. Layer by layer coating of poly electrolytes enables precise regulation of coating thickness around the engraft. Although, poly electrolytes have been commonly used in conformal coating, lack of well controlled porous properties still restrict their short and intermediate term cell therapy applications. This is due to the damage of immuno protective function of the entrapped cells as result of host antibody transmission failiure[133].

Nanofabricated membranes with uniform and reproducible porosity are superior for long term application of immuno isolation. Various nanoporous membranes, with pore sizes ranging from 10-55 nm, have been employed to enhance micro encapsulation[139]. However, reducing pore size to block antibodies, especially IgG is not in agreement with required sufficient perfusion of essential growth factors. Therefore, it is important to consider strategies for modifying nanopores with capacity to deactivate immunoglobulin in designing nanofabricated membranes[140].

1.11 Microfluidic system

Microfluidics is the science and technology of systems that process or control small volume of fluids, through channels with dimensions ranging from tens to hundreds of micrometres[141]. Applications of microfluidic technologies originated from their ability to use very small quantities of samples and reagents, and to carry out high resolution separations and detections with low cost and small footprints for the analytical devices[142]. Although microfluidics offers many advantages and so few disadvantages, it has not yet become widely used. The distant origins of microfluidics are microanalytical methods such as: gas phase chromatography (GPC), high pressure liquid chromatography (HPLC) and capillary electrophoresis (CE) which revolutionized chemical analysis by capillary format. These methods together with the power of the laser in optical detection enabled to simultaneously acquire high sensitivity and high resolution by using very small amounts of sample.

A second motivation for the development of microfluidic systems emerged after the end of the cold war by major military and terrorist threats of chemical and biological weapons. To counter these threats, the Defense Advanced Research Projects Agency (DARPA) of the US Department of Defence sponsored a series of

programmes in the 1990s with main focus on design and development of deployable microfluidic systems.

The third motivational force came from the field of molecular biology with the surge of genomics in the 1980s, followed by the development of other areas of micro-analysis related to molecular biology including high throughput DNA sequencing. Microfluidics offered approaches to overcome low throughput, sensitivity and resolution than had previously been observed in biology. The original application of microfluidics was photo lithography and associated technologies that were used in silicon microelectronics, and in microelectro mechanical systems (MEMS). The most highly developed of microfluidics applications is in screening conditions for example: pH, ionic strength and composition, cosolvents, and concentration for protein crystallization[143]. These techniques possess great potential to screen numerous quantity of conditions, to separate nucleation and growth of crystals and to reduce the damage to crystals caused by handling procedures. Other applications of microfluidic systems involve in separations coupled to mass spectroscopy, high throughput screening in drug development[144,145], bioanalyses[146], evaluation and manipulation of a single cell[147] or a single molecule[148] containing samples.

Jensen et al. described different types of systems for cell biology application. Attached and spread eukaryotic cells have linear dimensions of ranging from 10 to 100 µm which are well suited for current microfluidic devices. In addition, PDMS possesses excellent optical transparency, low toxicity and high permeability to oxygen and carbon dioxide that makes it uniquely suitable to grow and study cells in microchambers[149]. PDMS microfluidic systems have applications in the extensive study of many areas of cell biology such as: the cytoskeleton and the forces exerted by cells on the substrate[150]. Also, the contents of cells from cell aggregates down to the single cell level[151].

Microfluidic systems have been shown to adopt slowly in the development of new capabilities in chemical synthesis including organic and medicinal chemistry. Contributing factors are: the flexibility of conventional apparatus has not been matched by microfluidic systems and PDMS dissolves in, or is swelled by, many commonly used organic solvents[152]. Replacement of PDMS with silicon, glass[153,154], or other polymers[155], may solve this problem and enable reactions to occur at high temperatures and pressures, but the fabrication of systems with any of these materials is more challenging than with PDMS. Furthermore, pumping

and valving in rigid materials is generally accomplished through different strategies from those used in PDMS.

The impact of microfluidic technologies in the academic world has substantially increased in the recent years. Microfluidics is considered as a toolbox, which is required to develop innovative new products in the life sciences. Therefore, research community is the most widely application field for microfluidic technique and technologies that contribute in development of new products and solutions in such different application areas including biotechnology, diagnostics and medical/pharmaceutical industries[156].

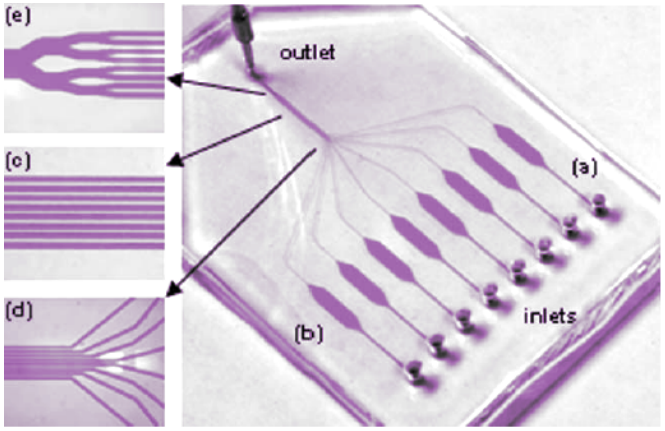


Figure 1.14: PDMS made microfluidic chip: (a) individual channel acting as a diffusion barrier; (b) reaction chamber;(c) network of channels; (d) assembly of the independent channels; (e) integrating the channels into an outlet channel that can be connected to the withdrawal mode of a syringe pump[9].

Current approaches for generation of mechanical stimulation imply dynamic bioreactor culture systems, for in-vitro cell culture and differentiation of tissue engineering constructs. Compared with static bioreactor system, dynamic bioreactors can enhance the mass transport of nutrients to the cells. In addition, cells that are subjected to the mechanical stimulation of dynamic media flow showed augmented osteogenesis and mineralization[157]. Because of bioreactors bulkiness and their limitation in processing large number of samples at the same time, microfluidic devices are ideal to overcome these restrictions and improve the overall efficiency of dynamic bioreactor systems. Many studies have reported the numerous applications for microfluidic systems in biochemical analysis, chemical reactions, and in cell-based assay[116,118].

The advantages of using this system over conventional bench-top systems include reduced size of operating systems, its flexibility in design modification, lower reagents consumption, lower wastes production and power requirements to operate, its disposability, increased speed of analyses, and system portability. One key factor in designing a functional microfluidic device is the type of material used for the fabrication of the device. This material should be economical and compatible with micro-fabrication techniques, while being perfectly matched with micrometer-scale structure and allowing the integration of functional components. In addition, chamber will enable chemical and mechanical stimulation of cells in a controlled environment, while reducing the overall volume of the systems enabling both reduction in cost and possibility of high throughput testing.

Popular polymers that have been used to fabricate microfluidic systems include: poly-dimethyl siloxane (PDMS), polyurethane, polyvinyl chloride, poly methyl methacrylate (PMMA), polyethylene terephthalate glycol (PETG), polycarbonate, polyethylene and, polystyrene[82]. Soft-polymeric systems, particularly systems made in PDMS, present many desirable properties for use in microfluidic devices. Soft lithography is a commonly used technique in fabrication of PDMS which involves elastomeric polymer molding by rapid prototyping of microfluidic devices[158]. PDMS made devices are easily integrated with outside components due to compatibility of this polymer with most materials. Because of its temperature stability in biological ranges (40-95 °C) PDMS have vast applications in processes requiring temperature gradient. PDMS optical transparency has made it compatible with conventional imaging techniques and optical detection methods in the visible and UV region. PDMS channels are perfectly suited for protein, cell based and biological assays due to their permeability to gases and their non-toxic nature. Some PDMS properties may be unfavourable in some applications including: its elastomeric nature that may cause shrinkage or sagging of device feature[159]. In addition PDMS incompatibility with many organic solvents may affect the non-specific adsorption in biological samples which could be rectified by improving its surface chemistry[121].

Soft lithography technique is currently moving towards commercialization. PDMS microfluidic chips used in development of DNA, protein, and cell-based assays accompanied by fabricating the microfluidic analytical systems is indeed an indication of great growing interest in polymeric microfluidic systems (Figure 1.14).

1.12 Potential clinical applications in regenerative medicine and tissue engineering

MSCs can be delivered into a tissue in undifferentiated status and the local microenvironment would direct the stem cells into specific differentiated cell lineage for regeneration. This approach is particularly useful in regenerating tissues such as intervertebral disc and bone and cartilage which microenvironment for differentiation is unknown[82].

A second approach involves inducing the differentiation of MSCs towards a specific lineage before delivery, providing the differentiation pathway is known. This approach prevents the risk of developing tumors after implantation as MSCs have already committed to specific lineage before delivery as well as enhancing the regeneration efficiency. The differentiated hMSCs have already started to make tissue specific matrix and the functional microtissues; therefore MSCs can be directly injected to the tissue for regeneration. As one of the native components of bone, collagen is an attractive osteoconductive material used in bone tissue engineering. Previous studies have used collagen to make porous scaffolds and embed specific drugs in these structures after the fabrication. Komasaka et al. study presented injectable collagen microspheres based protein delivery system for the sustained delivery of recombinant human vascular endothelial growth factor (rhVEGF) for tissue engineering application[160]. In another study Yang et al. investigated the therapeutic potential of collagen microspheres loaded with steroidal saponins as bone remodeling inducer factor for skeletal defects in in vitro model. Compared to the traditional drug impregnating approach, the advantages of this micro en-capsulation approach were even encapsulated drug distribution throughout the microsphere, and elimination of the drug impregnation step[161].

Nonetheless, there are several associated issues with cell based therapy and cell delivery including, identifying and imaging stem cells in adult tissues after implantation, tumorigenicity of the transplanted cell, immunological rejection and low survival rate of implanted cells. These issues cause hindrance in commercialisation of cell based therapy and prevent translation of cell implants research from the laboratory into clinical trials or market[26].

Collagen hES-MPs microspheres fabricated in this study can be used in both ap-

proaches. These microspheres are considered as excellent cell delivery system that provides physical protection and anchorage to MSCs while supporting cells growth, viability and migration. Moreover, progenitor cells in collagen microspheres are able to remodel the template collagen matrix into tissue specific matrix in response to differentiation signals[83]. Self assembled MSC collagen microspheres present exceptional cell delivery devices in bone healing and repair process that have addressed many inadequacies of the existing cell delivery approaches hence would facilitate the clinical application of cell-based therapy in local bone remodelling and regenerative medicine.

1.13 Aim and objectives

The aim of this PhD project is to manipulate the osteogenic differentiation of hES-MPs seeded in soft collagen microspheres by means of solely mechanical stimulation and investigate the significant effect of mechanical loading on osteogenesis of stem cells in the absence of chemical stimulation.

Main objectives of this project consist of:

1. Producing soft 3D environment from collagen I bovine and rat tail to support long term cell viability and proliferation.

2. Characterisation of seeded hES-MPs on collagen microspheres with different collagen concentration.

3. Explore the effect of different cell density on short and long term viability of seeded hES-MPs microspheres.

4. Investigate the osteogenic differentiation of seeded hES-MPs microspheres in the presence and absence of chemical stimulation.

5. Design a PDMS loading chamber for mechanical stimulation of cells.

6. Development of an appropriate loading protocol and condition for osteogenic commitment of cells.

7. Mechanically stimulate hES-MPs to differentiate into bone cells in 3D Collagen controlled microenvironment by using bose biodynamic system.

8. Compare the effect of mechanical and chemical stimulation on osteogenesis of hES-MPs.

9. Design a microfluidic system for parallel processing of stem cells aggregation which is compatible with current mechanical loading equipment in the lab and is highly cost effective.

10. Development of optimum compression and fluid flow protocols for osteogenic differentiation of cells.

11. Design a simple yet, effective system to apply fluid induced shear stress on 3D cell seeded construct.

12. Study the effect of low magnitude of fluid flow induced shear stress on osteogenic differentiation of hES-MPs 3D culture.

2

Materials and Methods

2.1 Materials

1. MG-63 human osteocarcoma cell line (kindly donated by Dr G. Reilly, University of Sheffield).

2. Human embryonic stem cell derived mesenchymal progenitor hES-MP 00.25 (hES-MP) cells (kindly donated by Dr G.Reilly, University of Sheffield).

3. Bovine collagen I with concentration of 5 mg/mL (Sigma, UK) for gelation process of collagen microspheres.

4. Rat-tail collagen I with concentration of 3.56 mg/mL solution in 0.02 N acetic acid (Becton Dickenson, USA) for gelation process of collagen microspheres.

5. L-glutamine 200 mM, penicillin 10.000 units, streptomycin 10 mg/mL, L-Glutamine penicillin streptomycin solution (L-glu P/S) (Sigma, UK) for mixing with culturing media of MG-63 and hES-MP cell lines.

6. 4 ng FGF-Basic (AA 10-155) recombinant human protein, FGF-β (life technologies, USA) for mixing with basal hES-MPs culture media.

7. hES-MPs basal culture media: α MEM supplement without L-glutamine (Lonza , UK) supplemented with 10% FBS, 1% (L-glu P/S) and FGF-β for culturing hES-MP cell line.

8. MG-63 basal culture media: Dulbecco's Modified Eagle's Medium (DMEM)

(Biosera, UK) supplemented with 10% Fetal Bovine Serum (FBS), 2 mM L-glutamine (L-glu) and 100 mg/ml penicillin and streptomycin (P/S) (both 1%).

9. Osteogenic media (OM): any basal media supplemented with 50 µg/ml ascorbic acid-2 phophate (Sigma, UK), 100 nM Dexamethasone (Dex)(Sigma, UK) and 5 mM β-glycerophosphate (Sigma, UK).

10. Loading media: α MEM supplemented with 10% FBS and 1% P/S and L-glu.

11. Porcine gelatine type A (Sigma, UK) for coating the cell culture flasks and well plates.

12. Alizarin red S stain (Sigma, UK) at concentration of 1 mg/mL in diH_2O for staining deposited calcium.

13. Quant-iT^{TM} PicoGreen® dsDNA reagent assay kit (Invitrogen, UK) for total DNA quantification.

14. Alkaline phosphatase Fluorometric Assay kit (abcam, UK) for quantification of total alkaline phosphatase activity level.

15. BCIP®/NBT Liquid Substrate System (Sigma, UK) for extracellular ALP staining of cells.

16. Glutaraldehyde, 25% (aqueous solution), Grade II (Sigma, UK) for SEM imaging of microspheres.

17. Hexamethyldisilazane (HMDS)(Sigma, UK) for sample preparation of SEM.

18. Oregon Green® 488 carboxylic acid succinimidyl ester with concentration of 1.5 µM dissolved in PBS (Invitrogen, UK) for fluorescent staining of bovine and rat-tail collagen I.

19. Trypsin-EDTA solution containing: 0.5 g porcine trypsin and 0.2 g EDTA and Hanks balanced salt solution with phenol red (Sigma, UK) for detachment of cells.

20. Perchloric acid 5% diluted in diH_2O (Sigma, UK) for dissolving the deposited calcium of cells.

21. Ethidium homodimer I solution 2 mM in DMSO (Sigma, UK) for fluorescent staining of dead cells.

22. Calcein green, AM 2 mM in DMSO (Life Technologies, USA) for Fluorescent staining of live cells.

23. Tris-chlorhydrate buffer solution 1.5 M for lysing cells prior to DNA and total ALP assays.

24. PrestoBlue® Cell Viability Reagent (Invitrogen, UK) for cell proliferation assay.

25. Triton X-100 (Sigma, UK) for lysing cells prior to DNA and total ALP assays.

26. Osmium tetraoxide (Sigma, UK) for fixing samples prior to SEM.

27. Formalin solution 10% neutral buffered (4% w/v formaldehyde)(Sigma, UK) for fixing cells.

28. PDMS SILGARD® 184 silicone elastomer kit for producing microfluidic and compression chambers.

29. Alcian Blue solution (Merck Millipore, UK) for staining of chondrogenic cells.

30. Bose ElectroForce® 5100 biodynamic system for mechanical testing and mechanical conditioning of samples equipped with 20 N load cell and Bose Knurled grips (ElectroForce System Group, BOSE, USA).

31. Platform rocker (STR6) (Stuart equipment, UK) for application of fluid-induced shear stress.

32. Tecan infinite F200 PRO micro plate reader (Labtech, UK).

33. Fluorescent microscope (Nikon Ti-E) (Nikon, UK) equipped with FITC/Cy2 and ET Texas red filters.

34. Zeiss Axioskop 2FS MOT laser scanning confocal microscope (upright and inverted) equipped with LSM 510 Meta detector (Carl Zeiss MicroImaging GmbH, Germany).

35. Scanning electron microscopy (SEM) (Philips XL-20, Cambridge, UK) (Department of Biomedical Science, University of Sheffield).

36. Orbital shaker basic IKA® KS 260 (Sigma, UK).

37. Inductively Coupled Emission Spectrometry (ICP-ES) (Department of Chemistry, University of Sheffield) for quantification of deposited minerals in cells.

38. Nano drop-3300 2.8.0 (Labtech, UK) for quantification of total ALP in cells.

39. ROBO Master-Pro software and Inkscape for microfluidic design, drawing and template print.

40. Image analysis software: LSM Image Browser (downloaded from Carl Zeiss microscopy).

41. Image analysis software: Image Processing and Analysis in Java (ImageJ).

42. Digital Image Correlation (DIC) analysis software Kelkins.

43. Data analysis software: GraphPad Prism 6 and Microsoft Excel.

44. GNU Image Manipulation Programme (GIMP) 2.8.0

2.2 Methods

2.2.1 Cell preparation

2.2.1.1 General cell culture conditions

All cells were cultured in T-75 or T-25 flasks using the appropriate basal media for proliferation and kept in a humidified incubator at 37 °C with 5% CO_2. Cells media was changed every 2-3 days with checking cells morphology and density under the microscope and cells passaged when reached confluency. Media was removed and cells were washed with PBS once before adding 3-5 mL of trypsin-ETDA and incubating for 2-3 min to detach cells from coated gelatin. Trypsin-EDTA was then neutralised with same volume of media and cell suspension were centrifuged at 2200 rpm for 3 min to form a cell pallet. The supernatant was discharged and cells were resuspended in a known volume of media and cell count was performed using heamocytometer and light microscope. Cells were suspended in a 10% DMSO in FBS solution and placed in isopropanol jacket and stored at −80 °C over night before being transferred to liquid nitrogen tank for long term storage. Thawed cells were suspended in fresh, warm media and seeded into culture flasks and incubated over night before being replaced with fresh media on the following day.

2.2.1.2 MG-63 cell line

MG-63 human osteocarcoma cells that were used in the presented work were selected from passages 50-60, split at ratio of 1:10 and cultured in MG-63 basal culture media containing Dulbecco's Modified Eagle's Medium (DMEM) (Biosera, UK) supplemented with 10% Fetal Bovine Serum (FBS), 2 mM L-glutamine (L-glu) and 100 mg/mL penicillin and streptomycin (P/S) (both 1%). Cells media was replaced with the fresh one every 2 /3 days. MG-63 cell line were used in this project to perform initial experiments to test the related protocols before being replaced by hES-MPs.

2.2.1.3 Human embryonic stem cell derived mesenchymal progenitors (hES-MPs)

hES-MP cell line were cultured on 0.1% gelatine coated surfaces and expanded and proliferated in media containing 4 nM fibroblast growth factor-basic recombinant human (FGF-β) as recommended by manufacturer (Cellartis). Cell passages of 3-7 were used in the experiments. hES-MPs can be expanded stably up to passage

30 according to the manufacturer but in this work, cells seemed to lose their fibroblastic morphology, ALP activity level and ability in depositing minerals after passage 13. The cells were passaged when cells had grown confluent and showed a swirly pattern, at a seeding density of 10.000 cells/cm^2. hES-MP cells are positive for CD105, CD73, CD166, HLA-ABC, CD44, CD146, CD90, and negative for CD45, CD34, CD14, CD31, CD117, CD19, CD 271, SSEA-4 and HLA-DR cell surface markers[162].

2.2.2 Cell culture in 2D

In all 2D experiments, the required number of cells was added to the known volume of media and seeded into well plate. Cell number was estimated based on initial seeding density and the length of the culture period.

2.2.3 Cell culture in 3D

2.2.3.1 Collagen microsphere formation

Rat-tail collagen type I and bovine collagen I were used in gelation process following (BD) protocol. Being placed on ice collagen I was neutralized by 1 N NaOH and 10X phosphate balance solution (PBS) and diluted into final concentrations of 0.5-3 mg/mL. Cells (hES-MP or MG-63) were suspended in the neutralized collagen solution to make up cell matrix mixtures with required cell densities. Collagen microspheres of 2.5-5 µL were dispensed onto 90 mm Petri dish covered with sterile, UV-irradiated parafilm and was incubated for 45 min at 37 °C and 5% CO_2 to induce gelation of collagen. Gelated collagen/hES-MPs/MG-63 spheres were then gently flushed with appropriate medium from the parafilm into the Petri dish and maintained free-floating. Microspheres were then inserted into compression and microfluidic chambers for mechanical stimulation or subjected to fluid shear stress by orbital shaker and rocker.

2.2.3.2 Cell seeding

Cells were seeded in the collagen microspheres at the same time of gelation and different seeding density were calculated based on the diameter of microsphere and concentration of collagen and cell type that were used in different experiments.

2.2.4 Fluorescent staining of live and dead cells

Cells were stained with calcein AM and ethidium bromide according to the manufacturer instruction (Life Technologies). Live cells are distinguished by the presence of ubiquitous intracellular esterase activity, determined by the enzymatic conversion of the virtually non fluorescent cell permeable calcein AM to the intensely fluorescent calcein. The poly anionic dye calcein is well retained within live cells, producing an intense uniform green fluorescence in live cells (λ_{ex}495 nm/λ_{em}515 nm). Ethidium bromide homodimer1 (EthD-1) enters cells with damaged membranes and undergoes a 40 fold enhancement of fluorescence upon binding to nucleic acids, producing a bright red fluorescence in dead cells (λ_{ex}495 nm/λ_{em}635 nm). EthD-1 is excluded by the intact plasma membrane of live cells. Briefly, working solution of 4 mM of calcein AM was generated by adding 12.5 µL of DMSO to 50 µg vial of calcein AM.
For preparation 4 µM EthD-1 solution, 20 µL of the supplied 2 mM EthD-1 stock solution was added to 10 mL sterile PBS. 5 µL of the supplied 4 mM calcein AM stock solution was then mixed with 10 mL EthD-1 solution to make 2 µM calcein AM solution. 250 µL of this mixture were then added to the formalin fixed microspheres and incubated in dark for 40 min at room temperature. Stained microspheres were then rinsed twice with PBS to wash off the excess stain and remained free floated in PBD during microscopic imaging. Stained samples were examined under the fluorescent microscope (Nikon Ti-E) and FITC/Cy2 (green) and ET Texas red filters for image acquisition.

2.2.5 Evaluation of cell viability and cell number

2.2.5.1 PrestoBlue assay

PrestoBlue is a ready to use cell permeable resazurin based reagent that functions as a cell viability and growth indicator. When cells are viable, they maintain a reducing environment within their cytosol. PrestoBlue fluorescent redox indicator dye uses that reducing ability to quantitatively measure cell growth, and therefore can be used to establish the relative viability of various reagents across many different cell types through viable cells ability to convert the dark blue oxidized form of the dye (resazurin) into a red-fluorescent reduced form as shown in Figure 2.1. PrestoBlue reagent contains a cell-permeant non fluorescent compound that is blue in colour. When added to cells, the PrestoBlue reagent is changed by the reducing environment of metabolically active cells and become highly fluorescent and its colour changed to red. This colour modification can be detected by fluorescence

or absorbance measurements of a micro plate reader (λ_{ex}535 nm/λ_{em}590 nm).

PrestoBlue assay was performed by removing media from cell seeded microspheres and washing them with PBS before incubating with 10 µL of 10X PrestoBlue reagent and 90 µL of media for 2 h at 37 °C. The fluorescent signal of resulting solution was determined using a 96 well plate reader between 535 nm and 590 nm.

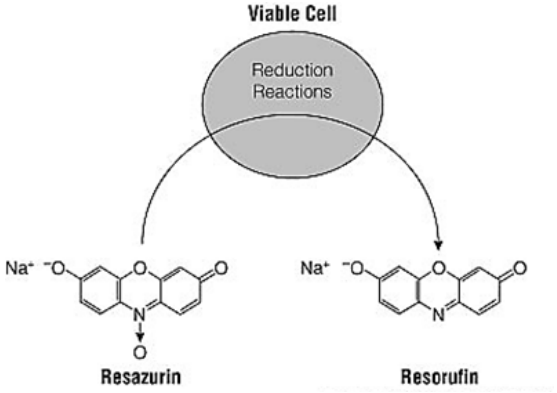


Figure 2.1: A schematic representation showing reduction of resazurin to resorofin. This reduction takes place in only viable cells. The resazurin is reduced by cells into a fluorescent red colour compound and the conversion is often used as an indicator of living cells. Adapted from www.promega.com/resources/protocols/technical-bulletins/101/celltiter-blue-cell-viability-assay-protocol.

2.2.5.2 Total DNA count

Total DNA was measured using a fluorescent Quant-iT dsDNA High-Sensitivity Assay Kit (Invitrogen, UK) which used DNA as an indicator of total cell number in each sample. Fluorescent markers bind to the double stranded DNA in the cells and provide an accurate reading of number of viable cells in each well plate. 2D cultured cells were detached from gelatin surface while 3D seeded cells were maintained in the microspheres. Cells/microspheres were then transferred into micro centrifuge tube, washed with PBS and lysed with 200 µL cocktail of cell digestion buffer consisting of: 10% of cell assay buffer that contained 1.5 M Tris-HCL, 1 mM $ZnCL_2$ and $MgCL_2$ in ddH_2O mixed with 1% Triton X-100 and incubated at 4 °C overnight. Cell lysate samples were then stored at 80 °C for 10 min before being incubated at 37 °C for 45 min and centrifuged at 10 000 rpm for 5 min. The resulting supernatant was used for DNA quantification. 200 µL of diluted cell lysate reagent (provided in the kit) and 20 µL of sample volumes were added into the wells of a microplate, mix and the fluorescence signal intensity was detected and recorded at ex/em485-520 nm. Total DNA was converted to ng DNA per sample using the following formula taken from a standard curve that was used in this work.

$$TotalDNA = Vsample \times (\frac{Y - 246.87}{361.85}) \quad (2.2.1)$$

Y: is fluorescent signal was read by microplate reader and V: is volume of sample added in the assay well (in mL).

2.2.6 Analysis of collagen fibres organisation and remodeling

2.2.6.1 Fluorescent staining of collagen fibres

Oregon Green 488 carboxylic acid, succinimidyl ester, 5-isomer fluorescent dye was used to stain bovine and rat tail collagen fibres in microspheres (Figure 2.2). Single 5-isomer of amine-reactive dye, Oregon Green 488 carboxylic acid, succinimidyl ester omit green fluorescence similar to that of fluorescein but are more photo stable. Oregon Green 488 dye has a lower pKa than fluorescein which makes this bright dye less pH sensitive in the physiological range. Fluorescent staining of collagen was performed with adding 6.54 mL of 1.5 µM Oregon Green 488 carboxylic acid, succinimidyl ester, 5-isomer collagen tracker in PBS to the samples that were kept incubated overnight at room temperature. Excess dye was then removed by three washes of PBS and samples were maintained in PBS during microscopic imaging process. Samples were visualised under a light microscope to identify the variability in collagen fibres organisation with and without cells and reorganising and remodelling the collagen fibre micro structure in different species.

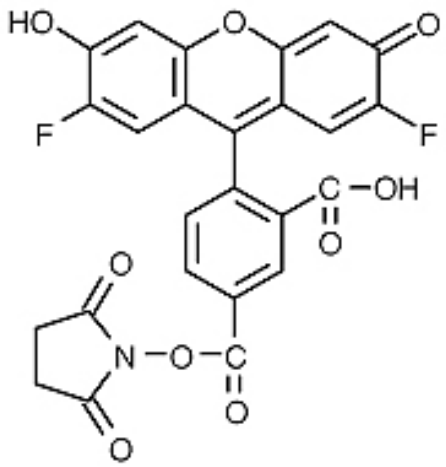


Figure 2.2: Molecular structure of Oregon Green 488 Carboxylic Acid, Succinimidyl Ester, 5-isomer fluorescent dye that used to stain collagen fibres of bovine and rat tail microspheres. Image was taken from www.thermofisher.com.

2.2.6.2 Second harmonic generation microscopic imaging

Natural collagen fibres in collagen microspheres and deposited ones in cells extracellular matrix were visualised through second harmonic generation (SHG) images obtained by Zeiss Axioskop 2FS MOT upright laser scanning confocal microscope equipped with tunable Chameleon Ti:sapphire multi photon laser. For wavelength dependence studies of collagen microspheres, excitation was performed using a range of wavelengths (760-950 nm) and collected as either a lambda stack or in the 10 nm bandpass filter at half the wavelength of the excitation laser. Lambda stacks were series of narrow 5 nm and 10 nm bandpass filters from 420-480 nm and collected using the LSM 510 Meta detector. For all imaging of microspheres collagen fibres, a 40X 1.3 NA oil immersion objective was used. Imaging of reoriented, deposited collagen fibres was performed using excitation wavelength of 940 nm and emission were collected in the 10 nm bandpass filter centred around 469 nm. The pinhole was set to 1000 nm for all conditions and each set of experiments. Fresh samples of seeded and non seeded collagen microspheres at different time points post en-capsulation were kept in PBS and room temperature and imaged while still wet.

2.2.7 Assessment of osteogenesis

2.2.7.1 BCIP/NBT Liquid Substrate System for extracellular ALP staining

BCIP/NBT Liquid Substrate System offers a convenient, ready-to-use substrate solution for visualizing alkaline phosphatase activity in immunoblotting and immunohistology. The 5-bromo-4-chloro-3-indolyl phosphate (BCIP)/nitro blue tetrazolium (NBT) Liquid Substrate System is an insoluble substrate for use with alkaline phosphatase that produces a visually observable blue-purple product. The resulting colour is very stable and will not fade upon exposure to light. Before application of stain media was removed from samples and two dH_2O (as a non-phosphate wash buffer) washes were carried out to ensure full media removal. Samples were covered with the reagent during colour development and Incubated for 10-20 min (depending on 2D and 3D cell cultures) at room temperature. Colour development was stopped and excess dye was removed by rinsing the specimen with dH_2O. The bound dye was observed either under a light microscope or using a digital camera.

2.2.7.2 Quantification of total ALP activity of cells

Alkaline phosphatase fluorometric assay kit (abcam, UK), is a fluorescent base quantitative method for assessing the total intracellular and extracellular ALP activity level of cells. The enzyme cleaves the phosphate group of the nonfluorescent 4-methylumbelliferyl phosphate disodium salt (MUP) substrate that generates an intense fluorescent signal ($\lambda_{ex}360\,\text{nm}/\lambda_{\ em}450\,\text{nm}$). ALP catalyses the hydrolysis of phosphate esters in alkaline buffer and produces an organic radical and inorganic phosphate. The change in alkaline phosphatase activity level is associated with numerous disorders and diseases in the liver and bones. For quantification of ALP, 20 µL of triplicate samples were directly added into 96 well plate and total volume brought to 110 µL with assay buffer. In order to avoid interference of components in the sample, sample background was set. Same volume of samples and assay buffer were added into separate wells with 20 µL stop solution and mixed well to terminate ALP activity in the sample. Required volume of 5 mM MUP substrate solution was diluted to 0.5 mM with assay buffer (1:10) and 20 µL of 0.5 mM MUP substrate solutions was then added to each well containing the test samples and background controls. Reaction was

incubated for 30-40 min at 25 °C while being protected from light. All reactions were stopped by adding 20 µL stop solution into each standard and sample reaction except the sample background control reaction. Fluorescence intensity was measured (λ_{ex}360 nm/λ_{em}445 nm) using a fluorescence Nano drop-3300 2.8.0 (Labtech, UK). ALP activity of the samples was calculated using following formula:

$$ALPactivity = \frac{\frac{A}{V}}{T}(\text{mU/ml}) \tag{2.2.2}$$

A is amount of 4-MU generated by samples (in nmol). V is volume of sample added in the assay well (in ml). T is reaction time (in min). Unit Definition: The amount of enzyme causing the hydrolysis of 1 µmol of MUP per minute at pH 10.0 and 25 °C (glycine buffer).

2.2.7.3 Alizarin red S staining

Alizarin red stain was used to determine the presence of calcium deposition by cells of an osteogenic lineage. Free (ionic) calcium forms precipitates with Alizarin, when immersed in Alizarin dye solution. After removing the media, samples were washed three times with PBS and fixed with 4% formaldehyde solution for 40 min at room temperature. Excess formaldehyde was removed from samples followed by three washes of dH_2O. 1% Alizarin red S dye in dH_2O was prepared and pH was adjusted to 4.1 with ammonium hydroxide before immersing the samples in the stain. Samples were placed on shaker under mild shaking for 30-35 min at room temperature. Excess dye was removed and samples were washed 4 times, for 5 min each, with dH_2O till solution that was surrounding the samples became completely cleared from stain. Samples were then air dried before qualitative analysis under a light microscope or with a digital camera. For quantitative analysis, each sample was destained with 200 µL of 5% perchloric acid for at least 20 min, resulting in a clear yellowish solution.

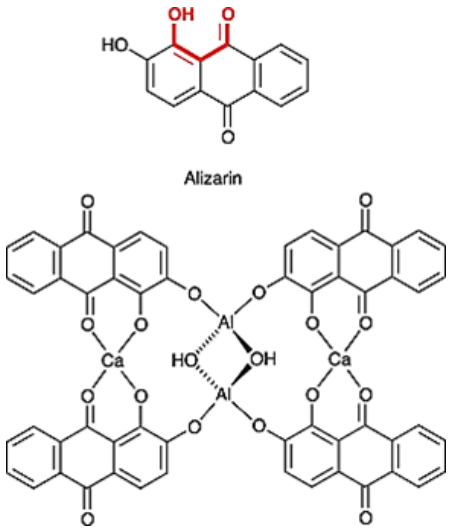


Figure 2.3: Molecular structure of Alizarin red dye in staining the deposited calcium in extracellular matrix of mineralised cells. Each calcium ion chelates with two molecules of Alizarin red[10].

Concentration of deposited calcium, zinc and phosphorous was the determined from Alizarin red stained samples using Inductively Coupled Emission Spectrometry (ICP-ES) (Department of Chemistry, University of Sheffield). Calcium and ALP staining of microspheres were not carried out on the same sample as they were both found to grossly interfere with each other. Still, calcium, Alcaine Blue and ALP staining of microspheres cross sections were performed using different cross sections of the same sample. Samples were digested in 5% w/v perchloric acid and were diluted by 10 fold prior to analysis. Samples then were mixed with 1% w/v nitric acid with ratio of 1:1 in the eppendorf tubes. Samples volume were brought to around 10 mL and the torch was turned on. An intense electromagnetic field was created within the coil by the high power radio frequency signal flowing in the coil. Instruments run at 40 mHz and the argon gas flown through the torch.

The argon gas was then ionized in the intense electromagnetic field and flows in a particular rotationally symmetrical pattern towards the magnetic field of the RF coil. A peristaltic pump deliverd an aqueous or organic sample into an analytical nebulizer and changed it into mist and introduced directly inside the plasma flame. The sample immediately collides with the electrons and charged ions in the plasma and was broken down into charged ions. The various molecules break up into their respective atoms which then lose electrons and recombine repeatedly in the plasma, giving off radiation at the characteristic wavelengths of the elements involved.

2.2.7.4 Alcian blue staining

Alcian blue is a member of polyvalent basic dyes family that is used to stain acidic polysaccharides such as glycosaminoglycans in cartilage, fibrous tissue and other body structures. Alcian blue can be used to determine proteins based on their resonance light scattering by strongly enhancing the signals. The dye selectivity enhances by increasing amounts of magnesium chloride in solution while, Alcian blue binding tendency to carboxylate or phosphate groups reduces when electrolyte concentration is low. An acetic acid-Alcian blue solution with pH of 2.5 is used for the specific staining of carboxylated and sulfatic proteoglycans. For staining, Alcian blue solution was added to the cross sections of formalin fixed samples through following steps:

1) rinsed with distilled water, 2) Alcian blue solution: added for 5 min, 3) running tap water for 3 min, 4) ethanol 70%: added for 2 min, 5) ethanol 96%: added for 2 min, 6) ethanol 100%: added for 2 min, 7) xylene: added for 5 min. After dehydration (ascending alcohol series) and clarifying cation with xylene, deposited blue stain on samples were visualised using 20X, a light microscope or a digital camera.

2.2.8 Scanning electron microscopy

Samples were fixed prior to SEM microscopy as following: primary fixation was performed using 2.5% glutaraldehyde in distilled water for 2 h and samples washed with dH_2O for 20 min. Secondary fixation was completed using 1% osmium tetroxide in distilled water for 1 h at room temperature in the dark followed by three washes with distilled water for 20 min. Dehydration was performed using, 30% ethanol balance with distilled water for 5 min, 50% ethanol balance with distilled water for 5 min, 70% ethanol balance with distilled water for 5 min, 80% ethanol balance with distilled water for 5 min and 90% ethanol balance with distilled water for 5 min before rehydration samples as following: 3:1 ethanol:HMDS for 10 min, 1:1 ethanol:HMDS for 10 min, 1:3 ethanol:HMDS for 10 min and 100% HMDS for 10 min and samples allowed to be air dried over night. Samples were then cut into half and mounted on a carbon dot stuck to a metal stub and sputter gold coated under vacuum for around 4 min to create a conductive surface for the electrons. For imaging the samples, an acceleration voltage of 10 kV was used and samples images were recorded at different time points and magnification in the Department of Biomedical Sciences at the University of Sheffield.

2.2.9 Histological staining of samples

Samples were fixed with the same protocol used in section 2.2.7.3 for Alizarin staining of deposited calcium. Samples then were frozen and cryosectioning of samples with thickness of 10 µm was performed using cryostat unit. Sample slides were then stained with Hematoxylin and Eosin (H&E) dyes by immersing samples in Haematoxylin for 4 min and washed with running water for 1 min. Samples then were dipped into Eosin for 2 min before removing the excess stain with running water. Series of dehydration with 70% to 100% ethanol were performed on samples before adding xylene for 1 min, slides were then coversliped using Permount and left overnight to be dried under the hood. All histological cryosectioning and staining procedures were completed in bone analysis laboratory, Mellanby Centre for Bone Research, Department of Human Metabolism at University of Sheffield.

2.2.10 Statistical analysis

All experiments were performed a minimum of two times with triplicate samples for each condition. For imaging, single images are representative of the experimental outcome and some experiments were limited to one sample per condition for each experiment run due to time restriction. Statistical significance was tested between samples mean. One way ANOVA was used followed by Tukey's or Sidak's post-hoc test. In all graphs mean ± SD are plotted unless stated otherwise and significant differences showed as $P<0.05$.

3

Cell Seeded Collagen Microspheres

3.1 Introduction

Stiffness and/or topography of cellular micro environment along with physical factors such as tension can dictate stem cell fate determination. Although physical cues control Mesenchymal Stem Cell (MSC) lineage specification by tuning the cytoskeleton, the full mechanism of how physical signals are sensed by cells and transformed into biochemical and biological signals remains unclear. Numerous studies have focused intensively on the effects of chemical signals in differentiation of stem cells; the effects of physical/mechanical signals of the micro environment on MSCs have long been neglected. However, few studies provided evidence that both direct and indirect mechanical signals are important in regulating a stem cell commitment. While most studies showed that compression forces can induce chondrogenic differentiation rather than osteogenesis, few studies have demonstrated the osteogenic effect of compressive loading on stem cells[16].

The encapsulation of living cells within a soft hydrogel matrix has numerous applications in many biomedical, clinical and biotechnological technologies, such as allogenic or xenogenic cell transplantation, cell-based biosensors and bio printing of three-dimensional scaffolds for tissue engineering and regenerative medicine. The aim of cell encapsulation is to entrap functional cells within a semi-permeable matrix. A suitable matrix must be biocompatible, support cell survival and also be permeable to oxygen, other nutrients and toxic metabolites.

Suitable materials for cell encapsulation should mimic the cells extracellular

matrix. Many of these materials are based on hydrogels, which are highly hydrated and composed of hydrophilic polymers that are cross-linked to form three-dimensional networks. Hydrogels derived from natural materials such as collagen have comparable structures to the extracellular matrix of many human tissues[126].

Agarose, polyethylene glycol, and sodium alginate are the most commonly used materials in this process. Yet, limitations of these materials in supporting cell attachment and growth in addition to being impermeable to the cells has made collagen a strong alternative supplement for enhancement in viability of the encapsulated cells. Collagen gels are more readily used in regenerative medicine and tissue engineering, which involves close host-implant interaction at the cellular level and uniform microsphere dimensions and morphology[120,121].

Natural extracellular polymers such as collagen are encapsulation materials of choice since they are the most abundant scaffold protein in tissues[122]. Their specific cell-binding sites are involved in normal cell function, and they have excellent bio-compatibility and negligible immunogenicity. Collagen has been used as carriers of antibiotics genes and proteins, as well as scaffolds[20]. However, because collagen has poor mechanical and shape stability and because no micro encapsulation system has been fully developed, they are incompatible with current micro encapsulation techniques, which involve vigorous mechanical disturbances including pressurized nozzle, emulsification or stirring during droplet generation[163].

Collagen microspheres generation involves forming micro droplets of cells in collagen via direct aliquoting or via emulsification, and consequently gelation of the collagen which forms microspheres. In emulsification, micro droplets are made by dispersing the aqueous collagen solution within a continuous oil phase solution and separating the microsphere from oil phase by centrifugation. In aliquoting, on the other hand, small volumes (a few micro litres) of aqueous collagen solution is dispersed onto a surface[123]. Major drawback of these techniques would be it requires each step of droplet generation, gelation, and extraction to be performed separately. Another downside would be the challenge to maintain uniform microsphere dimensions and shapes at a high production rate.

Few studies have used bio printing platform technique in producing cell encapsulated collagen droplets and examined long-term cell viability, multi layered 3D cell-laden hydrogel structures and high-throughput droplet generation, yet these techniques were unable to produce spherical collagen droplets due to gravity

effect. More recently, an integrated high-throughput microfluidic platform was designed to generate more uniform collagen microspheres size and shape with high cell viability. Since both the collagen micro droplet generation and the gelation processes occurred on a chip, the time lag between these two steps was adequately short to eliminate micro droplets coalescence. Also by employing microfluidic extraction approach cell viability was considerably improved[119].
Cell encapsulation offers an alternative approach for the long-term delivery of therapeutic products. A wide spectrum of cells and tissues can be immobilized, enhancing the potential applicability of this strategy in the treatment of multiple diseases, organ replacement and controlled drug delivery. Collagen micro en-capsulation technique represents entrapment of cells within natural, semi-permeable collagen fibres which safely isolates cells from host immune system, minimize the risk of immune response, prolong cell viability and function both in vitro, in vivo cell transplantation and formation of new tissues the absence of Immuno-repressive drugs[121,163].
In 2007 Chan and her group introduced a novel cell micro en-capsulation technique by entrapping hMSCs in a dense mesh-work of reconstructed rat tail collagen I fibres that generated self-assembled collagen/hMSC microspheres. Their approach illustrated the feasibility of utilising these microspheres for MSC delivery by investigating the microspheres injectability, the cellular growth kinetics and the migration capability in addition to their self-renewal capacity and multi-potent differentiating potential[120].

The objective of this study was to produce a soft 3D environment that consisted of self-assembled collagen I fibres to support long term viability and proliferation of human embryonic mesenchymal progenitors. Also to investigate the effect of 3D controlled environment in encouraging osteogenic differentiation of hES-MPs in the absence of external chemical and mechanical stimulation.

3.2 Methods

3.2.1 Collagen gelation procedure

Rat tail collagen type I (3.65 mg/ml) solution in 0.02 N acetic acid was purchased from Becton Dickenson (BD) and used in gelation process following BD protocol. Collagen I was neutralized by 1 N NaOH and 10X phosphate balance solution (PBS) and diluted into final concentrations of 0.5, 1, 2 or 3 mg/ml while was being placed on ice. Then, cells (hES-MPs or MG-63s) were suspended in the

neutralized collagen solution to make up cell/matrix mixtures with final cell densities of 5×10^5, 1×10^6 or 5×10^6cells/ml. Volume of each substance and number of cells required per droplet was calculated using the following equations:

$$v_1 = \frac{V}{10} \tag{3.2.1}$$

$$v_2 = \frac{V \times fc}{C} \tag{3.2.2}$$

$$v_3 = v_1 \times 0.023 \tag{3.2.3}$$

$$v_4 = V - (v_1 + v_2 + v_3) \tag{3.2.4}$$

Where V is the final volume, v_1 is the volume of $10 \times$ PBS, v_2 is volume of added collagen to the master mix, fc is the final collagen concentration in master mix, C is the initial collagen concentration in bottle, v_3 is the volume of 1 N NaOH, and v_4 is volume of cell suspension added to master mix. Then the number of cells per each droplet size was calculated by multiplying the number of cells in cell suspension required to make collagen master mix with dilution factor, that is unique for each cell concentration used in the experiment. The resulting number is multiplied again by droplet volume.

Collagen (mg/ml)	5×10^5 cells/ml	1×10^6 cells/ml	5×10^6 cells/ml
5 µl droplet			
0.5	1900	3800	19000
1	1545	3090	15450
1.5	1195	2390	11951
2	842	1685	8424
2.5 µl droplet			
0.5	950	1900	9500
1	722	1545	7725
1.5	597	1195	5975
2	421	842	4212

Table 3.1: Number of cells/droplet with different initial cell density, collagen concentration and droplet volume used in hES-MPs and MG-63s encapsulation.

Same procedure and cell number were followed for bovine collagen I solution with the concentration of 5 mg/mL. The number of seeded cells in 5 µL and 2.5 µL

collagen microspheres with collagen concentration of 2 mg/mL and initial cell density of 1×10^6 cells/mL and 5×10^5 cells/mL were calculated as 1400 and 700 respectively. For MG-63 cell line, 2800 cells with initial cell concentration of 10×10^6 cells/mL were seeded in 5 µL collagen droplets with collagen concentration of 3 mg/mL. No 2.5 µL droplet was made for 3 mg/mL collagen concentration. Collagen microspheres of 2.5 µL and 5 µL were dispensed onto 90 mm diameter Petri dish covered with UV-irradiated parafilm and was incubated for 45 min at 37 °C and with 5% CO2 for 45 min to induce gelation of collagen. Gelated collagen/hES-MPs or MG-63 spheres were then gently flushed with full medium containing: α DMEM, 10% FBS, 100 U/mL penicillin, 100 mg/mL streptomycin and 2 mmol/l L-glutamine from the parafilm into the Petri dish. Cell seeded microspheres were maintained free-floating and the medium was replaced with fresh complete media every 48 h.

3.2.2 Assessment of collagen mechanical properties

Mechanical properties of bovine collagen I gel with collagen concentration of 2 mg/ml were characterized by using rheometre at 37 °C and frequencies of 1.3-0.012 Hz. The elastic (storage, *G'*) and viscous (loss, *G"*) moduli were measured for each frequency step. The shear (complex, G) modulus was calculated as follows:

$$G = \sqrt{G'^2 \times G''^2} \tag{3.2.5}$$

The outputs were moduli vs. frequency plots, for the three groups of samples.

3.2.3 Evaluation of collagen fibres density and microstructure

Microstructure of cell seeded and non seeded collagen I fibres of bovine and rat tail was compared using SEM and SHG confocal microscopy and collagen I specific fluorescent marker. Nikon fluorescent microscope was then employed to identify the variability in collagen fibres organisation with and without cells and hES-MPs role in reorganising and remodelling the collagen fibre microstructure in different species. Non seeded collagen microspheres were examined at 24 h post encapsulation (pc) while, seeded collagen beads were assessed on day 7 pc.
All experiments and conditions that were applied on cell seeded collagen microspheres are presented in blow table. Experiments were carried out to characterise collagen fibre microstructure and to analyse cells behaviour within collagen gel

during 28 days post en-capsulation with and in the absence of chemical stimulation (Figure 3.1).

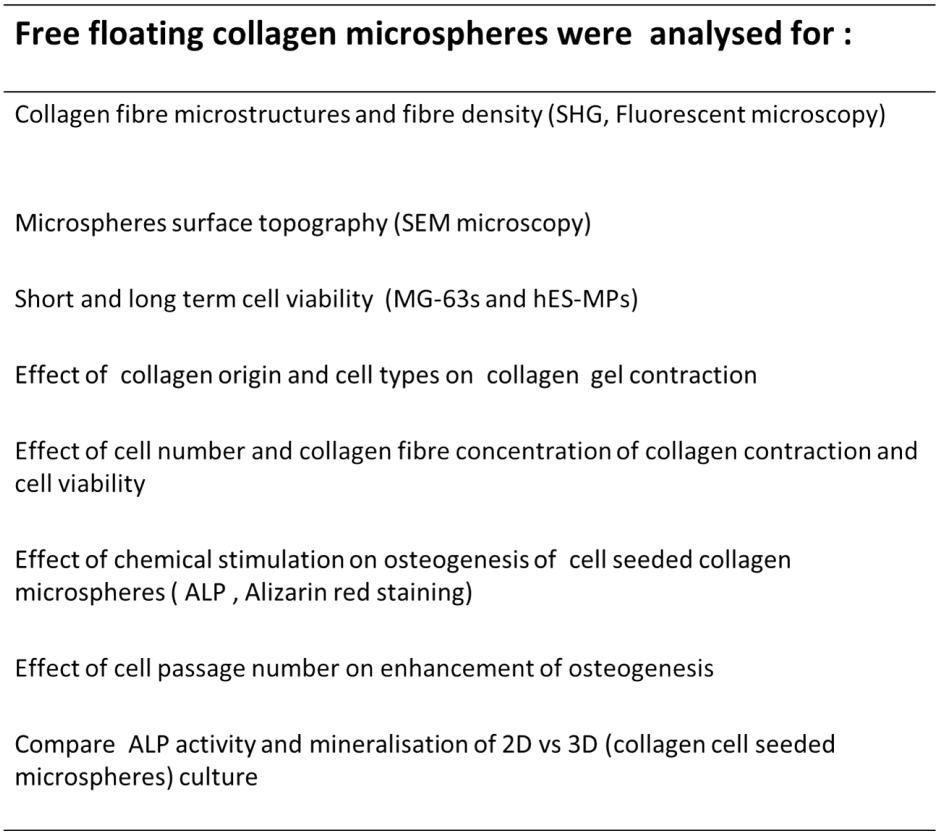


Figure 3.1: Undertaken experiments and conditions that applied on cell seeded collagen microspheres during 28 days pc.

3.2.4 Measurement of collagen microsphere contraction

For collagen concentration of 2 mg/mL, effect of hES-MPs and MG-63 cell line and collagen I sources from two species of bovine and rat tail on the contraction of collagen gel were compared with each other. For each time point, 12 collagen microspheres were selected and bead diameters were measured to compare collagen gel contractibility over 7 days experiment using ImageJ software.

3.2.5 Examining short and long cell viability of cell seeded collagen microspheres

Cell containing collagen microspheres with different collagen concentration and cell density were stained with calcein AM and ethidium homodimer-1 in DMSO for 45 min away from light. Collagen microspheres were flushed with full medium into 8 well micro slides ibiTreat purchased from Thistle Scientific to check the

cells viability and morphology at 8 h, 3, 5 and 7 days pc. Stained microspheres were examined under fluorescent microscope (Nikon Ti-E) and FITC/Cy2 and ET Texas red filters for image acquisition.

3.2.6 Assessment of collagen fibres micro structure in hES-MPs seeded bovine and rat tail collagen I microspheres

Microstructure of cell seeded collagen I samples of bovine and rat tail were compared at day 7 pc with non-seeded collagen I samples. Fluorescent staining of collagen was performed by adding 6.54 mL of 1.5 µM Oregon Green® 488 Carboxylic Acid, Succinimidyl Ester, 5-isomer collagen tracker in PBS to the samples and incubated overnight. Both samples were visualised under SHG confocal microscopy objective (EC plan-neofluar 40X/1.30 Oil DIC) (illumination 458-480 nm) and Nikon fluorescent microscope to identify the variability in collagen fibres organisation with and without cells and MSC's role in reorganising and remodelling the collagen fibre microstructure in different species.

3.2.7 Effect of different hES-MPs passages on level of ALP activity and calcium deposition

Passages 5 and 12 of hES-MP cell line were seeded in 2 mg/mL collagen microspheres. Fluorescent images of live and dead cells were recorded over 7 days pc. ALP staining and 1% Alizarin red staining of ECM calcium level of free floating samples were compared over 14 days pc. Three groups of samples were compared against each other: seeded hES-MPs collagen microspheres without added FGF-β to media, hES-MPs/collagen beads in added FGF-β to the media and hES-MPs/collagen microspheres in osteogenic media.

3.2.8 2D versus 3D hES-MP cell culture

Total DNA number, alkaline phosphatase activity level and 1% Alizarin red staining of 2D and 3D hES-MPs cultured with three conditions of: added FGF-β to media, control (nFGF-β) media and cultured in osteogenic media, were compared over 28 days pc to identify the effect of 3D micro-environment in differentiation of stem cells.

3.2.9 Cell culture

Two cell types were used in this study; human osteosarcoma-derived cell lines (MG-63s) and human embryonic cell-derived mesenchymal progenitor cell line hES-MP 002.5 (hES-MPs). hES-MP cells were used between passages 3-7 and passage 12.

3.2.10 Cellular assay

Cell growth and proliferation of hES-MP cell line of free floating controls were assessed using DNA pico-green assay at time 24 h, days 3, 4, 5, 6, 7 pc and standard curve shown in Figure 3.2.

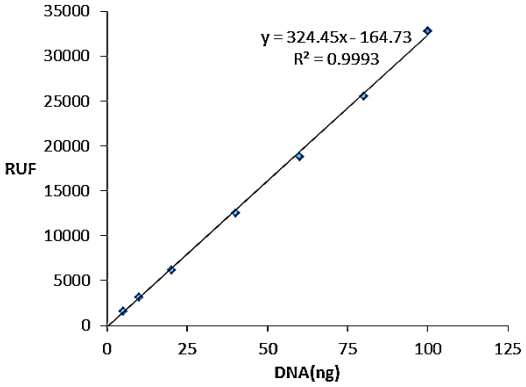


Figure 3.2: Standard curve of DNA pico green assay used to evaluate hES-MP cell viability within 28 days of post en-capsulation.

Cell viability was assessed by staining microspheres with 200 µL of 2 mM calcein AM in DMSO 495 nm-515 nm from Life Technologies and 4 mM ethidium homodimer-1 in DMSO 515 nm-635 nm purchased from Sigma for 45 min away from light. The microspheres were then washed with 500 µL PSB once to remove the excess fluorescent dye.

Extracellular matrix alkaline phosphatase activity of hES-MPs was evaluated by ALP staining of microspheres at 24 h, 6, 14, 21 and 28 days pc.

Deposited calcium of ECM was examined by staining the microspheres with 1% Alizarin red S staining at 24 h, 6, 21 and 28 days pc.
Collagen fibres micro structure and cell attachment were visualised using SEM microscope.

3.2.11 Statistics

Measurement of microspheres diameter were performed three times using 10-12 collagen beads for each repeat. Visualisation of cell viability at different time points and ALP and mineralisation staining was performed using bright field filter of (Nikon Ti-E) on two or three samples of each condition during experimental repeat. Statistical differences of seeded hES-MPs versus MG-63s microspheres contraction and bovine collagen I contraction against rat tail collagen I were completed using one-way ANOVA followed by Sidak's or Tukey's multiple comparisons test.

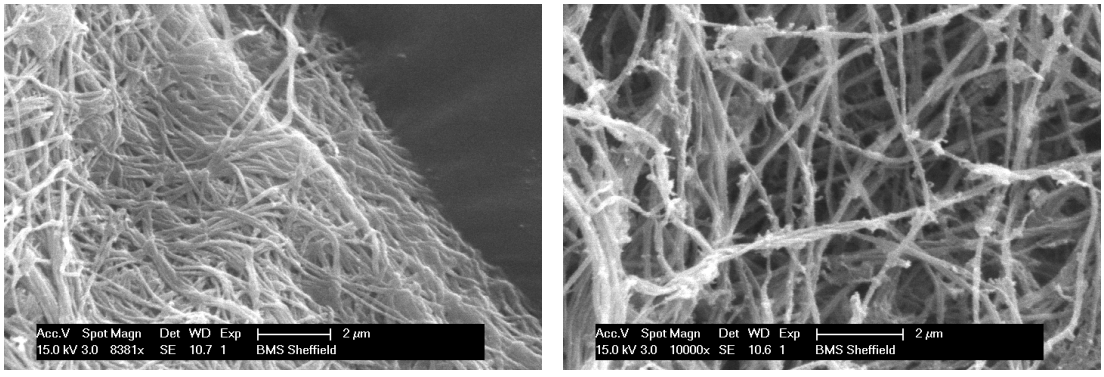
3.3 Results

3.3.1 Collagen gel mechanical properties

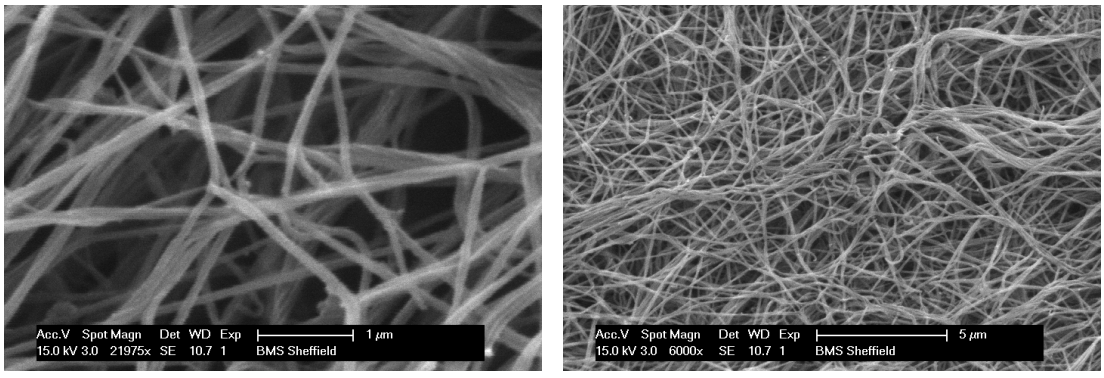
Viscoelastic properties and shear modulus of very soft collagen gel (0.2% of collagen/hydrogel) were measured by rheometre at 37 °C and 1.3-0.012 Hz. The elastic modulus varied from 0.0146 kPa at 1.3 Hz to 0.0077 kPa at 0.012 Hz, while the viscous modulus varied between 0.0037-0.0017 kPa. Average standard deviations were 0.0019-0.0005 kPa, respectively. The average shear moduli was calculated as 0.0103 kPa with standard deviation of 0.0019 , average elastic moduli was measured as 0.0101 kPa with standard deviation of 0.0019 , and average viscous moduli was calculated as 0.0023 kPa with standard deviation of 0.0005 kPa.

3.3.2 Identification of collagen fibre micro structure

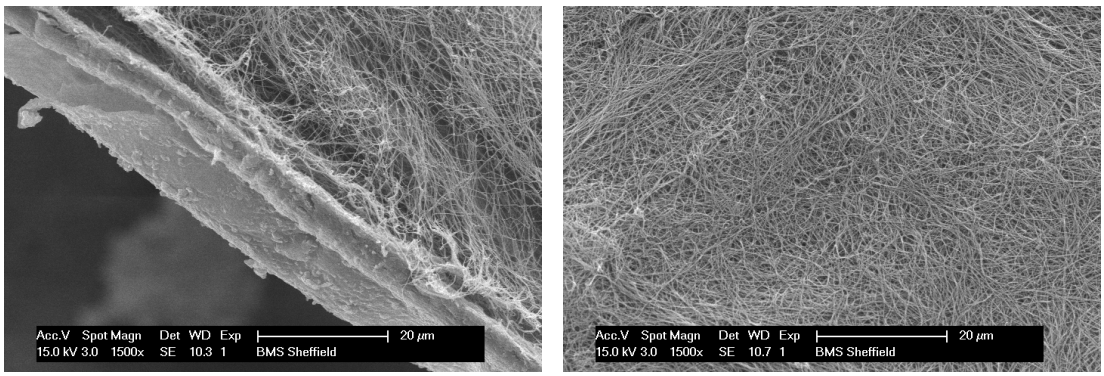
SEM microscopy showed highly porous surface structure of collagen gel and entrapment of hES-MPs within collagen matrix with little or no visible aligned fibres (Figure 3.3). Also amorphous fluffy structures of collagen gel with random orientation and mesh work of collagen fibres was confirmed by Col I specific fluorescent staining and SHG microscopy. The results from SHG confocal microscope showed no significant difference between microstructure of bovine and rat tail collagen I fibres. As shown in Figure 3.4 two non-seeded collagen microspheres for each specie were assessed under the microscope and presented similar collagen fibre organisation, with bovine sample emitting stronger signals and more visible aligned fibres. Images of collagen I fluorescent staining of bovine and rat tail collagen I beads showed very similar collagen fibres organisation but bovine collagen samples revealed slightly higher fibre density and network (Figure 3.5). Both samples presented amorphous fibrous structures and few visible alignments of collagen fibres. SEM images of seeded collagen microspheres presented well spread hES-MPs on collagen beads surface on day 7 pc and showed that cells migrated to the periphery of collagen gel and interacted with bovine collagen fibres as shown in Figure 3.6. Microscopic images of day 16 pc indicated higher interaction of elongated cells with collagen fibres and cell-cell network on the gel surface. Fibres microstructure was remodelled and reorganised by cells and more defined collagen fibres were visible on periphery of microspheres.



(a) **(b)**

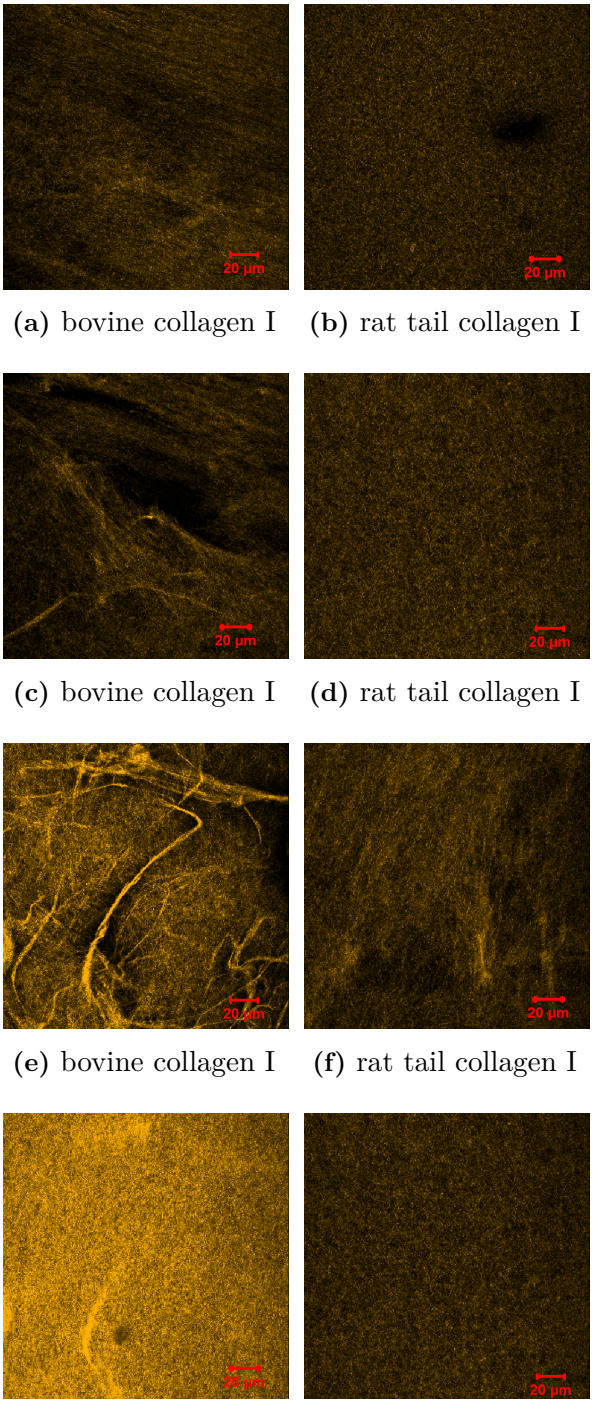


(c) **(d)**



(e) **(f)**

Figure 3.3: SEM images of bovine collagen I microspheres, micro structure and mesh work of collagen fibres after gelation, a-f; different cross section area and magnification of collagen gel. Scale bar for (a)-(b) 2 µm, (c) 1 µm, (d) 5 µm, (e)-(f) 20 µm.



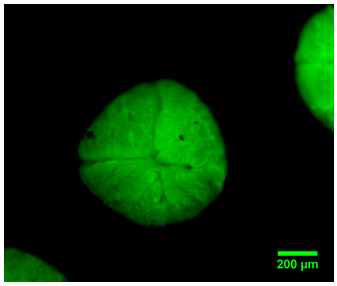
(a) bovine collagen I **(b)** rat tail collagen I

(c) bovine collagen I **(d)** rat tail collagen I

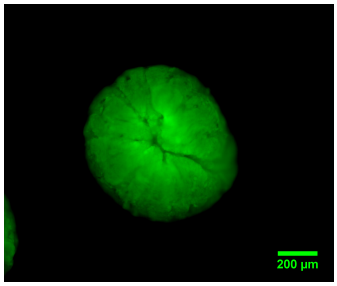
(e) bovine collagen I **(f)** rat tail collagen I

(g) bovine collagen I **(h)** rat tail collagen I

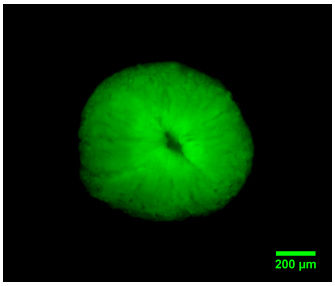
Figure 3.4: Microstructure and fibre density of three bovine and rat tail collagen I microspheres were compared using SHG confocal microscope at 24 h post gelation. Bovine collagen fibre presented higher intensity of signals suggesting the presence of more collagen fibres in the samples. Microscopic images were taken by Dr Green at Kroto Research Institute, Department of Material Sciences, University of Sheffield. Scale bar for (a)-(h) 20 µm.



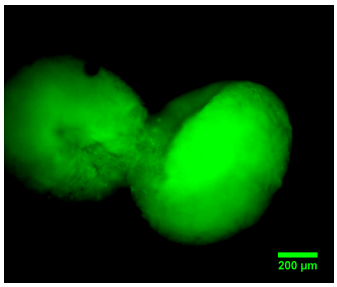
(a) fibres of bovine collagen I microsphere



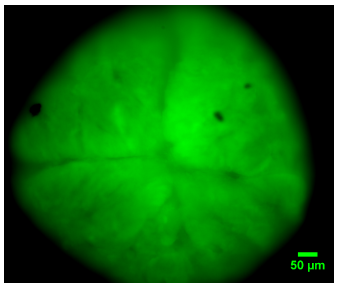
(b) fibres of bovine collagen I microsphere



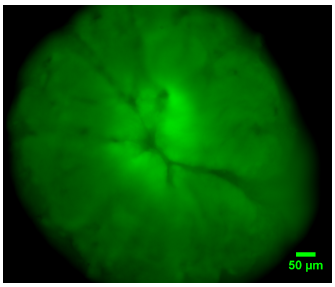
(c) fibres of rat tail collagen I microsphere



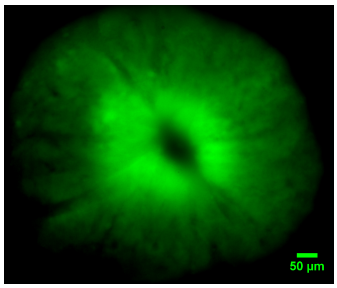
(d) fibres of rat tail collagen I microsphere



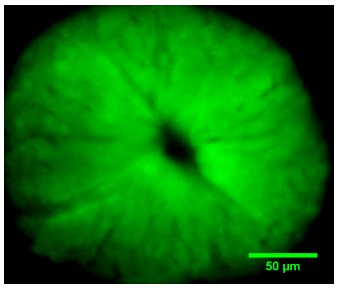
(e) fibres of bovine collagen I microsphere



(f) fibres of bovine collagen I microsphere

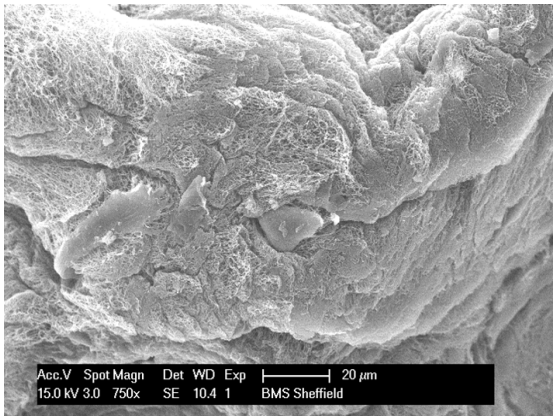


(g) fibres of rat tail collagen I microsphere

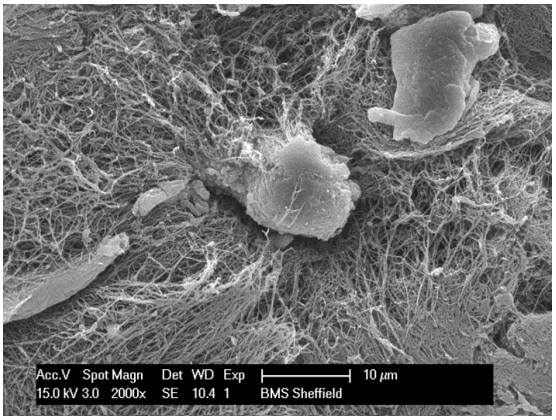


(h) fibres of rat tail collagen I microsphere

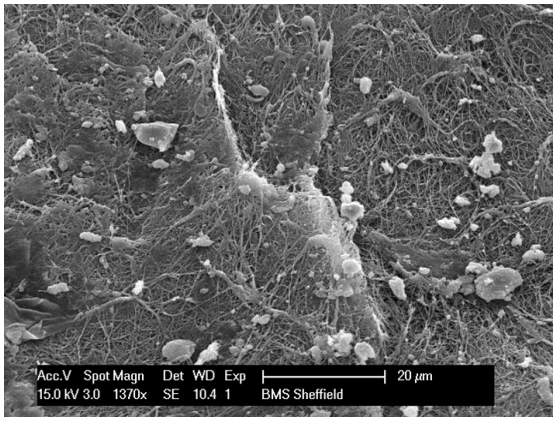
Figure 3.5: Microstructure and density of bovine and rat tail collagen I fibres were compared using Oregon Green® 488 carboxylic acid, succinimidyl ester, 5-isomer collagen tracker at 24 h post gelation. No considerable differences was recorded between microstructure of collagen fibres from bovine and rat tail origins. Scale bar for (a)-(d) 200 µm, (e)-(h) 50 µm.



(a) Day 7 post encapsulation



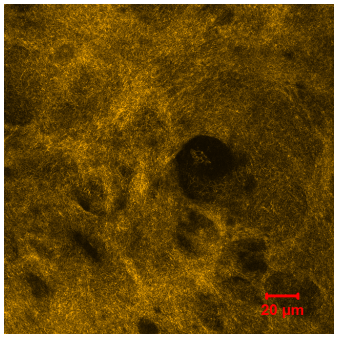
(b) Day 7 post encapsulation



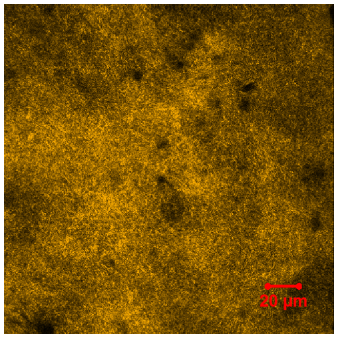
(c) Day 16 post encapsulation

Figure 3.6: SEM images of hES-MPs seeded bovine collagen I microspheres. Cells attached to the hydrogel surface and presented more elongated morphology on day 16 pc. Scale bars for (a) and (c) 20 µm and (b) 10 µm.

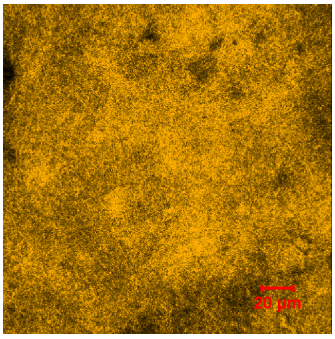
SHG images of seeded collagen microspheres revealed more organised fibre structure in bovine collagen I compared to rat tail collagen gel as shown in Figure 3.7. Although the signal is slightly stronger in rat tail samples, hES-MPs seemed to adapt better on bovine 3D gel and more defined fibres structure appeared within random organisation of collagen micro structure on 7 day pc. Remodelling of collagen microspheres was highly recognisable on day 21 pc with thicker and more visible extracellular collagen fibres around the darker areas that cells attached to the surface.



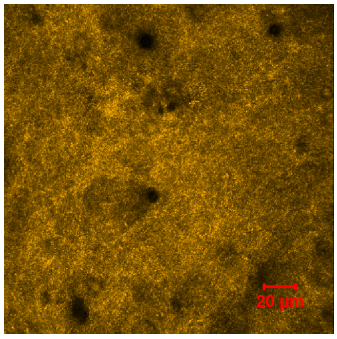
(a) Bovine collagen I day 7 pc



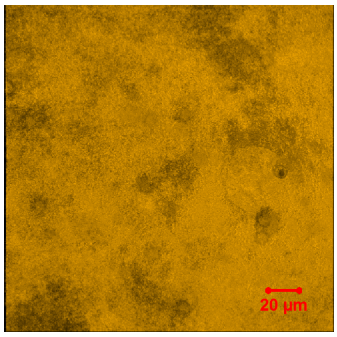
(b) Bovine collagen I day 7 pc



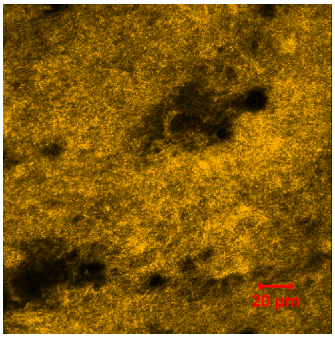
(c) Bovine collagen I day 7 pc



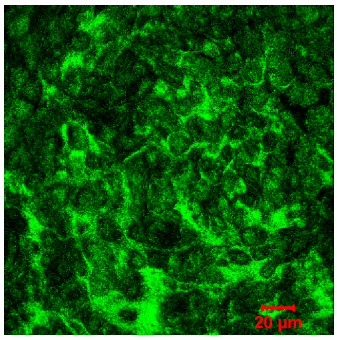
(d) Rat tail collagen I day 7 pc



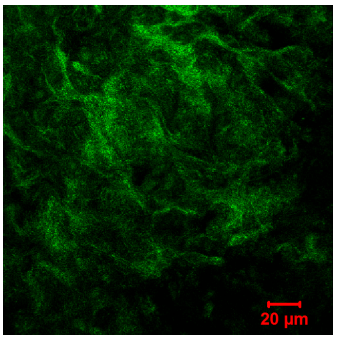
(e) Rat tail collagen I day 7 pc



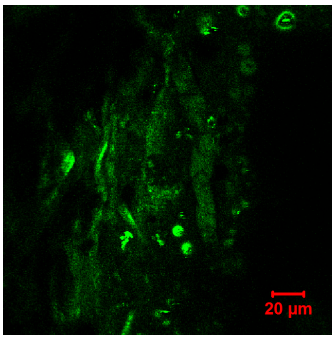
(f) Rat tail collagen I day 7 pc



(g) Bovine collagen I day 21 pc



(h) Bovine collagen I day 21 pc

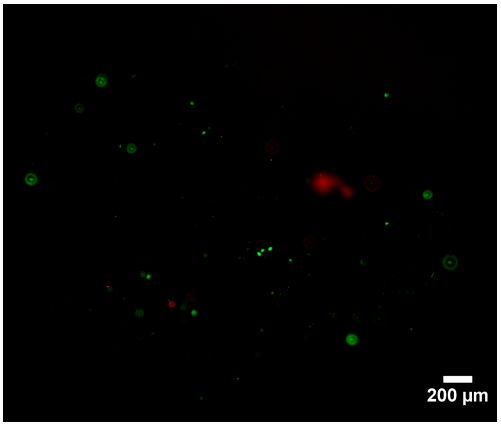


(i) Bovine collagen I day 21 pc

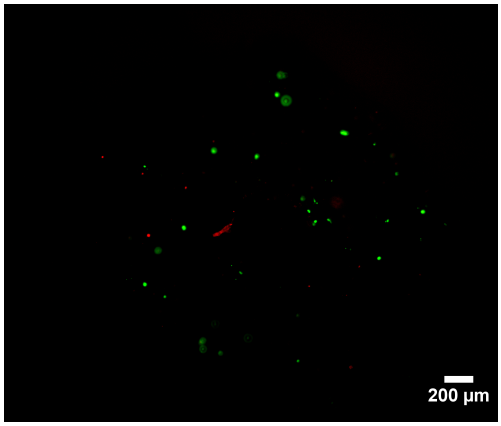
Figure 3.7: Microstructure and fibres density of hES-MPs seeded bovine and rat tail collagen I microspheres were compared using SHG confocal microscope. Rat tail collagen fibre presented slightly higher intensity of signals suggesting the presence of more collagen fibres in the samples on day 7 pc. Microscopic images were taken by Dr Green at Kroto Research Institute, Department of Material Sciences, University of Sheffield. Scale bars for (a)-(i) are 20 µm.

3.3.3 Assessment of short and long term cell viability of seeded hES-MPs/collagen microspheres

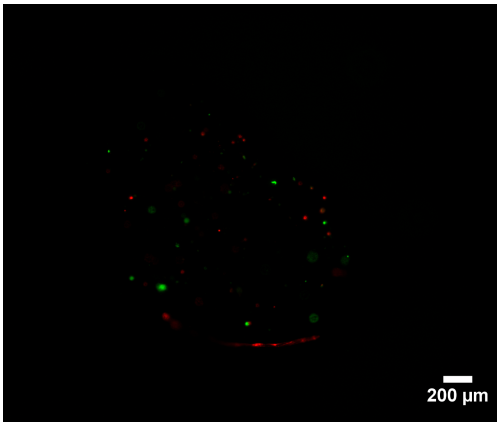
hES-MPs with cell density of 5×10^5 cells/mL and 1×10^6 cells/mL which were embedded in 1.5-2 mg/mL collagen I gel emitted strong green signal with calcein AM and low red signal with ethidium bromide homodimer within 8, 72, 120, and 168 h pc suggesting high viability and low mortality of cells (Figure 3.7). Also, higher number of elongated cells and better cell interactions were observed when 2 mg/mL of bovine collagen I was used for micro encapsulation of hES-MPs. In addition, cells tended to spread further and migrated to the periphery of collagen beads 48 h after the seeding. On the other hand collagen microspheres with cell populations of 5×10^6 cells/mL displayed very weak cell viability and most cells died within 24 h pc. Regardless of cell seeding density, very week or no green fluorescent signal was detected 24 h after encapsulation hES-MP cells in 0.5-1 mg/mL and 3 mg/mL collagen and cells shape mainly remained spherical.



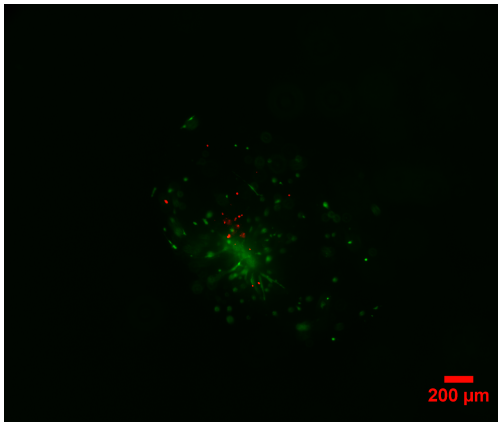
(a) 1×10^6cells/mL, c:0.5 mg/mL



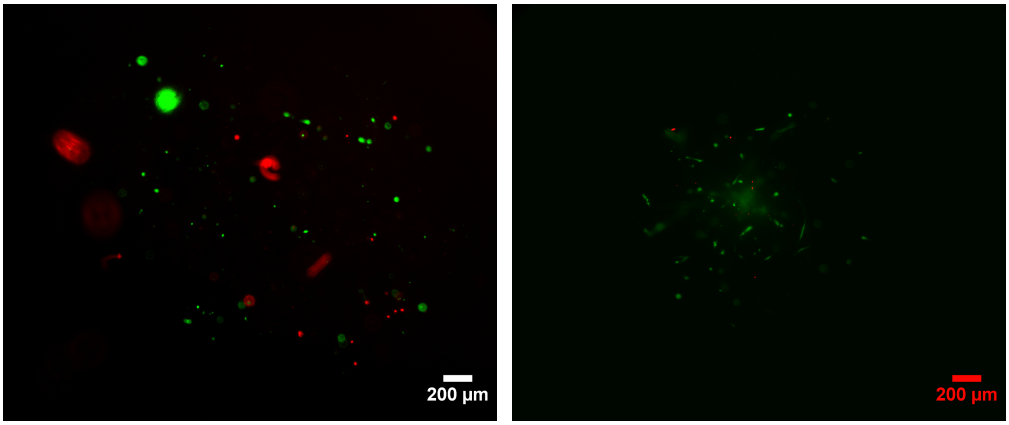
(b) 1×10^6 cells/mL, c:1 mg/mL



(c) 1×10^6 cells/mL, c:3 mg/mL



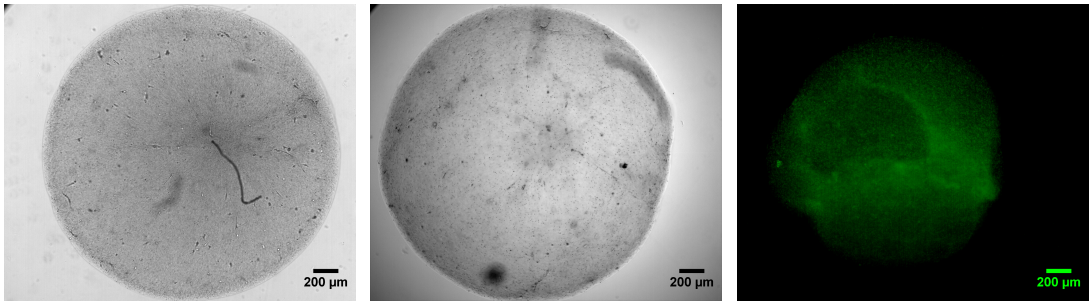
(d) 1×10^6 cells/mL, c:2 mg/mL



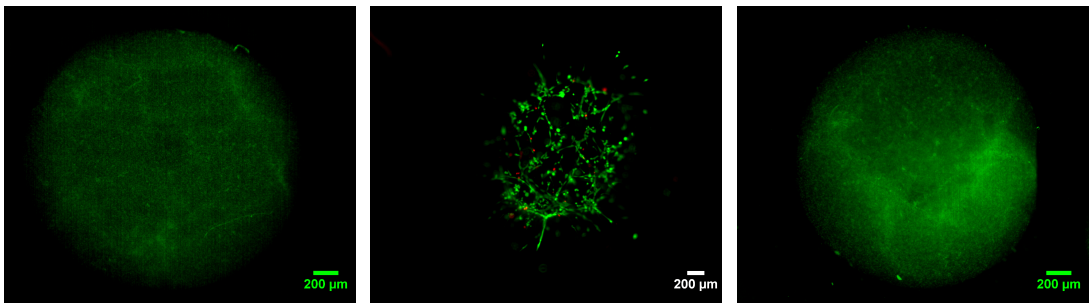
(e) 5×10^6 cells/mL, c:2 mg/mL **(f)** 5×10^5 cells/mL, c:2 mg/mL

Figure 3.7: Effect of collagen concentration and cell seeding density on viability of hES-MPs 24 h after encapsulation in bovine collagen I using fluorescence live and dead assay. c: collagen concentration. Scale bars for (a)-(f) are 200 µm.

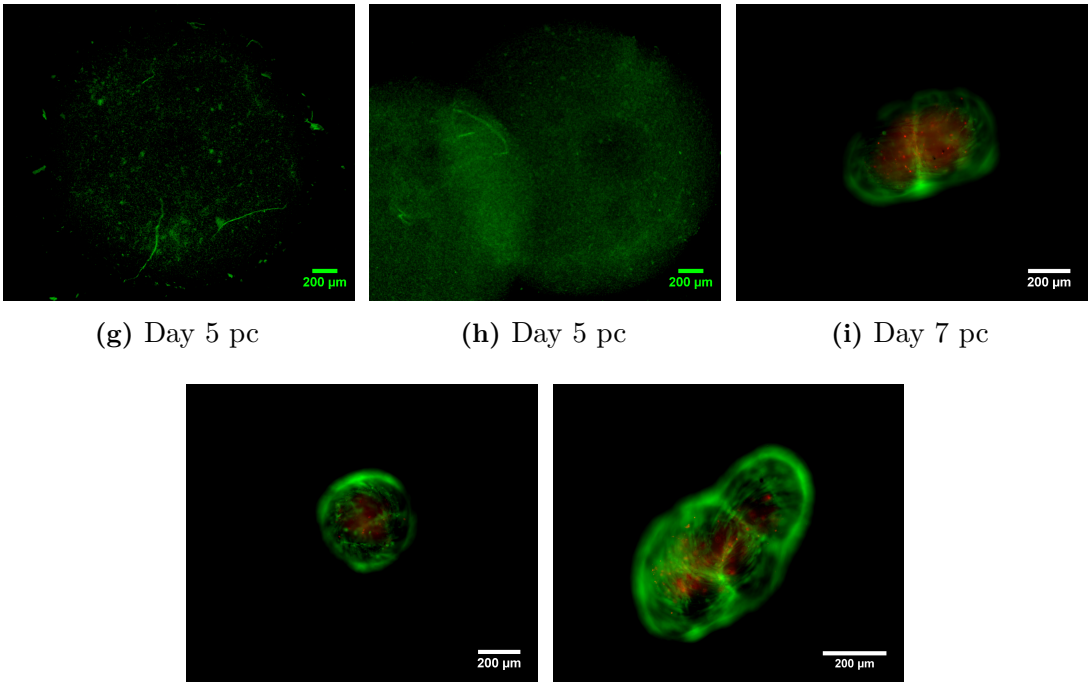
Those cells that stayed alive migrated to the surface of collagen beads and proliferated steadily till day 35 pc. Strong fluorescent signal of elongated viable cells indicated well established cell networks, cell-cell and cell-collagen fibres interactions in the collagen microspheres (Figure 3.7 and Figure 3.7).



(a) 24 h pc **(b)** 24 h pc **(c)** 48 h pc



(d) 48 h pc **(e)** Day3 pc **(f)** Day 3 pc

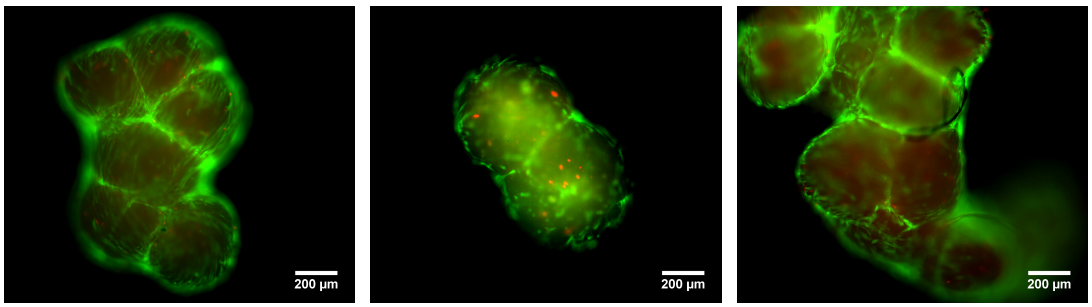


(g) Day 5 pc **(h)** Day 5 pc **(i)** Day 7 pc

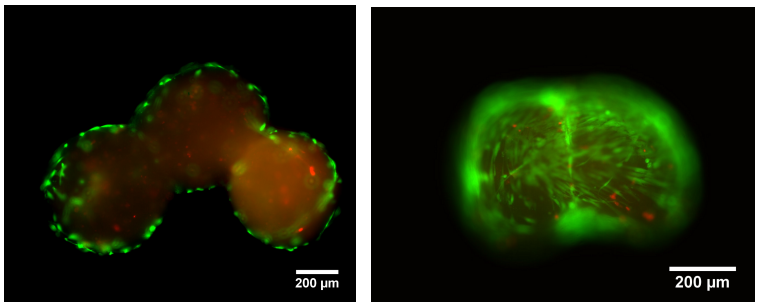
(j) Day 7 pc **(k)** Day 7 pc

Figure 3.7: Short term cell viability of seeded hES-MPs collagen I microsphere was checked by bright field and fluorescent imaging of live/dead cells over 7 days pc. Live cells were shown by green colour while, dead cells were stained red. Scale bars for (a)-(k) are 200 µm.

Results of DNA pico green assay indicated that the total DNA and cell number remained stable over 28 days pc. The cell number reduced by 14% between day 1 and day 6 before a steady increase of 6% on day 14 pc. The total DNA number alleviated to around 50 ng and reached the lowest cell number on day 21 then surged by 23% to 65 ng of DNA on day 28 pc as shown in Figure 3.8. No statistical significance was reported for the total DNA number over 7 days experiment.



(a) Day 35 pc **(b)** Day 35 pc **(c)** Day 35 pc



(d) Day 35 pc **(e)** Day 35 pc

Figure 3.7: Long term cell viability of seeded hES-MPs collagen I microsphere on day 35 pc was evaluated by fluorescent imaging of live/dead cells and presented by different magnification. Live cells were shown by green stain while, dead cells were stained red. Scale bars for (a)-(e) are 200 µm.

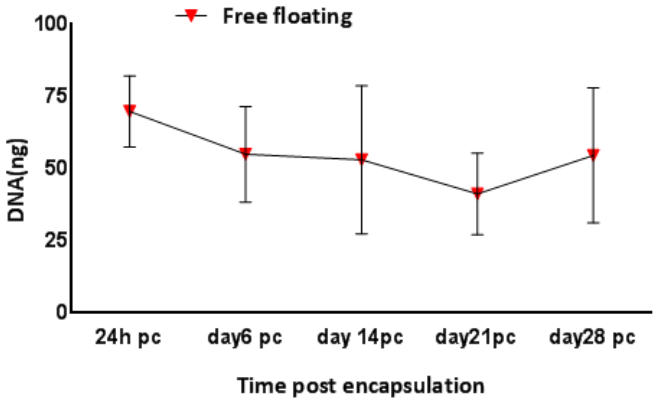
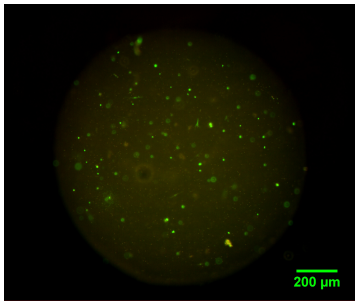


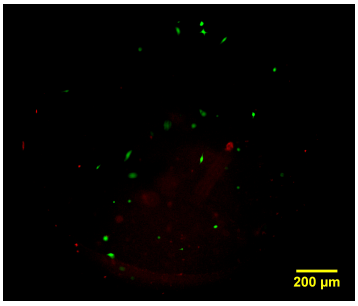
Figure 3.8: hES-MPs cell viability was evaluated over 28 days pc by using DNA pico green assay at different time points.

3.3.4 Determination of seeded MG-63s collagen I microspheres viability

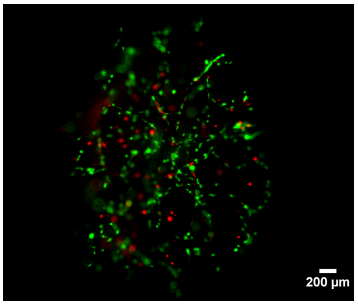
MG63 seeded in 3 mg/mL collagen I and at density of 1×10^6 cells/mL showed good viability within 7 days of experiment and up to 21 days pc (Figure 3.9). Cells elongated well and gathered to make cell clusters as observed on day 21. Other cell concentration did not survive beyond 24 h pc. MG-63 cell line also did not adapt to lower collagen concentration below 3 mg/mL, cells remained spherical with very low/no attachment to the collagen fibres and did not survive beyond 24 h.



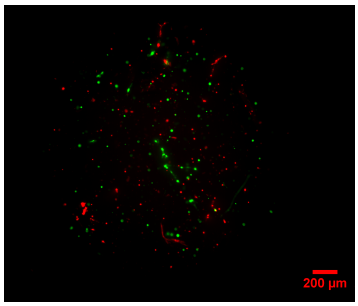
(a) 24 h pc



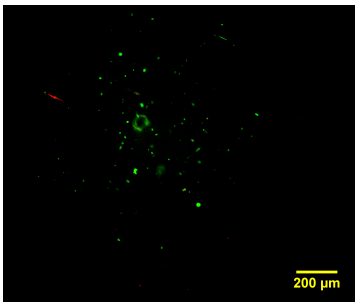
(b) 24 h pc



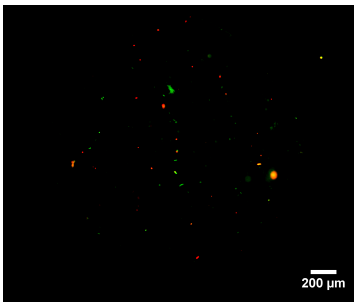
(c) 72 h pc



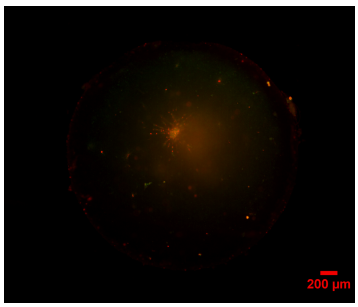
(d) 72 h pc



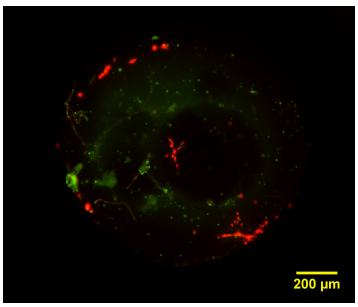
(e) Day 5 pc



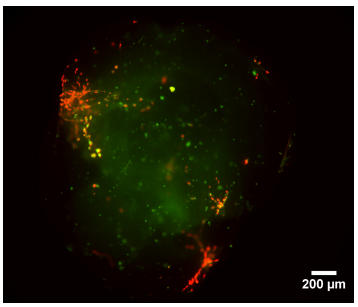
(f) Day 5 pc



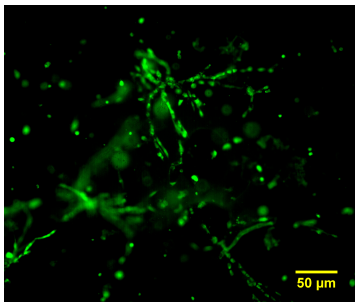
(g) Day 21 pc



(h) Day 21 pc



(i) Day 21 pc

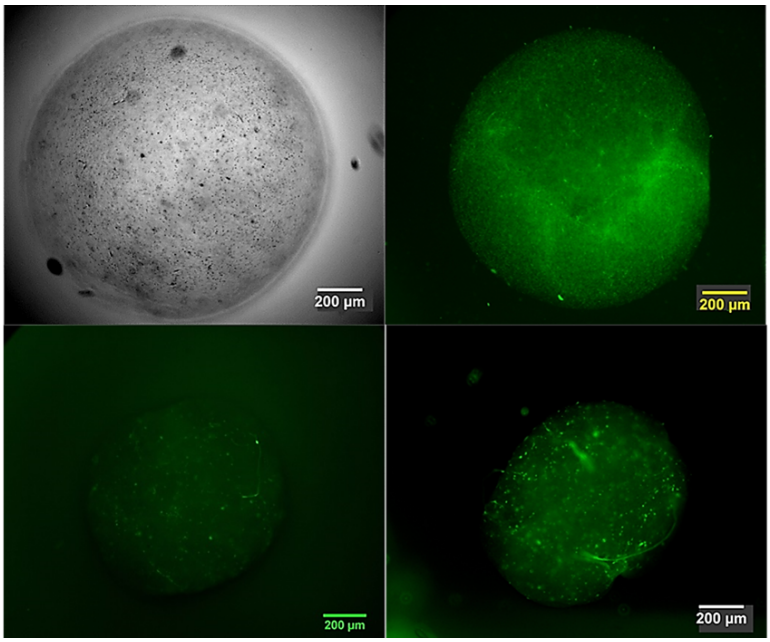


(j) Day 21 pc

Figure 3.9: Long term cell viability of seeded MG-63s collagen I microsphere was checked by fluorescent imaging of live/dead cells over 21 days pc. Scale bars for (a)-(i) are 200 µm and (j) 50 µm.

3.3.5 Collagen gel contraction

Results of hES-MPs/collagen beads monitoring demonstrated that collagen microspheres with collagen concentration of 2 mg/mL and cell number of 1×10^6 cells/mL significantly contracted by an average of 43% in diameter within 7 days pc, while other cell seeding density and collagen concentration showed no or small contraction over the same period of time (Figure 3.12 a). Average diameter reduction of 20% was reported between day 3 and day 5, while least contraction with only 14% change in diameter was observed between day 0 and 3 pc. Microspheres diameter was observed as 1410 µm on average at 8h pc then this figure was reduced to 1210 µm on day 3 and to 910 µm on day 5 before shrinking to the diameter of 815 µm on day 7 pc. The biggest drop in microspheres diameter and most substantial contraction was reported between day 3 and 7 pc (Figure 3.10).

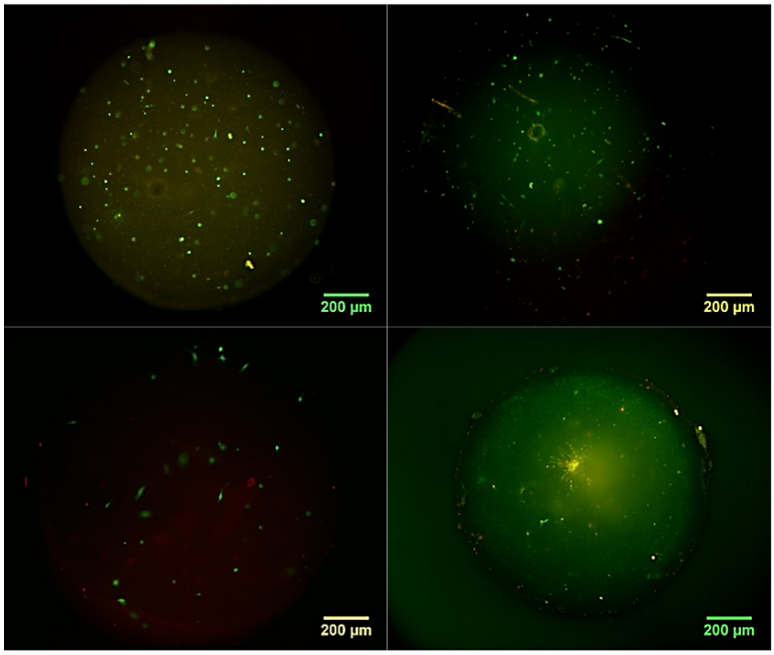


(a) hES-MPs

Figure 3.10: Microscopic images of cell seeded collagen I contraction over 7 days pc, from top left to bottom right, embedded hES-MPs ability to contract the collagen gel at 24 h, 72 h, 120 h and 168 h pc. Seeded hES-MPs contracted collagen gel to nearly half its diameter within first 7 days pc. Scale bars are 200 µm.

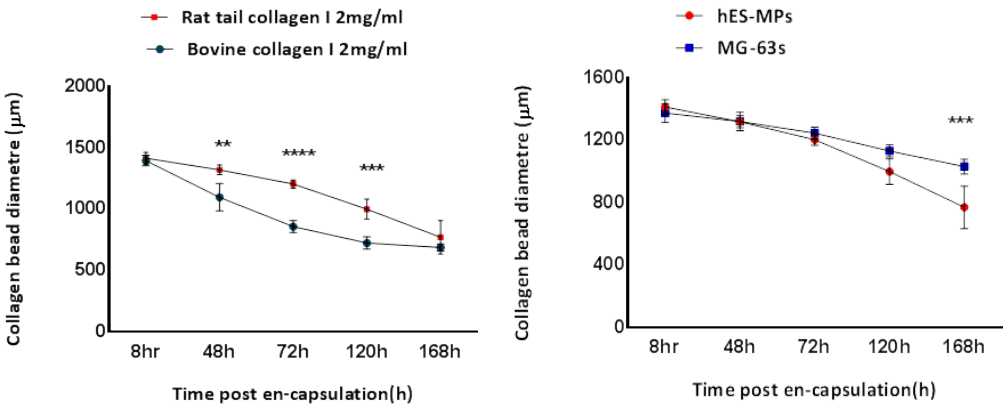
In contrast, seeded MG-63 cells in collagen microspheres contracted up to 15% over 7 days of experiment (Figure 3.12 b). At 8 h pc, collagen microspheres diameter were reported on average as 1385 µm, beads then marginally contracted by 10% and their diameter reduced to 1230 µm on day 3 pc. Collagen microspheres diameter was measured as 1192 µm and 1125 µm on day 5 and 7 pc respectively. Most significant contraction was 12% between 48 and 168 h of the experiment and

while least change (8%) was observed between hours 8 and 48 pc (Figure 3.11). Nonetheless, hES-MPs contracted collagen gel considerably more than MG-63 cells and their average diameter on day 7 pc was significantly smaller than MG-63s (28%, $p < 0.001$). The results of bovine and rat tail collagen gel contraction revealed that bovine collagen played greater role in supporting hES-MPs collagen contraction (Figure 3.12 b). Bovine collagen microspheres contracted more considerably within the first 72 h pc (39%), while rat tail collagen gel showed more stable contraction of 15% in same period of time. On average rat tail collagen gel contracted 29% ($p < 0.0001$) less than bovine within 72 h of gelation but, in the second half of experiment the average diameter of rat tail collagen microsphere dropped significantly by 35% compared to 20% decrease in bovine sample to reach around 700 µm on day 7 pc. Overall rat tail collagen gel contraction began much later than bovine and showed to be more subtle over the 7 days experiment.



(a) MG-63s

Figure 3.11: Microscopic images of cell seeded collagen I contraction over 7 days pc, from top left to bottom right, embedded MG-63s ability to contract the collagen gel at 24 h, 72 h, 120 h and 168 h pc. Seeded MG-63s contracted collagen gel far less that hES-MPs within first 7 days of en-capsulation. Scale bars are 200 µm.

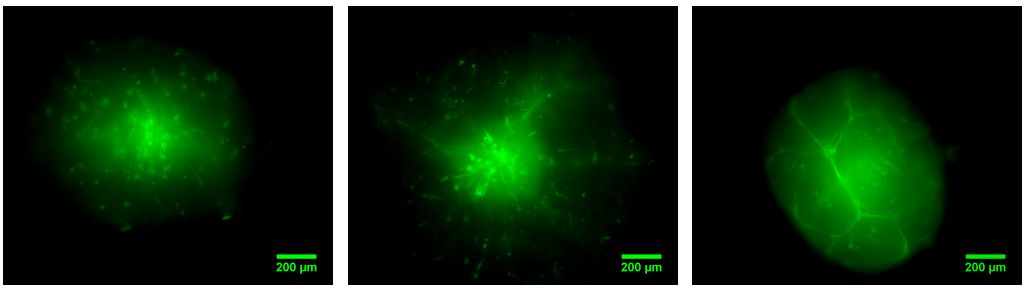


(a) **(b)**

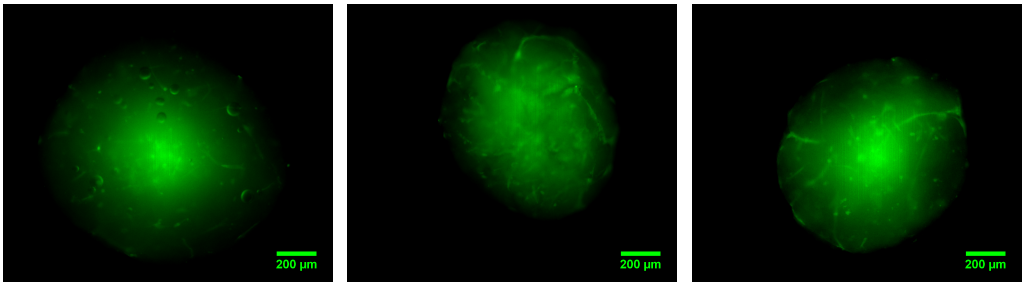
Figure 3.12: Effect of two cell lines and collagen I sources on the contraction of collagen I gel with concentration of 2 mg/mL were investigated, a: collagen contractibility of hES-MPs/bovine collagen I was compared with rat tail collagen I by measuring the diameter of 12 samples at each time point, b: ability of hES-MPs versus MG-63 cell line in contracting collagen gel was assessed,* indicates statistical significance, (** p <0.01, *** p <0.001, **** p <0.0001). Data is mean ± SD n=9.

3.3.6 Effect of different hES-MPs passages on level of ALP activity and calcium deposition

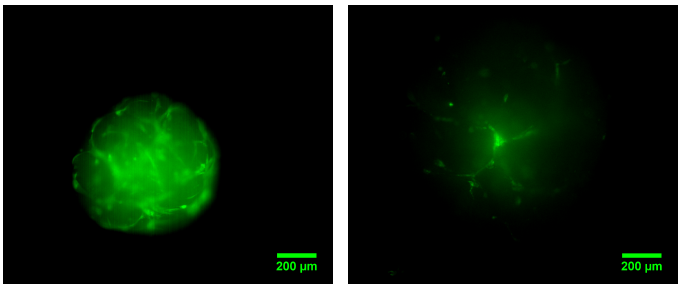
To characterise the consistency of the behaviour of different passages of hES-MPs/collagen microspheres and the effect of passage number on viability, alkaline phosphatase activity level and mineralisation within 3D environment passages (ps) 5 and 12 of hES-MP cell line were studied. Both passages presented similar cell viability over 7 days pc, collagen beads contracted well with cells elongated and migrated to the periphery of microspheres (Figure 3.12). Ps 5 hES-MPs microscopic images showed slightly stronger fluorescent signals and higher contraction of microspheres in comparison with ps 12.



(a) ps 5, 48 h pc **(b)** ps 12, 48 h pc **(c)** ps 5, day 3 pc



(d) ps 12, day 3 pc **(e)** ps 5, day 5 pc **(f)** ps 12, day 5 pc



(g) ps 5, day 7 pc **(h)** ps 12, day 7 pc

Figure 3.12: Microscopic images of hES-MPs live and dead assay and comparison of collagen gel contraction in different passages of hES-MP seeded hES-MPs collagen microsphere over 7 days pc. Ps5 hES-MPs showed slightly stronger fluorescent signals compared to Ps 12. Scale bars for (a)-(h) are 200 µm.

The results of ALP staining of two passages of seeded hES-MPs microspheres revealed very similar extra cellular matrix ALP activity level during 14 days experiment as shown in Figure 3.13. ALP staining intensity was similarly high on day one pc in both passages for FGF-β treated and osteogenic samples while, on days 5 and 7, passage 12 presented moderately higher ALP level in all three conditions compared to ps 5.

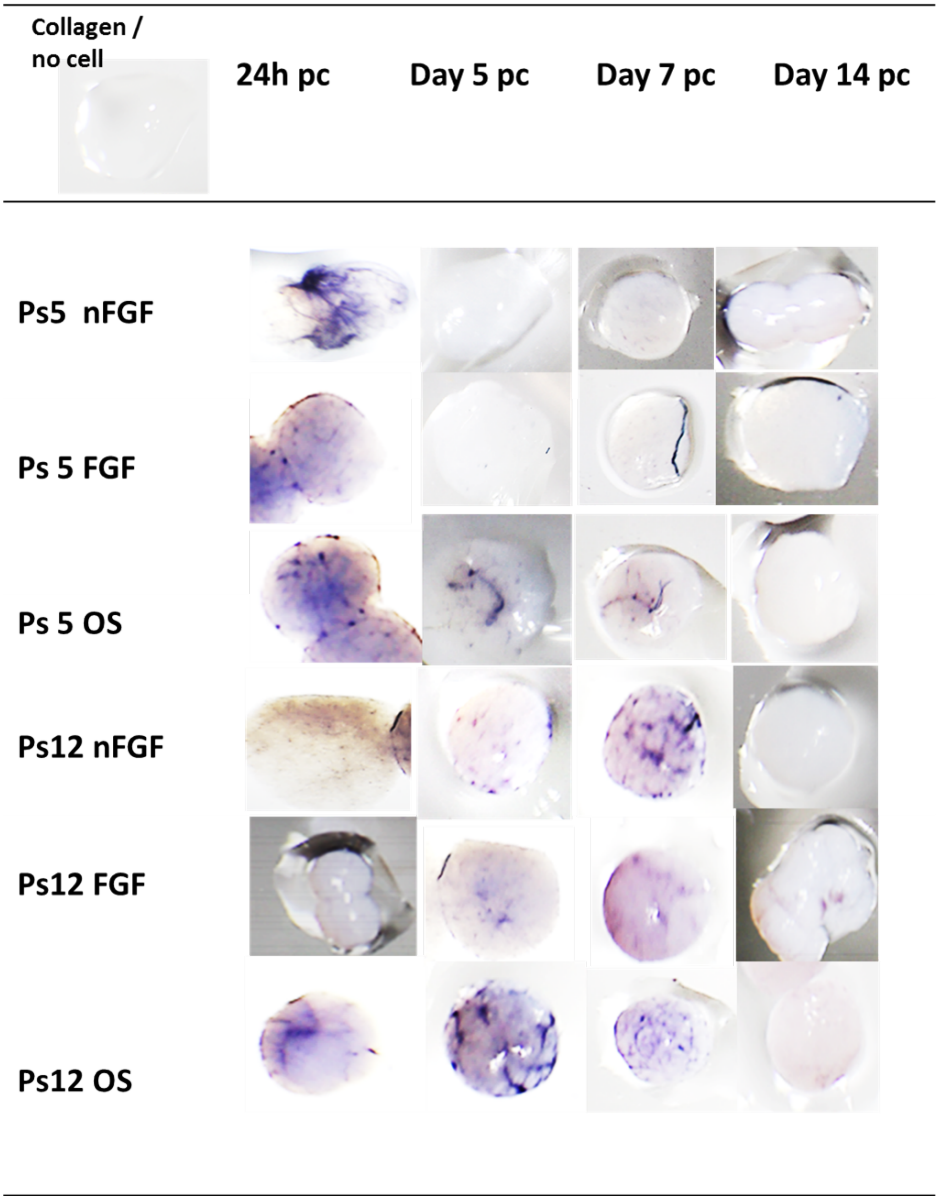


Figure 3.13: Alkaline phosphatase staining of different passages of hES-MPs seeded collagen microsphere over 14 days pc. OS media; osteogenic media, nFGF; control media with no treatment. ALP activity of both passages were similar during 14 day experiment with osteogenic media treated samples in both passages showed higher intensity of ALP stain from day 5 pc. Stain intensity in osteogenic media treated samples was reported as minimal on day 14 pc. All images taken by light microscope, 1.5x.

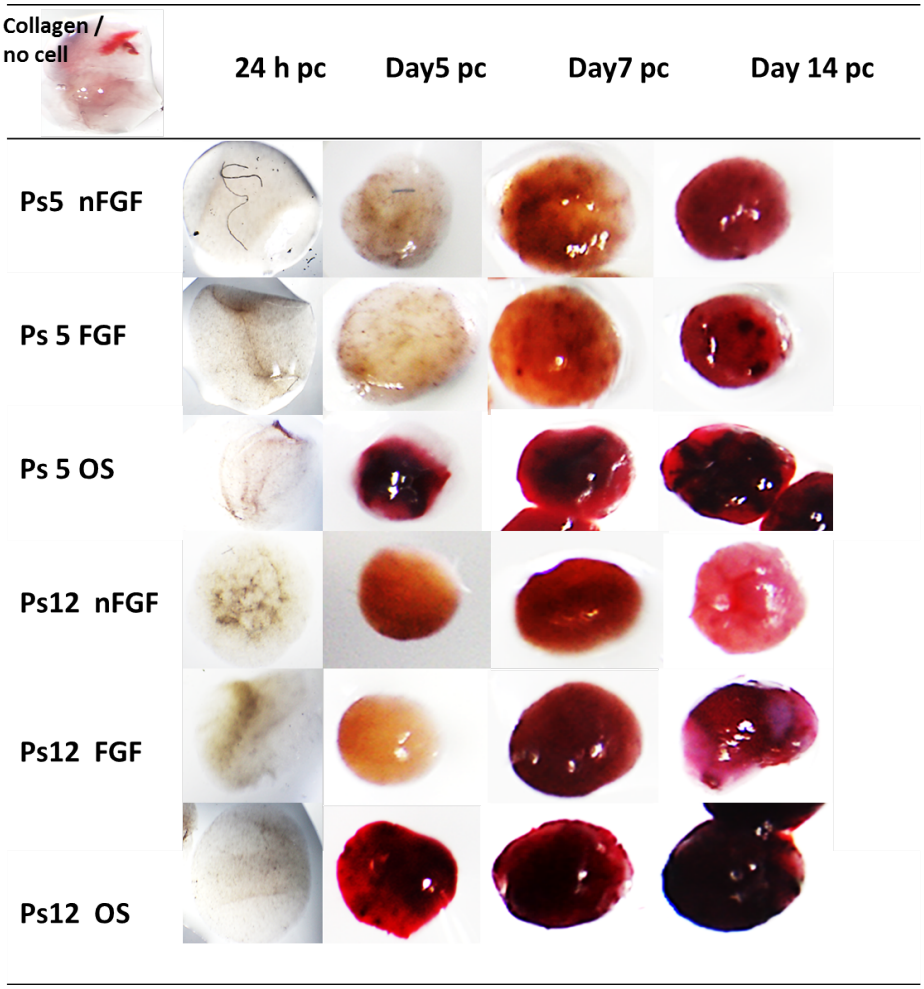
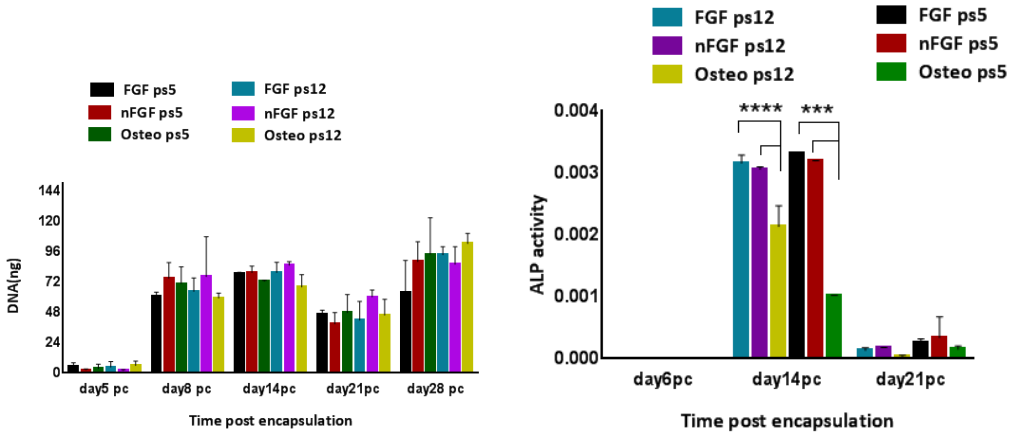


Figure 3.14: Alizarin red staining of different passages of hES-MPs seeded collagen microsphere over 14 days pc. OS media; osteogenic media, nFGF; control media with no treatment. Deposited stain accumulated much more in osteogenic media treated samples in both passages from day 5 pc. Stain intensity in osteogenic media treated samples was reported highest on day 14 pc in both passages but ps 12 showed slightly higher deposition of stain compared with ps 5. All images taken by light microscope, 1.5x.

Both passages showed low extra cellular ALP for all the experimental conditions on day 14 pc. Furthermore, osteogenic media treated samples in both passages presented higher colour intensity than other groups and non treated FGF-β samples in ps 12 showed darker purple colour than FGF-β treated samples on days 1, 5 and 7 pc. Yet, there was no noticeable difference between FGF-β treated and non treated conditions of passage 5 samples on any time points.

Alizarin staining results also showed similar colour intensity for all conditions in both passages as presented in Figure 3.14. Collagen microspheres that were treated with osteogenic media had highest calcium deposition compared to other experimental groups and both passages showed darker colour from day 5 pc. In addition, treated FGF-β samples in both passages appeared to have higher deposited calcium than non treated samples on day 7 and 14, still no significant difference was observed between two groups on day 1 and 5 pc. Interestingly, ps 12 picked slightly darker stain colour than ps 5 in all three conditions from day 5 onward.

DNA assay results indicated identical proliferation trends for both passages as in all three experimental groups and passages total DNA remained stable from day 8 to day 14 (Figure 3.15 a). Average hES-MPs cell number dropped by 42% on day 21 pc but, nearly doubled within 7 days to reach around 12,000 cells on day 28 pc. No statistical significance between passages or experimental conditions was reported. Furthermore, ALP activity level peaked on day 14 pc in both passages and groups and reduced by 90% to 0.00024 on day 21 pc (Figure 3.15 b). In both passages microspheres treated with osteogenic media showed significantly lower ALP activity level compared to other conditions ($p < 0.0001$) but, passage 5 ALP level showed 63% lower activity than passage 12. These findings were in disagreement with ALP staining results that showed very low to no extra cellular ALP level on day 14 pc and higher activity level on days 5 and 7 pc, while, no activity was detected with ALP fluorescent assay on day 6 pc in any passage conditions.



(a) (b)

Figure 3.15: Characterisation of hES-MPs/collagen microspheres behaviour in ps 5 and 12, a: cell proliferation of hES-MPs was assessed over 28 days pc using DNA pico green, b: total Alkaline phosphatase activity level was investigated by ALP fluorescent kit over 21 days pc, * indicates statistical significance, (*** p <0.0001). Data is mean ± SD n=9.

3.3.7 2D versus 3D hES-MP cell culture

2D culture of hES-MP cell line was compared with 3D seeded hES-MPs in bovine collagen I microspheres to identify the effect of 3D soft environment in osteogenic differentiation of stem cells with and without interfering of chemical stimulation. The results of alkaline phosphatase staining indicated that chemical stimulation of hES-MPs enhanced early ECM ALP activity compared to other experimental group (Figure 3.16). Stem cells cultured in osteogenic media expressed higher intensity of purple ALP stain from day 6 while, exhibition of ALP in non-treated FGF-β samples was noticeable only from day 14. Treated samples with FGF-β however, did not pick any ALP stain over 28 days experiment suggesting no osteogenic differentiation in that group.

Mineralisation of hES-MPs was assessed by Alizarin red staining of all three conditions (Figure 3.17). Those hES-MPs cultured in osteogenic media presented higher stain intensity and deposited calcium compared to other groups over 28 days, while, as expected, 2D samples that were treated with FGF-β showed no mineralisation. Chemical stimulation encouraged calcium deposition from day 6, yet manifestation of mineralisation started from day 21 in non treated FGF-β samples.

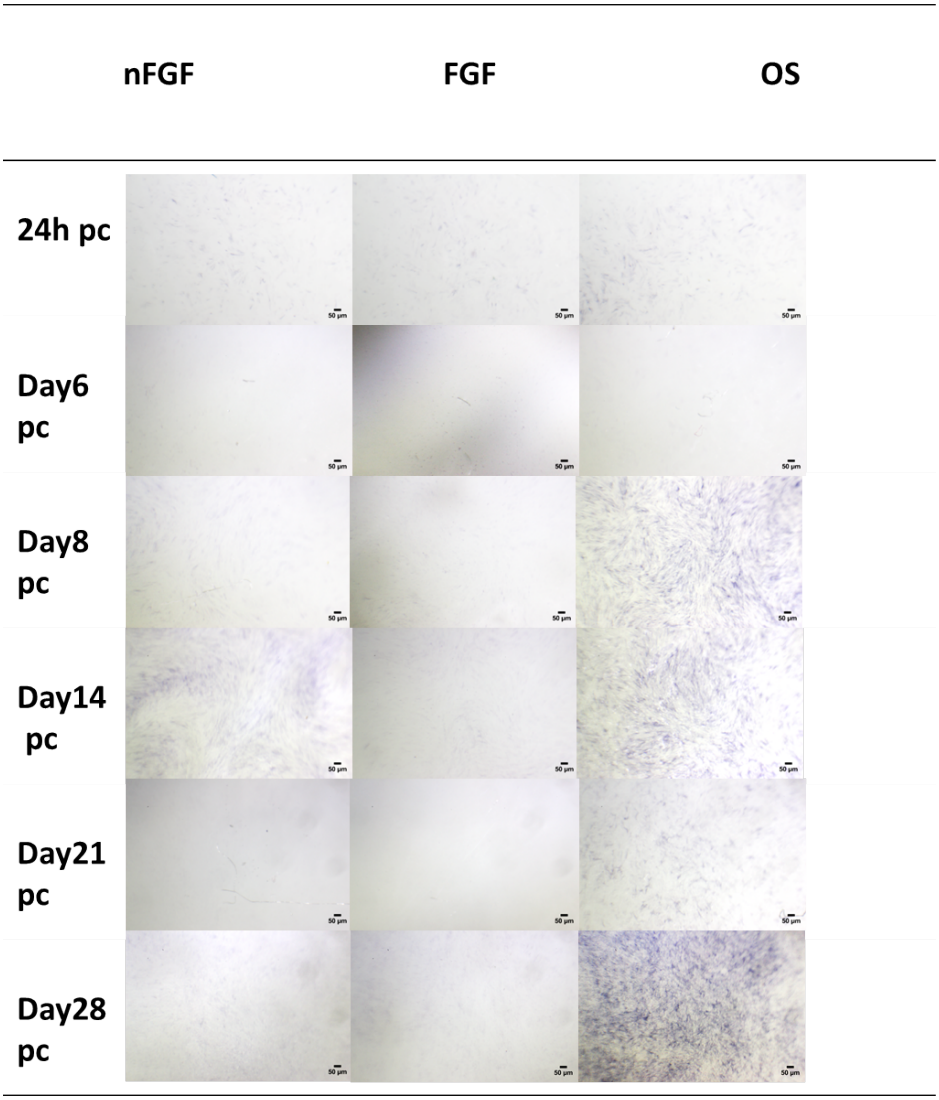


Figure 3.16: Alkaline phosphatase staining of 2D culture of ps 5 hES-MPs was assessed in three conditions of added FGF-β, nFGF-β (control media with no treatment) and cultured in osteogenic media (OS media) over 28 days. Ostegenic media treated samples showed higher deposition of ALP stain from day 8 pc onward. All images taken by light microscope, 10x.

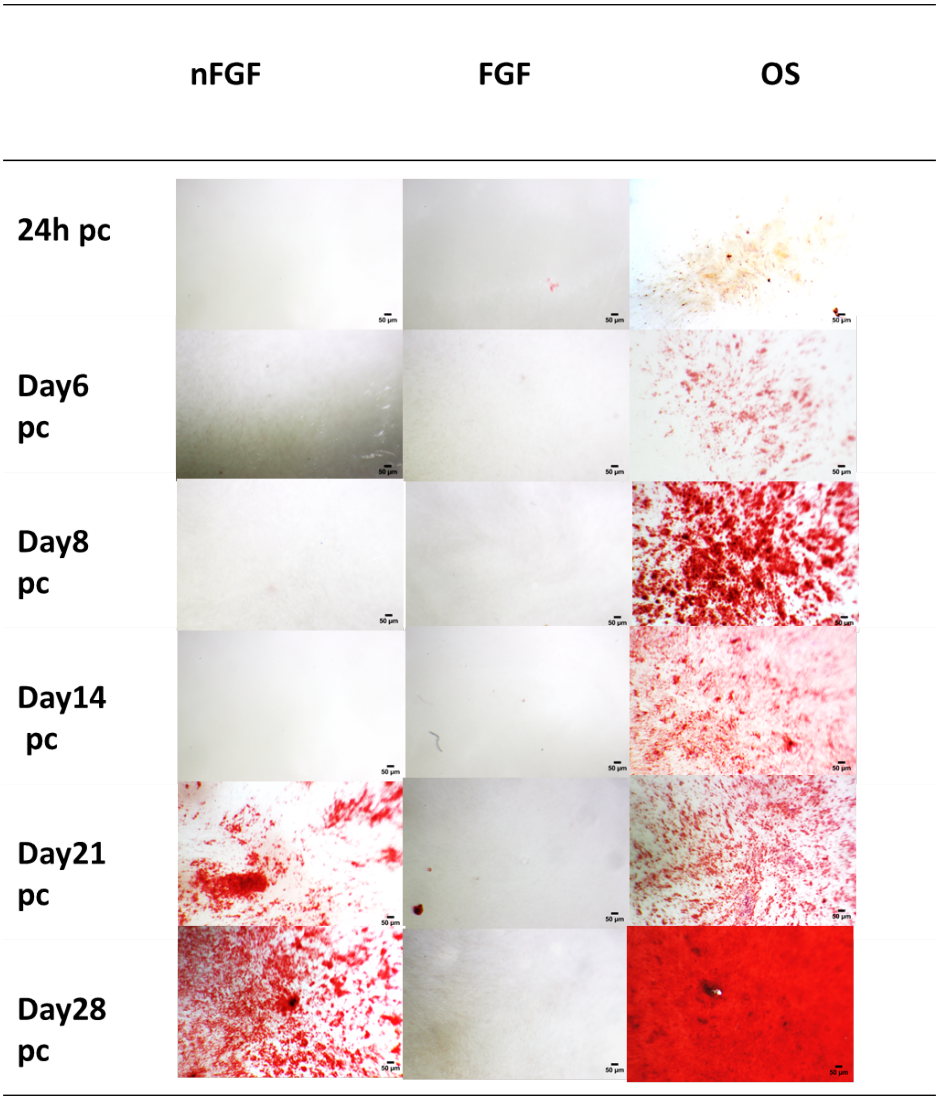


Figure 3.17: Alizarin red staining of 2D culture of ps 5 hES-MPs was examined in three conditions of added FGF-β, nFGF-β (control media with no treatment) and cultured in osteogenic media (OS media) over 28 days. Ostegenic media treated samples showed higher deposition of ALP stain from day 6 pc onward. All images taken by light microscope, 10x.

Total alkaline phosphatase activity of non treated FGF-β hES-MPs in 2D and 3D culture of seeded collagen I microspheres were evaluated and compared over 28 days as shown in Figure 3.18. Although the ALP level of both 2D and 3D culture were the same at 24 h pc (0.001), 2D culture showed greater activity level of alkaline phosphates after day 6. Enzyme activity increased up to day 28 in 2D samples, but in 3D samples ALP level peaked to 0.002 on day 14 pc before dropping to 0.0014 on days 21 and 28 pc. On day 28 pc, the normalised value of ALP in 2D samples was 5 times higher than 3D samples ($p < 0.05$).

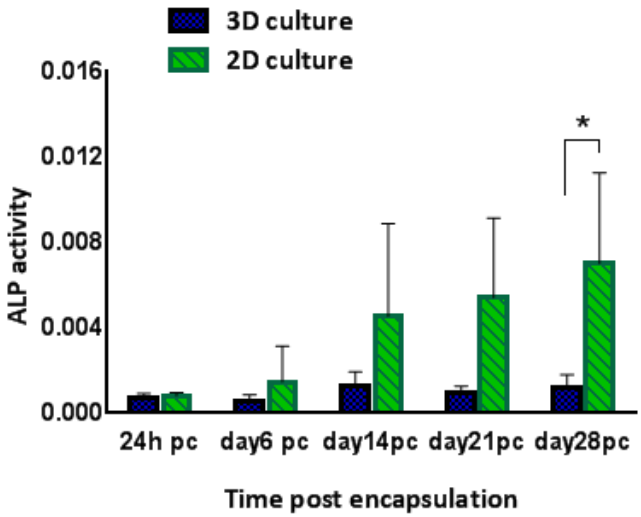


Figure 3.18: Total alkaline phosphatase activity of hES-MPs 2D culture was compared with seeded hES-MPs collagen microspheres over 28 days pc using ALP fluorescent kit,* indicates statistical significance, (* $p < 0.05$). Data is mean ± SD n=9.

3.4 Discussion

A variety of collagen concentrations and seeding cell densities were examined for optimum viability of hES-MPs and MG63 cell lines within low concentrations of bovine collagen I gel and to characterise cells behaviour (proliferation, migration and differentiation) in the 3D soft environment. Cell seeded collagen microspheres were produced successfully and both cells lines showed good survival and growth rate in their new environment. Different chemical stimulations were applied to fully characterise the progenitor cells behaviour in 2D and 3D environment. The results of this study indicated that collagen concentration, hence cells micro-environment mechanical properties, are important factors in the viability and proliferation of seeded cell on collagen microspheres. It also showed that undifferentiated and differentiated cells respond differently to the stiffness of their environment as hES-MPs adapted well with lower concentration of rat tail and bovine collagen I (1.5-2 mg/mL) compared to MG-63 cells. MG-63s on the other hand needed stiffer environment for their fully differentiated cellular stage and only grew on highest collagen concentration used in this experiment (3 mg/mL). These results are in agreement with the works published by Chan et al. and Hong et al.[119,120] that showed collagen concentration of 2 mg/mL for proliferation of MSCs and 3.5 mg/mL for human breast cancer cell line MDA-MB-231.

Microsphere cell seeding density was observed to be important in cell survival and growth process too. Higher cell concentration of both cell lines did not survive in their new environment and died within the first 24 h pc. Seeded cells with

concentration of 1×10^6 cells/mL showed optimum results in both hES-MPs and MG-63 cell lines. These findings are in agreement with Chan et al. study that showed optimum cell viability with cell density of 1×10^6 cells/mL[120].

Encapsulated hES-MPs contracted more significantly (43%) in comparison with MG-63 cells (15%). Contraction in both cell lines was not substantial between day 0 and day 3 and MG-63s showed more steady contraction between day 3 and 7 pc, while Chan et al. and Li et al. studies reported that contraction of collagen/MSCs were most significant within the first 30 h of pc[120,164]. hES-MPs/collagen microspheres proliferation results showed that cell growth reduced by up to 18% between 24 h and 120 h pc and then steadily increased which suggested that hES-MPs needed to remodel their new environment in order to survive and proliferate. The synergy between decreasing the cell number and no notable contraction indicated cell contraction is vital for their existence and elongation and proliferation in the new soft micro environment.

More elongated cell morphology was observed in MG-63s than hES-MPs. One possible explanation would be terminally differentiated MG-63s selectively proliferated on higher stiffness of collagen scaffold that applied more local strains to the cells compared with hES-MPs less stiff environment. Both cell lines showed enhanced cell-cell networks in microspheres peripheries 72 h after seeding with cell clustering that was observed from day 21 pc onwards. Cell concentration seemed to be more important than collagen concentration in microsphere contraction. As results indicated, collagen droplets with cell seeding density of 1200 cells/5 µL droplet and collagen concentration of 2 mg/mL contracted up to 15% within the first 30 h of gelation while, droplets with lower cell number showed a delayed (96 h pc) and less significant contraction (750 cells/5 µL, 8%).

Comparison between bovine and rat tail collagen I fibres micro structure presented similarities between two species. Both hES-MPs seeded collagen microspheres showed more amorphous structure and less organised collagen fibres compared to seeded samples. hES-MPs were added before polymerisation of collagen to the master mix which suggests that cells possibly digested and reorganised collagen fibres in a more random manner for their growth and viability. Nevertheless, more sample imaging for different time points and several areas/focal planes within each sample is needed to comment more accurately on the effect of species variability in cell triggered remodelling of collagen fibres.

Passage number did not have a major effect on cells contractibility and proliferation. Stained hES-MPs in both passage number expressed earlier and higher ALP activity in the presence of osteogenic media that started from day 5 post en-capsulation while, nFGF-β treated samples picked stain from day 7 onward. Nevertheless, results of fluorescent ALP assay was not in agreement with alkaline phosphatase staining as measuring ALP activity level suggested much less activity level in the presence of osteogenic media on days 14 and 21 pc. Although, both passage numbers manifested similar trend for ALP activity, with a peak of ALP on day 14 and significant drop on day 21 pc, the results also indicated that enzyme activity of passage 5 hES-MPS in osteogenic media was up to 63% lower in passage 12 on day 14 pc.

Mineralisation in different passages of seeded hES-MPs in collagen I was assessed by Alizarin red staining and presented higher deposited calcium in osteogenic media treated samples compared to other experimental groups. Chemical stimulation of microspheres favoured mineralisation by encouraging earlier and higher deposition of calcium which started from day 5 pc, yet non-treated samples with FGF-β expression of mineralisation began from day 7 pc onward and 1 week earlier than treated FGF-β microspheres.

To further characterise the behaviour of hES-MPs, ALP activity and mineralisation were compared in 2D and 3D cell cultures, that showed quite similar results in both conditions. Chemical stimulation forced early ECM ALP level and mineralisation as well as higher expression of deposited calcium and enzyme activity in both 2D and cell seeded microspheres, that initiated from day 5 pc. Yet again, samples that were treated with FGF-β in both groups presented lowest ALP level and mineralisation in all time points as was expected due to inhibition of differentiation which occurred in the presence of FGF-β. Interestingly, quantification of ALP activity revealed much higher enzyme level in 2D samples with continuous increase between 24 h and day 28 pc, but, seeded hES-MPs/microspheres presented a peak of ALP level on day 14 that dropped substantially by day 21 pc. One explanation would be delayed mineralisation in 2D culture because of consistently high level of ALP after day 14 whereas, mineralisation of hES-MPs begin soon after day 14 and complete by day 28 pc in 3D environment which was shown by very low level of ALP activity after day 14 pc. Nonetheless, our findings for ALP activity level in 2D culture is similar to the ALP level stated in Reilly et al. study that showed static 2D culture exhibited stable enzyme level between day 14 and 21 pc[165].

Furthermore, in a study that was carried out by Arpornmaeklong group ALP activity level of human embryonic stem cell-derived mesenchymal stem cells (hESC-MSCs) cultured in 2D, 3D collagen scaffold and osteogenic media was investigated[166]. The total ALP level of 2D culture in stem cell media and ostegenic media indicated much higher enzyme activity in the presence of osteogenic media on day 14 and 28 compared with non treated samples. Also, hESC-MSCs seeded in collagen scaffold in osteogenic media presented highest ALP activity level in comparison with 2D osteogenic media treated and non treated cells but there was no report of enzyme level of hESC-MSCs seeded in collagen scaffold without chemical stimulation[166]. The findings of this study on the effect of osteogenic media on 2D qualitative ALP activity level through ECM ALP staining were in agreement with Arpornmaeklong et al. results. However, comparing 2D and 3D culture was not possible due to lack of data presented on enzyme level in hES-MPs seeded in collagen scaffold.

3.5 Conclusions and future work

Collagen microspheres can act as an efficient cell supporting system, providing high viability and proliferation efficiency in hES-MPs post encapsulation. A variety of collagen concentrations and seeding cell densities were examined to achieve the best condition for viability and proliferation of hES-MPs and MG-63 cell lines. As there was no significant difference in collagen I microstructure between two species and bovine collagen I can be purchased at lower cost, it was chosen over rat tail collagen I. Cell/collagen microspheres were built successfully and both cell lines showed good survival and long term growth in their new environment while, hES-MPs collagen microspheres presented significantly higher contraction over MG-63 seeded collagen beads. Alkaline phosphatase activity and mineralisation were assessed in three groups of: treated with osteogenic media, treated with FGF-β and non treated FGF-β samples and our results indicated earlier and higher expression of ECM ALP and mineralisation in the presence of osteogenic media. In addition, cellular behaviour of hES-MPs 2D and 3D cultures were compared to identify the effect of 3D environment on mineralisation of stem cells. Interestingly, ALP activity showed much higher enzyme level in 2D samples with continuous increase between 24 h and day 28 pc compared to the peak of ALP level on day 14 pc in seeded hES-MPs/microspheres.The results of Alizarin red and ALP staining also showed higher accumulation of deposited stains in 3D culture of hES-MPs compared with 2D culture which suggests collagen 3D environment

stimulate/enhance early differentiation and mineralisation of hES-MPs. This study findings suggested that embedded hES-MP cells in collagen microspheres exhibited overall lower ALP over 28 days pc with a peak on day 14 pc while, ALP level was constantly higher in 2D culture and remained more or less stable during same period of time. Low and high passage of hES-MP cell line were compared to ensure that characteristic of these cell lines was consistent with change in passage number.

Nonetheless, stiffness of cell micro-environment can not provide all the necessary signals for full osteogenic commitment of hES-MPs and the role of other factors such as surface topography, porosity, mechanical and biochemical stimulations should also be considered to draw a more detailed and accurate map for interaction of cells with their environment. Also, optimization of collagen microsphere stability by coating techniques is needed to increase the collagen beads efficiency in supporting long term growth of stem cells. Also, evaluation of collagen biodegradability is necessary in future clinical application of microspheres as animal model and human implants.

4

Design of a microfluidic chamber for cell compression

4.1 Introduction

Current approaches for generation of mechanical stimulation imply dynamic bioreactor culture systems, for in vitro culture and differentiation of tissue engineering constructs. Compared with static bioreactor system, dynamic bioreactors can enhance the mass transport of nutrients to the cells. In addition, cells that are subjected to the mechanical stimulation of dynamic media flow showed augmented osteogenesis and mineralization[157]. Because of bioreactors bulkiness and their limitation in processing large number of samples at the same time, microfluidic devices are ideal to overcome these restrictions and improve the overall efficiency of dynamic bioreactor systems. Many studies have reported the numerous applications for microfluidic systems in biochemical analysis, chemical reactions, and in cell-based assay[116,118].

The advantage of using this system over conventional bench-top systems includes reduced size of operating systems, its flexibility in design modification, lower reagents consumption, lower wastes production and power requirements to operate, its disposability, increased speed of analyses, and system portability. One key factor in designing a functional microfluidic device is the type of material used for the fabrication of the device. This material should be economical and compatible with micro-fabrication techniques, while being perfectly matched with micrometer-scale structure and allowing the integration of functional components. In addition, the chamber should enable chemical and mechanical stimulation of cells in a controlled environment, while reducing the overall volume of the systems

enabling both reduction in cost and possibility of high throughput testing.

Popular polymers that have been used to fabricate microfluidic systems include: poly-dimethyl siloxane (PDMS), polyurethane, polyvinyl chloride, poly methyl methacrylate (PMMA), polyethylene terephthalate glycol (PETG), polycarbonate, polyethylene and, polystyrene[82]. Soft-polymeric systems, particularly systems made in PDMS, present many desirable properties for use in microfluidic devices. Soft lithography is a commonly used technique in fabrication of PDMS which involves elastomeric polymer molding by rapid prototyping of microfluidic devices[158]. PDMS made devices are easily integrated with outside components due to compatibility of this polymer with most materials. Because of its temperature stability in biological ranges (40-95 °C) PDMS have vast applications in processes requiring temperature gradient. PDMS optical transparency has made it compatible with conventional imaging techniques and optical detection methods in the visible and UV region. PDMS channels are perfectly suited for protein, cell based and biological assays due to their permeability to gases and their non-toxic nature. A couple of of PDMS properties may be unfavourable in some applications including: its elastomeric nature that may cause shrinkage or sagging of device feature[159]. In addition PDMS incompatibility with many organic solvents affects the non-specific adsorption in biological samples, but can be rectified by improving its surface chemistry[121]. Soft lithography technique is currently moving towards commercialization with using PDMS microfluidic chips to develop DNA, protein, and cell-based assays accompanied by fabricating the microfluidic analytical systems which is indeed an indication of great growing area of interest in polymeric microfluidic systems.

Microfluidic systems are used in a wide range of applications in many fields including biology, drug discovery, chemistry, food and cosmetics. Microfluidic techniques can be used in production of micro droplets that offer extremely consistent size of droplets, particles or emulsions. Microfluidics allows production of highly monodisperse droplets, emulsions, double emulsions, bubbles or particles and as well as performing chemical and biochemical reactions in droplets. Droplets size range from 1-100 µm with exceptionally high control and reproducibility from research to production scale and resulting droplets can be used as micro reactors to create complex formulations. Application of micro droplets include: encapsulation of cells, DNA or magnetic beads for research, analysis and diagnostics protein crystallisation, drug delivery and drug formulation. In addition, microfluidics are

widely used in cell isolation, analysis of individual cells from a population and analysis of small numbers of cells, or rare cells in a population[82].

This study aim was to stimulate osteogenesis of hES-MPs seeded collagen microspheres by applying solely mechanical loading. Microfluidic device was chosen as one mean of mechanical conditioning of cells which can offer a highly compatible microfluidic system for parallel processing of MSCs aggregation. Such a system would allow optimizing mechanical stimulation and fluid flow regime critical in mediating hES-MPs osteogenic differentiation. The method was developed following an iteration process where the microfluidic chamber was optimized through various steps which are described in each section. Microfluidic systems are mainly used in analysis of 2D cell culture and up to date there is no report of conditioning and analysing of 3D cell seeded constructs by such systems, therefore one of the objectives of this projects was to design a microfluidic device to apply mechanical stimulation to the cell seeded microspheres.

4.2 Methods

Loading protocol, experimental conditions and during of the applied mechanical stimulation on cell seeded collagen microspheres are summarized in Figure 4.1.

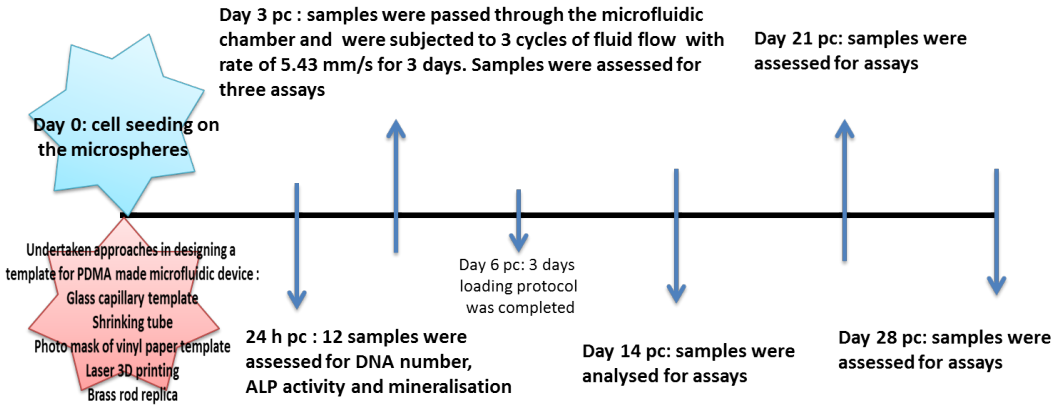


Figure 4.1: Schematic of various undertaken approaches in designing a PDMS made microfluidic chamber, loading/flow rate protocol and duration of experiment.

4.2.1 Fabrication of microfluidic chamber by glass capillary template

Capillary glass with inner diameter of 1 mm was pulled to 0.7, 0.6 and 0.5 mm using thin walled borosilicate glass micro-electrodes, manufactured with a Narishige PP830 vertical pipette puller. PDMS from Sylgard 184 was prepared by mixing a ratio of 10:1 of base to initiator. The resulting mixture was then stirred and degassed in a vacuum for 15 min and was poured on glass and left for 2 h at room temperature (RT) to set.The capillary glass was then removed from PDMS mold.



Figure 4.2: Vertical pipette puller, Narishige PP830

4.2.2 Fabrication of a microfluidic chamber using shrinking tube

Heat shrinking tube (Pro power HS510-1.22M, I.D=1.55 mm) was cut to 2 cm length pieces and heated to 120 °C for 30 s and pulled from both sides to create around 0.5 mm tube at the centre. PDMS was poured on top of the tube and left to solidify for 2 h at RT.

4.2.3 Fabrication of microfluidic chamber using play dough

Children play dough was covered with plastic food wrap and shaped into a main channel of around 1 mm and narrow middle channel of 0.5 mm using a pin roller. The template was baked at 110 °C for 15 min and cooled down at RT for 30 min. PDMS was poured over the dough and left for 2 h at RT to set. The dough was pulled out from PDMS mold by making small cut using surgical blade and tweezers.

4.2.4 Fabrication of microfluidic system by vinyl paper template

The geometry of chamber was drawn by inkscape software and consisted of 14 repeats of main channels (D=1 mm) with 2.5 mm length and 14 repeats of narrow channels (D=0.5 mm, L=2.5 mm) as shown in Figure 4.3. Dxf file of the drawing was loaded in ROBO Master Pro software that was connected to a Graphtec craft ROBO pro S cutter. Six vinyl papers were fixed on top of each other to provide the desired height of around 0.5 mm for the channels. Applied force for cutting was adjusted to 28 g, speed=2 mm/s and offset was set at 0. After cutting, the vinyl papers were adhered to a glass slide which its side lines were taped with 1 mm tickness sellotape. PDMS with 0.9 mm thickness was then poured into the created space and another glass slide was put on the top with 2 kg weight to apply necessary force for PDMS to fill the gaps between channels. PDMS curing took about 24 h at RT and vinyl paper was peeled off from cured PDMS.

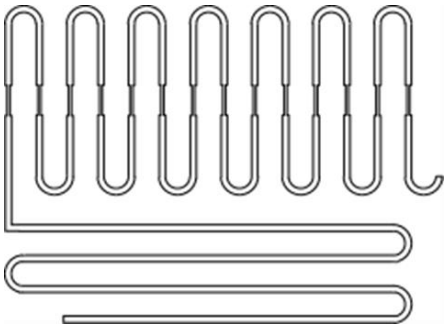


Figure 4.3: Geometry design of microfluidic chamber using inkscape software which contains 14 repeats of 1 mm diameter main channels with the length of 2.5 mm and 14 repeats of narrow channels (D=0.5 mm, L=2.5 mm).

4.2.5 Fabrication of rapid prototyping and photo mask of vinyl paper template

Vinyl paper template was created as described in section 4.2.4. But the main chamber template was removed from vinyl paper and the opposite part was adhered to a glass slide. A bigger glass slide (152 mm, 114 mm) was prepared by sticking 0.5 mm thick sellotape around its edges and was then treated with PEG. The template glass slide was placed on top of PEG treated slide to create a photo mask and was subjected to UV light 62% for 15 s and then, the PEG treated slide

was rinsed with methanol. This slide was used as a template to make PDMS chamber consequently.

4.2.6 Fabrication of microfluidic chamber via laser 3D printing

Initial geometry consisted of a main channel of 1 mm width and constricted channel of 0.5 mm as presented in Figure 4.4.

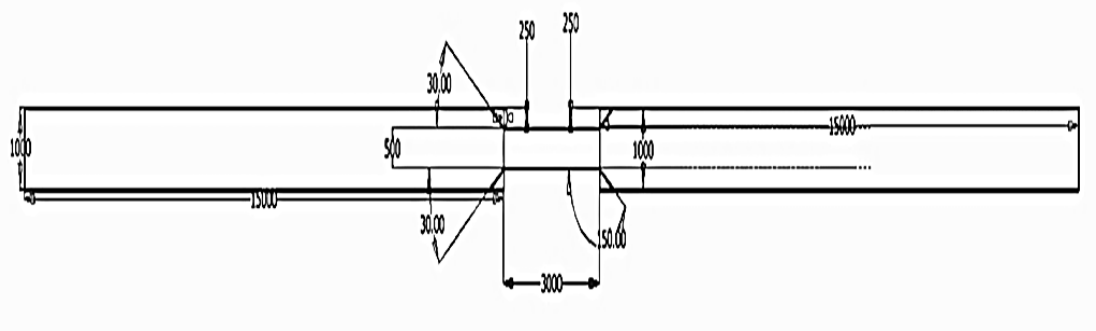


Figure 4.4: Geometry design of microfluidic chamber that contained a main channel (I.D=1 mm) and a narrow channel (I.D=0.5 mm).

The chamber optimised geometry was created using SolidWork software (2012 x64 Edition) and consisted of 10 repeats of main channels (I.D=1 mm) with 7.83 mm length and 10 repeats of narrow channels (O.D=0.75 mm, I.D=0.5 mm, L=7.68 mm) as shown in Figure 4.5.

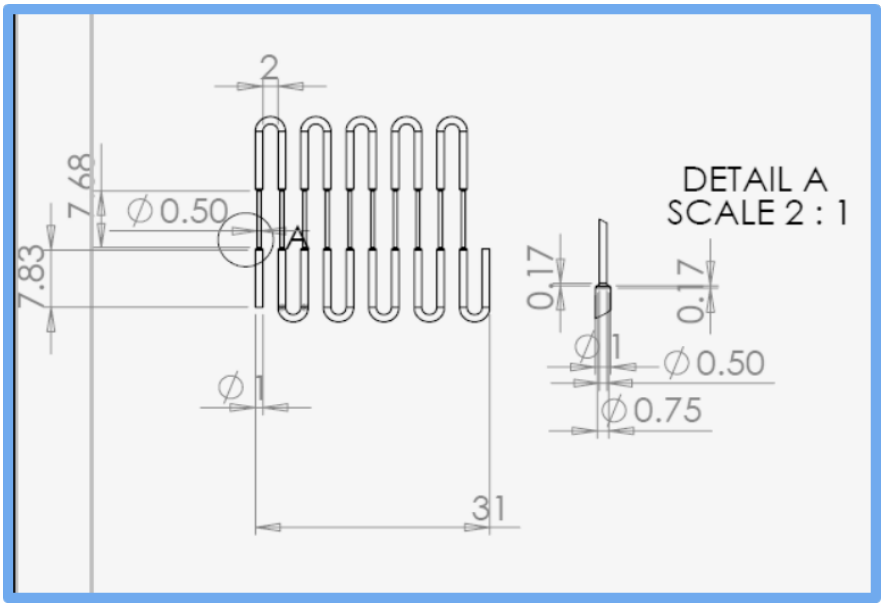


Figure 4.5: Geometry design of microfluidic chamber by solid work software that contained 10 repeats of 7.83 mm long main channels (I.D=1 mm) and 10 repeats of 7.68 mm long narrow channels (O.D=0.75 mm, I.D=0.5 mm).

4.2.6.1 Photo-curable monomer preparation

Photo-curable PEG was prepared by mixing PEG monomer (MW=258, sigma Aldrich) with 4% w of 1:1 photo-initiator blend of Diphenyl (2,4,6 trimethylbenzoyl) phosphineoxide and 2 hydroxy 2 methylpropiophenone.

4.2.6.2 UV laser set up

A UV laser (355 nm wavelength) was expanded and stabilised before being passed through a 10x microscope objective onto a motorised stage. The motorised stage could move in the x, y and z directions and was programmable using G-code. A well was made on a glass slide, which controlled the depth of the structure, and the photo-curable PEG was added to the well. The stage was programmed to write the outline of the Figure 4.4 creating a walled chamber. PEG was washed from the sample using methanol. PEG was then added to the channel and cured under a 150 W mercury lamp for 30 s. The manufacturing of the laser 3D print template was carried out by Dr Frederik Claeyssens group at the Kroto Research Institute in the Department of Materials Science and Engineering, University of Sheffield.

4.2.6.3 PDMS molding of microfluidic chamber

To prepare PDMS a ratio of 10:1 of base to initiator was mixed together. The silanising agent tridecafluoro-1h,1h,2h,2h-tetrahydrooctyl trichlorosilane was added to the surface of laser printed mold by vacuum deposition for 20 min. The PDMS was then poured on the mold containing slide in a container, which controlled the total thickness to 14 mm. The PDMS was cured at 60 °C for 3 h and then peeled and removed from the slide. A 2 mm biopsy punch was used to create the input/output channels. The polymer channel was then bound irreversibly to a glass slide using an air plasma machine at 50 W for 2 min. Flexible silicone tubes (2 mm external diameter and 0.5 mm internal diameter) were inserted into the channels to pump the calculated flow to the chamber using 5 ml syringes and syringe pumps. 70% ethanol was passed through the chamber several times and rinsed with PBS before overnight treatment with 1.5 mg/ml bovine serum albumin (BSA).

4.2.6.4 Flow regime and calculation of shear stress

Flow rate was initially set to 8.49 mm/s, to pump the collagen microspheres in to the microfluidic chamber which was later reduced by 20% to 6.79 mm/s and further 20% decrease to 5.43 mm/s using equation below.

$$\dot{m} = \rho \times v \times A \tag{4.2.1}$$

When $\dot{m}$ is mass flow rate kg/s, ρ is density kg/m^3, v is flow velocity mm/s and A is cross−sectional vector area/surface m^2

4.2.7 Fabrication of injected PEG as a template for microfluidic chamber

After making the 3D template with UV laser and being washed with methanol, PEG was poured on top of the mold and cured under a UV light for 15 s. The mold was treated with PEG again using capillary needle to carefully inject PEG drops on top of mold and cured under the UV lamp. This step was repeated several times to achieve the desired height of template. The PEG treated mold then was kept over night at RT and treated with silanising agent before adding PDMS. The PDMS was cured at 60 °C for 3 h and removed from the mold.

4.2.8 Fabrication of a microfluidic chamber by using brass rod replica

In the new design the chamber geometry was improved and optimised by eliminating both the main and repeats of compression channels. The optimised model consisted of only one constricted channel which was up to two times longer than the initial design (13-15 mm). Variety of brass rods with diameter ranging from 0.6 mm to 0.9 mm were used as a template to create microfluidic chamber. This diameter range enabled to build more specific channel for each experiment, according to the collagen microspheres contraction and their average diameter on day 6 post encapsulation, which minimised the inter-variability of average microspheres diameter in or between each experiment and repeats. Consequently, more unified compression forces would be delivered to cell seeded microspheres. The chamber template was placed at the bottom of a Petri dish and was fixed to two cylindrical shape PDMS segments by grips to provide a more horizontal and flatter mold. PDMS then was poured into the Petri dish and left to cure overnight at RT. The metal rod was taken out of PDMS by making very small cuts close to the inner surface of PDMS-rod. 2 mm holes were punched on the PDMS surface to create input/output, then as previously described, PDMS channel was sealed irreversibly to a glass slide using air plasma machine. 3 mL syringes were inserted directly to the chamber input/output channels and connected to the syringe pump.

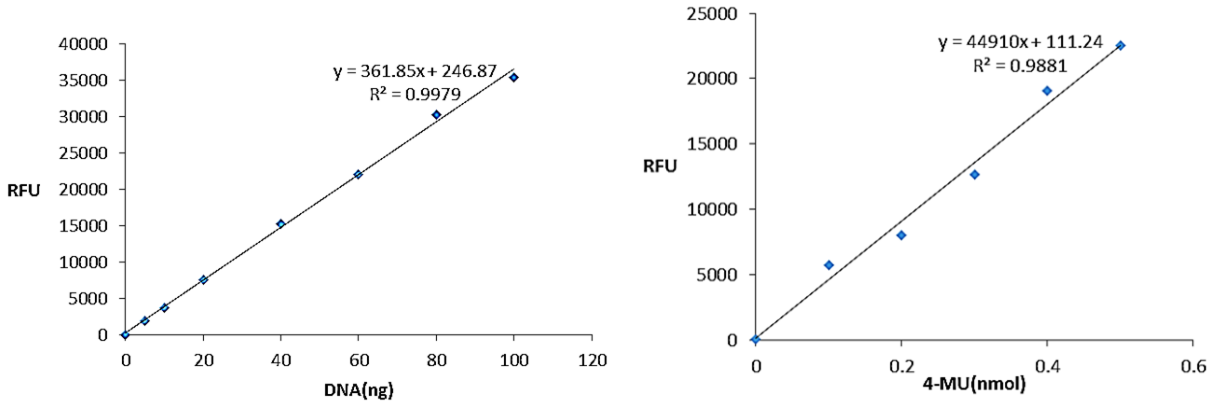
Flow rate was set to 8.49 mm/s to pump the microspheres containing media through the chamber.

4.2.9 Cell culture

Two cell types were used in this study; Human osteosarcoma-derived cell lines (MG-63s) and human embryonic cell-derived mesenchymal progenitor cell line hES-MP 002.5 (hES-MPs). hES-MP cells were used between passages 3-7. Both cell lines seeding density were 5×10^5 cells/mL that were embedded on collagen microspheres with bovine collagen I concentration of 2 mg/mL and 3 mg/mL.

4.2.10 Cellular assay

Cell viability and total DNA measurement were determined using DNA pico-green assay at 24 h, days 6, 14, 21 and 28 pc as shown in Figure 4.6.



(a) (b)

Figure 4.6: Standard curve of a; DNA pico green and b; ALP 4-MU that was employed to analyse hES-MPs viability and early stage mineralisation marker.

Cell growth and proliferation of MG-63 cell line of free floating controls versus compressed samples, were assessed using presto blue assay at time 24 h, days 3, 4, 5, 6, 7 pc and standard curve shown in Figure 4.7.

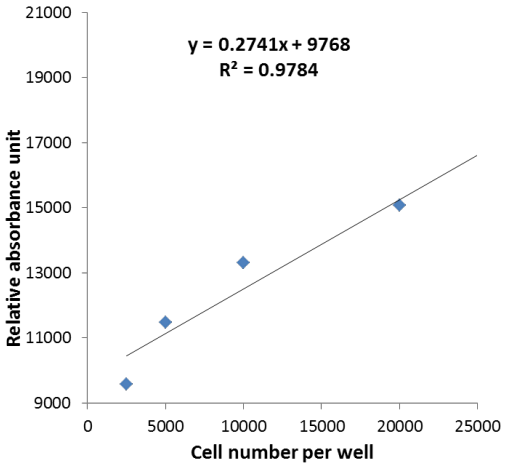


Figure 4.7: Standard curve of presto blue assay used to evaluate MG-63 cell viability at different time points.

Cell seeded collagen morphology, calcein AM and ethidium homodimer-1 stains were used to visualise live and dead cells on day 9 pc by fluorescent microscope (Nikon Ti-E).

ALP activity of hES-MPs was measured at 24 h, days 6 ,14, 21 and 28 pc. Quantification of deposited calcium was measured by 1% Alizarin red S staining at 24 h, days 6, 21 and 28 pc via ICP-ES. Samples were digested in 5% w/v perchloric acid and were diluted by 10 fold prior to analysis. Samples then were

mixed with 1% w/v nitric acid with ratio of 1:1 in the eppendorf tubes. Samples volume were brought to around 10 mL and the torch was turned on. An intense electromagnetic field was created within the coil by the high power radio frequency signal flowing in the coil. Instruments run at 40 mHz and the argon gas flown through the torch.
The argon gas was then ionized in the intense electromagnetic field and flows in a particular rotationally symmetrical pattern towards the magnetic field of the RF coil. A peristaltic pump deliverd an aqueous or organic sample into an analytical nebulizer and changed it into mist and introduced directly inside the plasma flame. The sample immediately collides with the electrons and charged ions in the plasma and was broken down into charged ions. The various molecules break up into their respective atoms which then lose electrons and recombine repeatedly in the plasma, giving off radiation at the characteristic wavelengths of the elements involved.

Phosphorous level of extra cellular matrix was assessed at 24 h, days 6, 21 and 28 pc by ICP-ES.

4.2.11 Statistics

All experiments were performed three times in triplicates (n=9). PDMS chambers visualisation by bright field filter were performed on two or three samples of each condition during experimental repeat. Cell viability at different time points, ALP and mineralisation comparison as well as statistical differences between free floating and compressed samples were completed using one-way ANOVA followed by Sidak‘s multiple comparisons test.

4.3 Results

4.3.1 Fabrication of microfluidic chamber using glass capillary, shrinking tubes or dough as a template

. PDMS molds using capillary glass, shrinking tubes and playing dough templates were produced and the micro structure of each channel was assessed under the microscope using bright field filter and objective 4x lens. As shown in Figure 4.8, the microscopic image of capillary glass made chamber revealed the remains of smashed glass stuck in the restrained channel and scratched the channels inner wall. PDMS chamber was flushed with PBS several times to remove the glass

pieces and debris but proved impossible to eliminate the broken glasses without severely damaging the microfluidic chamber.

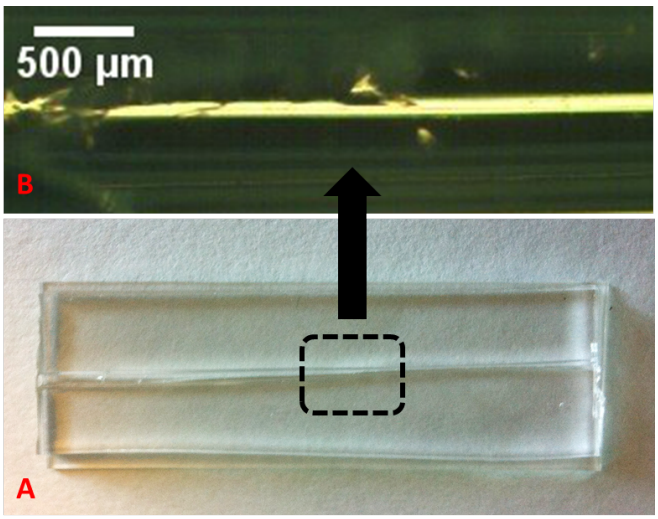


Figure 4.8: A; Capillary glass molded in PDMS, B; microscopic image of chamber micro structure bright filed filter 4x.

Microscopic images of PDMS chamber using shrinking tube as a replica presented severe rupture caused during the tube removal process which negatively affected the geometry of the designed channel. PDMS was ripped and generated uneven holes and grooves in the inner surface of both main and constricted channels, therefore increasing the chance of collagen microspheres damage while being trapped in the chamber (Figure 4.9).

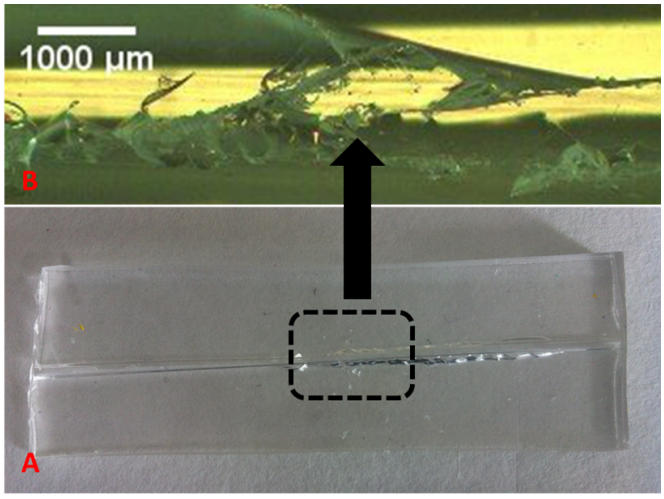


Figure 4.9: A; shrinking tubes molded in PDMS, B; microscopic image of chamber micro structure bright filed filter 4x.

Although removing the play dough from PDMS seemed less challenging, the resulting design lacked the smoothness needed for the inner channel surfaces.

Microscopic images of the chamber showed the presence of micro grooves and structures caused by uneven dough surface. Despite all the effort that was done to make a smooth template, removing the cling film left scratches and marks on the dough that was consequently transferred to the PDMS. Also controlling the geometry of both channels proved to be challenging therefore, this design was discarded (Figure 4.10).

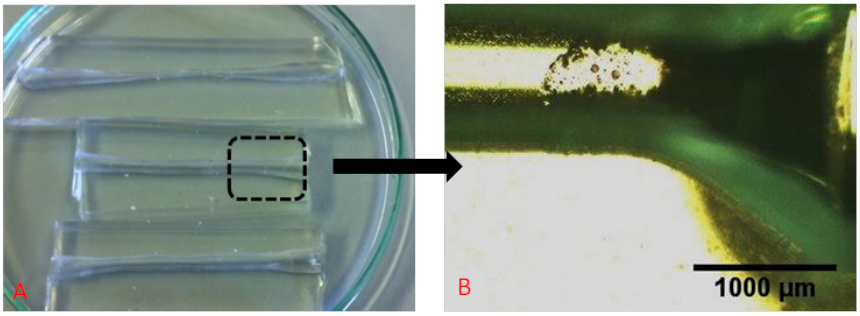


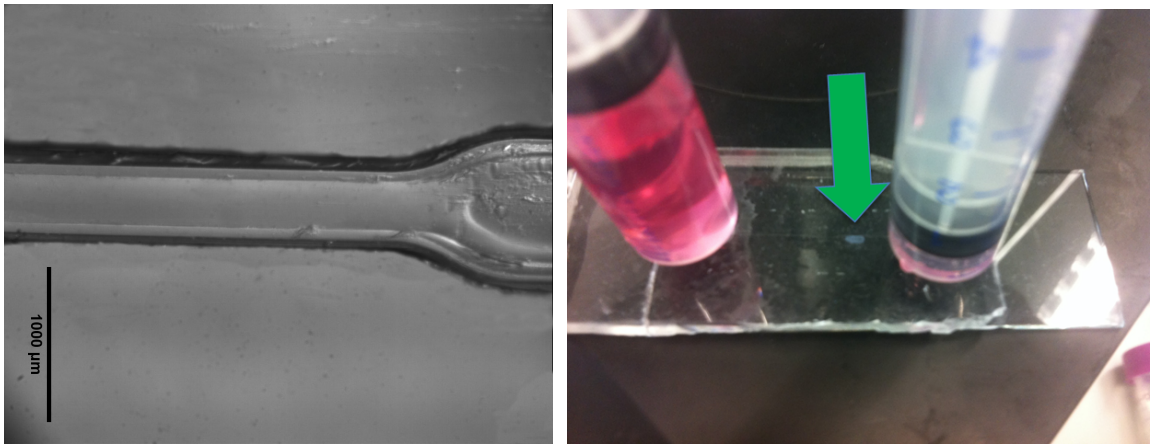
Figure 4.10: A; PDMS made chamber using play dough as a template, B; Microscopic image of chamber micro structure bright filed filter 4x.

4.3.2 Fabrication of microfluidic chamber via laser 3D printing

The microfluidic chamber that was made with laser 3D printing presented the most smooth inner and less channel surface among previously presented approaches with the least PDMS rupture as shown in Figure 4.11.

4.3.2.1 Compression of cell seeded collagen microspheres using microfluidic chamber

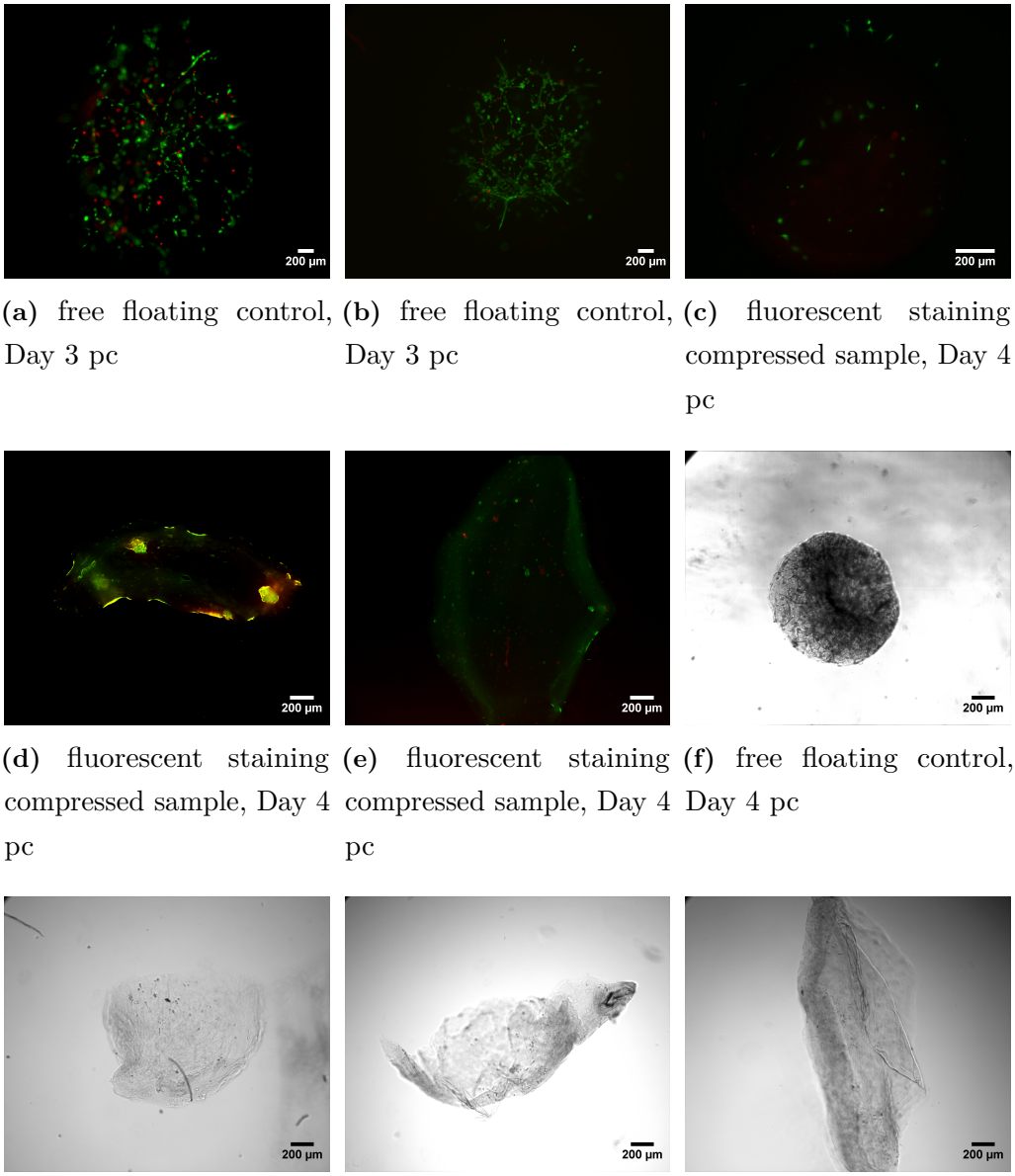
Twenty MG-63s seeded collagen microspheres were passed through the microfluidic chamber on day 3 pc. The initial fluid flow of 0.4 ml/min, equal to 8.49 mm/s, was used to push the microspheres through the channels. Average diameter of collagen microspheres was measured around 1.2 mm and cell viability and collagen integrity were assessed under the microscope as presented in Figure 4.12.



(a) **(b)**

Figure 4.11: a; microscopic images of PDMS chamber made by laser 3D printing, b; compression of collagen beads by being passed through microfluidic chamber

As shown in Figure 4.12, applying only one compression cycle caused rupture of collagen microspheres and cells to present round morphology. This finding revealed that the high flow rate could disrupt the collagen fibre structure which led to leakage and migration of MG-63 cells from collagen scaffold into the media. Furthermore, images of fluorescent staining proved that the cell viability was reduced considerably 24 h after the first day compression cycles and collagen morphology disrupted irreversibly.



(a) free floating control, Day 3 pc

(b) free floating control, Day 3 pc

(c) fluorescent staining compressed sample, Day 4 pc

(d) fluorescent staining compressed sample, Day 4 pc

(e) fluorescent staining compressed sample, Day 4 pc

(f) free floating control, Day 4 pc

(g) compressed sample, Day 4 pc

(h) compressed sample, Day 4 pc

(i) compressed sample, Day 4 pc

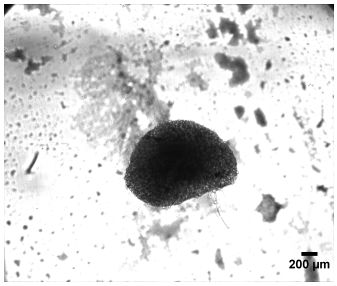
Figure 4.12: Microscopic images of viable MG-63s on day 3 pc before and 24 h after being subjected to flow rate of 0.4 ml/min using fluorescent live and dead stain and phase contrast microscopy. (g)-(i) shows collagen microspheres damage after being subjected to flow rate compared with free floating control (f). Scale bars for (a)-(i) are 200 µm.

4.3.2.2 Effect of optimisation of fluid flow rate on cell proliferation

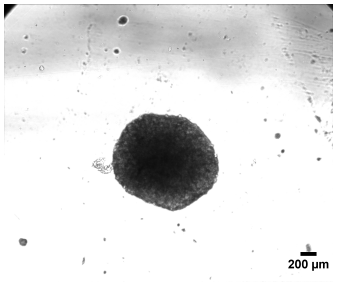
Fluid flow rate was reduced by 20% to 0.32 ml/min equivalent to 6.79 mm/s and cell viability and proliferation of seeded MG-63 cells was evaluated by fluorescent microscopy and presto blue assay. Microscopic images of compressed samples

showed intense fluorescent signal of live MG-63s 24 h after applying the first compression cycle. In contrast, control microspheres emitted stronger fluorescent signal of live cells and also showed less cell mortality. There was no evidence of collagen being torn by passing through the chamber and the scaffold retained its original round morphology as shown in Figure 4.13.

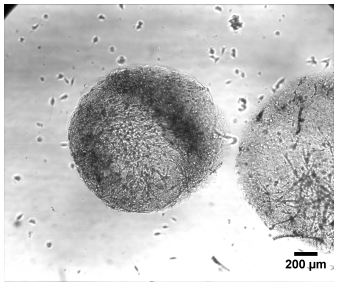
The compression cycles were applied for the following two days and cells viability of both control and compressed samples were assessed 24 h after each experiment and continued till day 7 pc. The results of fluorescent staining on day 5 and 7 revealed MG-63s substantial growth with more elongated morphology in comparison with day 4 pc while compressed samples emitted weaker fluorescent signal than free floating controls in both days (Figure 4.14). In addition, collagen microspheres shape remained spherical and no damage was observed on collagen bead's structures.



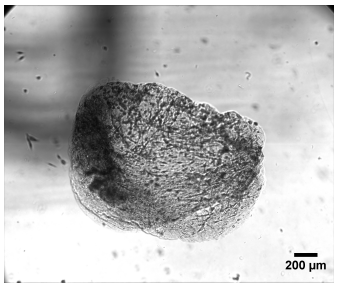
(a) free floating control, Day 5 pc



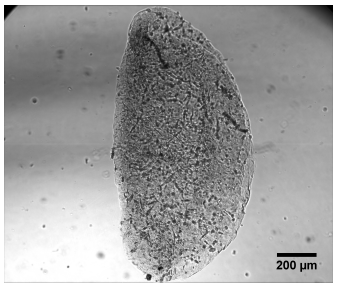
(b) free floating control, Day 5 pc



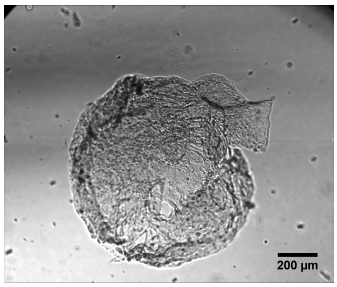
(c) free floating control, Day 5 pc



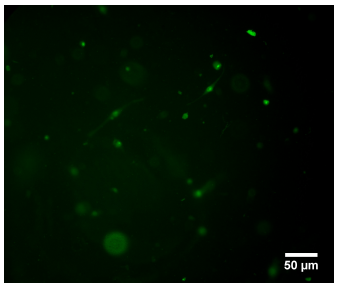
(d) free floating control, Day 5 pc



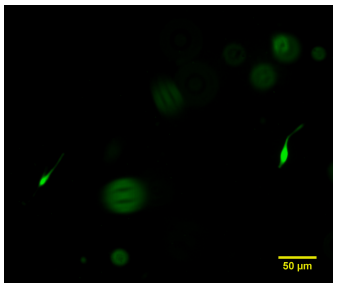
(e) compressed sample, Day 6 pc



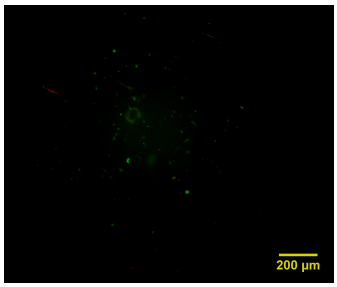
(f) compressed sample, Day 6 pc



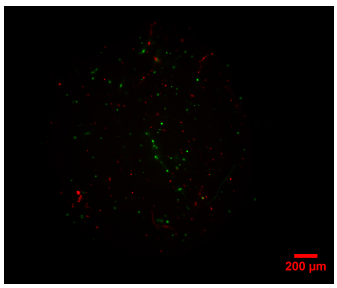
(g) fluorescent staining compressed sample, Day 6 pc



(h) fluorescent staining compressed sample, Day 6 pc

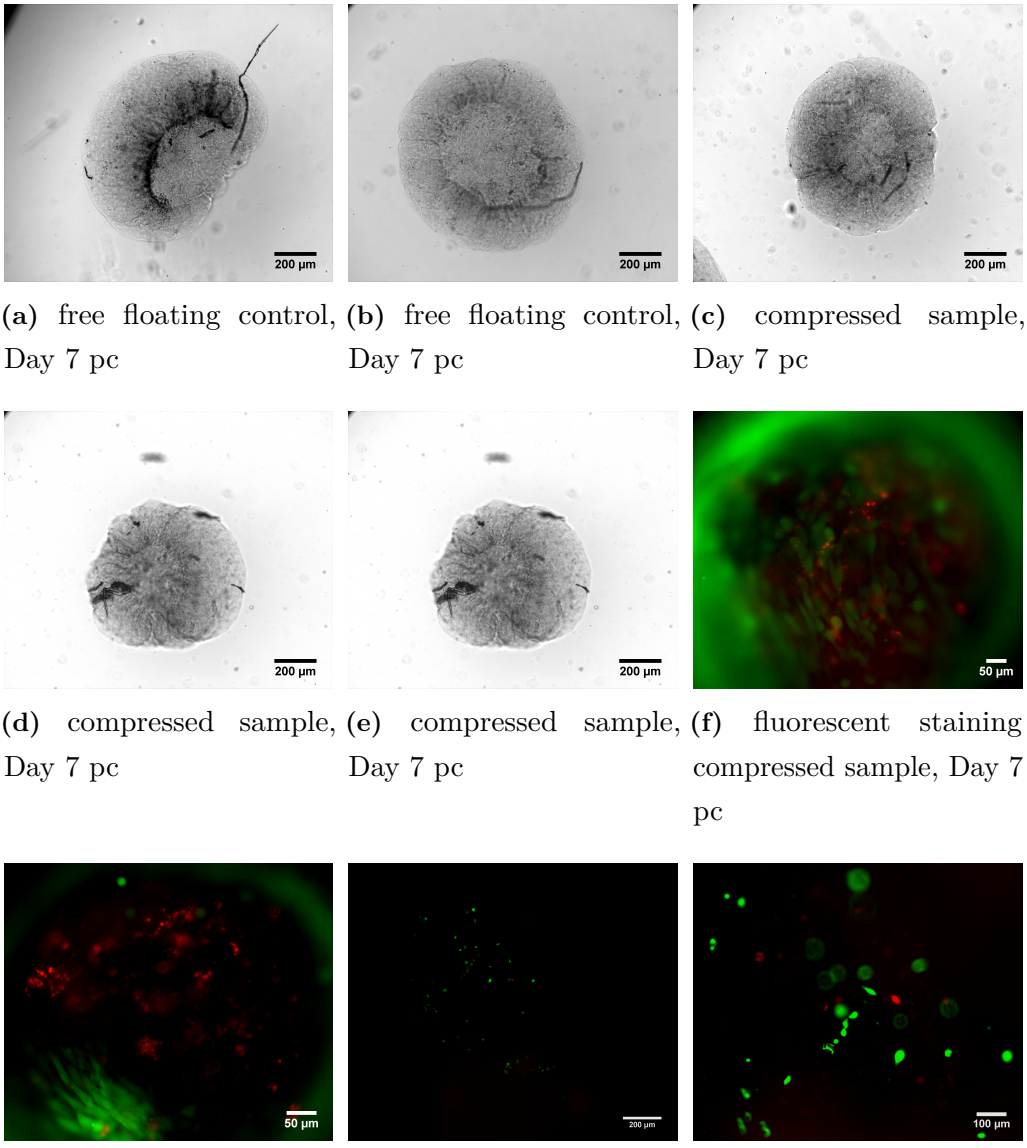


(i) fluorescent staining compressed samples, Day 6 pc



(j) fluorescent staining compressed samples, Day 6 pc

Figure 4.13: Microscopic images of viable MG-63s on day 5 pc before and 24 h after being subjected to flow rate of 0.32 ml/min. (a)-(f); phase contrast microscopy, scale bars are 200 µm, (g)-(i); live and dead fluorescent images of cell seeded microspheres, scale bars are 50 µm.



(a) free floating control, Day 7 pc

(b) free floating control, Day 7 pc

(c) compressed sample, Day 7 pc

(d) compressed sample, Day 7 pc

(e) compressed sample, Day 7 pc

(f) fluorescent staining compressed sample, Day 7 pc

(g) fluorescent staining compressed sample, Day 7 pc

(h) fluorescent staining compressed sample, Day 7 pc

(i) fluorescent staining compressed sample, Day 7 pc

Figure 4.14: Microscopic images of viable MG-63s on day 7 pc that were subjected to fluid flow compared with free floating controls. (a)-(e); phase contrast microscopy, scale bars are 200 µm, (f)-(i); live and dead fluorescent images of cells, scale bare for (f) and (g) are 50 µm and for (h) and (i) are 100-200 µm.

These findings were further confirmed by results of cell viability assay as shown in Figure 4.15.

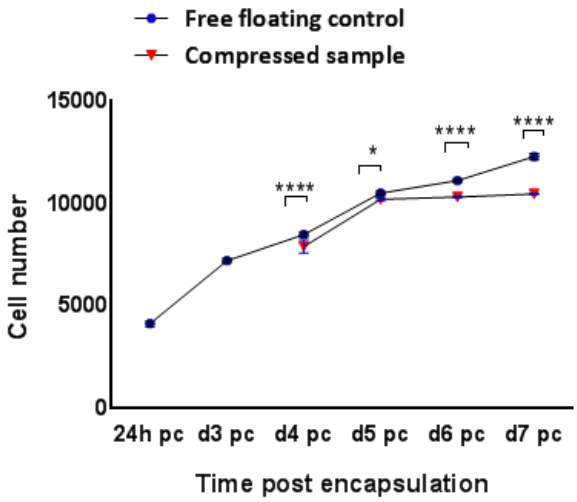


Figure 4.15: Cell viability of MG-63s seeded collagen microspheres. Comparison of compressed samples vs free floating controls using presto blue assay from 24 h to day 7 pc, * indicates statistical significance, (* p <0.01, **** p <0.0001). Data is mean ± SD for 9 samples.

Cell viability increased in both controls and samples over 7 days pc. Cell number enhanced remarkably by 31% from 8490 cells on day 4 to around 12 300 cells on day 7 in free floating controls compared to 24% rise in compressed sample over the same period of time. Compressed samples viability versus controls indicated significant drop of nearly 7%, 24h after application of first compression cycle (p <0.0001) while this gap reduced to only 3% on day 5 and expanded to 7% again on day 6 pc. Also, the number of cells in compressed samples considerably declined (15%) on day 7 in contrast to free floating controls (p <0.0001). Interestingly, cell viability of compressed samples showed a steady growth of around 3% from day 5 to day 7 whereas the viability of free floating controls increased significantly by 15% after completion of compression regime. Overall, compressed samples remained viable and could survive the compression cycles without disruption of collagen beads structure.

Despite good cell viability results, the collagen microspheres showed tendency to attach to the constricted channel and occasionally were required higher flow rate or an external force to be removed out of the chamber (Figure 4.16).

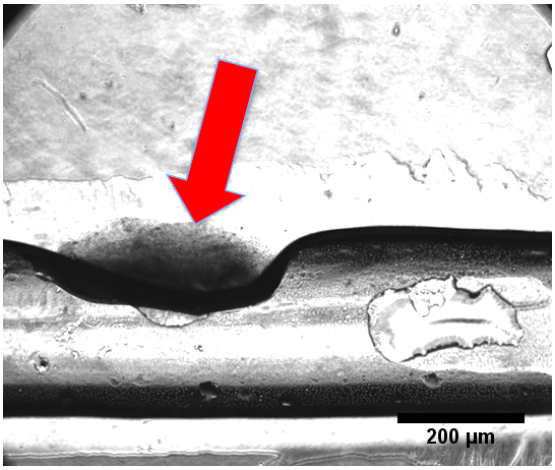


Figure 4.16: Collagen microspheres trapped in the constricted channel of microfluidic chamber objective 4x.

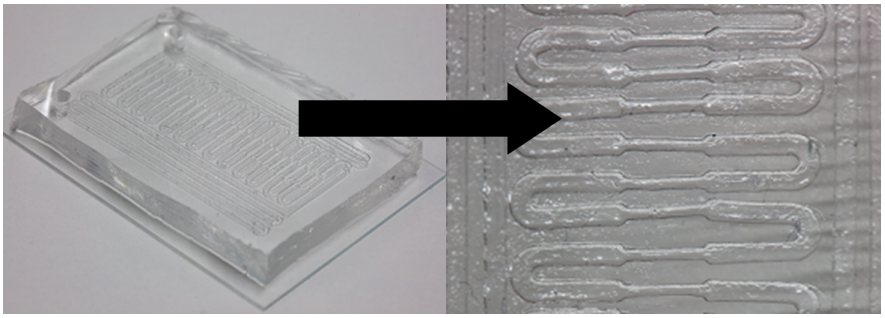
Reducing fluid flow to lower rate caused entrapment of collagen beads inside the narrow channel and made it impossible to move them through the chamber without permanent damage of collagen morphology and escalating MG-63s mortality. Therefore, an improved design of chamber was needed to tackle the challenge of microspheres being stuck to PDMS chamber and enhancing the microfluidic system efficiency by combining several chambers together. The advantage of such a system was to minimise the number of cycles and therefore, reduce the risk of cell infection, collagen destruction and handling during each experiment run.

4.3.3 Optimisation of chamber design

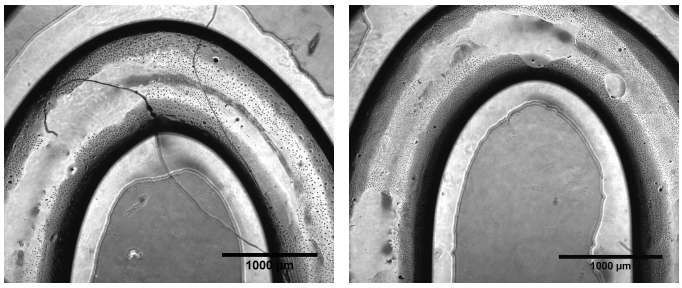
4.3.3.1 Enhancing the geometry via laser 3D print

The new chamber design consisted of multiple repeats of main and narrow channels which enabled reducing the compression cycles number as shown in Figure 4.17. Despite all the effort to make a more efficient chamber and to avoid collagen beads entrapment to the channel, several associated issues with the microfluidic chamber made it incompatible for the experimental purposes. The new chamber presented micro-grooves, and uncured PDMS near the narrow part of the chamber generated uneven surface structure in the inner wall of chamber. This rough surface structure of PDMS then caused severe entrapment of collagen beads and ruined the hydrogel geometry. Chemical treatment of the 3D template with vapour acetone did not improve the roughness. In addition, alteration of design caused insufficient gap

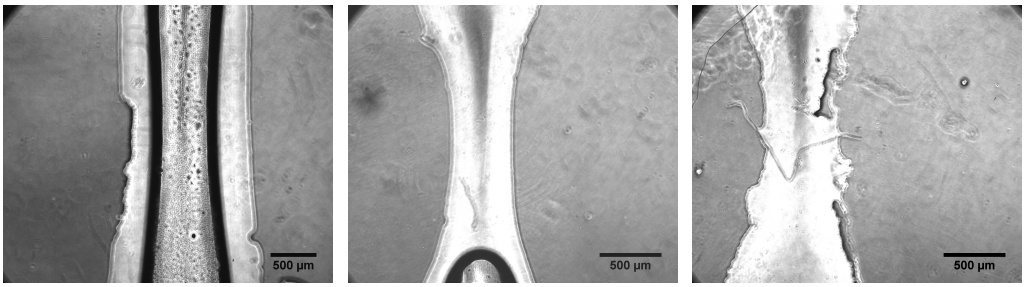
between each channel of chamber and appearance of the uncured parts in PDMS template that resulted in inadequate binding of the new mold to the glass slide through plasma binding. Consequently, the unsealed chamber triggered multiple leakage in the chamber during the experiment. Also, the channel's height of the new design could not reach the desired 3D dimension because of the limitation of laser print technique and therefore, did not exceed 0.4 mm. This defect of chamber geometry generated partially to fully blocked channels, especially in the narrow part of PDMS chamber and created further blockage of microspheres in the channel.



(a)



(b) channel's arch **(c)** channel's arch



(d) open channel **(e)** partially closed channel **(f)** fully closed channel

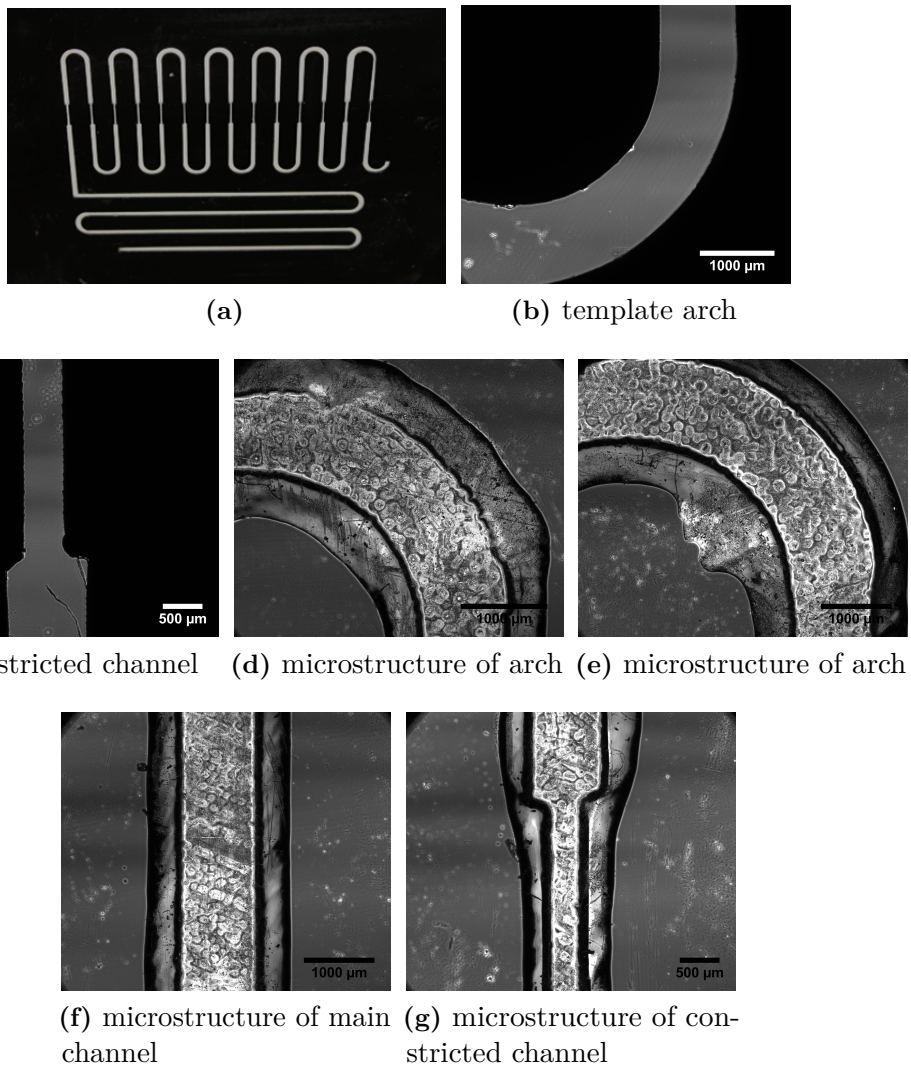
Figure 4.17: PDMS microfluidic chamber was made by laser 3D printing and its microstructure, a; PDMS chamber consisted of 14 repeats of main and restricted channels, images b-f show appearance of micro grooves, uneven inner surface on the channels and partially to fully blockage of narrow channels caused by uncured PDMS. Scale bars for (b) and (c) are 1000 µm and for (d)-(f) are 500 µm.

4.3.3.2 Rapid prototyping and photo mask of vinyl paper template

Vinyl paper was used as template to alter the rough inner surface of PDMS microfluidic chamber and to correct the channel's height. Although binding 6 vinyl papers together increased the height of the PDMS chamber from 0.4 mm to 0.52 mm in comparison with 3D template, yet again it failed to achieve the required height of 0.7 mm or more for the channels. This was due to the limitation of cutter machine to make precise cuts on thicker sheets and as shown in Figure 4.19, zigzag patterns were created on the wall of template and PDMS mold. For the same reason, the excess vinyl paper could not be fully removed without damaging the template and as result some parts of template remained blocked that was copied in to the PDMS replica and generated inconsistent and asymmetrical design for the microfluidic chamber. Furthermore, as indicated in images (f) and (g) of Figure 4.19, the inner surface of fabricated channels lacked the essential smoothness needed for the chamber as both main and narrow parts of PDMS channels were filled with micro patterns and grooves. Therefore, presence of micro patterns were not in favour of collagen microspheres passage through the chamber. The opposite part of vinyl paper template was used as mold in UV photo mask technique to improve the height and evenness of microfluidic chamber (Figure 4.19). The resulting silicon replica was very fragile and removing it left several breaks and missing pieces of PDMS in the chamber, which made it impossible to fully bind to the glass slide (Figure 4.18). Also, channels height did not surpass the rapid prototyping method and overall this technique was unsuccessful to improve the microfliudic chamber design.



Figure 4.18: Broken and missing parts in PDMS chamber caused by application of UV photo mask technique and vinyl paper template.



(a) **(b)** template arch

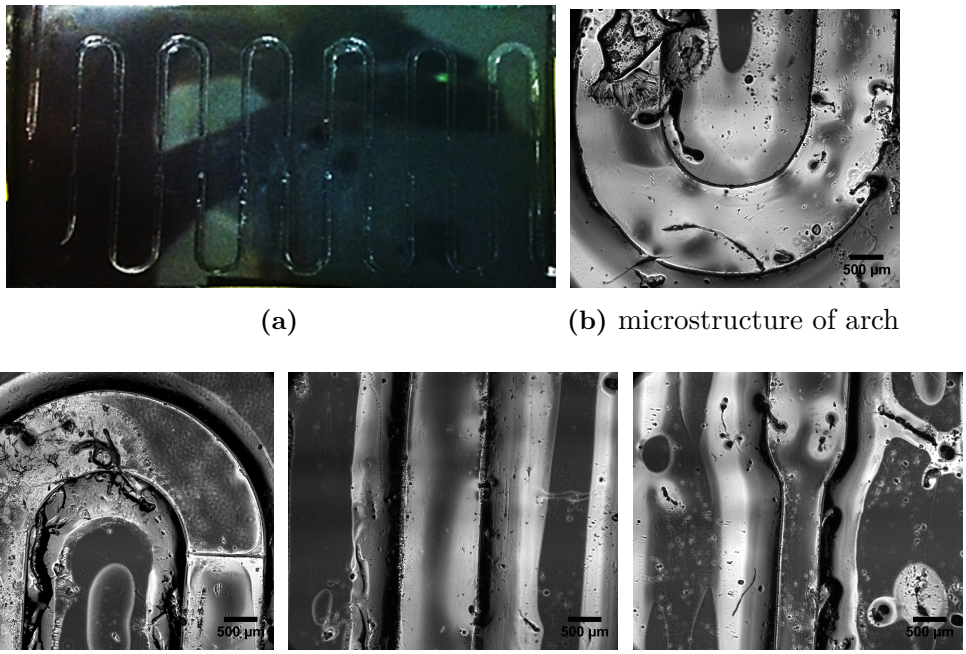
(c) constricted channel **(d)** microstructure of arch **(e)** microstructure of arch

(f) microstructure of main channel **(g)** microstructure of constricted channel

Figure 4.19: Vinyl paper used as a template to create microfluidic chamber. Images b-g show micro patterns and groove on the inner surface of template. Scale bars for (b), (d)-(f) are 1000 µm and for (c) and (g) are 500 µm.

4.3.3.3 Optimisation of chamber design via injected PEG method

Injected PEG method was employed to improve height and roughness of the microfluidic chamber. Injecting PEG layer by layer to the 3D print template remarkably enhanced the height from 0.4 mm to 0.6 mm. Despite the increase, channels height was not consistent through the 14 repeats and as shown in Figure 4.20, channels got thicker from left to right. This was due to the manual injection of PEG layers to the channels surface along with PEG overflow in thicker areas of template. Microscopic images of template surface indicated uncured PEG patches in some parts especially in the arch of template and confirmed the irregularity in channels height. Nevertheless, injected PEG technique did not improve the development of microfluidic chamber and this approach was not further used for the experiment.



(a) **(b)** microstructure of arch

(c) microstructure of arch **(d)** microstructure of main channel **(e)** microstructure of constrained channel

Figure 4.20: Vinyl paper template and UV photo mask were used to create microfluidic chamber. Scale bars for (b)-(e) are 500 µm.

4.3.3.4 Application of metal rod template in optimisation of chamber design

Metal rods with variety of outer diameter were used as a template to build microfluidic chamber. The resulting PDMS chamber solely consisted of one compression channel that was cylindrical and channel's height precisely matched the diameter

(Figure 4.21). Microscopic images of inner wall surface presented much smoother microstructure in comparison with other applied techniques. Elimination of the main channels along with the enhanced 3D geometry and smooth inner walls resulted in uninterrupted passage of microspheres through the channel without being stuck to the PDMS. In addition, measuring the average diameter of collagen beads on day 6 pc, facilitated fabrication of a unique chamber for each experiment that ensured all beads would be subjected to more uniform compression force. Therefore, by using the new design, the variability between experimental repeats has been greatly minimised.

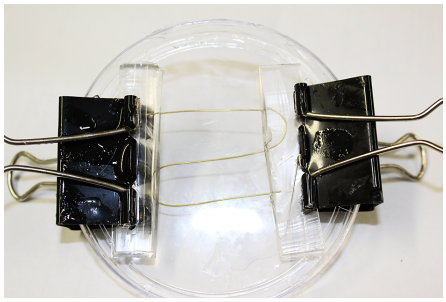
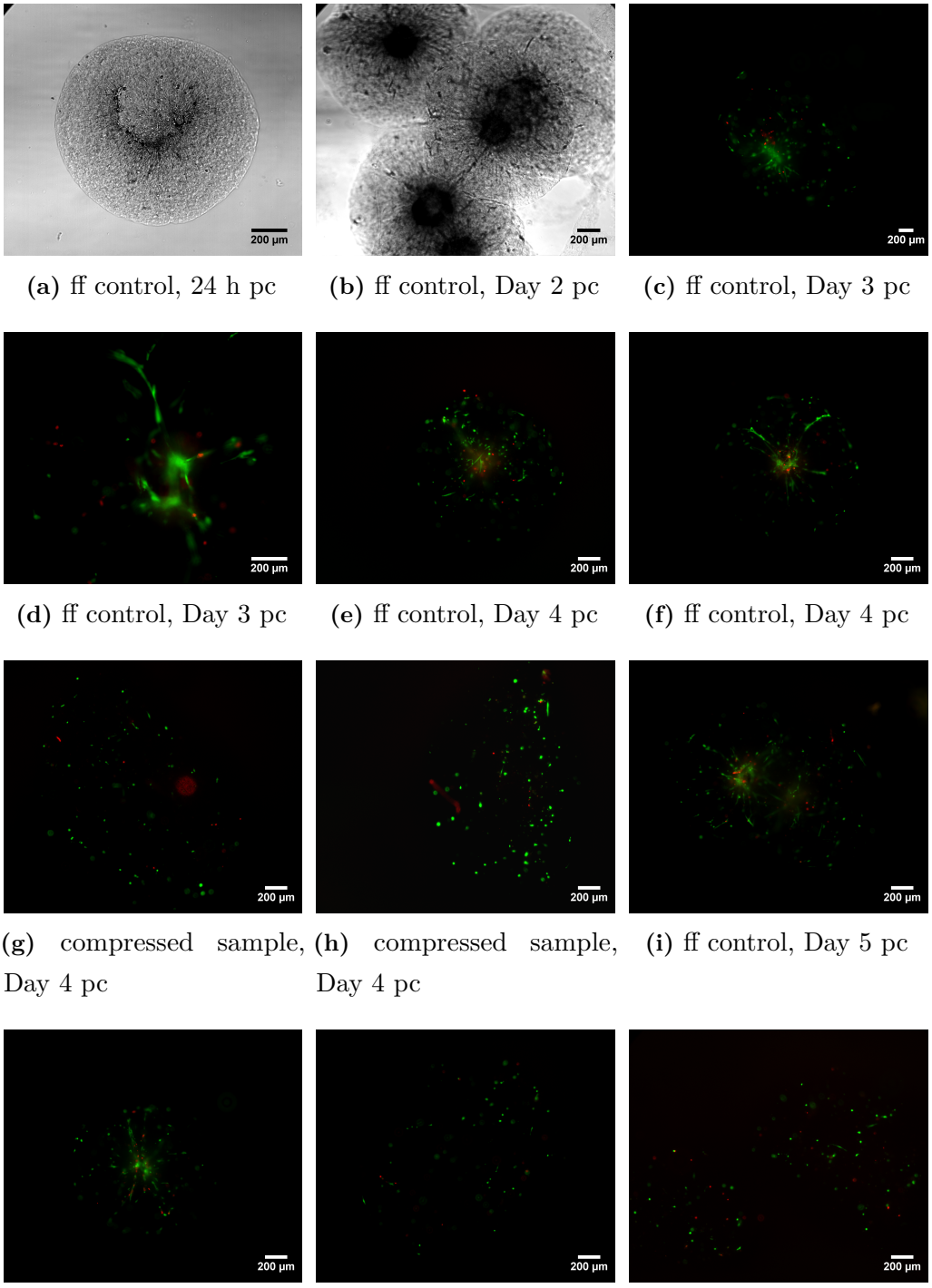


Figure 4.21: Metal rod was used as a template to fabricate PDMS microfliudic chamber.

4.3.4 Assessment of hES-MPs viability in microfluidic experiment

Microscopic images of compressed samples and free floating controls were compared to evaluate the seeded hES-MPs viability. Cell viability was maintained in both controls and samples over 8 day pc as presented in Figure 4.22 and Figure 4.23. Fluorescent staining of controls and samples during experiment revealed that hES-MPs subjected to 3 days compression cycle stayed alive and presented rounded morphology as opposed to more elongated cell form in free floating controls. Nonetheless, compressed cells stretched out to reach similar extended shape and size of free floating cells after completion of the microfluidic experiment on day 8 pc. Analysis of collagen microspheres integrity and structure showed stable and slightly out of shape morphology in compressed sample during and 48 h after being subjected to last compression cycle. Still free floating control microspheres presented more spherical and contracted form with more expended cells over 8 days pc. No visible damage of collagen beads was observed when exposed to compression and collagen fibres structure of samples and controls remained uniformly unchanged.



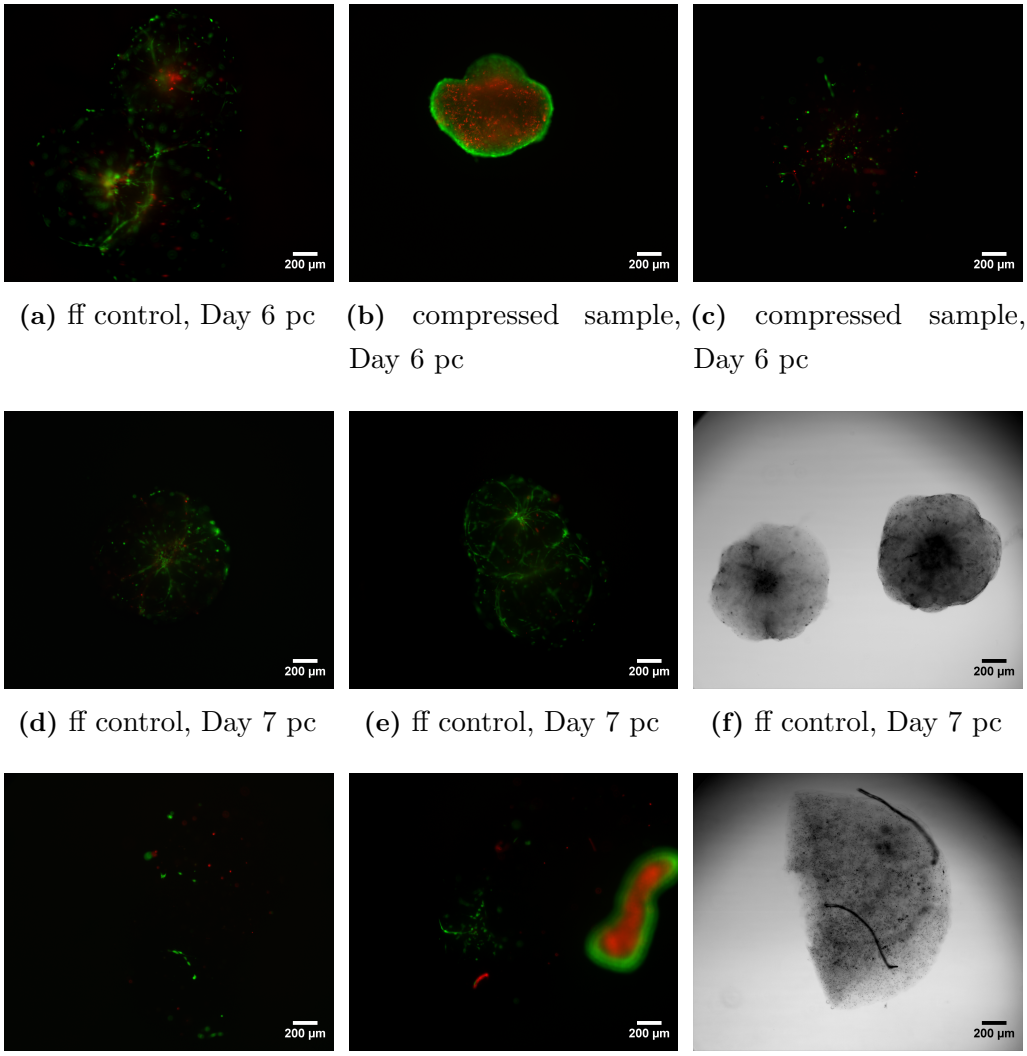
(a) ff control, 24 h pc **(b)** ff control, Day 2 pc **(c)** ff control, Day 3 pc

(d) ff control, Day 3 pc **(e)** ff control, Day 4 pc **(f)** ff control, Day 4 pc

(g) compressed sample, Day 4 pc **(h)** compressed sample, Day 4 pc **(i)** ff control, Day 5 pc

(j) ff control, Day 5 pc **(k)** compressed sample, Day 5 pc **(l)** compressed sample, Day 5 pc

Figure 4.22: Microscopic images of hES-MPs viability and collagen bead's geometry of free floating control on 24 h, days 2, 3, 4 and 5 pc. ff; free floating control. Samples were passed through the compression chamber on day 3 pc and fluorescent images of collagen microspheres were recorded 24 h after applying the first and the second compression cycles. Scale bars for images (a)-(i) are 200 µm.



(a) ff control, Day 6 pc **(b)** compressed sample, Day 6 pc **(c)** compressed sample, Day 6 pc

(d) ff control, Day 7 pc **(e)** ff control, Day 7 pc **(f)** ff control, Day 7 pc

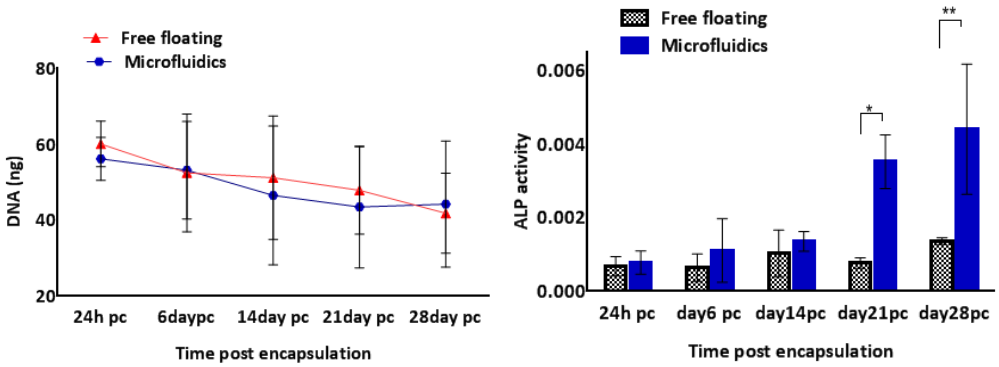
(g) compressed sample, Day 7 pc **(h)** compressed sample, Day 7 pc **(i)** compressed sample, Day 7 pc

Figure 4.23: Microscopic images of viable hES-MPs and collagen microspheres geometry of fluorescently stained free floating controls and compressed samples 24 h after applying 3rd compression cycle at day 6 and day 7 pc. ff; free floating control. Scale bars for (a)-(i) are 200 µm.

4.3.4.1 Microfluidic system can induce osteogenesis of hES-MPs by increasing early stage bone marker

The collagen microspheres that were passed through microfluidic chamber showed good cell viability over 28 days pc as presented in Figure 4.24. Early increase in cell proliferation was reported after day 6 and peaked by the total DNA content of 50 ng on day 14 pc. Cell growth then reached a plateau with a marginal fluctuation between days 21 and 28 pc while cell proliferation of free floating controls presented a steady drop over the same period of time. DNA content

decreased from over 60 ng on 24 h pc to just below 40 ng on day 28 pc, which indicated the positive effect of microfluidic system on viability and proliferation of hES-MP cell line.



(a) **(b)**

Figure 4.24: a; Cell proliferation comparison between free floating controls and microfluidic samples, b; alkaline phosphatase activity of free floating controls and compressed sample was assessed by fluorometric assay. * indicates statistical significance (* $p < 0.01$, ** $p < 0.001$). Data is mean ± SD for 9 samples.

Assessing alkaline phosphatase activity of compressed and control samples revealed that this early stage mineralisation marker level enhanced considerably over 28 days pc. ALP activity of compressed sample showed an increase up to 5 folds by day 28 pc while in free floating controls ALP peaked on day 14, dropped to half of its value on day 21 and reached to the same level as day 14 on day 28 pc. Although, both sample and control groups manifested similar ALP activity on day 14 pc (just above 0.001), compressed sample presented up to 4 times increase in alkaline phosphatase level on day 21 ($p < 0.01$) compared to controls and this figure also remained significantly higher on day 28 pc ($p < 0.001$). Our findings indicated that the mineralisation was still an ongoing event in compressed group, long after the completion of compression stimulation on day 11 pc whereas, free floating exhibited much earlier peak and on average very low ALP activity level per cell. Despite the high ALP activity level, the extra cellular calcium level revealed to be undetectable as the concentration of calcium was well below the threshold on all samples. Nevertheless, ICP-MS detected phosphorous on days 21 and 28 pc but the level presented to be much lower than controls group at the same time points. Phosphorous value reported up to four times higher in free floating controls than compressed sample on day 21 pc (4000 and 1000 µg/ml respectively) and its level increased to nearly 8000 µg/ml on day 28 pc in control group against 500 µg/ml in compressed sample ($p < 0.0001$). Overall, phosphorous level was considerably

lower compared to free floating controls which was in disagreement with ALP results.

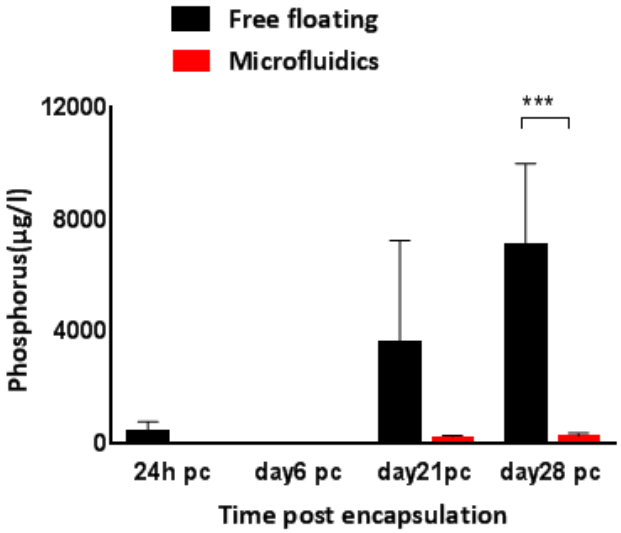


Figure 4.25: Evaluation of deposited extracellular matrix phosphorous level between microfluidic compressed samples and free floating controls over 28 days pc. * indicates statistical significance (*** p <0.0001). Data is mean ± SD for 9 samples.

4.4 Discussion

The aim of this study was to design a microfluidic chamber as an alternative to bulkier bioreactors to apply mechanical loading to cells seeded collagen constructs and stimulate hES-MPS osteogenic differentiation. Many studies showed the importance of integrating mechanical force and fluid flow to the cell's micro-environment to influence stem cells fate and induce the osteogenic differentiation. Recently, microfluidic system have been used to study the effect of these forces and fluid flow in particular, in stem cells commitment. Nonetheless, most of these researches, employed either 3D stem cells culture and microfluidic devices to mimic flow condition or microfluidic system to produce 3D micro droplets for tissue engineering applications[167].

Different approaches were implemented in building a microfluidic chamber from soft lithographic technique to rapid prototyping and replica molding to achieve appropriate geometry, height and surface structure. Our results indicated that the best outcome attained when metal rod was used as a replica while, other approaches failed to provide required height and surface smoothness for the chamber. Despite the reports from Wong et al.[168], Windvoel et al.[169] on surface modification

via physical adsorption for prevention of protein non specific binding, washing the chamber with BSA proved ineffective in preventing collagen microspheres entrapment in the channel. Furthermore, Cecchet[170] and Choi[171] studies revealed that treating the chamber with graft polymer coating of PEG or self assembled mono layer of PEG-silane could amplify the hydrophilicity and protein-resistance through formation of self assembly of poly (ethylene glycol methyl ether) (MPEG) film that leads to bonds between the substrate and the PDMS layer. Yet, PEG treatment did not show any positive effect on alteration of surface chemistry hence, prevention of collagen attachment to the chamber.

Surface roughness can also be modified at the nano scale through acetone vapour polishing that involved immersion of PDMS mold or 3D print template into an acetone bath and enhancing the hydrophilicity. However, our results showed that acetone vapour technique was unsuccessful in improving surface smoothness.
The height of chamber was calculated according to the measurement of collagen microspheres average diameter on day 6 pc to ensure a uniform compression load was sensed by all samples and to reduce the variability between repeat experiments. Still, changing the height of channel without adjusting the flow rate meant that the cells would be subjected to different shear stress conditions. Therefore, the outcome of this experiment could be inconsistent due to application of non identical mechanical stimulation regime on hES-MPs.

ICP-ES was employed to quantify the trace of ECM deposited minerals. This is a well-established technique in the field of geochemistry and is fast becoming the method of choice in identification of trace elements in biological tissues due to its high sensitivity and low detection limits[172]. ICP-ES technique can be used in determination of element concentrations and their distribution in different materials and physiological environment also, in imaging soft tissues, with relatively high sensitivity and spatial resolution[173]. Ricles et al.[174] used ICP-ES technique in assessing the nano particle loading and retention over time in differentiation of nano particle loaded MSCs into adipocytes and osteocytes. In addition, Tatavarty reported quantification of calcium/phosphorous in human mesenchymal stem cells/graphene oxide calcium phosphate nano composites using ICP-ES method[175] while others reported the application of ICP-ES in evaluation of the intracellular iron content in human adipose tissue-derived mesenchymal stem cells[176]. Due to use of very low cell number in our experiment and minimal calcium deposition, the common colorimetric methods for mineral quantification were not sensitive enough

to assess the level of mineralisation, therefore ICP-ES technique was employed to quantify extra cellular mineral trace (calcium, phosphorous and zinc).

Compression cycles were mostly in favour of hES-MPs viability as compressed sample proliferation showed only a marginal 6% decrease compared to free floating controls on day 14 and 21 pc. Yet, ALP activity and deposited phosphorous levels suggested very low or no influence of microfluidics on mineralisation and osteogenesis of seeded hES-MP/collagen microspheres (Figure 4.24). This was mainly due to high ALP activity level that was reported between days 21 and 28 pc and very low deposition of calcium and phosphorous on the same time points that indicated low or no mineralisation whereas deposition of minerals initiate after a peak in ALP activity followed by a substantial drop in enzyme level. These findings were then confirmed by non-detectable extracellular matrix phosphorous level shown in Figure 4.25. Therefore, the assessment of other bone markers such as osteocalcin, collagen I and RUNX2 and their genetic expression are needed to fully evaluate the osteogenic effect of microfluidic system on stem cells. In addition, the expression level of chondrogenic and adipogenic markers also needed to completely rule out the possibility of hES-MPs differentiation towards other cell lineages.

Direct evaluation of applied shear stress on cells was not completed as calculation of the flow that was passing through the microspheres as well as the fluid passing by collagen beads surface needed advanced numerical modelling. Furthermore, estimation of the transferred stress from the surface of microspheres to the cells which were located at the central area of beads and assessing the behaviour of cells located at the different areas of collagen microspheres to the local and combined global shear stress must be considered in the calculation. Therefore, due to the complex nature of this computational modelling, the shear stress that was sensed by cells or applied on the microspheres was not calculated and considered beyond the aim of the thesis. Due to the novelty of this experimental design, there were no comparable reports available to analyse the effect of applied compression through microfluidic chamber on osteogenesis of hES-MP cell line.

4.5 Conclusions and future work

A variety of approaches were taken to design a microfluidic chamber for application of mechanical stimulation on osteogenic differentiation of hES-MPs. Metal

rod replica was chosen as best candidate to provide the required geometry, surface smoothness and height of channel in PDMS made microfluidic chamber. A microfluidic chamber was made out of PDMS that consisted of a channel with diameter ranging from 0.6 mm to 0.9 mm for compression of the collagen beads. Movement of the microsphere and media is obtained by using syringe pumps. 5 µl collagen microspheres containing passages 3-6 of hES-MPs with collagen concentration of 2 mg/ml and cell density of 1200 cells per droplet were made.

Applied compressive force on the cell-seeded microspheres supported long term cell viability while partially encouraged the osteogenesis of hES-MPs and could be used as a model to further study the effect of mechano-stimulation on osteogenesis. Our finding indicates that microfluidic system can increase the ALP activity of compressed cells which imply mineralization while maintaining cells viability and proliferation over 28 days pc. Combining microfluidic systems with mechanical stimulation for osteogenesis represents a scientific and technological innovation that could greatly impact regenerative medicine. This chapter demonstrated a microfluidic chamber design for mechanical stimulation of flexible cellular microspheres and possibly a high-throughput microfluidic system for parallel processing of stem cell aggregation. The chamber enabled chemical and mechanical stimulation of cells in a controlled environment, while reducing the overall volume of the systems leading in both reduction in cost and possibility of high throughput testing.

The main focus of this study was to design a simple yet effective microfluidic chamber with optimised flow rate to enhance the viability, proliferation and differentiation of sensitive progenitors cells and to minimise the damage of soft collagen microspheres. This study also aimed to reduce the cell and collagen damage through optimising the starting day of experiment by analysing the contraction rate and diameter of microspheres. Nonetheless, visualisation of more detailed microstructure and cell/collagen fibres alignment of collagen microspheres through SEM and SHG microscopy is needed to provide better understanding of the effect of mechanical stimulation and full characterisation of the effect of compression particularly by using the microfluidic chamber on hES-MP cell line. Also, confirmation of osteogenesis by qPCR/real time PCR technique is required to compare the differential expressions of specific genes such as ALP, osteocalcin, osteonectin, Runx, BMP and ColI in compressed samples with free floating controls.

5

Mechanical conditioning of hES-MPs/collagen microspheres

5.1 Introduction

Many cell types including osteoblasts, chondrocytes, fibroblasts and endothelial cells are load sensitive and subjected to daily mechanical loading. Dense connective tissues like tendon and ligament are stretched frequently through muscle contraction caused by movement while bone is under dynamic loading to resist and adapt to the experienced forces by maintaining homoeostasis through tissue remodelling. Most of the forces applied in vivo are dynamic and cyclic that means often the tissue is under loading and resting cycles. For example leg bones undergo cyclic compression and tensile forces as human walks, therefore, it is possible that cells respond more to cyclic loading as opposed to constant load that could increase the risk of cells being overloaded and become unresponsive to the applied load. A key area of research in tissue engineering is concerned with finding the answers to how mechanical loading transfers to the cells, how cells sense mechanical forces and how and when cells response to the applied external stimuli. Both 2D and 3D cultures have been used to apply mechanical loading onto cells. Nevertheless, 2D experiments are carried out on flat surfaces and do not mimic in vivo 3D architecture. Therefore, 3D in vitro models may provide more physiologically relevant environments for mechanotransduction studies[177]. Studies have shown that cell response in 2D culture to dynamic stimulation is mainly due to the deformation of the substrate with additional minor fluid flow effects as there is little movement of fluid flow which provide minimal effect on the cell[178]. In contrast, cells response to the load in 3D constructs is related to both the mechanical stimulation that were initiated within the system as well as nutrient

transport mechanism generated by fluid movement through the scaffold[179]. As mentioned in Chapter 1 various techniques have been used to study the response of cells to mechanical stimulation. Yet, their main focus was on simple 2D surfaces such as coated gelatin, plastic and glasses that do not fully reflect the nature of the in vitro 3D environment. Therefore, these surfaces do not fulfil the necessary requirement in regeneration of functional tissue approach. Culturing cells on 3D environment will provide a more realistic and physiological model for studying load driven biochemical responses in cells and mimic in vivo conditions.

Many studies investigated the role of mechanical stimulation in the control of cell fate and mechanical conditioning of mesenchymal stem cells (MSCs) in directing MSC behaviour for tissue engineering applications. Delaine Smith reported that tensile loading favours osteogenesis through initiation of more fibrous matrix while, compression loading encourages generation of a more GAG rich matrix and chondrogenesis[16]. Other studies demonstrated the effect of longitudinal forces in up regulation of early ALP activity level and mineralisation markers both in the presence and absence of osteogenic media[88,180]. So far there are limited studies on the effect of compression loading on the osteogenesis of stem cells. Therefore, the aim of this chapter was to investigate the effects of cyclic mechanical-induced osteogenic differentiation and long term proliferation of progenitor cells and assess cellular mechanisms involved in mechanotransduction and osteogenesis of hES-MPs. The main purpose was to apply short bouts of mechanical loading, mainly tensile and compression, on the hES-MPs seeded collagen microspheres through shortening a channel in a microfluidic chamber. Another goal of this study was to investigate the effect of this mechanical stimulation on osteogenic differentiation of cells through quantification of ALP activity and deposited minerals levels in the hES-MPs seeded collagen microspheres. In addition, cellular matrix production and remodeling along with alignment of collagen fibre were evaluated to confirm load driven differentiation of cells. Applied loading regime was established by literature[16,90] and cells were subjected to indirect dynamic compression and tensile forces through a PDMS loading chamber.

5.2 Methods

5.2.1 Design of a PDMS made loading chamber

Needles with different outer diameter ranging from 0.6 mm to 0.9 mm were used as a template to create compression chamber. PDMS with the ratio of 10:1 of base to initiator was mixed, poured on top of the template and was baked at 60 °C for 1.5 h. The needle was removed from the set PDMS and PDMS mold was cut in a rectangular shape (length: 44 mm, width: 28 mm, thickness: 6 mm). Also, the same procedure was followed with 3 ml syringe which was used as a template to make a cylindrical chamber.

5.2.2 Characterisation of PDMS mechanical properties

Young's modulus, Poisson's ratio and plastic elongation of PDMS were calculated using high resolution digital imaging technique and digital image correlation (DIC) camera, Kelkins software and Bose bio-dynamic machine. For calculation of Young's modulus 10 block steps were completed as shown in Table 5.1:

Step 1	Sine wave	Level: 0.00 mm	Level: 2.35 mm
Step 2	Dwell	Time: 400 s	
Step 3	Ramp	Level: 2.4 mm	Rate: 0.01 mm/s
Step 4	Dwell	Time: 400 s	
Step 5	Ramp	Level: −2.4 mm	Rate: 0.01 mm/s
Step 6	Dwell	Time: 400 s	
Step 7	Ramp	Level: 2.4 mm	Rate: 8.4 mm/s
Step 8	Dwell	Time: 400 s	
Step 9	Ramp	Level: −2.4 mm	Rate: 8.4 mm/s
Step 10	Dwell	Time: 400 s	

Table 5.1: Mechanical properties of PDMS polymer were characterised using 10 step blocks of sinusoidal waves and ramps. Sine wave; sinusoidal wave of displacement to load. Dwell; sample was hold at a displacement level for a specific time. Ramp; sample was moved from displacement level 1 to displacement level 2 with specific rate. PDMS sample was subjected to relative tensile loading of 2.35 mm that applied from 0 mm to 2.35 mm, the sample was then hold at 2.35 mm for 400 s. PDMS sample then was pulled from relative 0 mm to 2.4 mm with rate of 0.01 mm/s, was hold for 400 s and moved back to relative 0 mm with the same rate. The experiment was repeated one more time with a different rate.

5.2.3 Cyclic compression protocol

Samples of 10-12 hES-MPs seeded collagen microspheres were transferred to the loading chamber on day 6 pc and were subjected to dynamic mechanical stimulation of 10% strain, 1 Hz for 15-40 min/day for 5 and 10 days using ElectroForce®5100 BioDynamic® test instrument and software Win Test 7 as illustrated in Figure 5.1 .

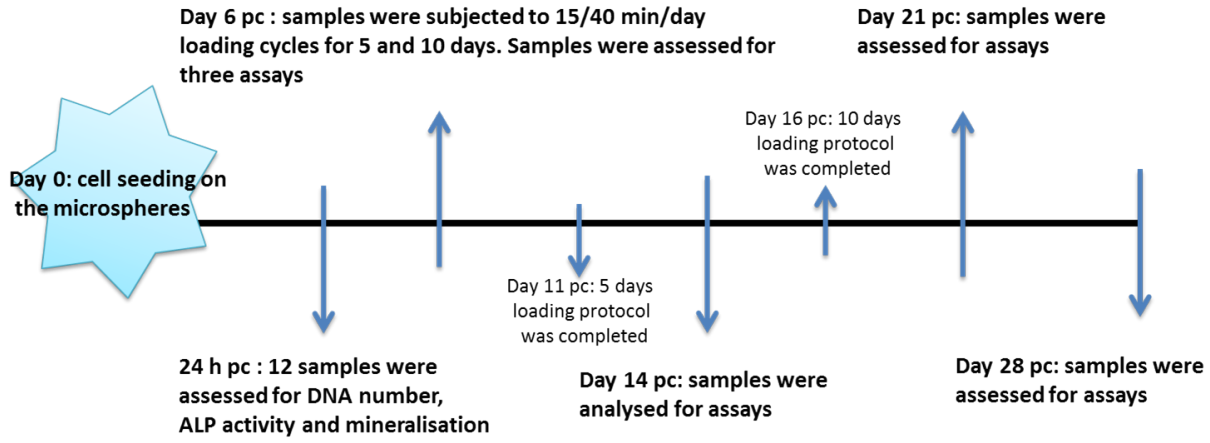


Figure 5.1: Schematic of the loading protocols, durations and mechanical conditioning of hES-MPs seeded collagen microspheres within 28 days post en-capsulation. Samples were subjected to either 15-40 mind, 10% strain, 1 Hz for 5 and 10 days. The DNA content, ALP activity level and mineralisation of 12 samples were analysed for each time points.

Cell viability, early stage mineralisation marker and level of mineral deposition of two experimental groups were tested against free floating controls and unloaded control microspheres that were kept in the loading chamber for 5 and 10 days. In 10 days loading experiment, 2 days rest was considered between each 5 days of mechanical conditioning. Constant strain protocol consisted of applying 10% strain, 1 Hz for 15-40 min/day for duration of 5 and 10 days whereas, in adjusted strain protocol plastic elongation of PDMS chamber was calculated for each day of experiment and the value was deducted from the applied 10% global strain till the plastic elongation value reached to 0.24 mm and remained constant (Figure 5.2 and Figure 5.3).

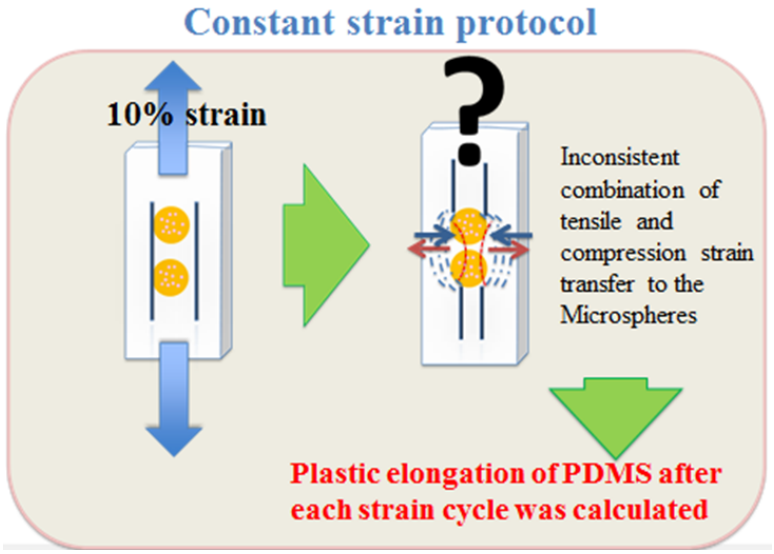


Figure 5.2: Schematic of the applied constant strain on PDMS made loading chamber which resulted in inconsistent load transfer to the microspheres.

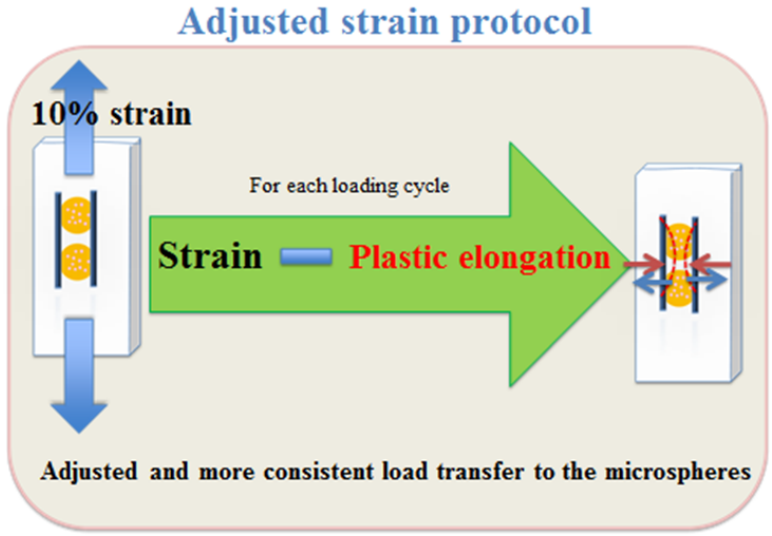


Figure 5.3: Schematic of the applied adjusted strain which shows subtracting the calculated PDMS plastic elongation from global strain may result in more consistent and uniform load transfer to the microspheres.

5.2.4 Assessment of collagen fibre alignment

Alignment of collagen fibres in control and loaded samples was compared using SHG confocal microscopy on day 21 pc.

5.2.5 Evaluation of collagen microsphere surface micro structure

Cell attachment, elongation and new ECM collagen lay down were examined by SEM on days 6, 16 and 28 pc. Also, microstructure of collagen beads and reorganisation of collagen fibres were assessed in the loaded samples versus free floating controls on day 21 pc.

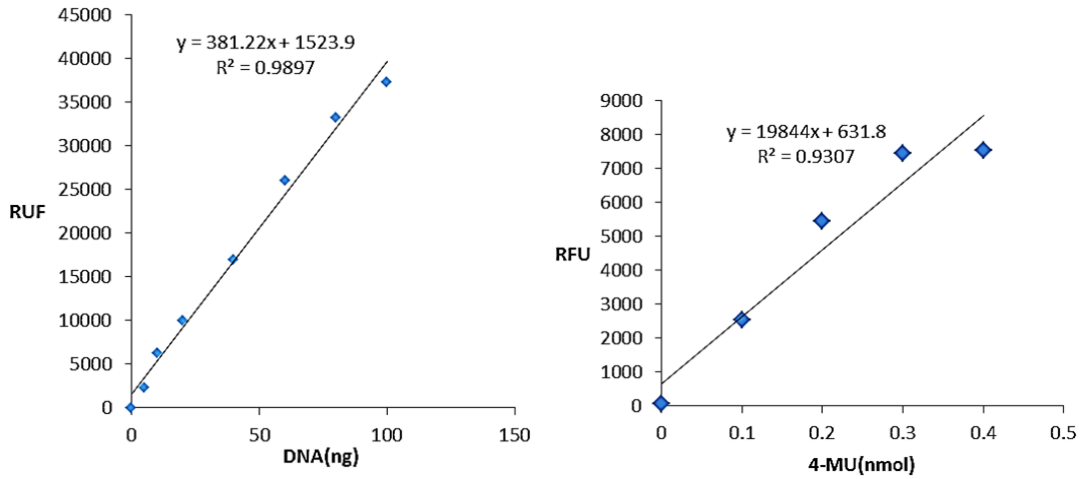
5.2.6 Cell culture

Human embryonic cell-derived mesenchymal progenitor cell line hES-MP 002.5 (hES-MPs) were seeded in bovine collagen I microspheres as was previously described in Chapter 2. Passages 3-7 of HES-MP cells were used in the experiments and cell seeding density was calculated as 5×10^5 cells/ml in collagen gel with collagen concentration of 2 mg/ml.

5.2.7 Cellular assay

Cell viability and total DNA measurement of hES-MP cells of free floating control versus loaded samples were determined using DNA pico-green assay at 24 h, days 6, 21 and 28 pc as shown in Figure 5.4.

ALP activity of compressed hES-MPs against free floating controls was measured at 24 h, days 6 ,14, 21 and 28 pc and was also visualised by ALP staining of microspheres cross sections (Figure 5.4).



(a) (b)

Figure 5.4: Standard curve of a; DNA pico green and b; ALP 4-MU that was employed to analyse hES-MPs viability and early stage mineralisation marker.

Quantification of deposited calcium was measured by 1% Alizarin red S staining at 24 h, days 6, 14, 21 and 28 pc via ICP-ES. Mineralisation was also visualised by 1% Alizarin red staining of loaded and control cross section samples over same period of time. Samples were digested in 5% w/v perchloric acid and were diluted by 10 fold prior to analysis. Samples then were mixed with 1% w/v nitric acid with ratio of 1:1 in the eppendorf tubes. Samples volume were brought to around 10 mL and the torch was turned on. An intense electromagnetic field was created within the coil by the high power radio frequency signal flowing in the coil. Instruments run at 40 mHz and the argon gas flown through the torch.
The argon gas was then ionized in the intense electromagnetic field and flows in a particular rotationally symmetrical pattern towards the magnetic field of the RF coil. A peristaltic pump deliverd an aqueous or organic sample into an analytical nebulizer and changed it into mist and introduced directly inside the plasma flame. The sample immediately collides with the electrons and charged ions in the plasma and was broken down into charged ions. The various molecules break up into their respective atoms which then lose electrons and recombine repeatedly in the plasma, giving off radiation at the characteristic wavelengths of the elements involved.

Phosphorous level of extra cellular matrix was assessed at 24 h, days 6, 21 and 28 pc by following above protocol for ICP-ES.

Extracellular matrix zinc level was quantified by ICP-ES following above protocol at 24 h, days 6, 21 and 28 pc.

5.2.8 Statistics

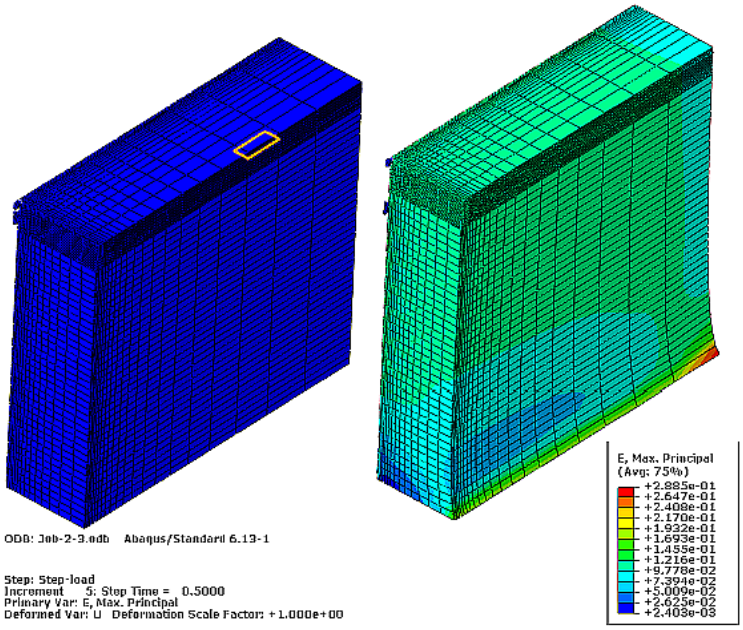
All experiments were performed three times in triplicates (n=9). Cell viability at different time points, ALP and mineralisation comparison as well as statistical differences between free floating, unloaded controls and loaded samples were completed using one-way ANOVA followed by Sidak's or Tukey's multiple comparisons test.

5.3 Results

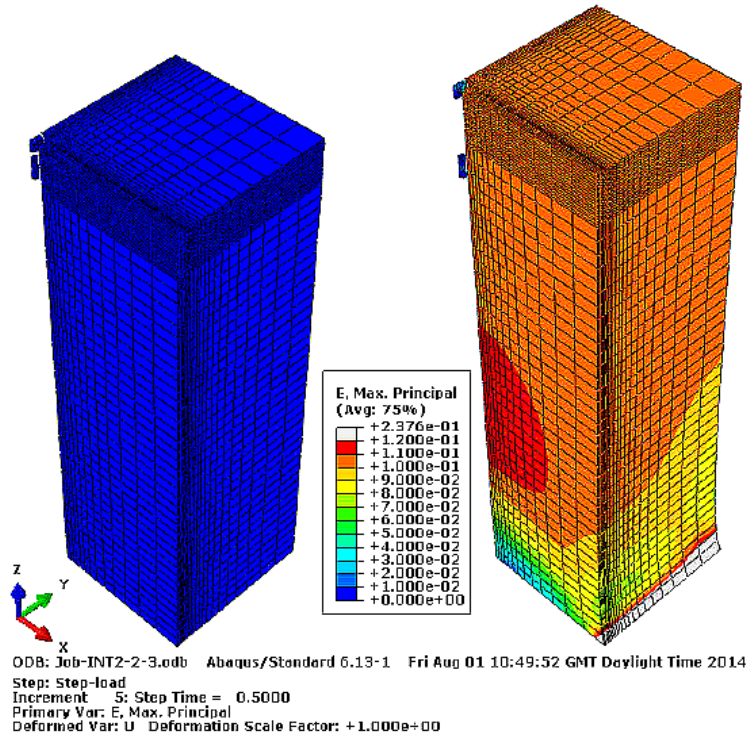
5.3.1 Design of a PDMS made compression chamber

A loading chamber was made out of PDMS and the central channel diameter was optimised based on the measurement of average collagen microspheres diameter (n=20) on day 6 pc as shown in Figure 5.7 a. Based on the computational modelling that was performed by Dr Baldit, chambers diameter was calculated and made in such a way that it was approximately 50 µm-80 µm bigger than the diameter of cell seeded collagen beads on day 6 pc[181]. This would ensure that collagen microspheres would not fall to the bottom of PDMS chamber when applying compression cycles. The diameter of chamber therefore, varied broadly from 600 µm-900 µm to fit the experiment more accurately. Clearly, strong stress appears close the sample ends but locally in the centre and along half sample height the strain is quite constant and close to 10% equivalent to the macroscopic load (Figure 5.5).

Also the computational modelling indicated that the microspheres inside the loading chamber would sense the maximal strain of around 5%. This is also consistent with the fact that the chamber needs to be stretched with a 5% strain to reach the contact with beads. In addition, the contact sensitivity is related the to the geometry of PDMS sample as with the rectangular cross section, it appears that the contact is first reached in the direction corresponding to the shortest geometry length compared with the square sample (Figure 5.6).

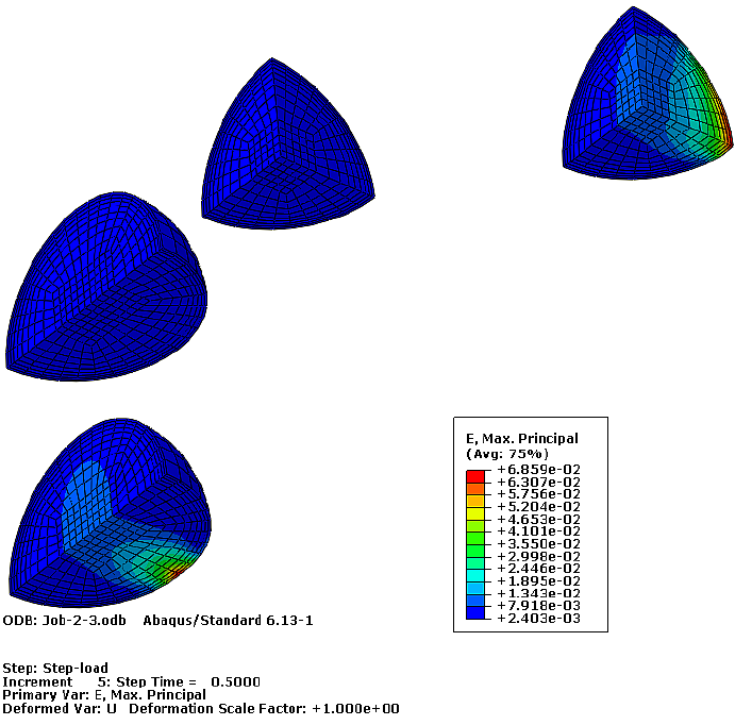


(a) rectangular cross section

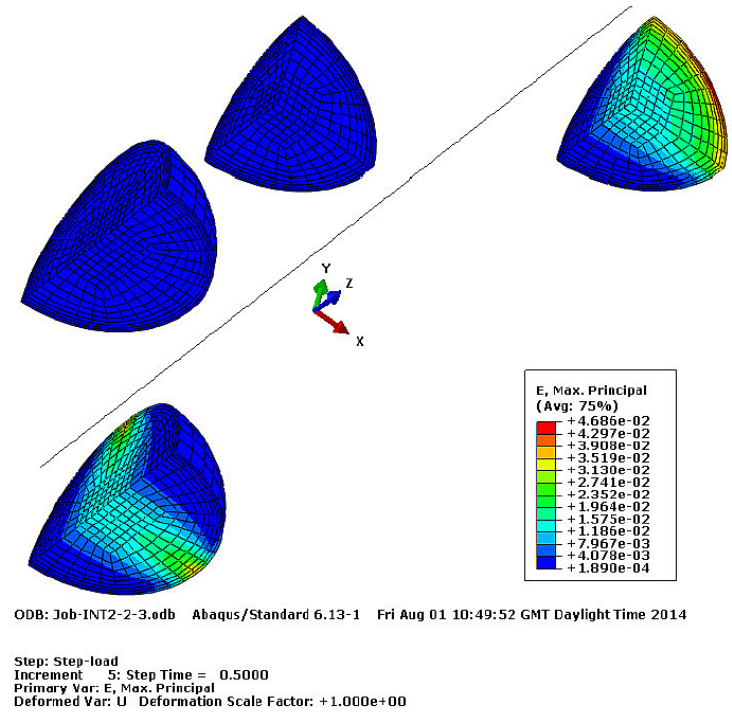


(b) squared cross section

Figure 5.5: PDMS strain field corresponding to 10% of strain applied macroscopically (Abaqus). Strong stress appears close the sample ends but locally in the centre and along half sample height the strain is quite constant and close to 10% equivalent to the macroscopic load.



(a) rectangular cross section

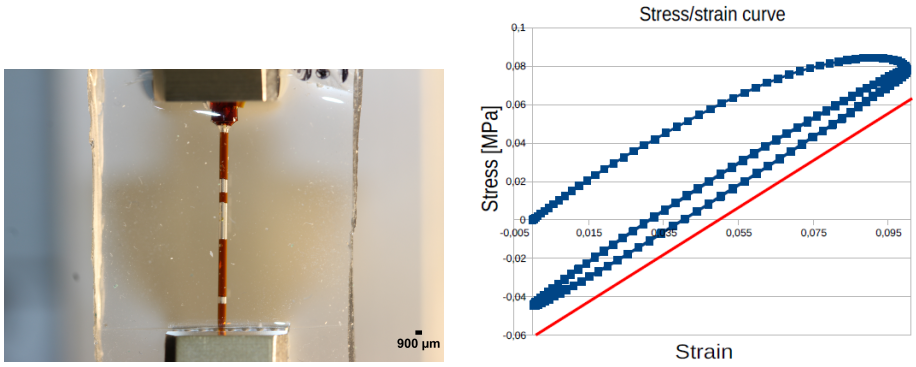


(b) squared cross section

Figure 5.6: Beads strain field corresponding to 10% of strain applied macroscopically on the PDMS sample (Abaqus). Microspheres inside the loading chamber would sense the maximal strain of around 5% by applying 5% tensile strain to the loading chamber to reach the contact with beads. Contact sensitivity is related the to the geometry of PDMS sample as with the rectangular cross section, it appears that the contact is first reached in the direction corresponding to the shortest geometry length compared with the square sample.

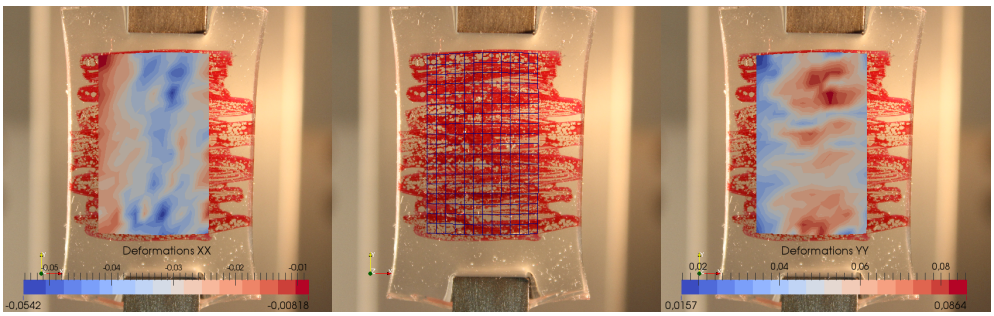
5.3.2 Characterisation of PDMS mechanical properties

PDMS is classed as a viscoelastic material as shown in stress/strain graph in Figure 5.7. The DIC software Kelkins calculated the displacement/strain on the surface of the PDMS and on average for the imposed 10% global strain, 7.5% strain along the vertical direction of solicitation and 3.75% strain along the horizontal transverse direction was measured as demonstrated in Figure 5.8. Poisson's ratio was then calculated as 0.5 which is consistent with the polymer behaviour. The difference between global and vertical direction strain can be related to strain localisation or sample slipping out of the grips during the experiment. Young's modulus of the polymer was calculated as 1000 kPa after relaxation and plastic deformation was calculated as 0.7 mm after applying 10% strain and using cycles blocks in Bose bio dynamic machine (Figure 5.9).



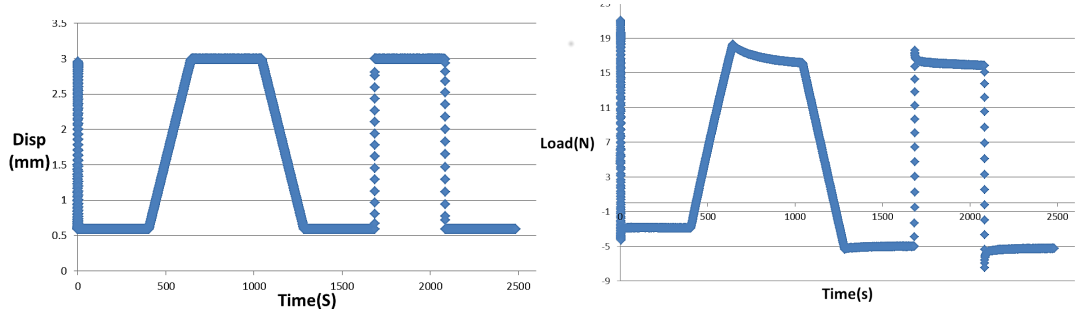
(a) Loading chamber **(b)** Stress-strain curve

Figure 5.7: PDMS made compression chamber, ID: 0.9 mm, a and viscoelastic behaviour of PDMS under 10% strain was shown by stress/strain curve along a cyclic loading, b.



(a) X-transverse strain **(b)** Mesh **(c)** Y-longitudinal strain

Figure 5.8: Measurement of transversal and longitudinal strains on the PDMS surface when subjected to 10% global strain using Kelkins software.



(a) PDMS displacement-time curve **(b)** PDMS load-time curve

Figure 5.9: Characterisation of PDMS Young's modulus and plastic elongation using Bose biodynamic system.

5.3.3 Application of cyclic mechanical conditioning

Cells were exposed to non-uniform strain in constant protocol, which suggested microspheres, and hence hES-MPs sensed inconsistent combination of tensile and compression loading. Calculating the plastic elongation of polymer and its subtraction from the total stain ensured transfer of more uniform strain to the cells and more importantly, obtaining positive values of load that guaranteed consistent mechanical stimulation of cell/collagen microspheres.

5.3.4 Comparison of cell proliferation, ALP activity and mineralisation between adjusted and constant loading protocols

DNA pico green assay results showed that cells remained viable and proliferated steadily well over 28 days pc in both constant and adjusted loading protocols as shown in Figures 5.10 a and 5.12 a. In constant loading regime, free floating controls had significantly higher total DNA content than other experimental groups on days 14, 21 and 28 pc ($p < 0.0001$). In addition, both 15 and 40 min/day loaded samples of 10 days regime showed slightly higher cell number than 5 days regime conditions by the end of 28 days experiment but no statistical significance was observed between the loaded conditions of 5 and 10 days. Also, in 10 days experiment, both 15 min/day and 40 min/day samples presented greater DNA content than unloaded controls ($p < 0.001$), with highest cell number for 40 min/day samples on day 28 pc (80 ng).

Although free floating controls seemed to have higher DNA content, no significant change in proliferation was detected between different conditions and time points

in the adjusted loading protocol. The only exception was day 14 pc in which proliferation in free floating controls (DNA content: 60 ng) was reported twice as high as 5 days for 15-40 min/day the loaded samples (30 ng, p <0.0001). Apart from free floating controls all other experimental groups had lower DNA content and cell number on day 14 pc. However, the total DNA content of all experimental groups increased by 35% to around 47 ng on day 21 pc in comparison with free floating controls. Both 5 days loaded groups demonstrated higher cell number in comparison with 10 days loading cycles. Nevertheless, the loaded and control samples in both protocols showed stable long term cell viability with no statistically significant drop in total DNA.

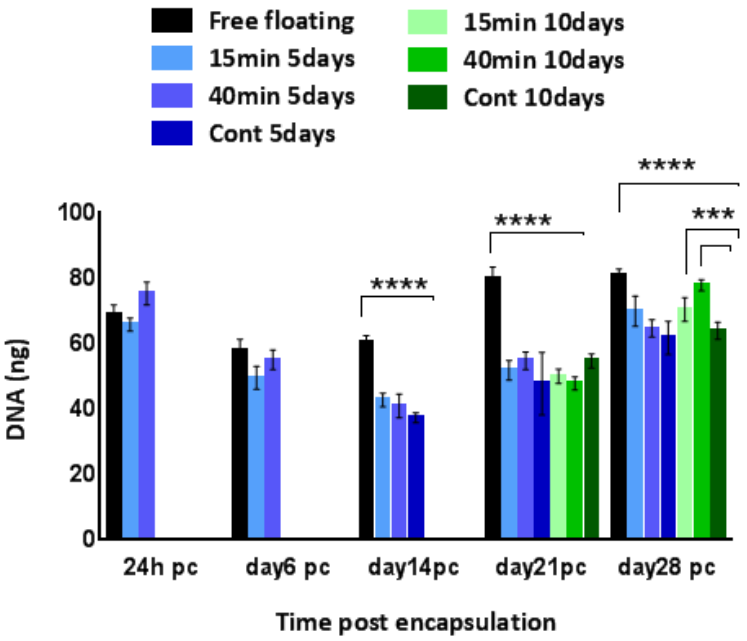


Figure 5.10: Evaluation of cell viability in loaded samples of constant protocol versus control over 28 day pc. Total DNA content of loaded samples 15 min/day and 40 min/day for 5 and 10 days, compared with controls in the constant protocol and DNA level shows steady viability of cells in all conditions. Free floating controls showed significant higher DNA concentration compared with other experimental samples. * indicates statistical significance, (**** p <0.0001, *** p <0.001). Data is mean ± SD n=9.

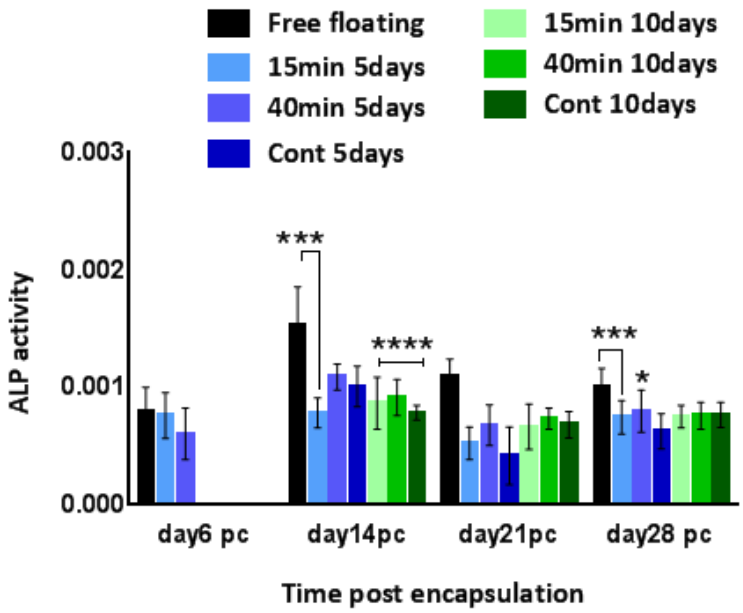


Figure 5.11: Evaluation of ALP activity in loaded samples of constant protocol versus control over 28 day pc. Enzyme level did not show any significant increase in different time points and apart from free floating controls, ALP activity remained unchanged during 28 day pc. * indicates statistical significance, (**** p <0.0001, *** p <0.001, * p <0.1). Data is mean ± SD n=9.

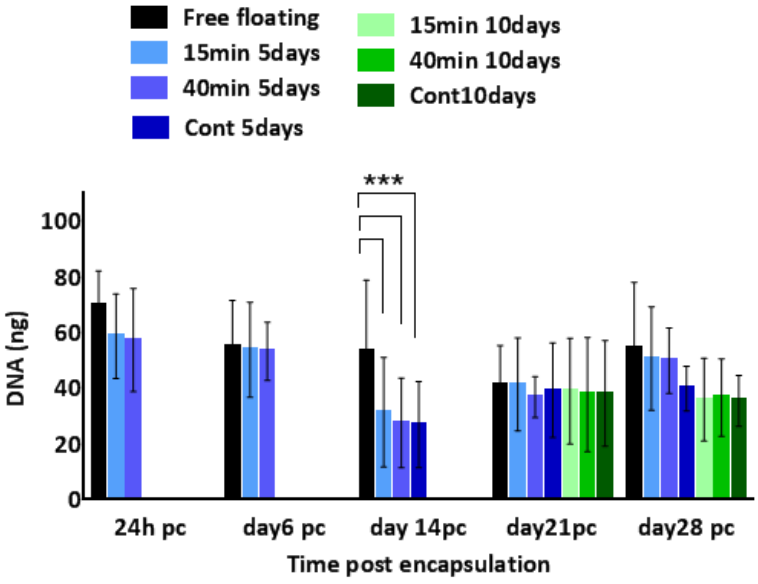


Figure 5.12: Evaluation of cell viability in loaded samples of adjusted protocol versus control over 28 day pc, a; total DNA content of loaded samples 15 min/day and 40 min/day for 5 and 10 days, compared with controls in the constant protocol. Total DNA concentration presented steady cell viability in all conditions during 28 day experiment with no significant changes between different time points. * indicates statistical significance, (*** p <0.001). Data is mean ± SD n=9.

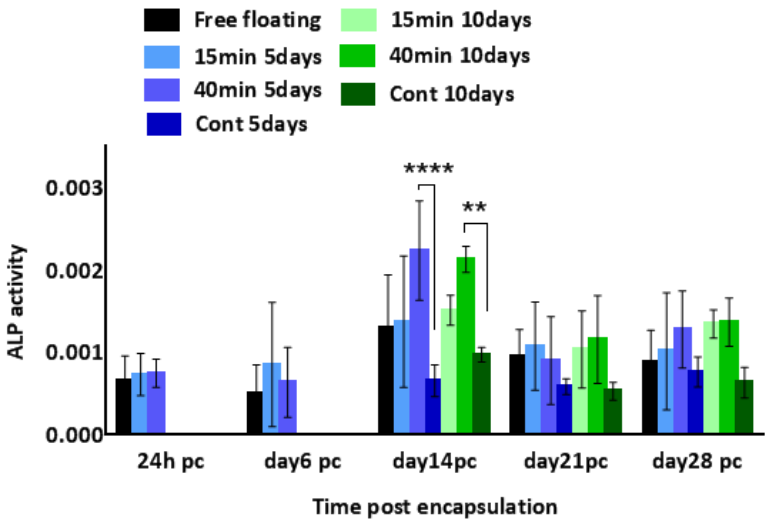


Figure 5.13: Evaluation of ALP activity in loaded samples of adjusted protocol versus control over 28 day pc. ALP activity reported significantly higher in loaded samples of 40 min in both 5 and 10 days loading regimes on day 14 pc in comparison with other conditions. Enzyme activity of all experimental conditions dropped to the lower level from day 21 pc onwards. * indicates statistical significance, (**** $p < 0.0001$, ** $p < 0.01$). Data is mean ± SD n=9.

The osteogenic differentiation of hES-MPs was investigated by measurement of ALP as an early stage mineralisation marker and was further confirmed by H&E and ALP staining in both constant and adjusted loading regimes. Measuring ALP activity level revealed no substantial change in the enzyme activity in the loaded samples compared to unloaded and free floating controls following applying the constant loading protocol over 28 days pc as shown in Figure 5.11.

ALP activity in free floating controls increased to the highest level on day 14 pc and reduced by half on days 21 and 28 pc. However, the enzyme activity did not show any increase on days 14, 21 and 28 pc in other experimental groups. ALP level reported stable around 0.0001 in all conditions on day 14 pc while free floating controls showed 50% higher alkaline phosphatase level ($p < 0.0001$ and 0.001) in comparison with both loaded samples and unloaded controls. Furthermore, 10 days loaded samples for both 15 min/day and 40min/day presented marginally more ALP activity level than 5 day loading regime on day 21 pc still, free floating controls reported higher enzyme activity level particularly in comparison with 5 day loaded samples of 15 min/day and 40min/day and unloaded controls ($p < 0.001$, 0.1 and 0.0001 respectively) on day 21 pc.

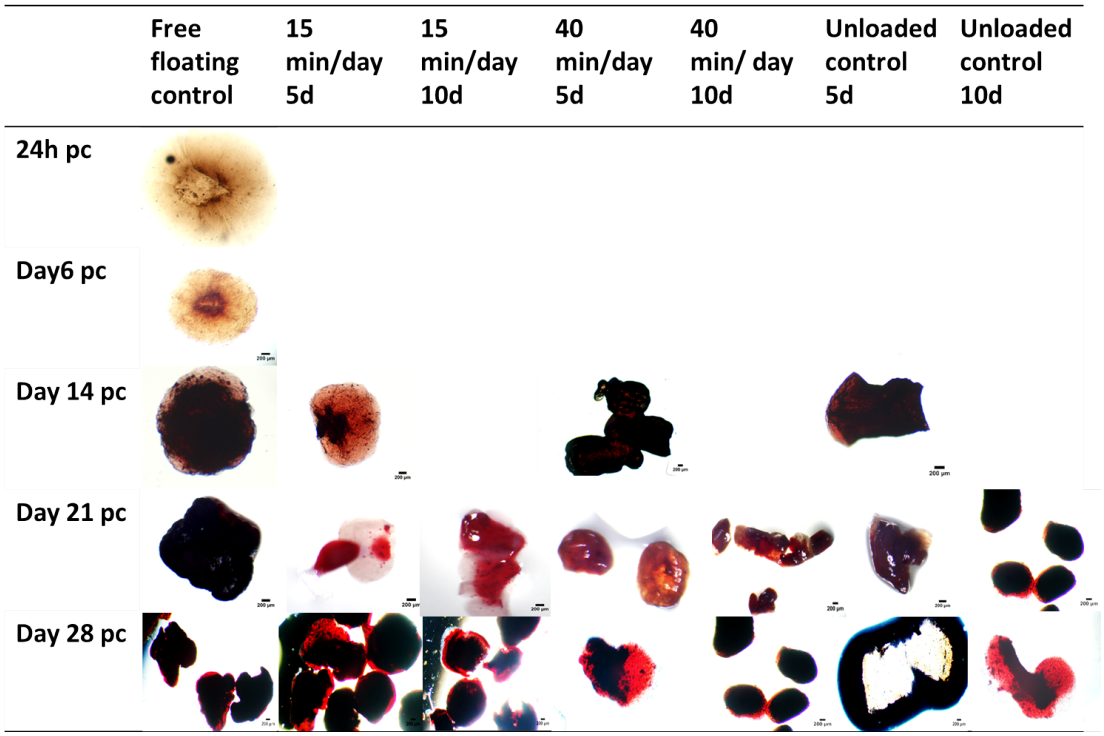
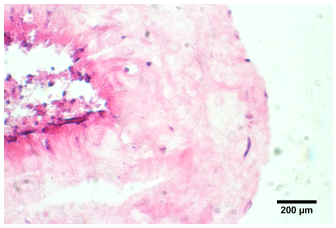


Figure 5.14: Alizarin red staining of hES-MPs seeded collagen microspheres loaded under constant loading protocol versus controls over 28 days pc. Both 15-40 min/day loaded samples of 5 and 10 days experiment presented higher accumulation of deposited Alizarin red stain compared to unloaded controls from day 21 pc onward. All images taken by light microscope, 20x.

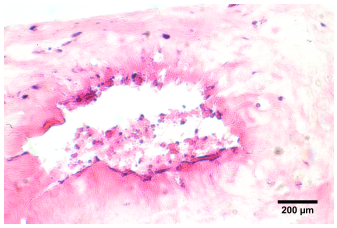
Alkaline phosphatase activity level in the adjusted loading protocol increased substantially from day 6 to day 14 pc when the activity level reached a peak, followed by a drop to nearly half the level on day 21, which then remained stable up to day 28 pc as presented in Figure 5.13. All conditions followed the same trend for ALP activity level which was normalised to the total DNA content of each sample. The ALP level in 5 and 10 days loading regimes, 40 min/day loaded samples surged significantly up 40% ($p < 0.0001$) of controls and 15 min/day samples activity level on day 14 pc. The enzyme level dropped to around 0.001 in free floating while 40 min/day loaded samples of 10 day regime presented marginally highest enzyme activity. In addition, all 10 days loading cycles samples showed slightly higher ALP activity levels compared to other conditions on day 28 pc, but no statistical significance was found between these experimental groups on day 28 pc. Interestingly, both 5 and 10 days unloaded controls that remained in the PDMS chamber presented marginally greater ALP level than free floating controls from day 14 pc onward.

Results of Alizarin red staining of loaded samples, unloaded and free floating control revealed higher deposited calcium in both free floating controls and 40 min/day loaded samples of 5 and 10 days loading experiments by showing higher deposition of red stain from day 14 pc onward as indicated in Figure 5.14. Considering that no statistically significant difference was detected between 15 min/day and 40 min/day loading of 5 and 10 days experiments in DNA content, ALP activity level and expression of mineralisation, 40 min/day of 10 days loading regime was chosen for further comparison between constant and adjusted loading protocols in quantification of deposited minerals and microspheres cross-section ALP, Alizarin red and Alcian blue staining.

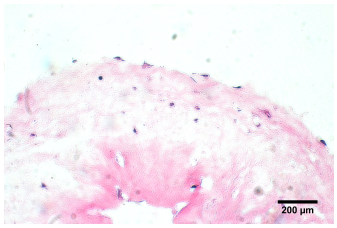
In contrary, ALP staining of samples cross sections revealed slightly different results as free floating controls exhibited more intense purple colour on days 21 and 28 pc compared to other conditions as indicated in Figures 5.16 and 5.17. Also, ALP colour intensity was considerably higher in loaded samples of adjusted strain of 40 min/day in 10 days loading regime in comparison with constant loading protocol and unloaded controls on day 28 pc. In addition, H&E staining of microspheres cross sections presented darker sections in the loaded samples that were subjected to the adjusted loading regime compared with constant protocol and unloaded controls as shown in Figure 5.15. Microscopic images of free floating controls cross sections also showed higher intensity of stains from day 21 pc.



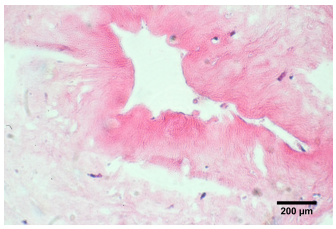
(a) ffc, 24 h pc



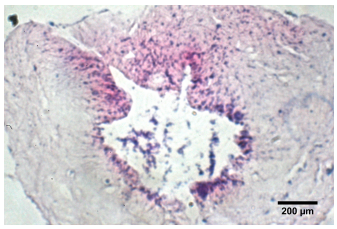
(b) ffc, 24 h pc



(c) ffc, day 6 pc



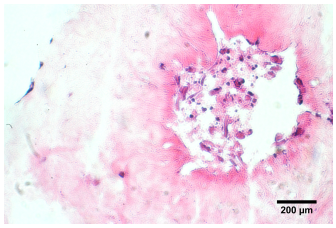
(d) ffc, day 6 pc



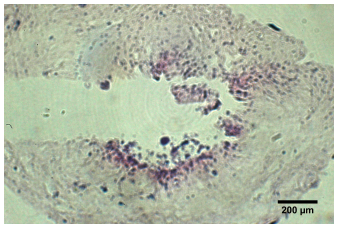
(e) ffc, day 21 pc



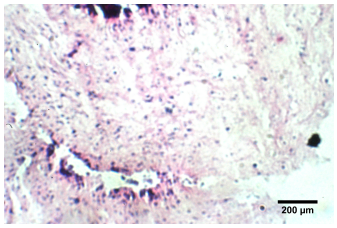
(f) cls 10 days, day 21 pc



(g) uc 10 days, day 21 pc



(h) als 10 days, day 21 pc



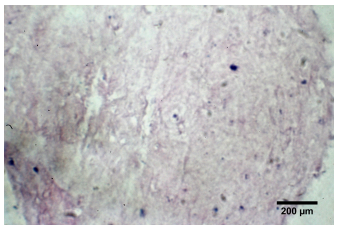
(i) ffc, day 28 pc



(j) cls 10 days, day 28 pc

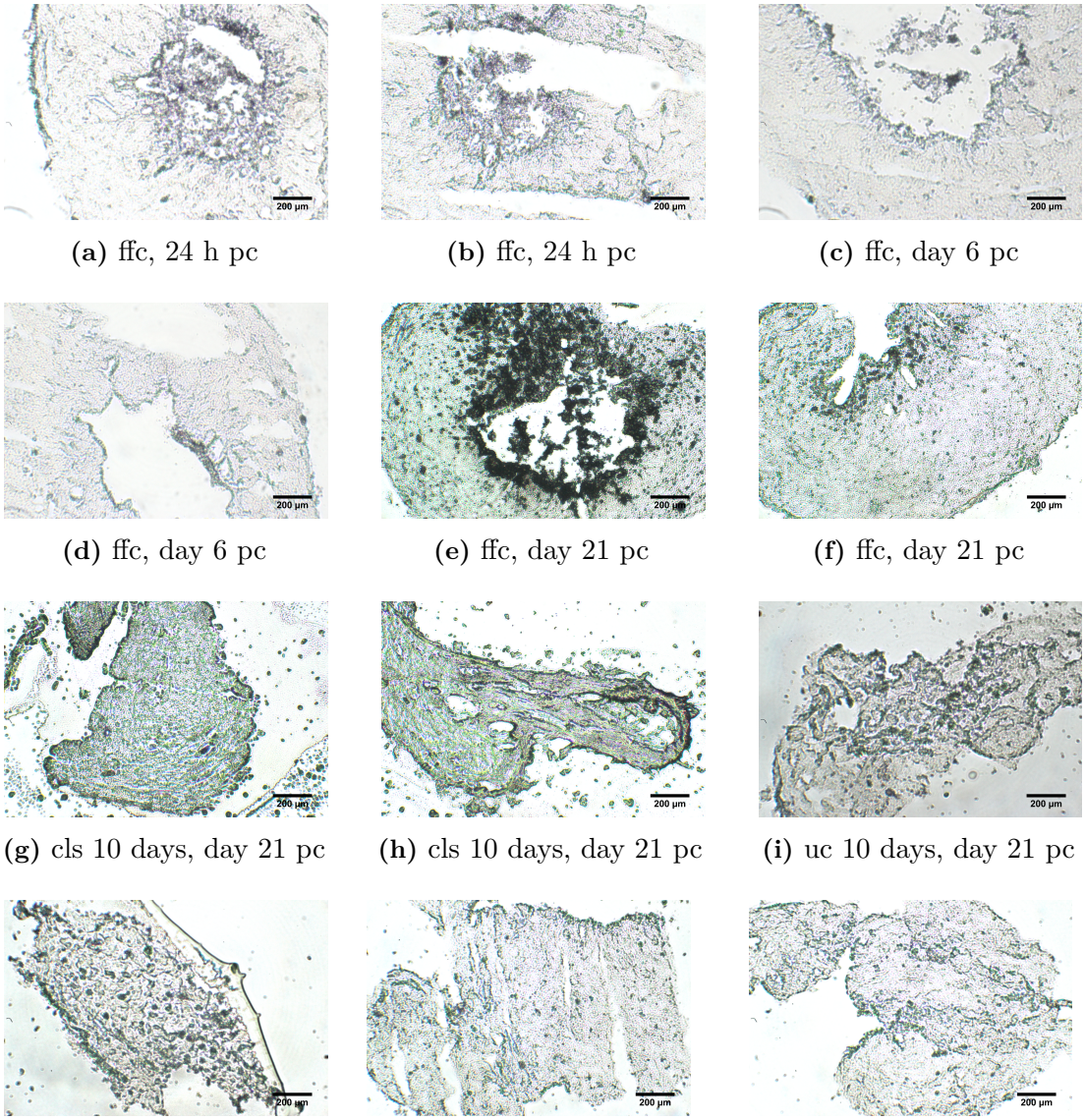


(k) uc 10 days, day 28 pc



(l) als 10 days, day 28 pc

Figure 5.15: H&E staining of 10 µm thick seeded hES-MPs collagen microspheres cross sections over 28 days pc in 10 days cyclic loading regime. ffc; free floating control. cls; constant loading sample. uc; unloaded control. als; adjusted loading sample. All images taken by light microscope, 20x.



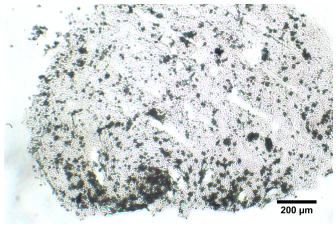
(a) ffc, 24 h pc **(b)** ffc, 24 h pc **(c)** ffc, day 6 pc

(d) ffc, day 6 pc **(e)** ffc, day 21 pc **(f)** ffc, day 21 pc

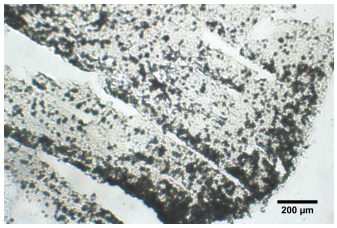
(g) cls 10 days, day 21 pc **(h)** cls 10 days, day 21 pc **(i)** uc 10 days, day 21 pc

(j) uc 10 days, day 21 pc **(k)** als 10 days, day 21 pc **(l)** als 10 days, day 21 pc

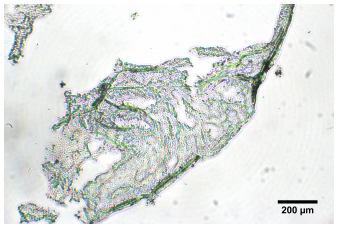
Figure 5.16: Alkaline phosphatase staining of 10 µm thick seeded hES-MPs collagen microspheres over 21 days pc in 10 days cyclic loading regime. ffc; free floating control. cls; constant loading sample. uc; unloaded control. als; adjusted loading sample. All images taken by light microscope, 20x.



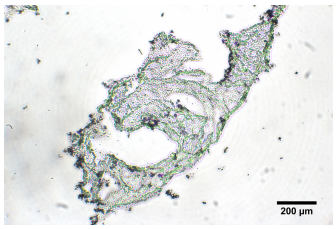
(a) ffc, day 28 pc



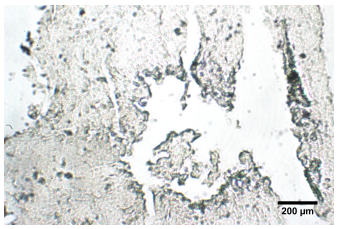
(b) ffc, day 28 pc



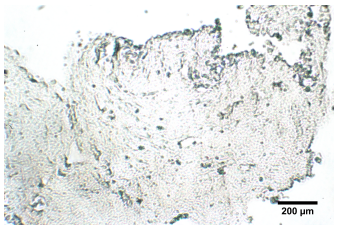
(c) cls 10 days, day 28 pc



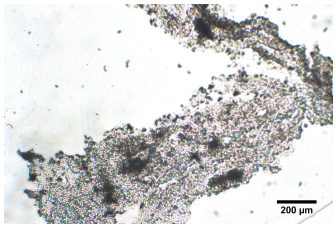
(d) cls 10 days, day 28 pc



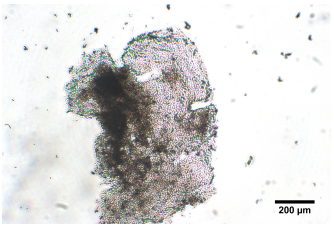
(e) uc 10 days, day 28 pc



(f) uc 10 days, day 28 pc

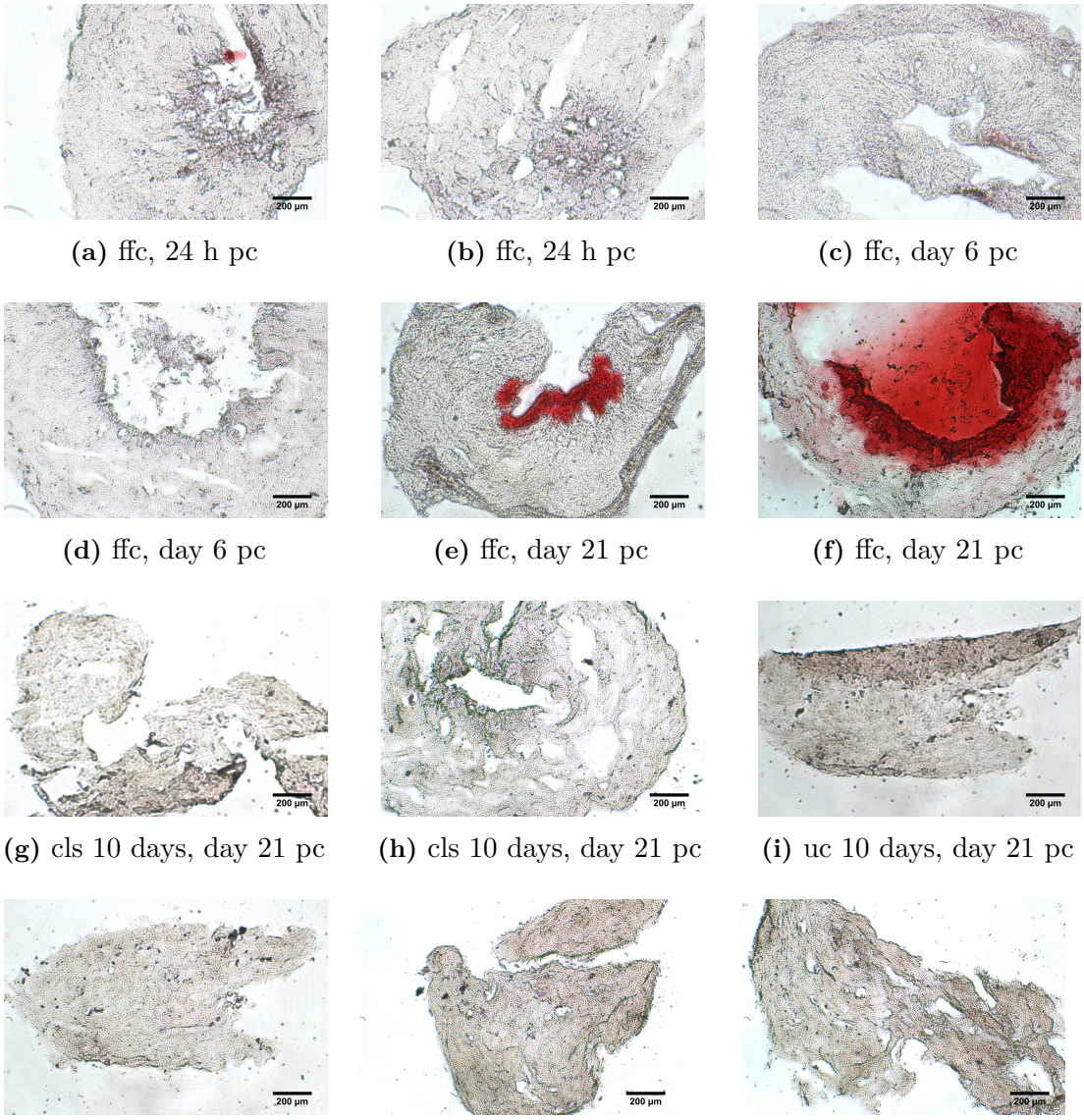


(g) als 10 days, day 28 pc



(h) als 10 days, day 28 pc

Figure 5.17: Alkaline phosphatase staining of 10 µm thick seeded hES-MPs collagen microspheres on day 28 pc in 10 days cyclic loading regime. ffc; free floating control. cls; constant loading sample. uc; unloaded control. als; adjusted loading sample. All images taken by light microscope, 20x.



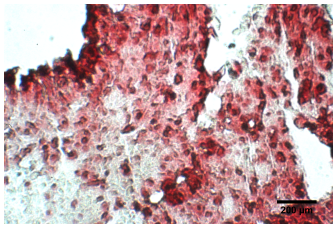
(a) ffc, 24 h pc **(b)** ffc, 24 h pc **(c)** ffc, day 6 pc

(d) ffc, day 6 pc **(e)** ffc, day 21 pc **(f)** ffc, day 21 pc

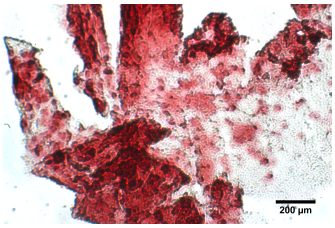
(g) cls 10 days, day 21 pc **(h)** cls 10 days, day 21 pc **(i)** uc 10 days, day 21 pc

(j) uc 10 days, day 21 pc **(k)** als 10 days, day 21 pc **(l)** als 10 days, day 21 pc

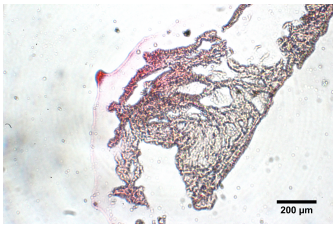
Figure 5.18: Alizarin red staining of 10 µm thick seeded hES-MPs collagen microspheres over 21 days pc in 10 days cyclic loading regime. ffc; free floating control. cls; constant loading sample. uc; unloaded control. als; adjusted loading sample. All images taken by light microscope, 20x.



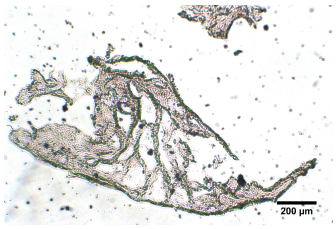
(a) ffc, day 28 pc



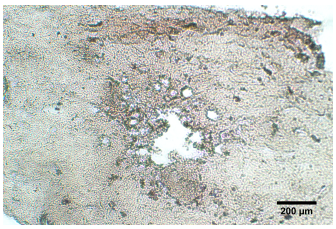
(b) ffc, day 28 pc



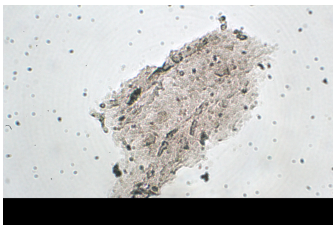
(c) cls 10 days, day 28 pc



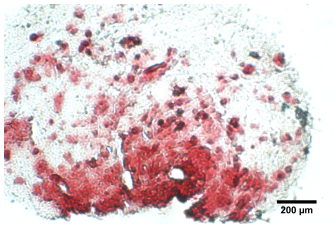
(d) cls 10 days, day 28 pc



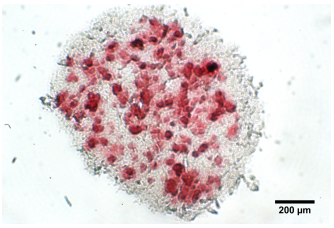
(e) uc 10 days, day 28 pc



(f) uc 10 days, day 28 pc



(g) als 10 days, day 28 pc



(h) als 10 days, day 28 pc

Figure 5.19: Alizarin red staining of 10 µm thick seeded hES-MPs collagen microspheres on day 28 pc in 10 days cyclic loading regime. ffc; free floating control. cls; constant loading sample. uc; unloaded control. als; adjusted loading sample. All images taken by light microscope, 20x.

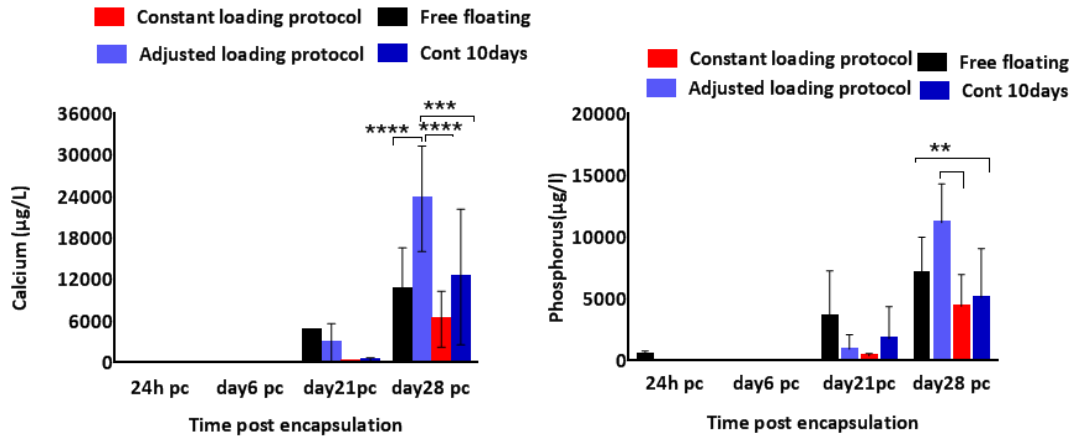
To assess osteogenic differentiation of hES-MPs under dynamic loading, extracellular matrix calcium and phosphorous levels as key parts of hydroxyapatite molecular structure as well as concentration of deposited zinc were quantified. Deposited calcium was detected from day 21 and showed significant increase on day 28 pc as shown in Figure 5.20. Loaded samples in adjusted loading protocol presented the highest calcium level compared to other groups on day 28 pc which was nearly twice as much as detected deposited calcium in free floating (27 000 µg/l, $p < 0.0001$). In addition, the calcium level of unloaded 10 days controls on day 28 pc was reported to be around 25% higher than free floating controls and 75% greater than its values in loaded samples that were subjected to the constant loading protocol.

On the other hand, loaded samples that were subjected to the constant loading

protocol presented lowest calcium level among other experimental groups with around 1000 µg/l and 8000 µg/l calcium was detected on day 21 and 28 pc. The calcium quantification results were further confirmed by Alizarin red staining of loaded and control samples cross sections. Both loaded samples under adjusted loading protocol and free floating controls presented more intense red colour in comparison with 10 days controls on day 28 pc. Yet, free floating controls showed highest stain intensity, particularly on day 28 pc that was in contrast with calcium quantification results. In addition, unloaded controls that presented higher calcium deposition compared to free floating and constant loading protocol samples showed indistinct to no stains on both days 21 and 28 pc. Furthermore, cross section staining results showed that free floating controls were the only group that positively stained with Alizarin red on day 21 pc while measurement of deposited calcium and Alizarin staining of microspheres matched calcium concentrations and stain intensity between free floating controls and loaded samples in the adjusted loading protocol on days 21 and 28 pc as presented in Figures 5.18 and 5.19.

Results of extracellular matrix phosphorous concentration revealed detection of deposited phosphorous from day 21 pc that peaked by day 28 pc as indicated in Figure 5.20. Free floating controls presented highest phosphorous level compared with other conditions on day 21 (nearly 500 µg/l) but loaded samples that were subjected to the adjusted loading protocol manifested the highest deposited phosphorous of 12 500 µg/l on day 28 pc. Phosphorous concentration of adjusted protocol loaded samples increased up to 80% from day 21 to 28 pc and its concentration was reported 2.5 times higher than that of loaded samples in constant protocol on day 28 pc ($p < 0.01$). Also free floating controls showed higher phosphorous level compared to unloaded controls and loaded samples of constant protocol (30%, $p < 0.01$ and 67% respectively) on day 28 pc.

Quantification of extracellular zinc level over 28 day pc presented detectable concentration of zinc from 24 h pc as shown in Figure 5.21. Zinc level of free floating controls was reported quite high on 24 h pc which was decreased to half by day 6 pc and steadily increased to around 70 µg/l on day 28 pc. In other experimental groups zinc concentration was detected from day 21 pc, and loaded samples in the adjusted loading protocol exhibited the highest level of deposited zinc on days 21 and 28 pc. Zinc level of loaded samples in the adjusted protocol was four times higher than its value in free floating controls (200 µg/l versus 47 µg/l, $p < 0.0001$) and nearly 10 times greater than of that in loaded samples of the constant protocol (200 µg/l and 23 µg/l respectively, $p < 0.0001$) on day 21 pc. Furthermore,



(a) calcium deposition **(b)** phosphorous deposition

Figure 5.20: Evaluation of deposited extracellular matrix calcium and phosphorous in loaded samples of 40 min/day in 10 days loading regime of constant and adjusted protocols versus controls over 28 days pc, a; measurement of deposited calcium in the loaded samples compared with controls, b; comparison of phosphorous level in the loaded samples versus controls, * indicates statistical significance, (**** p <0.0001, *** p <0.001, ** p <0.01). Data is mean ± SD n=9.

zinc concentration of loaded samples in the adjusted protocol declined by 25% and reached to 150 µg/l whereas, all the other groups presented higher level of zinc compared to the earlier time point on day 28 pc. Loaded samples in the constant strain protocol showed twice as high zinc level as day 21 pc, on day 28 while, free floating and unloaded controls zinc concentrations were increased up to 70% and 13% respectively. Nevertheless, deposited zinc of loaded samples in the constant protocol reported considerably lower than the amount in the adjusted protocol at both time points. To further confirm the osteogenic differentiation of hES-MPs and disprove the chondrogenic differentiation, microspheres cross sections were stained by Alcian blue stain as indicated in Figures 5.22 and 5.23. Our findings revealed that no substantial stain was deposited on any experimental group. Free floating controls showed deposited blue stain compared to other groups on days 21 and 28 pc while loaded samples of both loading protocols failed to absorb any stain. In addition, free floating controls showed week bright blue colour on day 6 pc which was faded on day 14 pc. In general, no deposited glycosaminoglycans was detected by Alcian blue staining of samples cross sections.

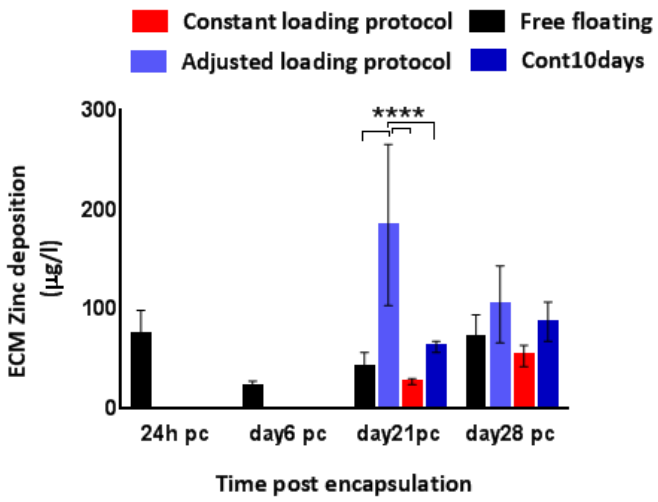
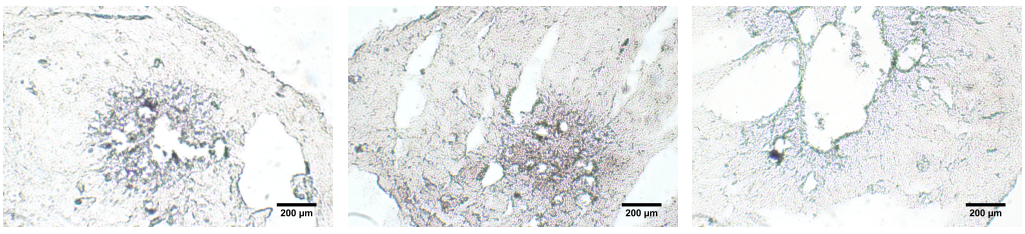
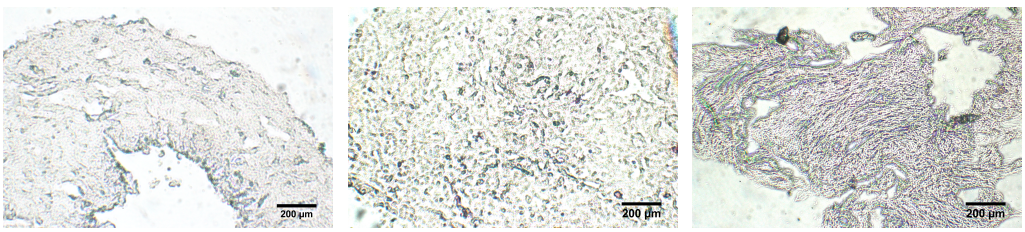


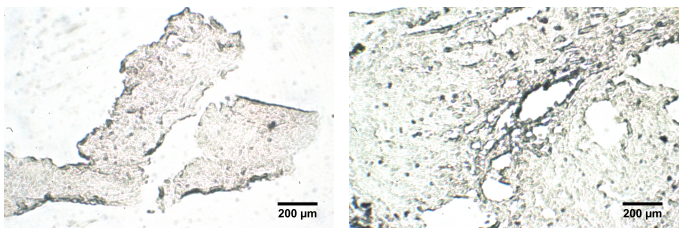
Figure 5.21: Measurement extracellular zinc level in the loaded samples of 40 min/day in 10 days loading regime of constant and adjusted protocols versus controls over 28 days pc, * indicates statistical significance, (**** p <0.0001). Data is mean ± SD n=9.



(a) ffc, 24 h pc **(b)** ffc, 24 h pc **(c)** ffc, day 6 pc

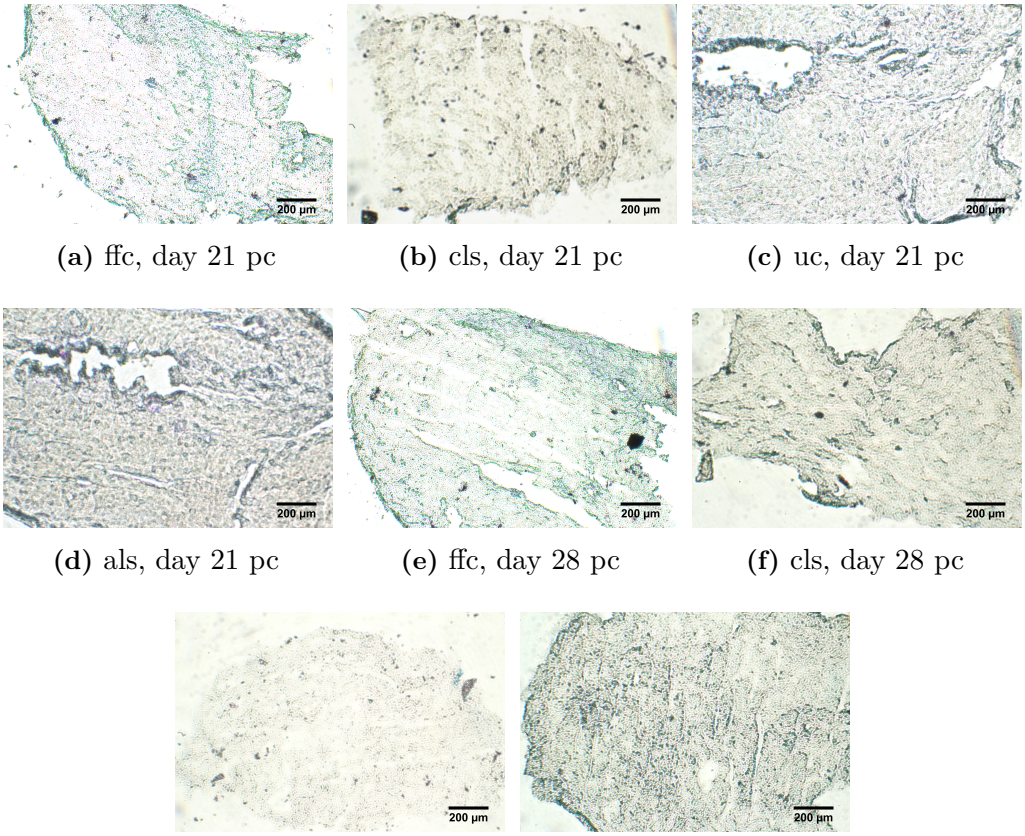


(d) ffc, day 6 pc **(e)** ffc, day 14 pc **(f)** cls, day 14 pc



(g) uc, day 14 pc **(h)** als, day 14 pc

Figure 5.22: Alcian blue staining of 10 µm thick seeded hES-MPs collagen microspheres over 14 days pc in 10 days cyclic loading regime, ffc; free floating control. cls; constant loading sample. uc; unloaded control. als; adjusted loading sample. All images taken under light microscope, 20x.



(a) ffc, day 21 pc **(b)** cls, day 21 pc **(c)** uc, day 21 pc

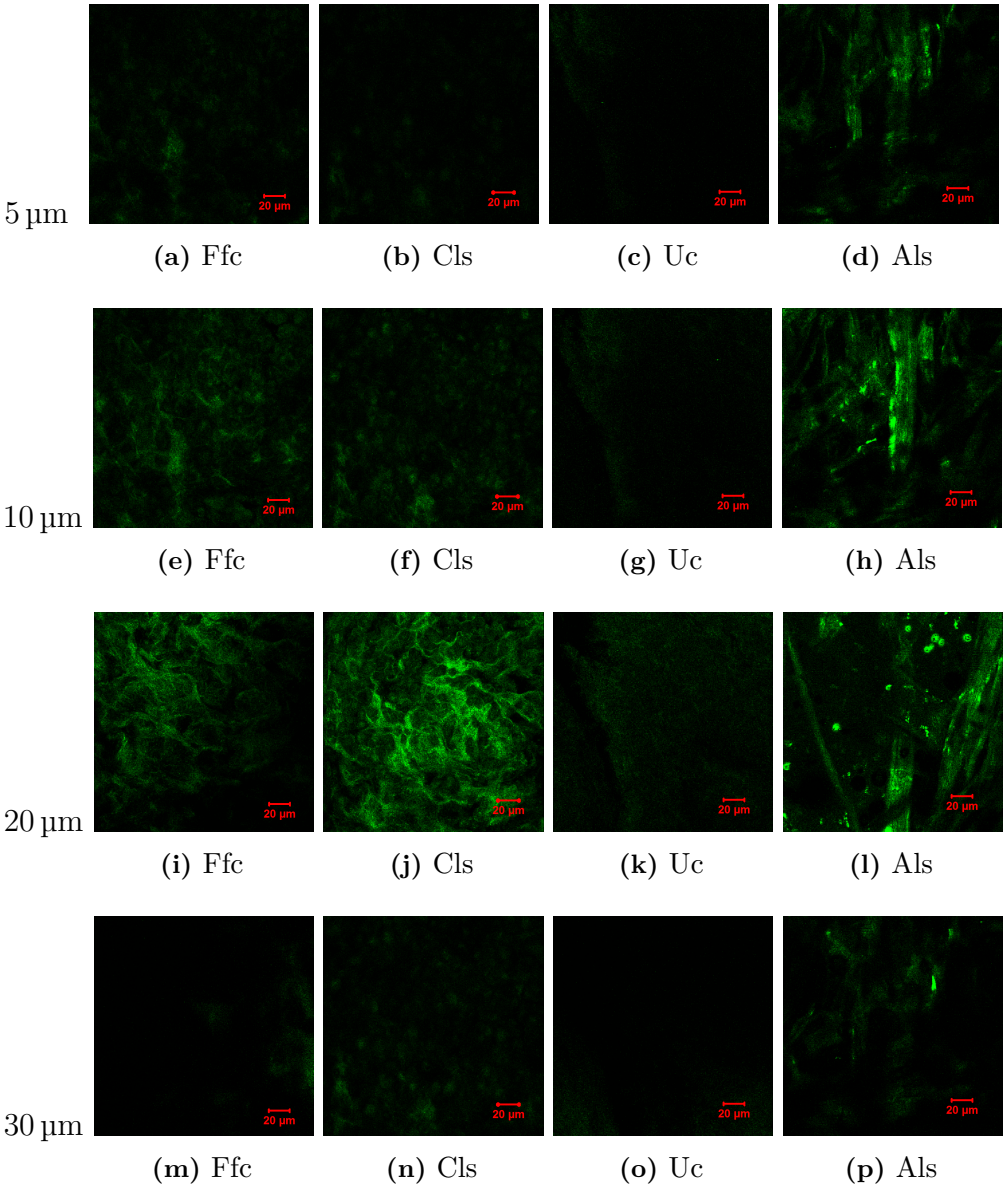
(d) als, day 21 pc **(e)** ffc, day 28 pc **(f)** cls, day 28 pc

(g) uc, day 28 pc **(h)** als, day 28 pc

Figure 5.23: Alcian blue staining of 10 µm thick seeded hES-MPs collagen microspheres on days 21 and 28 pc in 10 days cyclic loading regime, ffc; free floating control. cls; constant loading sample. uc; unloaded control. als; adjusted loading sample. All images taken by light microscope, 20x.

5.3.5 Assessment of collagen fibre alignment

SHG images were obtained by visualising collagen fibres of the seeded collagen microspheres at different depths on day 21 pc (Figure 5.24). The reorientation and more aligned organisation of collagen fibres in compressed samples of adjusted strain protocol was substantially more evident while control free floating samples and unloaded controls presented more fibrous structure of collagen fibres with no preferential orientation at all depths. The most intense SHG signal was recorded at depth 10-20 µm with less coverage area at 20 µm. The signal was very weak at 30 µm which indicated very low presence of collagen fibres at this point.



(a) Ffc **(b)** Cls **(c)** Uc **(d)** Als

(e) Ffc **(f)** Cls **(g)** Uc **(h)** Als

(i) Ffc **(j)** Cls **(k)** Uc **(l)** Als

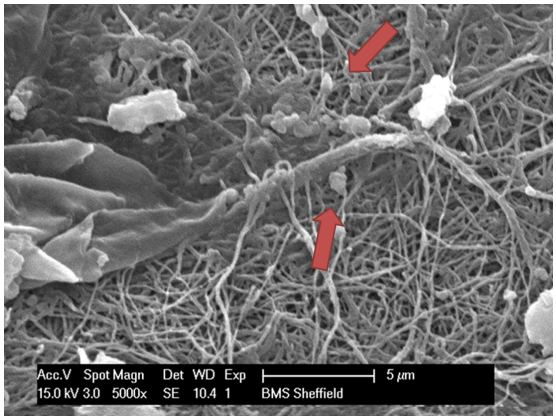
(m) Ffc **(n)** Cls **(o)** Uc **(p)** Als

Figure 5.24: SHG microscopic images of reorientation and alignment of collagen fibres on day 21 pc in 10 days cyclic loading experiment. SHG signal intensity was higher in loaded samples compared to the controls. Ffc; free floating control. Cls; constant loading sample. Uc; unloaded control. Als; adjusted loading sample. Collagen fibres of loaded sample in adjusted protocol visibly reorganised and aligned in comparison with more random organisation of collagen fibre in other conditions. Settings for images taken at 50-75 µm on all samples were optimised to visualise collagen SHG. All images taken by confocal microscope, EC 40x/1.3 plan-Neofluar oil DIC.

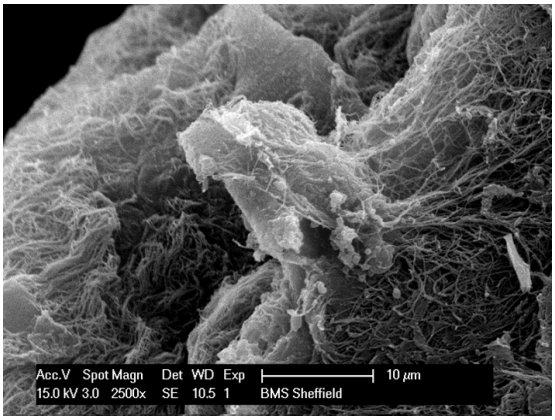
Loaded samples that were subjected to the adjusted loading protocol presented highest intensity of SHG signals which was more evident at 10-20 µm. These findings indicated more production, better reorientation and alignment of collagen fibre by loaded hES-MPs in the adjusted protocol. However, random collagen fibres in free floating controls and constant loading protocol showed more area coverage compared to loaded sample of the adjusted protocol, which again was more visible at 10-20 µm. All conditions noticeably showed different collagen fibres organisation in later time point in comparison with free floating controls on day 6 pc. Nevertheless, it was impossible to identify the axis of imposed strain due to random rotation of collagen microsphere in PDMS chamber during and after loading regime.

5.3.6 Evaluation of collagen fibre organisation using SEM microscopy

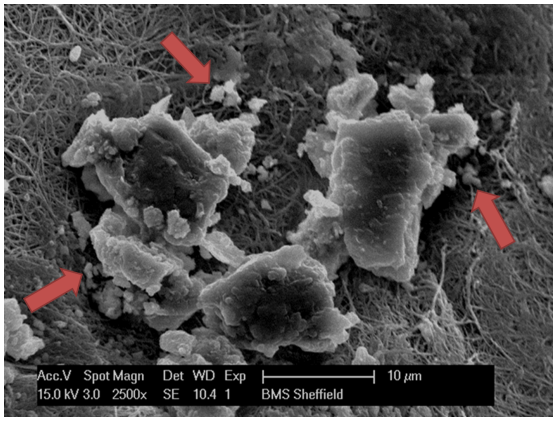
Surface structure of collagen microsphere, cellular elongation and extra cellular matrix reorganisation of collagen fibres was further assessed by SEM microscopy (Figure 5.25). All cell seeded microspheres were covered with cells and matrix at both time points. Cells and matrix on both time points and conditions did not present any preferential direction of orientation and no cellular or collagen fibre alignment was visible in loaded samples of the adjusted loading protocol versus free floating controls. In addition, deposition of mineral particles was apparent in both loaded samples and free floating controls on day 28 pc in comparison with day 6 pc. Appearance of these particles suggests osteogenic mineralisation that support calcium staining and quantification results. Furthermore, more and larger size of mineral particles were reported in the loaded samples than free floating controls which was in agreement with high concentration of deposited calcium presented in loaded samples subjected to the adjusted loading protocol on day 28 pc. Collagen fibres of microspheres in both samples and controls were visibly thinner compared to the produced extracellular matrix fibres on day 28 pc and showed more distinct organisation of fibres as opposed to free floating controls on day 6 pc.



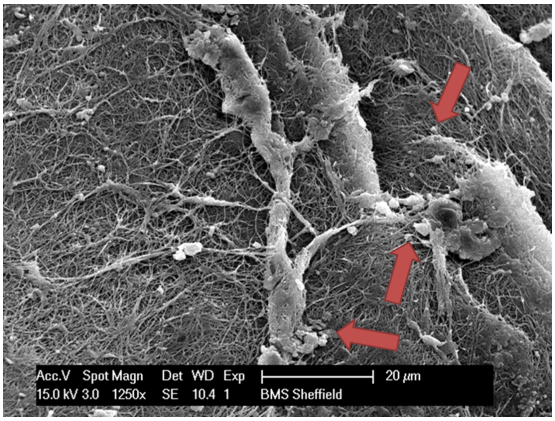
(a) ffc, day 28 pc



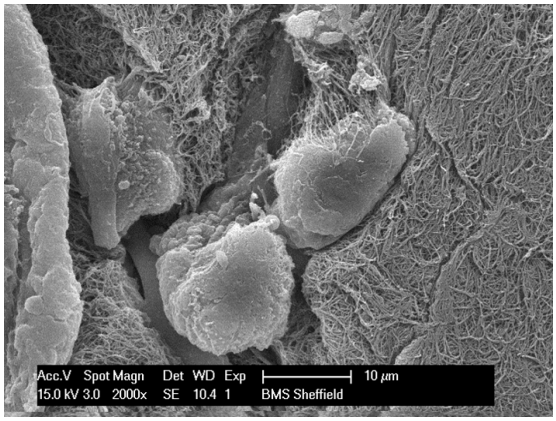
(b) ffc, day 28 pc



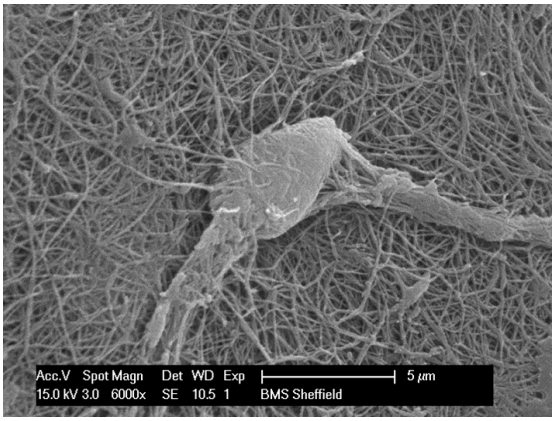
(c) als, day 28 pc



(d) als, day 28 pc



(e) ffc, day 6 pc



(f) ffc, day 6 pc

Figure 5.25: SEM microscopy of hES-MPs seeded collagen microspheres surface on day 28 pc. ffc; free floating control. cls; constant loading sample. uc; unloaded control. als; adjusted loading sample. Accumulation of mineral deposits is more evident in both loaded samples and free floating controls compared to free floating controls on day 6 pc.

5.4 Discussion

The main aim of this chapter was to assess the effect of mechanical stimulation on osteogenic differentiation of hES-MPs in soft 3D collagen environment, by monitoring the early stage mineralisation marker activity, matrix production and alignment as well as quantification of deposited minerals in the differentiated cells. Measuring the change in each of these aspects and discovering how closely related these cellular and molecular events are linked together, is crucial in understanding the process of regeneration of new bone from progenitor cells. Our results indicated that applying cyclic compression can induce osteogenic differentiation of progenitor cells by increasing ALP activity level on day 14 pc and elevate mineral deposition from day 21 pc.

A PDMS loading chamber was designed and made by taking into account the average diameter of collagen microspheres on day 6 pc before starting the loading regime. These measurements ensured accurate diameter of the loading chamber and maximised transmission of more uniformed load to the microspheres and cells. Computational modelling calculated the degree of freedom for the diameter of loading chamber between 50-80 µm, and these calculations allowed collagen microspheres, hence, progenitor cells to solely mechanically loaded during loading cycles while kept in the chamber for 5 and 10 days experiments.

Many studies reported the effect of longitudinal stretching on the osteogenesis of stem cells[95,96] while others revealed how compression could induce chondrogenic differentiation[91]. Still, to the author's knowledge, no studies reported the effect of compression on osteogenic differentiation of stem cells in soft scaffold. Therefore, analysing the combined effects of tensile and compression loading on the cell seeded microspheres was a main focus of this study. Two protocols were selected for loading regime and 10% global strains was applied for 15 min/day and 40 min/day for 5 and 10 days at 1 Hz as suggested by literature[16,90]. The reason behind the selection of 15 and 40 min/day loading cycles was to evaluate how duration of loading can influence the osteogenic differentiation. Also, to examine how long and how frequent, progenitor cells needed to be mechanically loaded to sense and respond to the stimuli and how repetition of load can encourage the mineralisation of hES-MPs. 40 min/day loading was chosen over 1 h as 40 min was the longest time hES-MPs survive without CO2 and added buffer agents.

Mechanical properties and plastic elongation of PDMS chamber was charac-

terised by DIC Kelkins software and repeated cycles of ramp and sinusoidal waves. These findings then were employed to optimise the loading protocol as deducting the calculated plastic elongation of polymer guaranteed the transmission of more homogeneous global load to the microspheres. In addition, subtracting the PDMS plastic elongation eliminated the persistent appearance of longitudinal strains with the negative load of up to $-5\,\mathrm{N}$ showing in the load displacement graph. It also reduced the inter-variabilities between repeats of experiment and 15 min/day and 40 min/day loading cycles as our results indicated a larger plastic deformation in 40 min/day loading chamber.

To evaluate the significance of these calculations on promotion of the osteogenic differentiation of hES-MPs seeded collagen microspheres and altering the level of deposited minerals, loaded samples of constant and adjusted protocols were compared against unloaded and free floating controls over 28 days pc. As it was reported in Chapter 2, hES-MPs go under osteogenic differentiation without any chemical and mechanical stimulation when seeded into the self assembly collagen microspheres and are kept free floating. Therefore this study aimed to encourage earlier and higher mineralisation level compared to free floating microspheres. Alkaline phosphatase activity level is an early stage mineralisation marker in osteogenic differentiation[182] that works through its enzymatic hydrolysis activity[183]. Several studies demonstrated a growth in the cellular ALP activity in the presence of osteogenic supplements while, it has been shown that shear stress had no effect on the cellular ALP levels in non-osteogenic conditions[184]. Grellier et al. revealed that hMSCs that were subjected to short bouts of FSS (30 min) in osteogenic conditions can up-regulate ALP mRNA but 90 min exposure had an opposite effect[109]. Furthermore, Sittichokechaiwut et al. suggested that compression loading at 5% global strain of seeded hMSCs on a porous scaffold increased ALP activity in non-osteogenic medium compared with the unloaded controls in static and osteogenic conditions[185] while others showed tensile loading of MSCs in polyurethane scaffold up-regulated the ALP activity in non-osteogenic conditions[186]. The results of these studies clearly suggested that the effect of mechanical stimulation on ALP activity level and the downstream signalling events of ALP are complex.

Monitoring alkaline phosphatase level reported significant increase in the enzyme activity by day 14 pc in loaded samples of 40 min/day adjusted loading protocol compared to free floating controls and 15 min/day loaded samples. Yet,

ALP activity did not show any considerable changes in any loaded samples of the constant protocol as enzyme level only fluctuated between values 0.001 and 0.0005 during 28 days experiment. Optimising the loading protocol stimulated higher ALP activity level and initiated early stage mineralisation in hES-MPs. Interestingly free floating controls enzyme level was much higher than the unloaded controls in both constant and adjusted strain protocols. One explanation would be that collagen microspheres and cells in free floating controls experience the combined effects of shear stress and hydrostatic pressure as opposed to the confined space of loading chamber that might encourage a considerable change in the ALP activity level at different time points[187].

Higher ALP level was reported in the constant and unloaded protocols than loaded samples of the adjusted loading regime on day 21 pc while stain intensity was visibly greater in the free floating controls and loaded samples of the adjusted protocol compared to other condition on day 28 pc. These findings were in contrast with the measurement of the ALP activity level. The reason behind this was due to the difference in the undertaken approaches to evaluate the ALP level as quantification of enzyme activity was based on combined intracellular and extracellular ALP level. Staining technique exclusively measured extracellular enzyme activity. Therefore, the presented values in the ALP graphs showed small changes in the total level of enzyme as intracellular ALP level down-regulated because of the initiation of mineralisation while the previously produced enzyme still in-fluxed to the extracellular matrix. Nevertheless, measuring the ALP activity at different and closer time points for example within few hours of the applied loading, would assist in better understanding the trend of enzyme activity level under the applied compression regime.

Mineralisation was assessed based on the concentration of deposited calcium, phosphorous and zinc levels in the extracellular matrix. Calcium concentration was highest in all conditions on day 28 pc and cells that were subjected to adjusted cyclic loading showed greatest calcium accumulation in comparison with other experimental conditions. These findings were in agreement with the Alizarin staining of samples cross sections while the results of Alizarin staining of microspheres was not conclusive due to the same colour intensity of the deposited stains that was reported in controls and loaded samples and between earlier and later time points of encapsulation. Stimulation of cells under adjusted loading protocol was significantly superior owing to the highest up-regulation of

phosphorous accumulation in loaded samples of the adjusted loading protocols on days 21 and 28 pc and were in agreement with the results of calcium deposition.

Zinc level was shown to have stimulatory effect on bone formation and mineralization, production of collagen and ALP activity level in vivo and in vitro[188]. Zinc plays a key role in mechanotransduction pathway and osteogenic differentiation as it is part of Osterix, a novel zinc finger containing transcription factor, that is specifically expressed in all developing bone[189]. Zinc is also part of matrix metalloproteinases (MMPs) molecular structure that is capable of degrading all kinds of ECM proteins and is particularly important in cell proliferation, ECM remodeling and differentiation[190,191]. Increase in extracellular zinc level could be linked to up-regulation of MMPs. Among MMPs, MMP3 and 10 are detected in human developing bone while MMP1 and 2 are isolated from human osteoblast cells and MMP14 are restricted to mature osteoblasts[192]. Other MMPs including MMP9 are expressed in osteoblasts, chondroclasts and endothelial cells and MMP13 are mostly detected in chondrocytes and newly recruited osteoblasts[79]. In addition, Anderson et al. reported of matrix vesicles, extracellular particles that are located at the site of mineralisation and are conspicuously high in zinc. The first hydroxyapatite crystals are found in the inner surfaces of these membrane invested particles and are initiated by high level of ALP activity and calcium binding molecules. Biologic mineralization phase begins with release of hydroxyapatite crystals into ECM space and continuous crystal deposition by homologous nucleation process[193].

Our results indicated that zinc accumulation was significantly up-regulated in loaded samples of adjusted loading protocol on day 21 pc and declined to half of its value on day 28 pc. However, other conditions and controls showed opposite trend for zinc on the above time points, with higher zinc expression level on day 28 pc. Up-regulation of zinc on day 21 pc and prior to increase in the deposited calcium and phosphorous could be explained by accumulation of zinc in the matrix vesicles that initiates the assembly of hydroxyapatite crystals and mineralisation and was reported on day 28 pc. Higher concentration of zinc might indicate mineralisation and osteogenic differentiation of hES-MPs through higher MMPs expression level in ECM but it also could mean chondrogenesis of progenitor cells. In order to dismiss this hypothesis, chondrogenic staining of microsphere cross sections was performed using Alcian blue stain that bonds to glycosaminoglycans. Our findings demonstrated a faint blue stain in samples and conditions particularly on day 21 and 28 pc compared with free floating controls at 24 h pc which suggested very

low/no chondrogenic differentiation. Still, low deposition of chondrogenic stain might be due to the low initial seeding density of hES-MPs in the microspheres that resulted in a week staining signal. Nevertheless, more studies on the role of zinc in calcification via matrix vesicles and expression level of osteogenic and chondrogenic MMPs needed to fully link the up-regulation of zinc with matrix vesicles and expression level of matrix metalloproteinase family members.

SHG microscopic images revealed more defined, aligned and reorganised lay down of new ECM in the loaded samples under adjusted loading regime on day 21 pc. It was more evident that cells and newly laid down collagen fibres were mostly located at 10-20 µm from the microspheres surface and it supported our results in Chapter 3 on migration of cells from central area to the microspheres periphery at later time points of encapsulation. Collagen fibres were visibly thicker and reoriented compared to other experimental conditions but it was impossible to define the axis of alignment due to rotation probability of microspheres in the loading chamber during and after cyclic loading. SEM images provided information of how cells spread on the surface of collagen microspheres and showed reorganisation and remodeling of ECM and new assembly of collagen fibres of microspheres on day 28 pc. Visualisation of numerous deposited mineral particles especially in the loaded samples of adjusted strain protocol suggested more mineralised tissue in comparison with free floating controls and once more was in agreement with mineral quantification and staining results.

5.5 Conclusions and future work

Applying mechanical stimulation can effect cell commitment but at the same time it shows that mechanical loading on its own fails to provide all necessary signals important for cell commitment and osteogenic differentiation of hES-MPs as compared to chemical stimulation. Combining mechanical and chemical stimulations can increase the osteogenesis as suggested in previous chapters and other studies. It was shown that loading of very low cell number seeded on soft natural scaffold can encourage osteogenesis of undifferentiated cells by enhancing both early stage bone marker and extracellular mineral deposition of calcium, phosphorous and zinc. Monitoring alkaline phosphatase level reported significant increase in the enzyme activity by day 14 pc in loaded samples of adjusted loading protocol compared to free floating controls. Staining of cross section was further confirmed the

enhancement of mineral deposition in the loaded samples in comparison with other experimental conditions at the later time points. In addition, SHG microscopic images revealed more defined, aligned and reorganised lay down of new ECM in the loaded samples under adjusted loading regime on day 21 pc compared with other conditions. Nevertheless, better handling of collagen beads is required as hydrogel soft geometry could easily be affected by transferring microspheres to the loading chamber. Due to very small size and light weight of microspheres, collagen microspheres may rotate through loading chamber and may cause non homogeneous transfer of forces to the cells as shown in histological staining of microspheres. Therefore, cells in different areas of a microsphere may experience more random mechanical forces and respond differently to the applied load.

Although this study revealed strong links between the deposited extracellular minerals and osteogenic differentiation more osteogenic specific protein quantification is required to define a complete signalling pathway (s) consist of genes, proteins and deposited minerals in mechanotransduction and osteogenesis process. Therefore, gene expression studies (qPCR) of bone and early stage mineralisation markers including ALP, osteocalcin, osteonectin, Runx, BMPs and ColI and ColII along with phenotyping of differentiated cells are recommended in the future. Furthermore, studying the combined and individual effects of applying direct cyclic loading with fluid flow and shear stress on cells is required to draw the map of load transfer between different layers of collagen microspheres and cells. Also, more sample imaging for different time points and several areas/focal planes within each sample is needed to comment more accurately on the effect of sample variability in cell triggered remodelling of collagen fibres. Application of cyclic loading on 3D culture of hES-MP cells could be used as a model to study the effect of mechano-stimulation on osteogenesis both in vitro and in silico.

6

Effect of fluid flow on osteogenesis of hES-MPs/collagen microspheres

6.1 Introduction

Our understanding of the potential and behaviour of stem cells from different adult tissue sources have come a long way in recent years but it is still not clear how to precisely control their differentiation and to develop more efficient and effective tissue engineering strategies. As presented in previous Chapters (3, 4 and 5) the fate and function of progenitor cells can be controlled by stiffness, geometry as well as physical and chemical stimuli in their micro environment. It has also been shown that mechanical forces can influence stem cell fate toward a specific cell linage. Oscillatory fluid shear forces caused by fluid movement around cells interstitial space is one of the major forces that define mechanical environment of bone cells and can also be experienced by cells in bone marrow cavity. Weinbaum et al. predicted the range of shear stress that is experienced by mature bone cells as (0.8-3 Pa)[194] but the magnitude of shear stresses that is sensed by cells in bone marrow cavity anticipated to be much lower because of lower stiffness of the marrow structure, albeit the true magnitude is not yet known[88]. In 3D culture, it is more complicated to calculate the cellular level of the applied shear forces, as these forces are strongly different from scaffold to scaffold[195].

As presented in Chapter 5, mechanical stimulation can induce osteogenic differentiation of hES-MPs. Still, the best conditions to enhance osteogenesis, for example combination of mechanical loading with FSSs and chemical stimuli or the effect of each of these protocols on their own is not fully understood. The microfluidic

system that was introduced in Chapter 4 or cyclic compression loading (Chapter 5) of cells may be suitable methods for studying the effectiveness of mechanical conditioning on osteogenic differentiation of progenitor cells but, seemed incomplete without examining the effect of FSSs on the soft cells 3D constructs. For this study, hES-MPs were chosen as a cell type for the results to be comparable with other mechanical forces that were employed in this report.
The aim of this chapter was to design a simple shaking and rocking technique to apply physiologically relevant shear stresses and also to calculate the magnitude of FSS at the centre of each well in shaking and rocking platforms. In addition, it was aimed to assess the effect of oscillatory FSSs on the osteogenic differentiation of hES-MPs seeded collagen microspheres by evaluating ALP activity and deposited mineral levels of subjected samples at different time points.

6.2 Methods

6.2.1 Application of fluid flow-induced shear stress on microspheres by orbital shaker

Cell seeded collagen microsphere with the seeding density of 1000-2000 cells per microspheres were placed on top of a mesh sheet and metal ring at the centre of each well in 12 well plates with their respective basal media. Microspheres were then exposed to FSS using an orbital shaker as shown in Figure 6.1. The shaker rotation regime consisted of 10 days experiment with speed of 50 rpm for 40 min/day that began from day 6 post en-capsulation. Cell seeded collagen microspheres were immersed in 2.5 mL media and kept either under static condition with no force or were subjected to FSS. The FSS generated were calculated at the centre of each well using previously described model by Dardik et al.[196]. All bouts of shaking experiment were performed inside an egg incubator to control the temperature and static samples remained in the main incubator. Shear stress was calculated using the following equation:

$$\tau_{max} = a\left(\eta\rho\left(2\pi f\right)^3\right)^{\frac{1}{2}} \tag{6.2.1}$$

Where a is the orbital radius of rotation of shaker (0.5 cm), ρ is the density of culture medium (0.1 g/ml), η is the viscosity of the medium (0.001 Pa s), and f is the frequency of rotation 50 rpm equal to 1.2 rotation/sec. Shear stress was calculated at the centre of well as 0.0597 Pa.

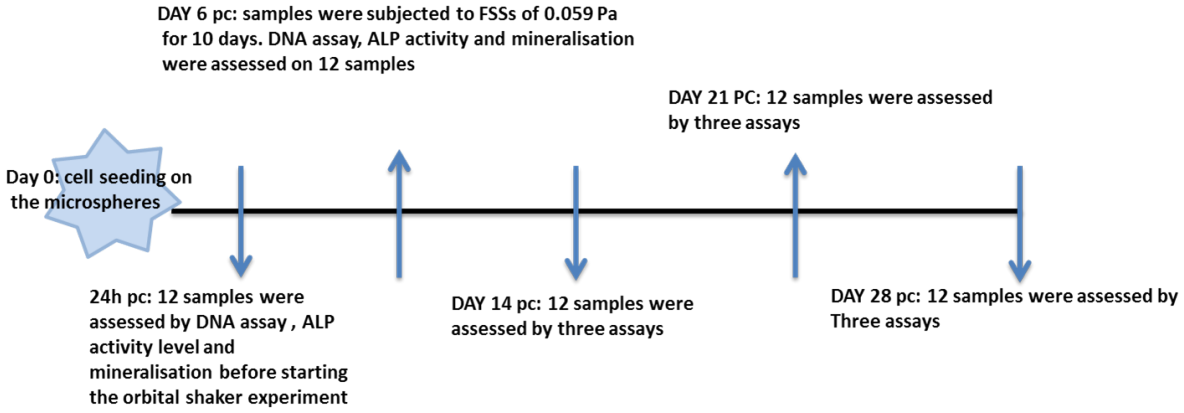


Figure 6.1: Cell seeding and experimental time line of orbital shaker experiment. (1000-2000) hES-MPs were seeded in collagen microspheres that were fixed at the centre of each well. DNA assay, ALP activity level and quantification of mineralisation were performed on samples at 24 h, day 6, 14, 21 and 28 pc.

6.2.2 Application of fluid flow-induced shear stress on microspheres by platform rocker

Rocker regime consisted of 45 cycles/min for 40 min/day for 10 days which started on day 6 post en-capsulation. Equation 6.2.2 was applied to calculate characteristic shear stress, defined as the shear stress at the centre of dish bottom when the dish is horizontal. When microspheres plate was placed on the platform, the see-saw rocking motion caused fluid in each well to move back and forth under the influence of gravity that forced shearing across the microspheres as shown in Figure 6.2. The FSS generated were calculated for one point at the centre of each well using previously described models by Zhou et al. and Delaine-Smith et al.[165,197]. All bouts of rocking were performed inside an egg incubator under the controlled temperature while static samples remained in the main incubator at the same time.

$$\tau_w = \frac{\pi \mu \theta_{max}}{2\delta^2 T} \tag{6.2.2}$$

Where μ is the fluid viscosity (0.001 Pa s), θ_{max} is the maximal flip angle (the rocking platform had a maximum tilt angle of 6°), δ is the ratio of the fluid depth to the wall length (3 and 7 ml respectively) and T is the time for one cycle. This model assumed that fluid movement was mainly caused by gravity and the fluid free surface remains horizontal. Also, the effect of centrifugal forces on the fluid was ignored due to the low angular acceleration and velocity. Shear stress at the centre of each well plate was calculated as 0.040 Pa.

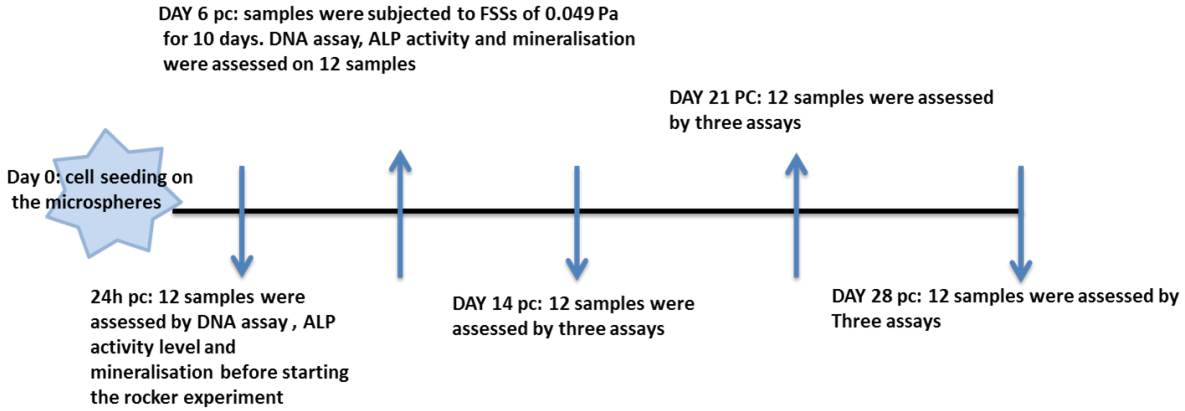


Figure 6.2: Cell seeding and experimental time line of platform rocker. (1000-2000) hES-MPs were seeded in collagen microspheres that were fixed at the centre of each well. DNA assay, ALP activity level and quantification of mineralisation were performed on samples at 24 h, day 6, 14, 21 and 28 pc.

6.2.3 Cell culture

Progenitor cell line hES-MP 002.5 (hES-MPs) were used for this experiment and cells were selected between passages 3-7. hES-MPs were seeded in bovine collagen I microspheres as was previously described in Chapter 2. hES-MP cell seeding density of 5×10^5 cells/ml and collagen concentration of 2 mg/ml were employed in this experiment.

6.2.4 Cellular assay

Total DNA measurement of hES-MPs cell line of controls versus samples that were subjected to orbital shaker and rocker generated shear stress were determined. DNA pico-green assay were used to detect total DNA and cell number at different time points of 24 h, days 6, 21 and 28 pc.

ALP activity of shear stress subjected samples against free floating controls was measured at 24 h, days 6, 14, 21 and 28 pc and was also visualised by ALP staining of microspheres cross sections.

Quantitative and qualitative deposited calcium staining were performed using 1% Alizarin red S staining at 24 h, days 6, 21 and 28 pc via ICP-ES.

Phosphorous level of extracellular matrix was assessed at 24 h, days 6, 21 and 28 pc by ICP-ES.

Extracellular matrix zinc level was quantified at 24 h, days 6, 21 and 28 pc by ICP-ES.

6.2.5 Statistics

All experiments were performed three times in triplicates (n=9). Cell viability at different time points, ALP and mineralisation comparison as well as statistical differences between static and shaker and rocker samples were completed using one-way ANOVA followed by Sidak's or Tukey's multiple comparisons test by GraphPad software.

6.3 Results

6.3.1 Effect of FSS on total DNA and proliferation of hES-MPs

HES-MPs seeded collagen microspheres were treated with three different conditions containing osteogenic media, hES-MPs basal media with and without added FGF-β. DNA number of cells was evaluated after being subjected to FSS in shaker experiment regime. The results of cell viability graph indicated that in all conditions cells proliferated well during the 28 days experiment (Figure 6.3). The early DNA concentration increased markedly after day 5 pc and continued to improve till day 14 pc followed by a drop on day 21 pc before surging to highest DNA number on 28 pc. All shaker sample and static control groups followed the same trend and there was no significant differences reported between groups over 21 days. On day 28 pc, however, samples treated with osteogenic media showed significantly higher DNA that those treated with FGF which kept the cells in undifferentiated status (110 ng compare to 75 ng, $p < 0.0001$). Furthermore, FGF treated samples that were subjected to shear stress also presented greater DNA compared to controls (102 ng and 75 ng respectively, $p < 0.001$). Nevertheless, non-chemically treated samples showed lower DNA content than controls ($p < 0.01$) on day 28 pc. Stem cells with different passage number were compared to rule out possible inter variability between older cells and no significant differences between cell passages DNA number was observed during shaker experiment.

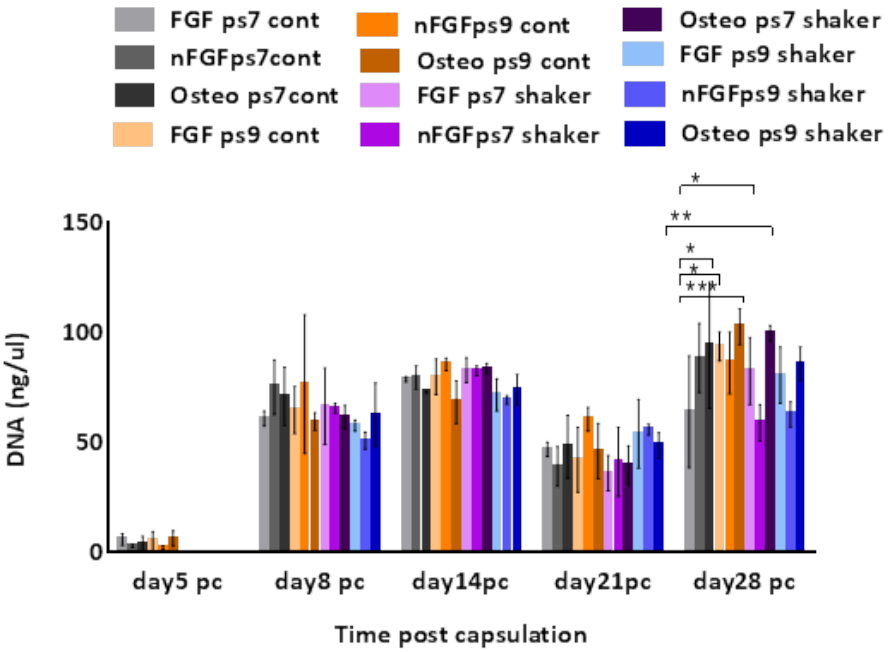


Figure 6.3: Cell viability of shear stress induced samples were assessed against static free floating controls over 28 days pc, total DNA measurement was performed for cell proliferation, * indicates statistical significance (*** p <0.001, ** p <0.01 and * p <0.1). Data is mean ± SD for n=9 samples.

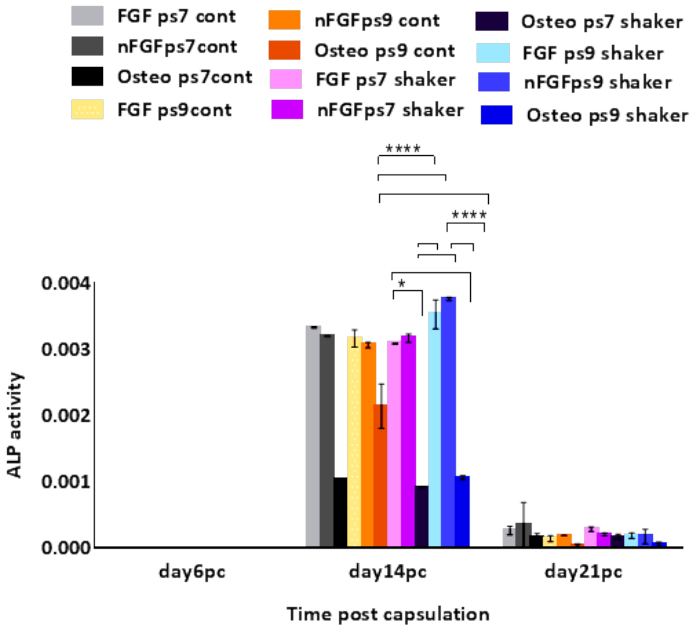


Figure 6.4: ALP activity level of shear stress induced samples were assessed against static free floating controls over 28 days pc, ALP activity was evaluated to study the osteogenic effect of fluid flow-induced shear stress on cells, * indicates statistical significance (**** $p < 0.0001$ and * $p < 0.1$). Data is mean ± SD for n=9 samples.

6.3.2 Evaluation of shear stress induced ALP activity level

ALP activity level of different conditions was compared to investigate the early sign of mineralisation (Figure 6.4). ALP level showed a peak on day 14 pc in all groups, in both passages samples and static controls that were treated with osteogenic media presented significantly lower level of ALP that was up to three times lower than other conditions. FSS induced samples of all experimental groups, however, manifested higher ALP level compared to osteogenic controls in both cell passages. Low ALP activity was detected in osteogenic media treated samples compared to both FGF-β and nFGF-β treated samples. This finding may suggest early differentiation and mineralisation of cells due to combined effect of osteogenic media and shear stress. Following the increase on day 14 pc alkaline phosphatase activity level reduced dramatically to 7 folds of its value and reached to around 0.0005 on day 21 pc. There was no significant changes of ALP activity found between different conditions and cells passage number on day 21 pc.

The effect of chemical stimulation combined with FSS were further tested by repeating the ALP activity measurement in shaker experiment with static controls

that were treated with and without osteogenic media compared with FSS induced samples (Figure 6.5 a). Both chemically stimulated samples and controls showed significantly higher ALP level on day 14 pc in comparison with non treated conditions. Osteogenic media treated free floating controls presented up to 3 folds higher ALP activity than non treated controls. ALP level in osteogenic media treated shaker samples was significantly higher and enzyme activity was reported 5 folds more than non treated shaker samples on day 14 pc ($p < 0.001$ and < 0.0001 respectively) but the ALP level reported lower than the static controls. Same pattern of ALP activity was detected on day 21 pc, yet non treated shaker samples showed lowest enzyme activity level compared to other conditions whereas, ALP level in chemically induced static controls was repeated the highest and close to its values on day 14 pc (0.0052 and 0.0043 respectively). Interestingly, extracellular ALP staining showed higher accumulation of deposited ALP stain in static controls than shaker samples on days 21 and 28 pc which was in contrast with quantitative ALP activity results (Figure 6.9).

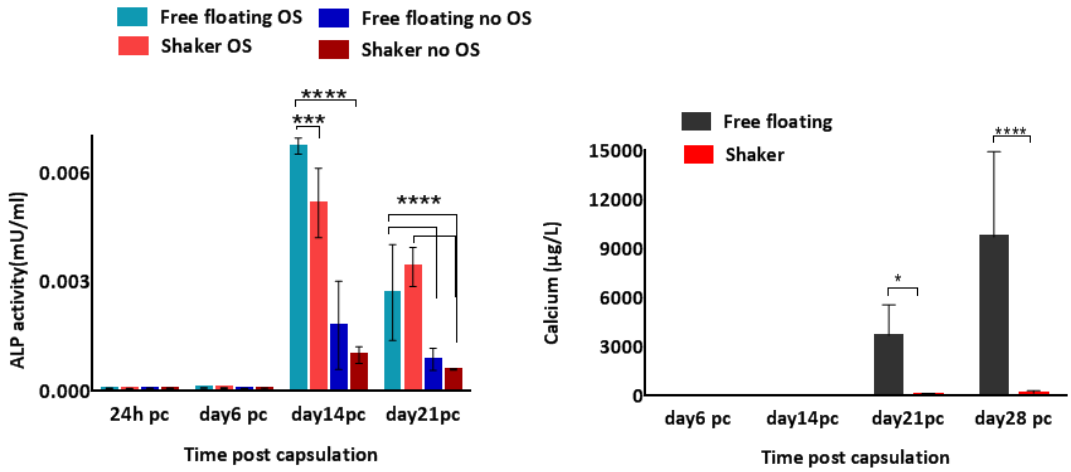


Figure 6.5: Measurement of alkaline phosphatase activity and deposited calcium in shaker experiment compared with static controls over 28 days pc, a; samples that were treated with osteogenic media (OS) presented significantly higher ALP level from day 14 pc onward, b; deposited calcium up regulated considerably from day 21 pc onward in static controls compared with the shaker samples, * indicates statistical significance (**** $p < 0.0001$ and *** $p < 0.001$). Data is mean ± SD for n=9 samples.

6.3.3 Assessment of mineralisation

Applying shear stress combined with chemical stimulation presented highest effect in initiation of mineralisation that was supported by Alizarin red staining of all three conditions in shaker experiment (Figure 6.6). Osteogenic samples and controls showed more calcium than other conditions in all time points. Both treated samples in FGF-β and nFGF-β media presented relatively higher calcium deposition from day 14 pc onward. Yet, the effect of shear stress in mineralisation of chemically and non-chemically treated samples was inconclusive.

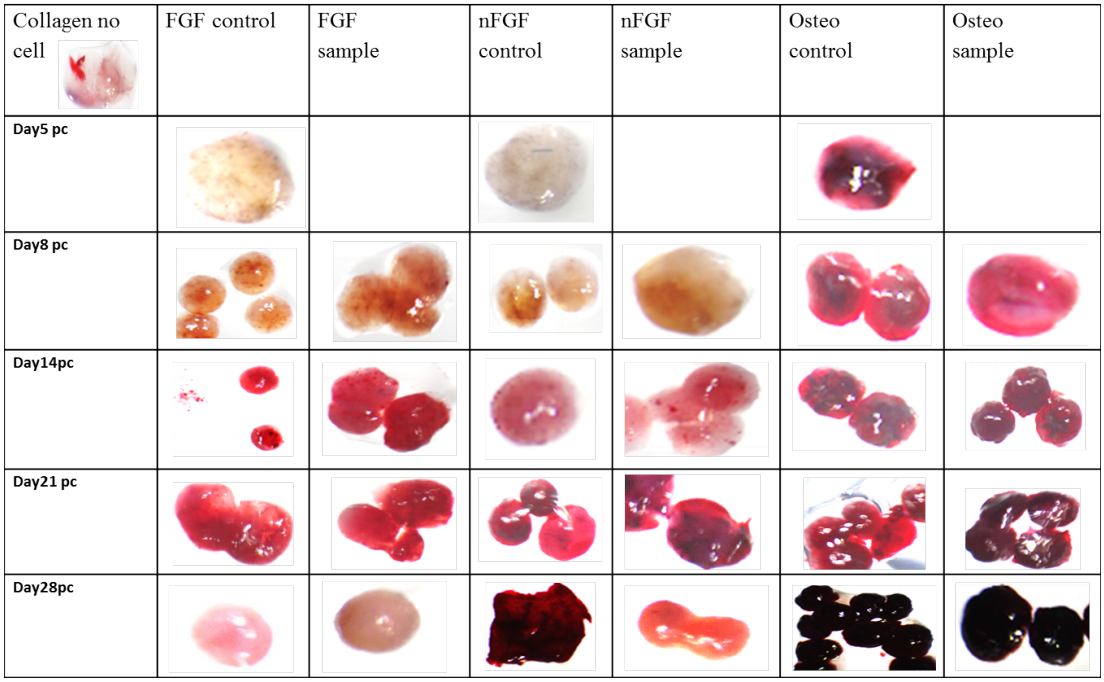


Figure 6.6: Comparison of ARS red S staining intensity between shaker samples and static free floating controls that were treated with osteogenic, basal media with added FGF-β and basal media. Deposited ARS stain was considerably higher in shaker samples that were treated with osteogenic media compared with other experimental conditions from day 14 pc onward.

These finding however, were not in agreement with the results of calcium deposition measurement that indicated significantly higher calcium level in free floating controls than shear stress subjected samples on days 21 and 28 pc (Figure 6.6 b). Chemical stimulation had the most effect in initiation of mineralisation and mechanical forces and the level shear stress on its own, may not be sufficient to encourage osteogenic differentiation. The results of ARS staining of shaker

samples and static controls cross sections also presented more deposited staining static controls that was visually detectable from day 21 pc, while shaker samples only picked a weak colour of ARS stain on day 28 pc that was mainly restricted to the centre of cross section (Figure 6.10). In addition, H&E staining of shaker samples and controls cross sections further confirmed the more mineralised tissue in static controls than shaker samples from day 21 pc onward with visibly darker purple colour around cells (Figure 6.11). Quantification of phosphorous level also indicated significant up regulation from day 21 pc while, shaker samples presented substantially low phosphorous concentration which was close to the threshold (Figure 6.7 b). The results of deposited zinc measurement presented up regulation of zinc concentration in both samples and controls on days 21 and 28 pc yet, static controls deposited zinc level was slightly higher than shaker samples (165 µg/l and 53 µg/l). No statistically significant difference was found between shaker samples and static controls at any time points.

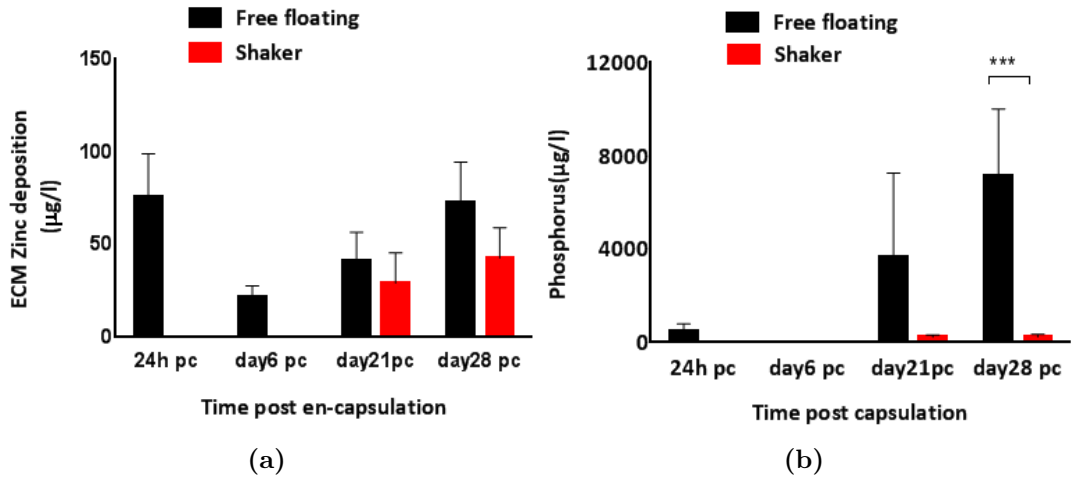


Figure 6.7: Deposited zinc and phosphorous level of shear stress induced samples were assessed against static free floating controls over 28 days pc, a; quantitative measurement of deposited zinc showed significantly higher concentration of minerals in static controls that fluid flow induced samples was performed for cell proliferation, b; phosphorous level was up regulated significantly in static controls than shaker samples, * indicates statistical significance (*** $p < 0.001$). Data is mean ± SD for n=9 samples.

In a separate study the osteogenic differentiation of subjected hES-MPs to shear stress was examined and compared using orbital shaker and rocker (Figure 6.8). Applied shear stress by orbital shaker proved to be more in favour of mineralization compared to rocker as higher ALP activity was reported on both days 21 and 28 pc.

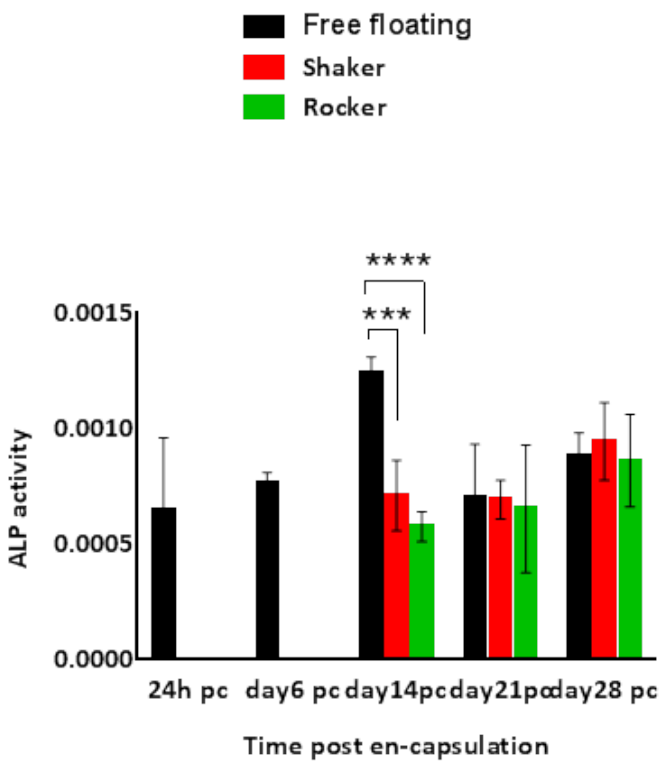
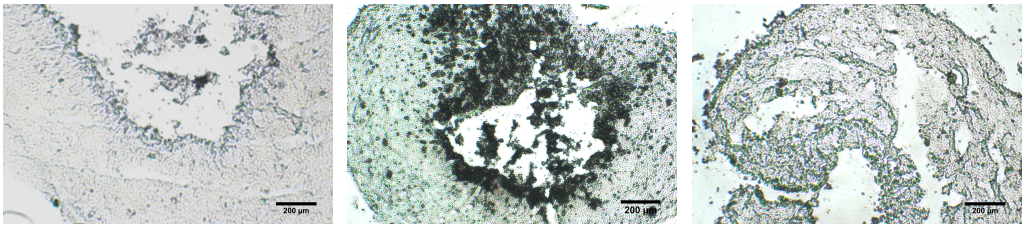
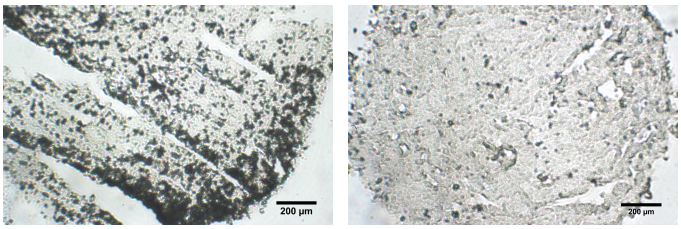


Figure 6.8: Comparison of ALP activity level between shaker, platform rocker samples and free floating controls over 28 day pc. Alkaline phosphatase level was reported significantly higher free floating controls compared to fluid flow-induced samples of rocker and orbital shaker conditions. * indicates statistical significance (*** $p < 0.001$ and **** $p < 0.0001$). Data is mean ± SD for n=9 samples.

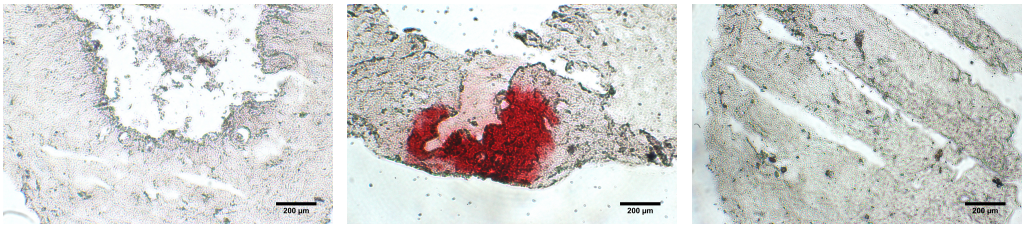


(a) ff, Day 6 pc **(b)** ff, Day 21 pc **(c)** ss, Day 21 pc

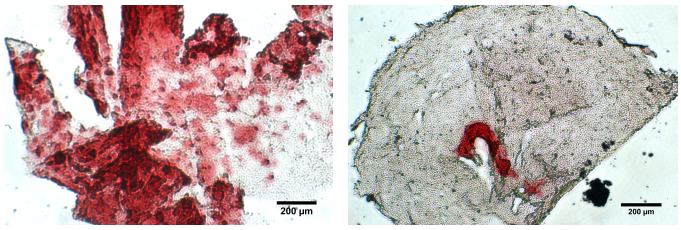


(d) sc, Day 28 pc **(e)** ss, Day 28 pc

Figure 6.9: ALP staining of 10 µm thick cross sections of of shear stress induced samples were performed against static free floating controls over 28 days pc. ff; free floating control, sc; static control, ss; shaker sample. Static free floating controls presented higher ALP stain intensity on both days 21 and 28 pc compared to shaker experiment samples.

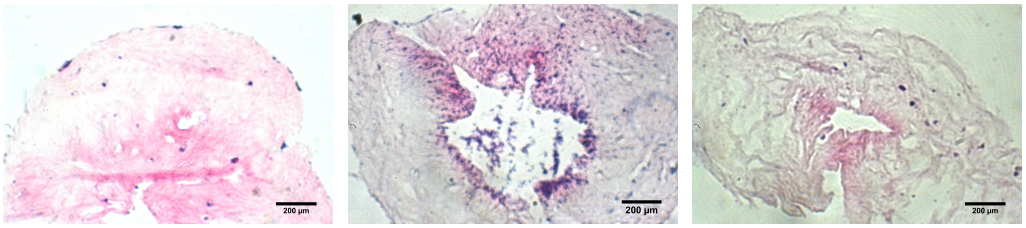


(a) sc, Day 6 pc **(b)** ff, Day 21 pc **(c)** ss, Day 21 pc

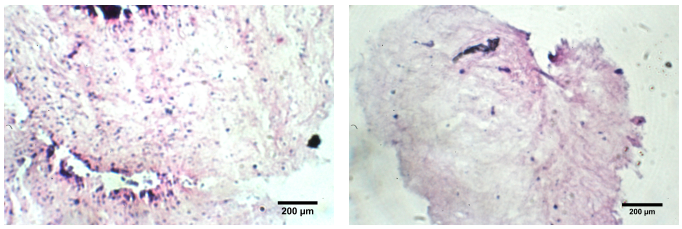


(d) sc, Day 28 pc **(e)** ss, Day 28 pc

Figure 6.10: Alizarin red S staining of 10 µm thick cross section of shear stress induced samples were assessed against static free floating controls over 28 days pc. ff; free floating control, sc; static control, ss; shaker sample . Static controls presented more accumulation of deposited ARS stain on both days 21 and 28 pc compared to shaker experiment samples.



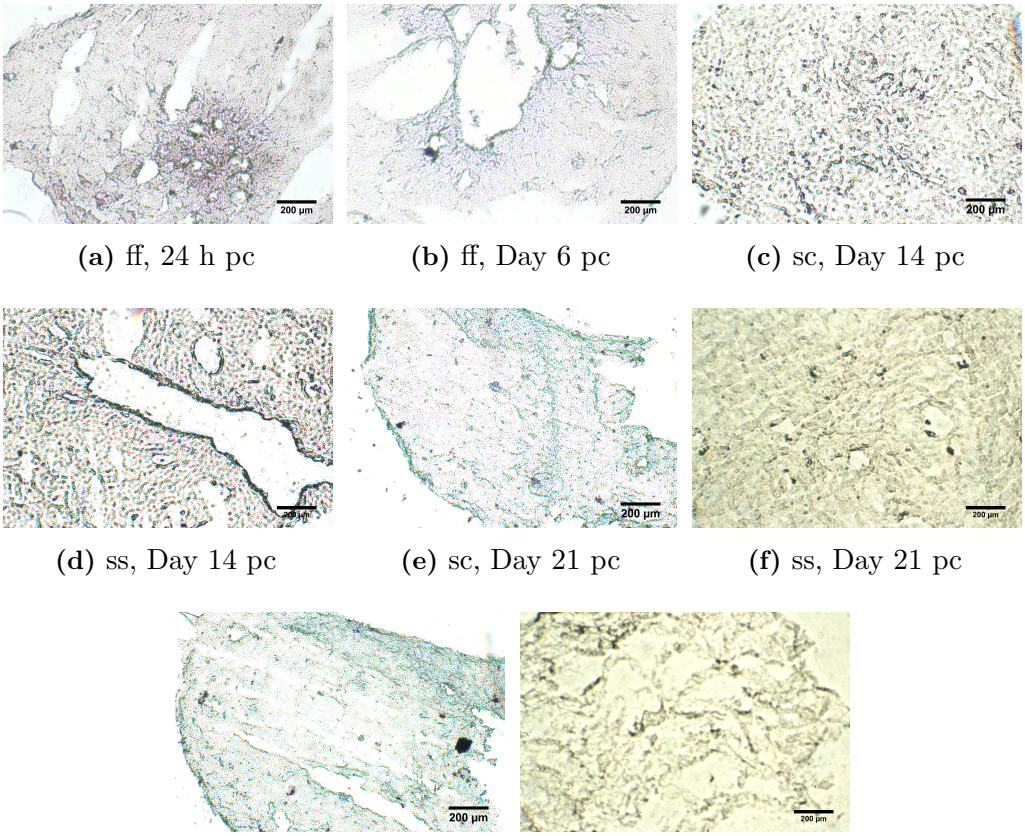
(a) ff, Day 6 pc **(b)** ff, Day 21 pc **(c)** ss, Day 21 pc



(d) sc, Day 28 pc **(e)** ss, Day 28 pc

Figure 6.11: Histological staining of 10 µm thick cross section of shear stress induced samples against static free floating controls over 28 days pc. ff; free floating control, sc; static control, ss; shaker sample. Static controls presented darker stain colour that suggested more mineralised cells on both days 21 and 28 pc compared to shaker experiment samples.

Shaker and rocker samples presented very similar values and intensity for ALP activity but much lower compared with free floating controls. Yet again extracellular calcium and phosphorous level of rocker samples that were subjected to FSSs were undetectable and therefore did not indicate mineralisation in rocker experiment. In contrast to static controls the ALP level of both rocker and shaker samples was reported as the lowest on day 14 pc which was increased marginally by day 21 and 28 pc. Free floating static controls showed statistically significant higher ALP level compared to shaker and rocker conditions on day 14 pc ($p < 0.001$ and < 0.0001 respectively). However extracellular ALP level of free floating controls showed higher intensity of stain on day 21 pc in comparison with shaker samples that was in contrast with the result of ALP activity level presented in Figure 6.8. The results of Alcian blue staining showed higher deposition of stain in shaker samples particularly on day 14 pc that faded by day 21 and 28 pc. These finding suggested the chondrogenic differentiation of hES-MPs under FSS. The intensity of Alcian blue stain however, remained stable over the time in static controls.



(a) ff, 24 h pc **(b)** ff, Day 6 pc **(c)** sc, Day 14 pc

(d) ss, Day 14 pc **(e)** sc, Day 21 pc **(f)** ss, Day 21 pc

(g) sc, Day 28 pc **(h)** ss, Day 28 pc

Figure 6.12: Alcian blue staining of 10 µm thick cross section of shear stress induced samples against static free floating controls over 28 days pc. ff; free floating control, sc; static control, ss; shaker sample. Shaker sample presented higher accumulation of deposited stain on day 14 pc that suggested initiation of chondrogenic differentiation compared to static controls.

6.4 Discussion

The main aim of this chapter was to evaluate the effectiveness of a simple methodology (a shaking or a rocking platform) to apply oscillatory fluid flow induced shear stress to progenitor cells for stimulating osteogenic differentiation. This study to our knowledge is the first to apply this simple methodology on soft 3D culture of progenitor cells. Its has been shown that stem cells respond to different types of mechanical stimuli in both 2D and 3D bioreactor conditions[16]. For 2D systems, various experimental apparatus, including the cone and plate system[111], rotating disk or radial flow devices[198], oscillating orbital shaker system[197], and a rocking see-saw system[111] have been used to study the effects of shear stress on monolayers of cells. More recently, 3D cultures of cells in bioreactors were designed to apply flow-induced shear forces to cell seeded scaffolds[104] that include

rotating wall vessels, spinner flasks, and perfusion systems. In 3D cultures, it is more complicated to calculate the cellular level of the applied shear forces, as these forces are strongly different from scaffold to scaffold. Jungreuthmayer et al. reported that applying the same fluid flow resulted in generation of much higher shear stresses within a collagen/GAG scaffold than a calcium phosphate scaffold[195].

The calculated shear stress in this study for both shaker and rocker experiments were much lower than those estimated to occur within mature bone (0.3-8 Pa)[194], and were at 0.04 Pa for rocker and 0.0597 Pa for shaker experiments at the centre of well culture and very close to FSS that was reported for 2D cell culture by Delaine-Smith[165]. But also was much lower than the calculated FSS reported for 2D and 3D culture of osteoblast cells in McCoy and Sittichokechaiwut studies[106,185].

It has been demonstrated that higher magnitudes and longer period of exposure to shear stress can lead to cell detachment of both progenitor and osteoblasts cells[106]. However, mature bone cells can resist higher magnitudes of FSS better than progenitors cells as, these cells are encased in a more mineralised collagen matrix compared to stem cells. Furthermore, higher shear stresses that were used in in vivo experiments may not be suitable or required for in vitro conditioning of 3D constructs. While, the true value of shear stress forces experienced by stem cell environment in vivo is not yet known, it is likely that the magnitude of FSS will be much lower than that in mature bone cells because of higher porosity and lower stiffness of progenitor micro environment[88]. In addition, it is still not clear whether in tissue engineering application the attempt should be on replicating mature bone environment or more developmental and healing environment that encourage osteogenic differentiation of progenitor cells. As developing bone tissue are not yet a mature tissue the experienced FSSs forces are likely to be different from those of a fully developed one, but little is known so far[199]. In a study that was carried out by Nauman et al. the effect of continuous pulsatile fluid shear stresses on production of prostaglandin E2 (PGE_2) in osteoblasts was investigated. It showed that low shear stress (0.06 Pa, 3 Hz) have no effect on the production of PGE_2 and initiation of mineralisation but, can increase ALP activity[200]. In addition, other studies indicated that applying shear stress with magnitude of 0.06 Pa and above can promote cytosolic calcium concentration in osteoblasts 2D culture[201].

Cell seeded collagen microspheres were fixed at the centre of each well by a

thin fabric mesh to ensure that fluid flow and shear stress can reach the construct hence cells more homogeneously. Fluid flow induced shear stress was applied to microspheres and osteogenic markers were analysed to check whether low magnitude of FSS can provide all the necessary signals required for initiation of osteogenic differentiation in hES-MPs. Also, the uniaxial direction of fluid flow was compared with rotational/swirl flow to evaluate the validity of flow direction and the generated FSSs on the osteogenic differentiation of progenitor cells.

Our results indicated that chemical stimulation encouraged considerably higher osteogenic differentiation of all 3D hES-MPs culture conditions compared to FSS as ALP level and deposited Alizarin red S stain up regulated more and at earlier time points in both shaker samples and static controls that were treated with osteogenic media. Non chemically treated shaker samples and static controls ALP activity, however did not change significantly which suggests ineffectiveness of applied FSS on the osteogenesis of cells seeded microspheres. These findings were further supported by results of qualitative ARS staining that showed chemical stimulation was more dominant than FSS in determination of hES-MPs fate. Different passage number of cells and treatment with basal media with no added FGF-β showed little impact on osteogenesis as suggested by lower intensity of ARS but interestingly even lower deposited ARS stain was detected in combination basal media with FSS from day 14 pc onward.

Mineralisation was further assessed in shaker samples and static controls by quantification of deposited minerals using ICP-ES. Concentration of deposited calcium and phosphorous in shaker samples reported significantly lower than static controls and was confirmed by Alizarin red S staining of samples and controls cross sections at different time points. Free floating controls presented higher deposition of stain on both day 21 and 28 pc that indicated higher mineralisation in controls than samples and was further confirmed by histological staining of cross sections. H&E staining of samples and controls revealed darker purple colour in free floating controls in comparison with shaker samples on days 21 and 28 pc which once more suggested more mineralised tissue in controls than those subjected to FSSs.

The result of deposited zinc concentration however, showed higher zinc level in shaker samples compared with other deposited minerals but free floating controls presented more up regulation of zinc than shaker samples. As was reported in previous chapter high zinc level can be linked to chondrogenic differentiation

of cells therefore, these findings were evaluated more by Alcian blue staining of samples and control cross sections that revealed higher deposition of stain in shaker samples compared with controls on day 14 pc. Nevertheless, the intensity of detected Alcaine blue stain in shaker samples was reported much lower than controls in days 21 and 28 pc. These inconclusive results require further analysis of both osteogenic and chondrogenic markers to confirm particular linage differentiation of hES-MPs under the applied FSSs. Because there was no similar study on the effect of FSS on soft cell seeded collagen microspheres reported (to the best of author knowledge), no data comparison were possible for this experiment.

In a separate study, hES-MPs seeded microspheres were fixed at the centre of each well and were subjected to FSSs by using a rocking platform and osteogenic differentiation of cells were assessed by measurement of ALP activity and mineralisation markers level. Alkaline phosphatase level of rocker samples reported lower than both shaker samples and static controls from day 14 pc onward and unlike the free floating controls enzyme activity which was reduced by day 21 pc, ALP level continued to be up regulated till day 28 pc and indicated an opposite trend in comparison with other conditions. Yet, no calcium and phosphorous was detected in rocker samples by ICP-MS which suggested inhibition of mineralisation by this experiment. Our results are comparable with Delaine-Smith study that showed applying 0.04 Pa magnitude of FSS by rocking platform can't induce osteogenic differentiation of 2D hES-MPs culture within osteogenic media treatment[165]. ALP activity level of hES-MPs 2D culture did not show any up regulation on days 14 and 21 while our findings indicated an up regulation of enzyme activity level up to day 28 pc. One reason could be higher sensitivity of fluorometric ALP assay that was employed in our experiment to detect lower ALP activity level in comparison with colorimetric pNPP assay that was used in their studies. In addition, FSS stimulated mineralisation of hES-MPs 2D culture by up regulation of deposited calcium up to day 21 pc whereas applying fluid flow induced shear stress was not effective to enhance mineralisation of hES-MPs seeded microspheres.
While other studies have shown that fluid flow induced shear stress and other mechanical forces alone can induce osteogenesis of stem cells[184,202], in this study FSSs alone was not effective in significantly enhancing ALP activity or initiating the mineralisation. The applied FSSs might only be effective in promoting osteogenesis of hES-MPs 2D culture and it is possible that 3D soft collagen hyrogel is not an appropriate construct for transmission of low magnitudes of FSSs to the cells. In addition, the calculated values of FSSs are specifically valid for the cells on the

surface of the microspheres, therefore the inconsistency between our results could be due to random spreading manner and arbitrary number of cells in collagen beads. Supplementation with Dex and increasing the FSSs magnitude might be required to enhance osteogenic differentiation response while assessment of chondrogenic and adipogenic markers is necessary to rule out hES-MPs differentiation in to other cell linages.

6.5 Conclusions and future work

The effect of mechanical forces on progenitor cells and their potential to aid healing and induce direct differentiation is now of a major focal points for musculoskeletal tissue engineering applications. The formation of a suitable tissue engineered construct requires mechanical conditioning to endure the forces it will experience in the body. Shaker and rocker systems that were employed here created FSSs that up regulated ALP level but failed to enhance mineralisation and osteogenic differentiation of soft hES-MPs seeded collagen hydrogel in the absence of osteogenic media. Static free floating controls showed higher alkaline phosphatase activity and deposited minerals in both presence and absence of osteogenic media which was indicated ineffectiveness of the applied shear stress in osteogenesis. The role of shear stress in initiation of osteogenesis in cells 3D culture still has not been well defined. It was shown that combination of chemical stimulation and shear stress can promote osteogenesis but fluid flow alone may not provide all the necessary signals for osteogenic differentiation. Therefore, more studies are needed to fully unveil the role of shear stress and mechanical stimulation in mechanotransduction and determination of stem cells fate. The system itself however have several advantages that includes: its simple design, can accommodate numerous experimental samples and allows to study a wide range of loading parameters (for example: load days, load frequency) in combination with different supplements. Additionally, the system allows to study and understand the related biochemical events and activation of genes/proteins pathways in mechanotransduction.
Optimisation of the fluid flow rate, shear stress magnitude, frequency and duration of experiment are needed to obtain the best protocols for shaker and rocker experiments to enhance osteogenesis of cells. Further evaluation of chondrogenic markers and related genes is also required in comprehending the role of employed shear stress regime in chondrogenesis of hES-MPs 3D culture. It is equally necessary to asses the effect of combining chemical and FSS stimulation on regulation of osteogenic gene markers to establish better understanding of fluid flow induced

shear stress on osteogenic differentiation of progenitor cells.

7

Discussion and Conclusions

The main aim of this research project was to study the effect of mechanical stimulation on the osteogenic differentiation of hES-MPs seeded collagen microspheres. The overall goal was to assess whether osteogenic differentiation and mineralisation of progenitor cells can be manipulated by mechanical forces without interfering of chemical stimulation? In other words, are mechanical forces on their own enough to provide all the necessary biochemical signals required in mineralisation of hES-MPs 3D culture? The hypothesis was that mechanical and physical cues in microenvironment of stem cells can promote osteogenesis of soft 3D progenitor cells and our results showed that physical cues (bovine collagen I microspheres) and external mechanical forces (cyclic compression, tension and FSS) both influence and control cells behaviour, mineralisation and matrix reorganisation and alignment.

7.1 Collagen I microspheres

Physical cues in scaffolds including: collagen concentration, degree of fibres cross linking, and pore size influence collagen fibres organisation and collagen gel mechanical properties. This study showed that different concentrations of collagen can affect the gel's mechanical properties and are important in cell viability and proliferation. It also showed that undifferentiated and differentiated cells respond differently to stiffness of their environment as progenitor cells proliferated more and spread on lower concentration of rat tail collagen I gel (1.5-2 mg/mL) while more differentiated cells (MG-63s) adapted to the stiffer environment (3 mg/mL) with declined viability on the softer surfaces. These results are in agreement

with the works published by Chen et al. and Kameoka et al.[119,120] that showed collagen concentration of 2 mg/mL and 3.5mg/mL support proliferation of MSCs and human breast cancer cell line MDA-MB-231 respectively.

In addition, cell seeding density was shown to be dominant in survival and growth of encapsulated cells. Seeding with low cell number indicated reduced cell viability within the first 24 h of encapsulation in both cell lines. Concentration of 1×10^6 cells/mL showed the highest cell viability and number over 7 days pc in both hES-MPs and MG-63 cell lines. These findings are in line with Chan et al. study which showed optimum cell viability with cell density of 1×10^6 cells/mL[120].

Encapsulated hES-MPs contracted collagen microspheres much higher than MG-63s. Collagen contraction in both cell lines was most substantial between day 3 and 7 pc, which was in contrast with Chan et al. and Li et al. studies reporting the most significant collagen contraction within the first 30 h of pc[120,164]. Furthermore, seeded hES-MPs proliferation results presented a delayed in cell growth between 24 h and 120 h pc that was followed by an steady increase in cell number. This finding suggests that hES-MPs remodel and reorganise their new environment before spreading and proliferation. The synergy between decreasing the cell number and no notable contraction confirmed cell contraction is vital for their existence, elongation and proliferation in the new soft micro environment.

Cell concentration seemed to be more influential with respect to collagen concentration in microsphere contraction. As results indicated, collagen droplet with cell seeding density of 1200 cells/5 µL droplet and collagen concentration of 2 mg/mL, contracted up to 15% within 30 h of pc, while contraction in microspheres with cell concentration of 750 cells/5 µL droplet was observed much later (within 96 h) and less significant. Comparison between bovine and rat tail collagen I fibres micro structure presented close similarities between two species. Both hES-MPs seeded collagen microspheres showed more amorphous structure and less organised collagen fibres compared to seeded samples. hES-MPs were added before polymerisation of collagen to the master mix which suggests that cells possibly digested and reorganised collagen fibres in a more random manner for their growth and viability.

Moreover, different passages of hES-MPs were compared to assess the consistency of stem cells behaviour when treated with osteogenic media, with FGF-β and without FGF-β. It been shown in Chapter 3 that chemical stimulation pro-

mote and enhance osteogenic differentiation of cells in both passages by increasing ALP activity and deposited calcium while without FGF-β treated samples expressed delayed and lower alkaline phosphatase activity level and mineralisation. Comparing 2D and 3D cultures of hES-MPs indicated a peak in ALP level of 3D culture of hES-MPs on day 14 pc that dropped by day 21 pc while, 2D culture showed a continuous increase of ALP activity over 28 days pc. These findings were further confirmed by calcium staining and measuring ALP activity level which followed similar trend in both 2D and 3D cultures, but chemical stimulation enhanced osteogenic differentiation and early mineralisation of hES-MPs that began from day 5 pc.

7.2 Mechanical conditioning of cells

7.2.1 Microfluidics

A microfluidic chamber was designed as an alternative approach to bioreactors and osteogenic differentiation of hES-MPs was assessed under the mechanical conditioning of cells . Although numerous studies showed the importance of integrating the microenvironment with mechanical force and fluid flow to influence stem cells fate by employing microfluidic system, they failed to use 3D stem cells culture to mimic in vivo flow condition[167]. Therefore, the effect of applying external mechanical stimulation on the osteogenesis of 3D soft environment of progenitor cells was analysed using microfluidic device and the osteogenic markers level was measured at different time points.

Several approaches were used in building a microfluidic chamber including soft lithographic technique, rapid prototyping and replica molding to achieve appropriate geometry, height and surface structure. Apart from using a metal rod as a replica, all the other attempts failed in providing the required height and surface roughness for the microfluidic chamber. Surface modification via physical adsorption, rinsing the chamber with BSA and PEG PEG/silane treatment of the chamber did not change the chamber surface chemistry and proved to be ineffective in preventing collagen microspheres attachment to the chamber's wall[168 169 171]. In addition, alteration of surface roughness was employed through acetone vapour polishing but did not improve surface smoothness.

Although compression cycles did not adversely affect the viability and proliferation of hES-MPs, the ALP activity and deposited phosphorous levels proved ineffective in enhancing mineralisation and osteogenesis of seeded hES-MP/collagen microspheres. As high ALP and very low deposited minerals were reported at the later time points (days 21 and 28 pc). These findings were further confirmed by minute ECM calcium level and very low intensity of deposited Alizarin red stain.

The main focus of this study was to build a microfluidic device with optimum height, surface chemistry and roughness to be suitable in applying mechanical loading. Thus, cellular response of hES-MPs require more assessment and meticulous evaluation by measuring other bone markers including osteocalcin, collagen I and RUNX2 and their genetic expression. Also, chondrogenic and adipogenic differentiation of hES-MPS under the applied cyclic compression loading should fully be evaluated before confirming the validity of the applied loading protocol on osteogenesis of the cells.

Furthermore, better characterisation of the transferred forces to the cells under external loading is needed to establish the dominance of load type while considering the significant effect of other forces for example the effect of shear stress from fluid flow in compression system. These forces have combined impact on mass transport and biochemical availability and may intervene with effect of loading on cell differentiation process or cause a misinterpretation in analysing the obtained results. Albeit, in tissue engineering the main focus is on the overall response and not the specific mechanism behind it, it is equally crucial to identify the exact type of load(s) that promote specific tissue formation to simplify the further system designs. Computational modelling of loading system is also needed to help better characterisation of stresses and strains that are being experienced throughout the scaffold and by the cells[94].

7.2.2 Mechanical stimulation

Cell seeded collagen microspheres were mechanically stimulated by applying initial 10% global strain, 15-40 min/day for 5 and 10 days starting from day 6 pc. Constant and adjusted loading protocols were performed and compared to achieve the optimum required mechanical conditioning for osteogenesis of hES-MPs. The effect of osteogenic differentiation of these mechanical loadings on hES-MPs was studied by quantification of osteogenic markers including ALP, calcium, phos-

phorous and zinc and immuno-histological staining of microspheres cross sections over 28 days pc. The ALP activity level of adjusted loading protocol samples indicated a peak with significant changes in the enzyme activity on day 14 pc compared with constant loading, free floating and unloaded controls. Measuring ECM minerals also presented significantly higher concentration of calcium and phosphorous in loaded samples of adjusted strain protocol compared to other experimental conditions on day 28 pc. Zinc concentration in the adjusted loading samples showed an early peak on day 21 pc that was in contrast with the peak concentrations of the other two minerals and suggested the possibility of chondrogenic differentiation of the cells. However, negative Alcian blue staining of microspheres cross sections together with positive staining of Alizarin red staining of adjusted loading samples indicated osteogenic differentiation of progenitor cells under mechanical stimulations. These finding were further confirmed by SHG images of substantial reorganised and reoriented collagen fibres near the periphery of collagen beads, in addition to SEM images of more visible deposited minerals on the surface of collagen microspheres in the adjusted loading samples on day 28 pc.

Although various studies showed the effect of tensile and compression loading in enhancing the osteogenesis of primary cells, experimental models still do require meticulous design to allow transmission of appropriate and effective global strain to cells local micro environment. Different studies reported the effect of longitudinal stretching on the osteogenesis and compression on chondrogenic differentiation of stem cells[95,96]. Yet, it is not very clear whether compression can induce osteogenesis of stem cells on soft scaffold[91]. In reality and in vivo condition mechanical strain modes are complex and combined mechanical forces act together to influence stem cells fate in the body. Thus, it is somehow more relevant to study the joint effect of external mechanical forces on osteogenesis of progenitor cells[203]. Therefore, analysing the combined effects of tensile and compression loading on the cell seeded microspheres was a main focus of this study.

Two protocols were selected for loading regime and 10% global strains was applied for 15 min/day and 40 min/day for 5 and 10 days at 1 Hz as suggested by literature[16,90]. 40 min/day loading was chosen over 1 h as 40 min was the longest time hES-MPs survive without CO2 and added buffer agents.

The results of mechanical stimulations of progenitor cells indicated the effec-

tiveness of the adjusted loading protocol in enhancing osteogenesis of the cells. Yet, there are multiple factors that contribute in failure to obtain more significant and accurate outcome in this study. Controlling these factors might provide more accuracy and less variabilities in measuring osteogenesis markers and increase the validity of the effect of mechanical loading on osteogenic differentiation of hES-MPs soft 3D cultures.

One of the most important factors is the geometry of the collagen microspheres that determine the transmission of loads (compression and tensile) through collagen fibres and into the cells. The geometry of collagen beads was assumed spherical and as it was calculated by computational modelling applying 10% global strain results in transferring of around 5% compression to the centre and more tensile loads to the periphery of the spheres. Due to non-homogeneous distribution of the cells in the microspheres and cells tendency to migrate to the surface of collagen beads, in theory, hES-MPS would sense more tensile loads compared to compression. In addition, applying tensile load to the PDMS and compression of the chamber will cause collagen microspheres to be pulled in longitudinal direction (top to bottom) that would change the geometry of the beads during the experiment. This alteration of beads geometry in opposite direction of being confined and compressed by the PDMS under the loads would also adds to the complexity of load transfer. In reality, microsphere geometry varies considerably depending on the number of seeded cells from being close to spherical, oval or three quarter of a sphere that once again increase the variability between samples, experimental conditions and repeats.

In addition, numerical modelling indicated that when 10% strain is applied to the construct, embedded cells receive different magnitude of strain that decrease exponentially with increasing the distance from the construct surface[204]. Theses findings were confirmed by Pfeiler et al.[205] model that evaluated the local loading conditions on hMSCs seeded in 3D collagen scaffold that was exposed to cyclic tensile strain. Their study concluded that globally strain applied tensile strain of 10% resulted in 18.3% local strain because of geometric variation in the gel shape.

Furthermore, osteogenic markers assays were performed on a pool of total extracted cells from the collagen microspheres without considering the local cell number on the specific area (centre or periphery) of the beads and dominance of load type. Therefore, they can't be true representatives of the effectiveness of

the applied mechanical strain on the cells. As a result, cells in different areas of microspheres would sense non identical load transfer that may lead in inconsistent cellular response and promotion of differentiation. Theses variabilities were confirmed by assessing the histological staining of collagen beads cross sections that indicated random accumulation of osteogenic markers stains with no significant preference of the deposited stains intensity in the periphery or centre of the cross sections and also between different cross sections of one sample. In addition, the intervaribility between samples caused by very low initial seeded cells and proliferated cells in random areas of beads periphery increased the inconsistency of the results. The intensity of the deposited stain can be affected by very low cell number in specific area of the beads despite assuming that the optimum load transfer condition was carried out.

Advanced computational modelling is required to define a more detailed and accurate map of load transfer for specific areas of the collagen microspheres. Such a map would improve our understanding in transmission of loads and load types to the cells and therefore, would assist in developing an optimum protocol to study the effect of mechanical loading on the cells and cellular response. In addition, conventional in vitro osteogenic marker assays are not sensitive enough for low cell number therefore, even with an optimised mechanical conditioning regime quantification and analysis of the changes in osteogenic markers would not be valid.

7.2.3 Fluid flow induced shear stress

The effectiveness of applied oscillatory fluid flow induced shear stress to progenitor cells for enhancing osteogenic differentiation was tested by simple methodology (a shaking or a rocking platform). This study to our knowledge is the first to apply this simple methodology on soft 3D culture of progenitor cells. Previously, its has been shown that stem cells respond to different types of mechanical stimuli and shear stress in both 2D and 3D bioreactor conditions[16,104,198].

The applied shear stress for both shaker and rocker experiments were much lower than those estimated to occur within mature bone [194] and 2D and 3D culture of osteoblast cells[106,185], and were calculated as 0.04 Pa for rocker and 0.0597 Pa for shaker experiments at the centre of well culture and very close to FSS that was reported for 2D cell culture by Delaine-Smith[165].

Fluid flow induced shear stress was applied on hES-MPs seeded collagen microspheres that were fixed at the centre of each well and osteogenic markers were analysed to check whether low magnitude of FSS can provide all the necessary signals required for initiation of osteogenic differentiation in hES-MPs. The uniaxial direction of fluid flow was compared with rotational/swirl flow to assess the role of flow direction and the generated FSSs on the osteogenic differentiation of progenitor cells.

Evidently, chemical stimulation enhanced osteogenic differentiation of all 3D hES-MPs culture conditions compared to FSSs. The stimulation was confirmed by higher ALP activity level and increased intensity of deposited mineralisation stains at earlier time points in both osteogenic media treated samples of shaker experiment and static controls. Also, cells passage number and treatment with basal media with no added FGF-β indicated little impact on osteogenesis. Mineralisation was further analysed by quantification of deposited minerals and revealed significantly lower calcium and phosphorous level in shaker samples compared to the static controls. Free floating controls presented higher deposition of stain and higher mineralisation at later time points (days 21 and 28 pc) than shaker samples that was supported by histological staining of cross sections.

Interestingly, concentration of the deposited zinc in shaker samples was quite similar to zinc level in free floating controls and its value was detectable in both conditions from day 21 pc. Possibility of chondrogenic differentiation of hES-MPs was evaluated by Alcian blue staining of samples and control cross sections that revealed higher deposition of stain in shaker samples compared with controls on day 14 pc. However, the stain intensity in shaker samples was reported much lower than controls at later time points.

In addition, hES-MPs seeded microspheres were subjected to FSS by using a rocking platform and osteogenic differentiation of cells was analysed by evaluation of ALP activity and mineralisation markers level. The ALP level of rocker samples indicated lower enzyme activity compared with shaker samples and static controls from day 14 pc onward while, the free floating controls ALP activity reduced by day 21 pc. No detectable calcium and phosphorous concentration was reported in rocker samples that suggested initiation of mineralisation was blocked by the

imposed experimental condition. Nonetheless, these findings are comparable with Delaine-Smith study that suggested applying lower magnitude of FSSs by rocking platform inhibit osteogenic differentiation of 2D hES-MPs culture in osteogenic media[165].

Albeit, it has been shown that fluid flow induced shear stress single handedly can induce osteogenesis of stem cells[184,202], the results of this study failed to prove the effectiveness of FSSs in amplifying the ALP activity and promoting mineralisation. These inconsistent and inconclusive results may require further analysis of both osteogenic and chondrogenic markers in supporting specific linage differentiation of hES-MPs under the applied FSSs.
This study showed that stiffness (collagen concentration) and/or topography of cellular micro environment along with mechanical conditioning (tension, compression and FFSs) can manipulate stem cells fate. Its also showed that low concentration of collagen can be an efficient cellular microenvironment which supports long term cell viability. In addition, contraction of the encapsulated hES-MPs proved to be crucial in cell adaptation to their new environment. The results of this study also presented that mechanical stimulation of very low cell number seeded on soft collagen scaffold can encourage osteogenesis of undifferentiated cells by enhancing both early stage bone marker and mineralisation. Although tensile and compression loading shown to be more effective than FSSs in promoting osteogenesis of the cells. Applying mechanical stimulation can effect cell commitment but mechanical loading may not provide the necessary signals for full cell commitment and osteogenesis, thus, combining mechanical and chemical stimulation is critical in osteogenic differentiation of hES-MPs as been suggested in other studies.

7.3 Conclusions

The main finding of this project was to show that mechanical loading can regulate osteogenic differentiation of hES-MPs seeded in soft collagen microspheres in the absence of chemical stimulation. Mechanical loading of samples was applied through three different approaches including the use of loading chamber and bose bioreactor, applied compression by microfluidic device and FSSs by using orbital shaker and rocker. A variety of collagen concentrations and seeding cell densities were examined for optimum viability of hES-MPs and MG63 cell lines within low concentrations of bovine collagen I gel. Cell seeded collagen microspheres were produced successfully and both cells lines showed good survival and growth rate

in their new environment. Different chemical stimulations were applied to fully characterise the progenitor cells behaviour in 2D and 3D environment. Furthermore, A PDMS microfluidic chamber was designed and fabricated using metal rods and proved to be the best approach in building the desired micro chamber for mechanical conditioning of cells. The chamber enabled application of mechanical stimulation of hES-MPs in a controlled environment while reducing the overall volume of the systems enabling both reduction in cost and possibility of high throughput testing. ALP activity level of the compressed samples was reported higher than free floating controls during 28 days experiment while mineralisation was not enhanced. In addition, mechanical conditioning of cells was performed using Bose bioreactor and a PDMS loading chamber and loading condition was optimised by subtracting the plastic elongation of PDMS from the applied 10% global strain. 40 min/day loading cycles were carried out for 10 days and demonstrated to be effective in promoting osteogenesis of hES-MPs by enhancing ALP activity and mineralisation. A simple shaker and rocker experiment were successfully set up to analyse the effect of FSSs on osteogenic differentiation of hES-MPs seeded microspheres and results showed that low magnitudes of FSSs can't enhance osteogenic commitment and mineralisation of the cells compared to 2D culture.

Understanding the integrated mechanobiology of bone tissue regeneration is crucial to develop new strategies and therapies in bone tissue engineering. In vitro models, by their nature are simplified representatives of reality that help deepen our knowledge in identifying the controllable factors of regenerative mechanisms. Studies of such models must incorporate profound biological analysis and insightful mechanical understanding to allow clinically relevant and truly translational application.

Physical and mechanical cues are potent controlling factors in cells differentiation and can be implemented as guide to study cellular response, matrix production and tissue regeneration. Assessing their effects offer more improved conditioning of cells in the implantable scaffold or advance design of more clinically relevant constructs that so far has been unsuccessful. In addition, a better understanding of the mechanical micro environment of progenitor cells allows tunable modulation of cells migration and differentiation towards a particular tissue. Despite the design of numerous experimental models of constructs and cell loading devices, the generated results are not fully comparable because of wide diversity in source of the cells, cells pre conditions, scaffold materials, loading device and the applied

loading regimes. Minute changes in biochemical factor, physical/mechanical stimuli and time of applied external load can hugely affect stem cells fate thus, deep understanding of the role of these individual factors is essential in optimisation of the new experimental models.

Cells in 3D culture sense and respond to their mechanical environment in a complex and dynamic manner and as a result of an integrated effect of the mechanical behaviour of the ECM, the biology of the mechanotransduction, and local gradient of the secreted molecules. While, 2D models continue to offer valuable insights into cytoskeletal mechanics and cellular mechanisms in interacting with their physical microenvironment, more work in 3D environments is needed to more effectively link those results with in vivo conditions.

The results of this study revealed that mechanical stimulation on its own failed to provide all the necessary signals in enhancing the osteogenesis of hES-MPs. Combining mechanical, physical and chemical modulators would offer a more complete model in studying stem cells fate. A part from dynamic loading of cells by bose bioreactor that enhanced osteogenic differentiation of the cells, microfliudic device and fluid flow induced FSSs proved to be ineffective in stimulating the osteogenic markers. Osteogenic specific protein quantification, gene expression studies (qPCR) of bone and early stage mineralisation markers including ALP, Osteocalcin, Osteonectin, Runx, BMPs and ColI and ColII along with phenotyping of differentiated cells are recommended in the future work plan. Studying the combined and individual effects of applying direct cyclic loading with fluid flow and FSSs on cells is crucial to draw the map of load transfer in relation with the distance from the surface of collagen microspheres. Application of cyclic loading on 3D culture of hES-MP cells could be used as a model to regulate mechano-stimulation and linage differentiation both in vitro and in silico. Researchers would benefit from the results of hES-MPs characterization in 3D soft environment and mechanically stimulated hES-MPs collagen microspheres can be used as cells and therapeutic carriers or implants in bone and cartilage healing application. The result of this study can also be used as a tool to built more optimised construct to transfer mechanically stimulated stem cells to the specific area of a defeated bone. Such cells would differentiate to appropriates mature cells crucial in making a new bone thus the results would make a breakthrough in bone regeneration processes.

Bibliography

[1] L. L. And, J. Rao, G. Li, and Xiaofeng Qian and Beicheng Sun and Xuehao Wang, "Immunology of liver transplantation," *Exp. Clin. Transplant.*, vol. 12, no. 1, pp. 10–15, 2014.

[2] I. R. Reid, "Vitamin D let's get back to the evidence base," *IBMS Bonekey*, vol. 7, no. 7, pp. 249–253, 2010.

[3] S. Sundelacruz and D. L. Kaplan, "Stem cell- and scaffold-based tissue engineering approaches to osteochondral regenerative medicine," *Semin. Cell Dev. Biol.*, vol. 20, no. 6, pp. 646–655, 2009.

[4] A. M. DiMarino, A. I. Caplan, and T. L. Bonfield, "Mesenchymal Stem Cells in Tissue Repair," *Front. Immunol.*, vol. 4, no. September, pp. 1–9, 2013.

[5] F. DAngelo, R. Tiribuzi, I. Armentano, J. M. Kenny, S. Martino, and A. Orlacchio, "Mechanotransduction: Tuning Stem Cells Fate," *J. Funct. Biomater.*, vol. 2, no. 2, pp. 67–87, 2011.

[6] N. Shah, Y. Morsi, and R. Manasseh, "From mechanical stimulation to biological pathways in the regulation of stem cell fate.," *Cell Biochem. Funct.*, vol. 32, no. 4, pp. 309–25, 2014.

[7] J.-H. Chen, C. Liu, L. You, and C. a. Simmons, "Boning up on Wolff's Law: Mechanical regulation of the cells that make and maintain bone," *J. Biomech.*, vol. 43, no. 1, pp. 108–118, 2010.

[8] B. Trappmann, J. E. Gautrot, J. T. Connelly, D. G. T. Strange, Y. Li, M. L. Oyen, M. a. Cohen Stuart, H. Boehm, B. Li, V. Vogel, J. P. Spatz, F. M. Watt, and W. T. S. Huck, "Extracellular-matrix tethering regulates stem-cell fate.," *Nat. Mater.*, vol. 11, pp. 642–9, jul 2012.

[9] M. Perán, M. A. García, E. López-Ruiz, M. Bustamante, G. Jiménez, R. Madeddu, and J. a. Marchal, "Functionalized nanostructures with application in regenerative medicine," *Int. J. Mol. Sci.*, vol. 13, no. 3, pp. 3847–3886, 2012.

[10] E. C. Constable and C. E. Housecroft, "Coordination chemistry: the scientific legacy of Alfred Werner.," *Chem. Soc. Rev.*, vol. 42, no. 4, pp. 1429–39, 2013.

[11] M. M. Nava, M. T. Raimondi, and R. Pietrabissa, "Controlling self-renewal and differentiation of stem cells via mechanical cues," *J. Biomed. Biotechnol.*, vol. 2012, 2012.

[12] S. Ding and P. G. Schultz, "A role for chemistry in stem cell biology," *Nat. Biotechnol.*, vol. 22, no. 7, pp. 833–840, 2004.

[13] P. Macchiarini, P. Jungebluth, T. Go, M. A. Asnaghi, L. E. Rees, T. a. Cogan, A. Dodson, J. Martorell, S. Bellini, P. P. Parnigotto, S. C. Dickinson, A. P. Hollander, S. Mantero, M. T. Conconi, and M. a. Birchall, "Clinical transplantation of a tissue-engineered airway," *Lancet*, vol. 372, no. 9655, pp. 2023–2030, 2008.

[14] D. E. Discher, D. J. Mooney, and P. W. Zandstra, "Growth factors, matrices, and forces combine and control stem cells," *Science (80-.).*, vol. 324, no. 5935, pp. 1673–1677, 2009.

[15] D. A. Lee, M. M. Knight, J. J. Campbell, and D. L. Bader, "Stem cell mechanobiology," *J. Cell. Biochem.*, vol. 112, no. 1, pp. 1–9, 2011.

[16] R. M. Delaine-smith and G. C. Reilly, *The Effects of Mechanical Loading on Mesenchymal Stem Cell Differentiation and Matrix Production*, vol. 87. Vitamins & Hormones, 1 ed., 2011.

[17] T. M. Skerry, "One mechanostat or many? Modifications of the site-specific response of bone to mechanical loading by nature and nurture.," *J. Musculoskelet. Neuronal Interact.*, vol. 6, no. 2, pp. 122–127, 2006.

[18] J. Iqbal and M. Zaidi, "Molecular regulation of mechanotransduction.," *Biochem. Biophys. Res. Commun.*, vol. 328, pp. 751–5, mar 2005.

[19] T. M. Skerry, "The response of bone to mechanical loading and disuse: fundamental principles and influences on osteoblast/osteocyte homeostasis.," *Arch. Biochem. Biophys.*, vol. 473, pp. 117–23, may 2008.

[20] Z. Ruszczak, "Collagen as a carrier for on-site delivery of antibacterial drugs," *Adv. Drug Deliv. Rev.*, vol. 55, pp. 1679–1698, nov 2003.

[21] F. Guilak, D. M. Cohen, B. T. Estes, J. M. Gimble, W. Liedtke, and C. S. Chen, "Control of stem cell fate by physical interactions with the extracellular matrix.," *Cell Stem Cell*, vol. 5, pp. 17–26, jul 2009.

[22] J. H. Wang and B. P. Thampatty, "Mechanobiology of Adult and Stem Cells," *Int. Rev. Cell Mol. Biol.*, vol. 271, no. 08, 2008.

[23] N. Desprat, W. Supatto, P. A. Pouille, E. Beaurepaire, and E. Farge, "Tissue Deformation Modulates Twist Expression to Determine Anterior Midgut Differentiation in Drosophila Embryos," *Dev. Cell*, vol. 15, no. 3, pp. 470–477, 2008.

[24] P. Patwari and R. T. Lee, "Mechanical control of tissue morphogenesis," *Circ. Res.*, vol. 103, no. 3, pp. 234–243, 2008.

[25] C. T. Laurencin, A. M. Ambrosio, M. D. Borden, and J. A. Cooper, "Tissue engineering: orthopedic applications.," *Annu. Rev. Biomed. Eng.*, vol. 1, no. FEBRUARY 1999, pp. 19–46, 1999.

[26] A. R. Amini, C. T. Laurencin, and S. P. Nukavarapu, "Bone tissue engineering: recent advances and challenges.," *Crit. Rev. Biomed. Eng.*, vol. 40, no. 5, pp. 363–408, 2012.

[27] E. M. Younger and M. W. Chapman, "MORBIDITY AT BONE GRAFT DONOR SITES," *J. Orthop. Trauma*, vol. 3, no. January 1982, pp. 192–195, 1989.

[28] B. Y. C. F. Lord, H. J. M. Mankin, G. Boston, W. Massachusetts, H. Cancer, and O. Oncology, "Infection in bone allografts. Incidence, nature, and treatment.," *J Bone Jt. Surg Am*, vol. 70, no. 3, pp. 369 –376, 1988.

[29] C. Delloye, O. Cornu, V. Druez, and O. Barbier, "Bone allografts: What they can offer and what they cannot.," *J. Bone Joint Surg. Br.*, vol. 89, no. 5, pp. 574–579, 2007.

[30] T. Kaully, K. Kaufman-Francis, A. Lesman, and S. Levenberg, "Vascularization–the conduit to viable engineered tissues.," *Tissue Eng. Part B. Rev.*, vol. 15, no. 2, pp. 159–169, 2009.

[31] S. J. Hollister and W. L. Murphy, "Scaffold Translation: Barriers Between Concept and Clinic," *Tissue Eng. Part B Rev.*, vol. 17, no. 6, pp. 459–474, 2011.

[32] A. S. Greenwald, D. P. Oxon, S. D. Boden, V. M. Goldberg, M. Yaszemski, C. S. Heim, and B. Sc, "BONE-GRAFT SUBSTITUTES : FACTS , FICTIONS & APPLICATIONS Prepared by :," *J Bone Jt. Surg Am*, vol. 83, pp. 98 –103, 2001.

[33] R. Dimitriou, E. Jones, D. McGonagle, and P. V. Giannoudis, "Bone regeneration: current concepts and future directions.," *BMC Med.*, vol. 9, p. 66, 2011.

[34] C. Zuo, Y. Huang, R. Bajis, M. Sahih, Y. P. Li, K. Dai, and X. Zhang, "Osteoblastogenesis regulation signals in bone remodeling," *Osteoporos. Int.*, vol. 23, no. 6, pp. 1653–1663, 2012.

[35] F. Shapiro, "BONE DEVELOPMENT AND ITS RELATION TO FRACTURE REPAIR. THE ROLE OF MESENCHYMAL OSTEOBLASTS AND SURFACE OSTEOBLASTS," *Eur. Cells Mater.*, vol. 15, pp. 53–76, 2008.

[36] F. J. O'Brien, "Biomaterials & scaffolds for tissue engineering," *Mater. Today*, vol. 14, no. 3, pp. 88–95, 2011.

[37] G. H. Altman, R. L. Horan, H. H. Lu, J. Moreau, I. Martin, J. C. Richmond, and D. L. Kaplan, "Silk matrix for tissue engineered anterior cruciate ligaments," *Biomaterials*, vol. 23, no. 20, pp. 4131–4141, 2002.

[38] D. W. Hutmacher, "Scaffolds in tissue engineering bone and cartilage.," *Biomaterials*, vol. 21, no. 24, pp. 2529–2543, 2000.

[39] Edward A. Phelps and Natalia Landázuri and Peter M. Thulé and W. Robert Taylor and Andrés J. García, "Bioartificial matrices for therapeutic vascularization," *Proc. Natl. Acad. Sci.*, vol. 107, no. 8, pp. 3323–3328, 2010.

[40] F. J. O'brien, B. Harley, I. V. Yannas, and L. J. Gibson, "The efect of pore size on cell adhesion in collagen GAG scaffolds," *Anat. Artic.*, vol. 1, no. 2, 2005.

[41] T. J. Blokhuis and J. J. C. Arts, "Bioactive and osteoinductive bone graft substitutes: Definitions, facts and myths," *Injury*, vol. 42, no. SUPPL. 2, pp. S26–S29, 2011.

[42] E. Verron, I. Khairoun, J. Guicheux, and J.-M. Bouler, "Calcium phosphate biomaterials as bone drug delivery systems: a review.," *Drug Discov. Today*, vol. 15, no. 13-14, pp. 547–552, 2010.

[43] P. Habibovic, U. Gbureck, C. J. Doillon, D. C. Bassett, C. a. van Blitterswijk, and J. E. Barralet, "Osteoconduction and osteoinduction of low-temperature 3D printed bioceramic implants," *Biomaterials*, vol. 29, no. 7, pp. 944–953, 2008.

[44] U. Ripamonti, J. Crooks, L. Khoali, and L. Roden, "The induction of bone formation by coral-derived calcium carbonate/hydroxyapatite constructs," *Biomaterials*, vol. 30, no. 7, pp. 1428–1439, 2009.

[45] M. Rahaman, D. Day, B. S. Bal, and Q. Fu, "Bioactive glass in tissue engineering," *Acta Biomater.*, vol. 7, no. 6, pp. 2355–2373, 2011.

[46] A. M. C. Barradas, H. Yuan, C. a. van Blitterswijk, and P. Habibovic, "Osteoinductive biomaterials: current knowledge of properties, experimental models and biological mechanisms.," *Eur. Cell. Mater.*, vol. 21, pp. 407–429, 2011.

[47] B. D. Ulery, L. S. Nair, and C. T. Laurencin, "Biomedical applications of biodegradable polymers," *J. Polym. Sci. Part B Polym. Phys.*, vol. 49, no. 12, pp. 832–864, 2011.

[48] M. D. Cato, L. S. Nairc, S. P. Nukavarapuc, S. G. Kumbar, T. Jianga, N. R. Krogmand, A. Singhd, H. R. Allcockd, and C. T. Laurencin, "Miscibility and in vitro osteocompatibility of biodegradable blends of poly[(ethyl alanato) (p-phenyl phenoxy) phosphazene] and poly (lactic acid-glycolic acid)," *Biomaterials*, vol. 29, no. 3, pp. 337–349, 2008.

[49] G. Wei and P. X. Ma, "Structure and properties of nano-hydroxyapatite/polymer composite scaffolds for bone tissue engineering," *Biomaterials*, vol. 25, no. 19, pp. 4749–4757, 2004.

[50] C. V. M. Rodrigues, P. Serricella, a. B. R. Linhares, R. M. Guerdes, R. Borojevic, M. a. Rossi, M. E. L. Duarte, and M. Farina, "Characterization of a bovine collagen-hydroxyapatite composite scaffold for bone tissue engineering," *Biomaterials*, vol. 24, no. 27, pp. 4987–4997, 2003.

[51] N. R. Krogman, A. L. Weikel, K. a. Kristhart, S. P. Nukavaropu, M. Deng, L. S. Nair, C. T. Laurencin, and H. R. Allcock, "The Influence of Side

Group Modification in Polyphosphazenes on Hydrolysis and Cell Adhesion of Blends with PLGA," *Biomaterials*, vol. 30, no. 17, pp. 3035–3041, 2009.

[52] P. X. Ma, R. Zhang, G. Xiao, and R. Franceschi, "Engineering new bone tissue in vitro on highly porous poly(alpha-hydroxyl acids)/hydroxyapatite composite scaffolds.," *J. Biomed. Mater. Res.*, vol. 54, no. 2, pp. 284–293, 2001.

[53] E. Ho, E. Ho, A. Lowman, A. Lowman, M. Marcolongo, and M. Marcolongo, "Synthesis and characterization of an injectable hydrogel with tunable mechanical properties for soft tissue repair.," *Biomacromolecules*, vol. 7, no. 11, pp. 3223–8, 2006.

[54] R. K. Roeder, G. L. Converse, R. J. Kane, and W. Yue, "Hydroxyapatite-reinforced polymer biocomposites for synthetic bone substitutes," *JOM*, vol. 60, no. 3, pp. 38–45, 2008.

[55] J. M. Saul and D. F. Williams, "Hydrogels in Regenerative Medicine," *Princ. Regen. Med.*, pp. 637–661, 2011.

[56] C. E. Semino, "Self-assembling Peptides : From Bio-inspired Materials to Bone Regeneration," *J Dent Res*, vol. 87, no. 7, pp. 606–616, 2008.

[57] P. M. Mountziaris, P. P. Spicer, F. K. Kasper, and A. G. Mikos, "Harnessing and Modulating Inflammation in Strategies for Bone Regeneration," *Tissue Eng. Part B Rev.*, vol. 17, no. 6, pp. 393–402, 2011.

[58] J. M. A. Chang, A. Rodriguez, and D. T., "Foreign Body Reaction To Biomaterials," *Semin Immunol*, vol. 20, no. 2, pp. 86–100, 2008.

[59] B. Veleirinho, D. S. Coelho, P. F. Dias, M. Maraschin, R. Pinto, E. Cargnin-Ferreira, A. Peixoto, J. a. Souza, R. M. Ribeiro-do Valle, and J. a. Lopes-da Silva, "Foreign body reaction associated with PET and PET/chitosan electrospun nanofibrous abdominal meshes.," *PLoS One*, vol. 9, no. 4, p. e95293, 2014.

[60] . Ami R. Amini1, James S. Wallace1, and Syam P. Nukavarapu1, 2, "Short-Term and Long-Term Effects of Orthopedic Biodegradable Implants," *J LongTerm Eff Med Implatns*, vol. 21, no. 2, pp. 93–122, 2011.

[61] H. Wang, X. Li, E. Tomin, S. B. Doty, J. M. Lane, D. H. Carney, and J. T. Ryaby, "Thrombin peptide (TP508) promotes fracture repair by up-regulating inflammatory mediators, early growth factors, and increasing angiogenesis," *J. Orthop. Res.*, vol. 23, no. 3, pp. 671–679, 2005.

[62] V. M. Paralkar, F. Borovecki, H. Z. Ke, K. O. Cameron, B. Lefker, W. a. Grasser, T. a. Owen, M. Li, P. DaSilva-Jardine, M. Zhou, R. L. Dunn, F. Dumont, R. Korsmeyer, P. Krasney, T. a. Brown, D. Plowchalk, S. Vukicevic, and D. D. Thompson, "An EP2 receptor-selective prostaglandin E2 agonist induces bone healing.," *Proc. Natl. Acad. Sci. U. S. A.*, vol. 100, no. 11, pp. 6736–6740, 2003.

[63] B. L. P. Knowles, "What Are Stem Cells and Where Do They Come From ? Are All Stem Cells the Same :," *Stem Cell Netw.*, vol. 1, pp. 5–12, 2013.

[64] B. A. J. Friedenstein, "Osteogenesis in transplants of bone marrow cells," *J.Embryol.exp.Moph*, vol. 16, no. December, pp. 581–390, 1966.

[65] M. Dominici, K. Le Blanc, I. Mueller, I. Slaper-Cortenbach, F. Marini, D. Krause, R. Deans, a. Keating, D. Prockop, and E. Horwitz, "Minimal criteria for defining multipotent mesenchymal stromal cells. The International Society for Cellular Therapy position statement.," *Cytotherapy*, vol. 8, pp. 315–7, jan 2006.

[66] V. Vogel, "Mechanotransduction involving multimodular proteins: converting force into biochemical signals.," *Annu. Rev. Biophys. Biomol. Struct.*, vol. 35, pp. 459–88, jan 2006.

[67] J. Rubin, C. Rubin, and C. R. Jacobs, "Molecular pathways mediating mechanical signaling in bone.," *Gene*, vol. 367, pp. 1–16, feb 2006.

[68] H. L. Morris, C. I. Reed, J. W. Haycock, and G. C. Reilly, "Mechanisms of fluid-flow-induced matrix production in bone tissue engineering," *Proc. Inst. Mech. Eng. Part H J. Eng. Med.*, vol. 224, pp. 1509–1521, dec 2010.

[69] A. M. D. Malone, C. T. Anderson, P. Tummala, R. Y. Kwon, T. R. Johnston, R. Zhang, D. H. Dowhan, Y. R. Miao, M. Gewirtz, S. C. Barry, R. G. Ramsay, J. Thomas, F. Depreux, N. Kraeva, R. E. Loy, A. Sanjeewa, S. Boncompagi, A. Kraev, O. Anthony, R. T. Dirksen, C. Franzini-armstrong, C. E. Seidman, J. G. Seidman, D. H. Maclennan, E. Zvaritch, E. Ryan, S. A. Goonasekera, S. Boncompagni, A. O. Gramolini, and T. Robert, "Primary cilia mediate

mechanosensing in bone cells by a calcium-independent mechanism," *PNAS*, vol. 104, no. 13325-13330, 2007.

[70] J. R. Glossop and S. H. Cartmell, "Effect of fluid flow-induced shear stress on human mesenchymal stem cells: differential gene expression of IL1B and MAP3K8 in MAPK signaling.," *Gene Expr. Patterns*, vol. 9, pp. 381–8, jun 2009.

[71] C. A. Simmons, S. Matlis, A. J. Thornton, S. Chen, C.-Y. Wang, and D. J. Mooney, "Cyclic strain enhances matrix mineralization by adult human mesenchymal stem cells via the extracellular signal-regulated kinase (ERK1/2) signaling pathway," *J. Biomech.*, vol. 36, pp. 1087–1096, aug 2003.

[72] N. Case, B. Sen, J. A. Thomas, M. Styner, Z. Xie, C. R. Jacobs, and J. Rubin, "Steady and oscillatory fluid flows produce a similar osteogenic phenotype.," *Calcif. Tissue Int.*, vol. 88, pp. 189–97, mar 2011.

[73] M. C. T. E. Osteoblasts, J. You, G. C. Reilly, X. Zhen, C. E. Yellowley, Q. Chen, J. Henry, C. R. Jacobs, and H. J. Donahue, "TRANSDUCTION : Osteopontin Gene Regulation by Oscillatory Fluid Flow via Intracellular Calcium Mobilization and Activation of Mitogen-activated Protein Kinase in Osteopontin Gene Regulation by Oscillatory Fluid Flow via Intracellular Calcium Mobilization," *J.Biol.Chem*, vol. 276, pp. 13365–13371, 2001.

[74] J. G. McGarry, J. Klein-Nulend, and P. J. Prendergast, "The effect of cytoskeletal disruption on pulsatile fluid flow-induced nitric oxide and prostaglandin E2 release in osteocytes and osteoblasts.," *Biochem. Biophys. Res. Commun.*, vol. 330, pp. 341–8, apr 2005.

[75] S. M. Tanaka, H. B. Sun, R. K. Roeder, D. B. Burr, C. H. Turner, and H. Yokota, "Osteoblast responses one hour after load-induced fluid flow in a three-dimensional porous matrix.," *Calcif. Tissue Int.*, vol. 76, pp. 261–71, apr 2005.

[76] M. Stem, G.-I. Im, Z. Quan, and D. Ph, "The Effects of Wnt Inhibitors on the Chondrogenesis," *Tissue Eng. Part A*, vol. 16, no. 7, pp. 103–120, 2010.

[77] Y. Gong, R. B. Slee, N. Fukai, G. Rawadi, S. Roman-roman, A. M. Reginato, H. Wang, T. Cundy, F. H. Glorieux, D. Lev, M. Zacharin, K. Oexle, J. Marcelino, W. Suwairi, S. Heeger, G. Sabatakos, S. Apte, W. N. Adkins,

J. Allgrove, M. Arslan-kirchner, J. A. Batch, P. Beighton, G. C. M. Black, R. G. Boles, L. M. Boon, C. Borrone, H. G. Brunner, G. F. Carle, B. Dallapiccola, A. D. Paepe, B. Floege, M. L. Halfhide, B. Hall, R. C. Hennekam, T. Hirose, A. Jans, C. A. Kim, K. Keppler-noreuil, A. Kohlschuetter, D. Lacombe, M. Lambert, E. Lemyre, T. Letteboer, L. Peltonen, R. S. Ramesar, M. Romanengo, H. Somer, E. Steichen-gersdorf, B. Steinmann, B. Sullivan, A. Superti-furga, W. Swoboda, V. D. Boogaard, W. V. Hul, M. Vikkula, M. Votruba, B. Zabel, T. Garcia, R. Baron, B. R. Olsen, and M. L. Warman, "LDL Receptor-Related Protein 5 (LRP5) Affects Bone Accrual and Eye Development," *Cell*, vol. 107, pp. 513–523, 2001.

[78] V. K. Yadav, J.-H. Ryu, N. Suda, K. F. Tanaka, J. a. Gingrich, G. Schütz, F. H. Glorieux, C. Y. Chiang, J. D. Zajac, K. L. Insogna, J. J. Mann, R. Hen, P. Ducy, and G. Karsenty, "Lrp5 controls bone formation by inhibiting serotonin synthesis in the duodenum.," *Cell*, vol. 135, pp. 825–37, nov 2008.

[79] T. F. Day, X. Guo, L. Garrett-Beal, and Y. Yang, "Wnt/beta-catenin signaling in mesenchymal progenitors controls osteoblast and chondrocyte differentiation during vertebrate skeletogenesis.," *Dev. Cell*, vol. 8, pp. 739–50, may 2005.

[80] T. P. Hill, D. Später, M. M. Taketo, W. Birchmeier, and C. Hartmann, "Canonical Wnt/beta-catenin signaling prevents osteoblasts from differentiating into chondrocytes.," *Dev. Cell*, vol. 8, pp. 727–38, may 2005.

[81] S. L. Etheridge, G. J. Spencer, D. J. Heath, and G. Genever, "Expression Profiling and Functional Analysis of Wnt Signaling Mechanisms in Mesenchymal Stem Cells," *Stem Cells*, vol. 22, pp. 849–860, 2004.

[82] A. Augello and C. D. Bari, "Review The Regulation of Differentiation in Mesenchymal Stem Cells," *Hum. Gene Ther.*, vol. 21(10), no. October, pp. 1226–1238, 2010.

[83] I. Sekiya, B. L. Larson, J. T. Vuoristo, R. L. Reger, and D. J. Prockop, "Comparison of effect of BMP-2, -4, and -6 on in vitro cartilage formation of human adult stem cells from bone marrow stroma.," *Cell Tissue Res.*, vol. 320, pp. 269–76, may 2005.

[84] R. Tuli, S. Tuli, S. Nandi, X. Huang, P. a. Manner, W. J. Hozack, K. G. Danielson, D. J. Hall, and R. S. Tuan, "Transforming growth factor-beta-

mediated chondrogenesis of human mesenchymal progenitor cells involves N-cadherin and mitogen-activated protein kinase and Wnt signaling cross-talk.," *J. Biol. Chem.*, vol. 278, pp. 41227–36, oct 2003.

[85] D. J. Rickard, L. C. Hofbauer, S. K. Bonde, F. Gori, T. C. Spelsberg, and B. L. Riggs, "Bone morphogenetic protein-6 production in human osteoblastic cell lines. Selective regulation by estrogen.," *J. Clin. Invest.*, vol. 101, no. 2, pp. 413–422, 1998.

[86] R. Modarresi, T. Lafond, J. a. Roman-Blas, K. G. Danielson, R. S. Tuan, and M. R. Seghatoleslami, "N-cadherin mediated distribution of beta-catenin alters MAP kinase and BMP-2 signaling on chondrogenesis-related gene expression.," *J. Cell. Biochem.*, vol. 95, pp. 53–63, may 2005.

[87] J. Eyckmans, S. J. Roberts, J. Schrooten, and F. P. Luyten, "A clinically relevant model of osteoinduction: a process requiring calcium phosphate and BMP/Wnt signalling.," *J. Cell. Mol. Med.*, vol. 14, pp. 1845–56, jun 2010.

[88] W. L. Weldon School of Biomedical Engineering, Purdue University, 206 S. Martin Jischke Drive, "The Mechanical Environment of Bone Marrow : A Review," *Ann. Biomed. Eng.*, vol. 36, no. 12, pp. 1978–1991, 2008.

[89] P. Angele, D. Schumann, M. Angele, B. Kinner, and C. Englert, "Cyclic , mechanical compression enhances chondrogenesis of mesenchymal progenitor cells in tissue engineering scaffolds," *Biorheology*, vol. 41, pp. 335–346, 2004.

[90] J. K. Mouw, J. T. Connelly, C. G. Wilson, K. E. Michael, and M. E. Levenston, "Dynamic compression regulates the expression and synthesis of chondrocyte-specific matrix molecules in bone marrow stromal cells.," *Stem Cells*, vol. 25, pp. 655–63, mar 2007.

[91] R. L. Mauck, B. A. Byers, X. Yuan, and R. S. Tuan, "Regulation of cartilaginous ECM gene transcription by chondrocytes and MSCs in 3D culture in response to dynamic loading.," *Biomech. Model. Mechanobiol.*, vol. 6, pp. 113–25, jan 2007.

[92] A. H. Huang, M. J. Farrell, M. Kim, and R. L. Mauck, "LONG-TERM DYNAMIC LOADING IMPROVES THE MECHANICAL PROPERTIES OF CHONDROGENIC MESENCHYMAL STEM CELL-LADEN HYDROGELS," *Eur. Cells Mater.*, vol. 19, no. 215, pp. 72–85, 2010.

[93] S. D. Thorpe, C. T. Buckley, T. Vinardell, F. J. O'Brien, V. a. Campbell, and D. J. Kelly, "The response of bone marrow-derived mesenchymal stem cells to dynamic compression following TGF-beta3 induced chondrogenic differentiation.," *Ann. Biomed. Eng.*, vol. 38, pp. 2896–909, sep 2010.

[94] M. S. Thompson, D. R. Epari, F. Bieler, and G. N. Duda, "¡i¿In vitro¡/i¿ models for bone mechanobiology: applications in bone regeneration and tissue engineering," *Proc. Inst. Mech. Eng. Part H J. Eng. Med.*, vol. 224, pp. 1533–1541, dec 2010.

[95] X. Yang, P. Gong, Y. Lin, L. Zhang, X. Li, Q. Yuan, Z. Tan, Y. Wang, Y. Man, and H. Tang, "Cyclic tensile stretch modulates osteogenic differentiation of adipose-derived stem cells via the BMP-2 pathway.," *Arch. Med. Sci.*, vol. 6, pp. 152–9, apr 2010.

[96] M. Ngiam, S. Liao, T. Ong Jun Jie, Xiaodi Sui, Yixiang Dong, S. Ramakrishna, and C. K. Chan, "Effects of mechanical stimulation in osteogenic differentiation of bone marrow-derived mesenchymal stem cells on aligned nanofibrous scaffolds," *J. Bioact. Compat. Polym.*, vol. 26, pp. 56–70, dec 2010.

[97] M. Jagodzinski, M. Drescher, J. Zeichen, S. Hankemeier, C. Krettek, U. Bosch, M. V. Griensven, and S. Traumatology, "EFFECTS OF CYCLIC LONGITUDINAL MECHANICAL STRAIN AND DEXAMETHASONE ON OSTEOGENIC DIFFERENTIATION OF HUMAN BONE," *Eur. Cells Mater.*, vol. 7, pp. 35–41, 2004.

[98] J. R. Mauney, S. Sjostorm, J. Blumberg, R. Horan, J. P. O'Leary, G. Vunjak-Novakovic, V. Volloch, and D. L. Kaplan, "Mechanical stimulation promotes osteogenic differentiation of human bone marrow stromal cells on 3-D partially demineralized bone scaffolds in vitro.," *Calcif. Tissue Int.*, vol. 74, pp. 458–68, may 2004.

[99] C.-H. Huang, M.-H. Chen, T.-H. Young, J.-H. Jeng, and Y.-J. Chen, "Interactive effects of mechanical stretching and extracellular matrix proteins on initiating osteogenic differentiation of human mesenchymal stem cells.," *J. Cell. Biochem.*, vol. 108, pp. 1263–73, dec 2009.

[100] E. M. Byrne, E. Farrell, L. a. McMahon, M. G. Haugh, F. J. O'Brien, V. a. Campbell, P. J. Prendergast, and B. C. O'Connell, "Gene expression by marrow stromal cells in a porous collagen-glycosaminoglycan scaffold is

affected by pore size and mechanical stimulation.," *J. Mater. Sci. Mater. Med.*, vol. 19, pp. 3455–63, nov 2008.

[101] J. T. Connelly, E. J. Vanderploeg, J. K. Mouw, C. G. Wilson, M. E. Levenston, D. Ph, E. J. Vanderploeg, J. K. Mouw, C. G. Wilson, and M. E. Levenston, "Tensile loading modulates bone marrow stromal cell differentiation and the development of engineered fibrocartilage constructs.," *Tissue Eng. Part A*, vol. 16, no. 6, pp. 1913–1923, 2010.

[102] F. Colazzo, P. Sarathchandra, R. T. Smolenski, A. H. Chester, Y.-T. Tseng, J. T. Czernuszka, M. H. Yacoub, and P. M. Taylor, "Extracellular matrix production by adipose-derived stem cells: implications for heart valve tissue engineering.," *Biomaterials*, vol. 32, pp. 119–27, jan 2011.

[103] J. Klein-Nulend, R. G. Bacabac, and M. G. Mullender, "Mechanobiology of bone tissue.," *Pathol. Biol. (Paris).*, vol. 53, pp. 576–80, dec 2005.

[104] A J EI Haj and S H Cartmell, "Bioreactors for bone tissue engineering," *Proc. Inst. Mech. Eng. Part H J. Eng. Med.*, vol. 224, pp. 1523–1532, dec 2010.

[105] A. D. Bakker, K. Soejima, J. Klein-nulend, and E. H. Burger, "The production of nitric oxide and prostaglandin E 2 by primary bone cells is shear stress dependent," *J. Biomech.*, vol. 34, pp. 671–677, 2001.

[106] R. J. Mccoy, D. Eng, F. J. O. Brien, and D. Ph, "Influence of Shear Stress in Perfusion Bioreactor Cultures for the Development of Three-Dimensional Bone Tissue Constructs : A Review," *Tissue Eng. Part B Rev.*, vol. 16, no. 6, pp. 50–61, 2010.

[107] F. Maes, P. Van Ransbeeck, H. Van Oosterwyck, and P. Verdonck, "Modeling fluid flow through irregular scaffolds for perfusion bioreactors.," *Biotechnol. Bioeng.*, vol. 103, pp. 621–30, jun 2009.

[108] S. B. Vangordon, R. S. Voronov, T. B. Blue, R. L. Shambaugh, D. V. Papavassiliou, and V. I. Sikavitsas, "Effects of Scaffold Architecture on Preosteoblastic Cultures under Continuous Fluid Shear," *Ind. Eng. Chem. Res*, vol. 50, pp. 620–629, 2011.

[109] M. Grellier, R. Bareille, and C. Bourget, "Responsiveness of human bone marrow stromal cells to shear stress," *J Tissue Eng Regen Med*, vol. 3, no. March, pp. 302–309, 2009.

[110] M. J. Jaasma and F. J. O'Brien, "Mechanical Stimulation of Osteoblasts Using Steady and Dynamic Fluid Flow," *Tissue Eng. Part A*, vol. 14, pp. 1213–1223, jul 2008.

[111] C. R. Jacobs, C. E. Yellowley, B. R. Davis, Z. Zhou, J. M. Cimbala, and H. J. Donahue, "Differential effect of steady versus oscillating flow on bone cells," *J. Biomech.*, vol. 31, pp. 969–976, 1998.

[112] V. I. Sikavitsas, G. N. Bancroft, H. L. Holtorf, J. A. Jansen, and A. G. Mikos, "Mineralized matrix deposition by marrow stromal osteoblasts in 3D perfusion culture increases with increasing fluid shear forces," *PNAS*, no. 33, pp. 2–7, 2003.

[113] S. Srinivasan, D. A. Weimer, S. C. Agans, S. D. Bain, and T. E. D. S. Gross, "Low-Magnitude Mechanical Loading Becomes Osteogenic When Rest Is Inserted Between Each Load Cycle," *J. BONE Miner. Res.*, vol. 17, no. 9, pp. 1613–1620, 2002.

[114] J. O. H. N. A. P. Edersen and M. E. A. S. Wartz, "Mechanobiology in the Third Dimension," *Ann. Biomed. Eng.*, vol. 33, no. 11, pp. 1469–1490, 2005.

[115] S. Khetan, M. Guvendiren, W. R. Legant, D. M. Cohen, C. S. Chen, and J. a. Burdick, "Degradation-mediated cellular traction directs stem cell fate in covalently crosslinked three-dimensional hydrogels.," *Nat. Mater.*, vol. 12, pp. 458–65, may 2013.

[116] L. G. Vincent and A. J. Engler, "Stem cell differentiation: Post-degradation forces kick in.," *Nat. Mater.*, vol. 12, pp. 384–6, may 2013.

[117] C. Grashoff, B. D. Hoffman, M. D. Brenner, R. Zhou, M. Parsons, M. T. Yang, M. a. McLean, S. G. Sligar, C. S. Chen, T. Ha, and M. a. Schwartz, "Measuring mechanical tension across vinculin reveals regulation of focal adhesion dynamics.," *Nature*, vol. 466, pp. 263–6, jul 2010.

[118] N. Huebsch, P. R. Arany, A. S. Mao, D. Shvartsman, O. a. Ali, S. a. Bencherif, J. Rivera-Feliciano, and D. J. Mooney, "Harnessing traction-mediated manipulation of the cell/matrix interface to control stem-cell fate.," *Nat. Mater.*, vol. 9, pp. 518–26, jun 2010.

[119] S. Hong, H.-J. Hsu, R. Kaunas, and J. Kameoka, "Collagen microsphere production on a chip.," *Lab Chip*, vol. 12, pp. 3277–80, sep 2012.

[120] B. P. Chan, T. Y. Hui, C. W. Yeung, J. Li, I. Mo, and G. C. F. Chan, "Self-assembled collagen-human mesenchymal stem cell microspheres for regenerative medicine.," *Biomaterials*, vol. 28, pp. 4652–66, nov 2007.

[121] B. Engineering, C. S. Building, and T. G. G. Ab, "Technology of mammalian cell encapsulation," *Adv. Drug Deliv. Rev.*, vol. 42, pp. 29–64, 2000.

[122] G. A. Di Lullo, S. M. Sweeney, J. Korkko, L. Ala-Kokko, and J. D. San Antonio, "Mapping the ligand-binding sites and disease-associated mutations on the most abundant protein in the human, type I collagen.," *J. Biol. Chem.*, vol. 277, pp. 4223–31, feb 2002.

[123] E. Brouzes, M. Medkova, N. Savenelli, D. Marran, M. Twardowski, J. B. Hutchison, J. M. Rothberg, D. R. Link, N. Perrimon, and M. L. Samuels, "Droplet microfluidic technology for single-cell high-throughput screening," *PNAS*, vol. 25, no. 106, pp. 195–200, 2009.

[124] Y. Deng, N. Zhang, L. Zhao, X. Yu, X. Ji, W. Liu, S. Guo, K. Liu, and X.-Z. Zhao, "Rapid purification of cell encapsulated hydrogel beads from oil phase to aqueous phase in a microfluidic device.," *Lab Chip*, vol. 11, pp. 4117–21, dec 2011.

[125] R. Parenteau-Bareil, R. Gauvin, and F. Berthod, "Collagen-Based Biomaterials for Tissue Engineering Applications," *Materials (Basel).*, vol. 3, pp. 1863–1887, mar 2010.

[126] L. Gasperini, J. F. Mano, and R. L. Reis, "Natural polymers for the microencapsulation of cells.," *J. R. Soc. Interface*, vol. 11, no. 100, p. 20140817, 2014.

[127] B. Sahithi, A. Sk, H. Sk, G. Sahithya, D. P. M, and Y. Lakshmi, "A review on collagen based drug delivery systems," *Int. J. Pharm. Teach. Pract.*, vol. 4, no. 4, pp. 811–820, 2013.

[128] J. A. Ramshaw, J. A. Werkmeister, and V. Glattauer, "Collagen-based biomaterials," 1996.

[129] A. R. Bender, H. V. Briesen, J. Kreuter, I. B. Duncan, R. G. Kreuter, I. a. N. B. Duncan, A. R. Bender, and H. V. O. N. Briesen, "Efficiency of Nanoparticles as a Carrier System for Antiviral Agents in Human Immunodeficiency Virus-Infected Human Monocytes/Macrophages In Vitro," *Antimicrob. AGENTS Chemother.*, vol. 40, no. 6, pp. 1467–1471, 1996.

[130] R. Khan and M. H. Khan, "Use of collagen as a biomaterial: An update.," 2013.

[131] M. Hamidi, A. Azadi, and P. Rafiei, "Hydrogel nanoparticles in drug delivery," *Adv. Drug Deliv. Rev.*, vol. 60, no. 15, pp. 1638–1649, 2008.

[132] D. Swatschek, W. Schatton, W. E. G. Müller, and J. Kreuter, "Microparticles derived from marine sponge collagen (SCMPs): preparation, characterization and suitability for dermal delivery of all-trans retinol," *Eur. J. Pharm. Biopharm.*, vol. 54, no. 2, pp. 125–133, 2002.

[133] C. Qi, X. Yan, C. Huang, A. Melerzanov, and Y. Du, "Biomaterials as carrier, barrier and reactor for cell-based regenerative medicine," *Protein Cell*, vol. 6, no. 9, pp. 638–653, 2015.

[134] G. D. Nicodemus and S. J. Bryant, "Cell encapsulation in biodegradable hydrogels for tissue engineering applications.," *Tissue Eng. Part B. Rev.*, vol. 14, no. 2, pp. 149–165, 2008.

[135] H. Zimmermann, D. Zimmermann, R. Reuss, P. J. Feilen, B. Manz, a. Katsen, M. Weber, F. R. Ihmig, F. Ehrhart, P. Geßner, M. Behringer, a. Steinbach, L. H. Wegner, V. L. Sukhorukov, J. a. Vásquez, S. Schneider, M. M. Weber, F. Volke, R. Wolf, and U. Zimmermann, "Towards a medically approved technology for alginate-based microcapsules allowing long-term immunoisolated transplantation," *J. Mater. Sci. Mater. Med.*, vol. 16, no. 6, pp. 491–501, 2005.

[136] R. Mahou, R. R. H. Meier, L. H. Bühler, and C. Wandrey, "Alginate-poly(ethylene glycol) hybrid microspheres for primary cell microencapsulation," *Materials (Basel).*, vol. 7, no. 1, pp. 275–286, 2014.

[137] N. V. Krishnamurthy and B. Gimi, "Encapsulated cell grafts to treat cellular deficiencies and dysfunction.," *Crit. Rev. Biomed. Eng.*, vol. 39, no. 6, pp. 473–91, 2011.

[138] S. Krol, S. Del Guerra, M. Grupillo, A. Diaspro, A. Gliozzi, and P. Marchetti, "Multilayer nanoencapsulation. new approach for immune protection of human pancreatic islets," *Nano Lett.*, vol. 6, no. 9, pp. 1933–1939, 2006.

[139] W. de Graaff, D. Tomotsune, T. Oosterveen, Y. Takihara, H. Koseki, and J. Deschamps, "Randomly inserted and targeted Hox/reporter fusions tran-

scriptionally silenced in Polycomb mutants.," *Proc. Natl. Acad. Sci. U. S. A.*, vol. 100, no. 23, pp. 13362–13367, 2003.

[140] T. A. Desai, D. Hansford, and M. Ferrari, "Characterization of micromachined silicon membranes for immunoisolation and bioseparation applications," *J. Memb. Sci.*, vol. 159, no. 1-2, pp. 221–231, 1999.

[141] G. M. Whitesides, "The origins and the future of microfluidics.," *Nature*, vol. 442, no. 7101, pp. 368–373, 2006.

[142] A. Manz, D. J. Harrison, E. M. J. Verpoorte, J. C. Fettinger, A. Paulus, H. Lüdi, and H. M. Widmer, "Planar chips technology for miniaturization and integration of separation techniques into monitoring systemsCapillary electrophoresis on a chip," *J. Chromatogr. A*, vol. 593, no. 1-2, pp. 253–258, 1992.

[143] C. L. Hansen, E. Skordalakes, J. M. Berger, and S. R. Quake, "A robust and scalable microfluidic metering method that allows protein crystal growth by free interface diffusion.," 2002.

[144] J. Pihl, M. Karlsson, and D. T. Chiu, "Microfluidic technologies in drug discovery," *Drug Discov. Today*, vol. 10, no. 20, pp. 1377–1383, 2005.

[145] L. Kang, B. G. Chung, R. Langer, and A. Khademhosseini, "Microfluidics for drug discovery and development: From target selection to product lifecycle management," *Drug Discov. Today*, vol. 13, no. 1-2, pp. 1–13, 2008.

[146] S. K. Sia and G. M. Whitesides, "Microfluidic devices fabricated in poly(dimethylsiloxane) for biological studies," *Electrophoresis*, vol. 24, no. 21, pp. 3563–3576, 2003.

[147] A. A. Werdich, E. A. Lima, B. Ivanov, I. Ges, M. E. Anderson, J. P. Wikswo, and F. J. Baudenbacher, "A microfluidic device to confine a single cardiac myocyte in a sub-nanoliter volume on planar microelectrodes for extracellular potential recordings.," *Lab Chip*, vol. 4, no. 4, pp. 357–362, 2004.

[148] P. S. Dittrich and A. Manz, "Single-molecule fluorescence detection in microfluidic channels-the Holy Grail in uTAS," *Anal. Bioanal. Chem.*, vol. 382, no. 8, pp. 1771–1782, 2005.

[149] G. M. W. Wikswo, J. Saic, A. Richmond, M. Stremler, C. Y. Chung, and J. P., "Effects of flow and diffusion on chemotaxis studies in a microfabricated gradient generator," *Lab Chip*, vol. 5, no. 6, pp. 611–618, 2012.

[150] H. Lu, L. Y. Koo, W. M. Wang, D. a. Lauffenburger, L. G. Griffith, and K. F. Jensen, "Microfluidic shear devices for quantitative analysis of cell adhesion," *Anal. Chem.*, vol. 76, no. 18, pp. 5257–5264, 2004.

[151] A. R. Wheeler, W. R. Throndset, R. J. Whelan, A. M. Leach, R. N. Zare, Y. H. Liao, K. Farrell, I. D. Manger, and A. Daridon, "Microfluidic device for single-cell analysis," *Anal. Chem.*, vol. 75, no. 14, pp. 3581–3586, 2003.

[152] J. N. Lee, C. Park, and G. M. Whitesides, "Solvent Compatibility of Poly(dimethylsiloxane)-Based Microfluidic Devices," *Anal. Chem.*, vol. 75, no. 23, pp. 6544–6554, 2003.

[153] H. Löwe and W. Ehrfeld, "State-of-the-art in microreaction technology: concepts, manufacturing and applications," *Electrochim. Acta*, vol. 44, no. 21-22, pp. 3679–3689, 1999.

[154] K. F. Jensen, "Silicon-Based Microchemical Systems: Characteristics and Applications," *MRS Bull.*, vol. 31, no. 02, pp. 101–107, 2006.

[155] J. P. Rolland, R. M. Van Dam, D. a. Schorzman, S. R. Quake, and J. M. DeSimone, "Solvent-resistant photocurable liquid fluoropolymers for microfluidic device fabrication [corrected].," *J. Am. Chem. Soc.*, vol. 126, no. 8, pp. 2322–2323, 2004.

[156] S. Haeberle and R. Zengerle, "Microfluidic platforms for lab-on-a-chip applications.," *Lab Chip*, vol. 7, no. 9, pp. 1094–1110, 2007.

[157] M. E. Gomes, V. I. Sikavitsas, E. Behravesh, R. L. Reis, and A. G. Mikos, "Effect of flow perfusion on the osteogenic differentiation of bone marrow stromal cells cultured on starch-based three-dimensional scaffolds," *J Biomed Mater Res A*, vol. 1, no. 67, pp. 87–95, 2003.

[158] C. Perrault, "Microfluidic chipn for mechanobioengineering," *Univ. Sheff.*, pp. 3–8, 2012.

[159] T. W. Odom, J. C. Love, D. B. Wolfe, K. E. Paul, and G. M. Whitesides, "Improved Pattern Transfer in Soft Lithography Using Composite Stamps," *Langmuir*, vol. 18, no. 9, pp. 5314–5320, 2002.

[160] N. Nagai, N. Kumasaka, T. Kawashima, H. Kaji, M. Nishizawa, and T. Abe, "Preparation and characterization of collagen microspheres for sustained release of VEGF," *J. Mater. Sci. Mater. Med.*, vol. 21, no. 6, pp. 1891–1898, 2010.

[161] C. Yang and J. Wang, "Preparation and Characterization of Collagen Microspheres for Sustained Release of Steroidal Saponins," *Mater. Res.*, vol. 17, no. 6, pp. 1644–1650, 2014.

[162] A. Bergman, "Differentiation of human pluripotent stem cell- derived mesenchymal progenitors into osteogenic , chondrogenic and adipogenic lineages Differentiation of human pluripotent stem cell-derived mesenchymal progenitors into osteogenic , chondrogenic and adipog," *Chalmers Univ. Technol.*, pp. 1–54, 2012.

[163] D. Wallace, "Collagen gel systems for sustained delivery and tissue engineering," *Adv. Drug Deliv. Rev.*, vol. 55, pp. 1631–1649, nov 2003.

[164] C.-h. Li, M. Phil, T.-K. Chik, B. Eng, A. H. W. Ngan, D. Ph, S. C. H. Chan, D. K. Y. Shum, and B. P. Chan, "Correlation between compositional and mechanical properties of human mesenchymal stem cell-collagen microspheres during chondrogenic differentiation.," *Tissue Eng. Part A*, vol. 17, pp. 777–88, mar 2011.

[165] R. M. Delaine-Smith, S. MacNeil, and G. C. Reilly, "Matrix production and collagen structure are enhanced in two types of osteogenic progenitor cells by a simple fluid shear stress stimulus.," *Eur. Cell. Mater.*, vol. 24, pp. 162–74, jan 2012.

[166] P. Arpornmaeklong, S. E. Brown, Z. Wang, and P. H. Krebsbach, "Phenotypic characterization, osteoblastic differentiation, and bone regeneration capacity of human embryonic stem cell-derived mesenchymal stem cells.," *Stem Cells Dev.*, vol. 18, no. 7, pp. 955–968, 2009.

[167] Y. Ma, M. P. Neubauer, J. Thiele, A. Fery, and W. T. S. Huck, "Artificial microniches for probing mesenchymal stem cell fate in 3D," *Biomater. Sci.*, vol. 2, pp. 1661–1671, 2014.

[168] I. Wong and C. M. Ho, "Surface molecular property modifications for poly(dimethylsiloxane) (PDMS) based microfluidic devices," *Microfluid. Nanofluidics*, vol. 7, no. 3, pp. 291–306, 2009.

[169] T. Windvoel Mbanjwa, M., Mokone, N., Mogale, A., Land, K., "Surface Analysis of Polydimethylsiloxane Fouled with Bovine Serum Albumin," *Waset*, vol. 61, p. 3, 2010.

[170] F. Cecchet, B. De Meersman, S. Demoustier-Champagne, B. Nysten, and A. M. Jonas, "One step growth of protein antifouling surfaces: Monolayers of Poly(ethylene oxide) (PEO) derivatives on oxidized and hydrogen-passivated silicon surfaces," *Langmuir*, vol. 22, no. 3, pp. 1173–1181, 2006.

[171] H. Choi, P. Boccazzi, P. E. Laibinis, A. J. Sinskey, and K. F. Jensen, "POLY (ETHYLENE GLYCOL) (PEG) - MODIFIED POLY (DIMETHYL-SILOXANE) (PDMS) FOR PROTEIN- AND CELL-RESISTANT SURF âĂŹ ACES IN MICROBIOREACTOR," *7th Int. Cenferenceon Miniaturized Chem. Biochem. Anal. Syst.*, vol. 1, pp. 1105–1108, 2003.

[172] J. Chou, C. Austin, P. Doble, B. Ben-Nissan, and B. Milthorpe, "Trace elemental imaging of coralline hydroxyapatite by laser-ablation inductively coupled plasma-mass spectroscopy," *J. Tissue Eng. Regen. Med.*, no. July, pp. n/a–n/a, 2012.

[173] J. S. Becker, R. C. Dietrich, a. Matusch, D. Pozebon, and V. L. Dressler, "Quantitative images of metals in plant tissues measured by laser ablation inductively coupled plasma mass spectrometry," *Spectrochim. Acta - Part B At. Spectrosc.*, vol. 63, no. 11, pp. 1248–1252, 2008.

[174] L. M. Ricles, S. Y. Nam, K. Sokolov, S. Y. Emelianov, and L. J. Suggs, "Function of mesenchymal stem cells following loading of gold nanotracers.," *Int. J. Nanomedicine*, vol. 6, pp. 407–416, 2011.

[175] R. Tatavarty, H. Ding, G. Lu, R. J. Taylor, and X. Bi, "Synergistic acceleration in the osteogenesis of human mesenchymal stem cells by graphene oxidecalcium phosphate nanocomposites," *Chem. Commun.*, vol. 50, no. 62, p. 8484, 2014.

[176] C. Song, J. Wang, C. Mo, S. Mu, X. Jiang, X. Li, S. Zhong, Z. Zhao, and G. Zhou, "Use of Ferritin Expression, Regulated by Neural Cell-Specific Promoters in Human Adipose Tissue-Derived Mesenchymal Stem Cells, to Monitor Differentiation with Magnetic Resonance Imaging In Vitro," *PLoS One*, vol. 10, no. 7, p. e0132480, 2015.

[177] M. J. Barron, C.-J. Tsai, and S. W. Donahue, "Mechanical stimulation mediates gene expression in MC3T3 osteoblastic cells differently in 2D and 3D environments.," *J. Biomech. Eng.*, vol. 132, no. 4, p. 041005, 2010.

[178] J. Juhásová, S. Juhás, J. Klíma, J. Strnádel, M. Holubová, and J. Motlík, "Osteogenic differentiation of miniature pig mesenchymal stem cells in 2D and 3D environment.," *Physiol. Res.*, vol. 60, no. 3, pp. 559–571, 2011.

[179] X.-F. Tian, B.-C. Heng, Z. Ge, K. Lu, a. J. Rufaihah, V. T.-W. Fan, J.-F. Yeo, and T. Cao, "Comparison of osteogenesis of human embryonic stem cells within 2D and 3D culture systems.," *Scand. J. Clin. Lab. Invest.*, vol. 68, no. 1, pp. 58–67, 2008.

[180] E. M. Kearney, E. Farrell, P. J. Prendergast, and V. a. Campbell, "Tensile strain as a regulator of mesenchymal stem cell osteogenesis," *Ann. Biomed. Eng.*, vol. 38, no. 5, pp. 1767–1779, 2010.

[181] Adrien Baldit and Ana Campos and Marzia Brunelli and Cécile Perrault and Damien Lacroix, "Mutlti-scale modeling in tissue engineering: a Virtual Physiological approach," *VPH Conf.*, vol. 18, no. 8, pp. 624–631, 2014.

[182] Ellis E. Golub and Kathleen Boesze-Battaglia, "The role of alkaline phosphatase in cartilage mineralization.," *Bone Miner.*, vol. 17, no. 2, pp. 273–278, 1992.

[183] Y. Sugawara, K. Suzuki, M. Koshikawa, M. Ando, and J. Iida, "Necessity of enzymatic activity of alkaline phosphatase for mineralization of osteoblastic cells.," *Jpn. J. Pharmacol.*, vol. 88, no. 3, pp. 262–269, 2002.

[184] G. Yourek, S. M. McCormick, J. J. Mao, and G. C. Reilly, "Shear stress induces osteogenic differentiation of human mesenchymal stem cells," *Regen Med*, vol. 5, no. 5, pp. 713–724, 2010.

[185] A. Sittichokechaiwut, J. H. Edwards, a. M. Scutt, and G. C. Reilly, "Short bouts of mechanical loading are as effective as dexamethasone at inducing matrix production by human bone marrow mesenchymal stem cell.," *Eur. Cell. Mater.*, vol. 20, pp. 45–57, 2010.

[186] G. Friedl, H. Schmidt, I. Rehak, G. Kostner, K. Schauenstein, and R. Windhager, "Undifferentiated human mesenchymal stem cells (hMSCs) are highly sensitive to mechanical strain: transcriptionally controlled early osteochondrogenic response in vitro," *Osteoarthr. Cartil.*, vol. 15, no. 11, pp. 1293–1300, 2007.

[187] R. Hess, T. Douglas, K. A. Myers, B. Rentsch, C. Rentsch, H. Worch, N. G. Shrive, D. a. Hart, and D. Scharnweber, "Hydrostatic pressure stimulation of human mesenchymal stem cells seeded on collagen-based artificial extracellular matrices.," *J. Biomech. Eng.*, vol. 132, no. 2, p. 021001, 2010.

[188] H.-J. Seo, Y.-E. Cho, T. Kim, H.-I. Shin, and I.-S. Kwun, "Zinc may increase bone formation through stimulating cell proliferation, alkaline phosphatase activity and collagen synthesis in osteoblastic MC3T3-E1 cells.," *Nutr. Res. Pract.*, vol. 4, no. 5, pp. 356–361, 2010.

[189] K. Nakashima, X. Zhou, G. Kunkel, Z. Zhang, J. M. Deng, R. R. Behringer, and B. De Crombrugghe, "The novel zinc finger-containing transcription factor Osterix is required for osteoblast differentiation and bone formation," *Cell*, vol. 108, no. 1, pp. 17–29, 2002.

[190] R. K. Schneider, A. Puellen, R. Kramann, K. Raupach, J. Bornemann, R. Knuechel, A. Pérez-Bouza, and S. Neuss, "The osteogenic differentiation of adult bone marrow and perinatal umbilical mesenchymal stem cells and matrix remodelling in three-dimensional collagen scaffolds," *Biomaterials*, vol. 31, no. 3, pp. 467–480, 2010.

[191] F. Mannello, G. M. Tonti, G. P. Bagnara, and S. Papa, "Role and function of matrix metalloproteinases in the differentiation and biological characterization of mesenchymal stem cells.," *Stem Cells*, vol. 24, no. 3, pp. 475–481, 2006.

[192] C. Filanti, G. R. Dickson, D. Di Martino, V. Ulivi, C. Sanguineti, P. Romano, C. Palermo, and P. Manduca, "The expression of metalloproteinase-2, -9, and -14 and of tissue inhibitors-1 and -2 is developmentally modulated during osteogenesis in vitro, the mature osteoblastic phenotype expressing metalloproteinase-14.," *J. Bone Miner. Res.*, vol. 15, no. 11, pp. 2154–2168, 2000.

[193] H. C. Anderson, "Matrix vesicles and calcification.," *Curr. Rheumatol. Rep.*, vol. 5, no. 3, pp. 222–226, 2003.

[194] S. Weinbaum, S. C. Cowin, and Y. Zeng, "A model for the excitation of osteocytes by mechanical loading-induced bone fluid shear stresses," *J. Biomech.*, vol. 27, no. 3, pp. 339–360, 1994.

[195] A. . Al-Munajjed, N. . Plunkett, J. P. Gleeson, T. Weber, C. Jungreuthmayer, T. Levingstone, J. Hammer, and F. J. O'Brien, "Development of a biomimetic

collagen-hydroxyapatite scaffold for bone tissue engineering using a SBF immersion technique," *J. Biomed. Mater. Res. - Part B Appl. Biomater.*, vol. 90, no. 2, pp. 584–591, 2009.

[196] A. Dardik, L. Chen, J. Frattini, H. Asada, F. Aziz, F. a. Kudo, and B. E. Sumpio, "Differential effects of orbital and laminar shear stress on endothelial cells," *J. Vasc. Surg.*, vol. 41, no. 5, pp. 869–880, 2005.

[197] X. Z. Wang, D. Liu, L. You, , and Liyun, "Quantifying Fluid Shear Stress in a Rocking Culture Dish," *J Biomech*, vol. 43, no. 8, pp. 1598–1602, 2010.

[198] D. D. Deligianni, N. Katsala, S. Ladas, D. Sotiropoulou, J. Amedee, and Y. F. Missirlis, "Effect of surface roughness of the titanium alloy Ti-6Al-4V on human bone marrow cell response and on protein adsorption," *Biomaterials*, vol. 22, no. 11, pp. 1241–1251, 2001.

[199] B. M. Willie, A. Petersen, K. Schmidt-Bleek, A. Cipitria, M. Mehta, P. Strube, J. Lienau, B. Wildemann, P. Fratzl, and G. Duda, "Designing biomimetic scaffolds for bone regeneration: why aim for a copy of mature tissue properties if nature uses a different approach?," *Soft Matter*, vol. 6, no. 20, p. 4976, 2010.

[200] E. A. NAUMAN and R. L. SATCHER and T. M. KEAVENY and B. P. HALLORAN and and D.D BIKLE, "Osteoblasts respond to pulsatile fluid flow with short-term increases in PGE(2) but no change in mineralization.," *J. Appl. Physiol.*, vol. 90, no. 5, pp. 1849–1854, 2001.

[201] S. Kou, L. Pan, D. van Noort, G. Meng, X. Wu, H. Sun, J. Xu, and I. Lee, "A multishear microfluidic device for quantitative analysis of calcium dynamics in osteoblasts," *Biochem. Biophys. Res. Commun.*, vol. 408, no. 2, pp. 350–355, 2011.

[202] Mathews .S and Mathew .SA and Gupta .PK nad Bhonde .R and Totey .S, "Study the effect of various extracellular matrix proteins on adhesion , proliferation and osteoblast differentiation of bone marrow derived human mesenchymal stem cells," *J Tissue Eng Regen Med*, vol. 8, no. 2, pp. 143–52, 2014.

[203] C. Moraes, Y. Sun, and C. a. Simmons, "(Micro)managing the mechanical microenvironment.," *Integr. Biol. (Camb).*, vol. 3, no. 10, pp. 959–71, 2011.

[204] A. R. Stern, M. M. Stern, and M. E. Van Dyke, "Transduction of Strain To Cells Seeded Onto Scaffolds Exposed To Uniaxial Stretching: a Three Dimensional Finite Element Study," *J. Mech. Med. Biol.*, vol. 12, pp. 1–16, mar 2012.

[205] T. W. P. Loboa, R. D. Sumanasinghe, and E. G., "Finite Element Modeling of 3D Human Mesenchymal Stem Cell- Seeded Collagen Matrices Exposed to Tensile Strain," *J Biomech*, vol. 41, no. 10, pp. 2289–2296, 2008.